MATRIX METALLOPROTEINASE REQUIREMENTS FOR NEUROMUSCULAR SYNAPTOGENESIS

By

Mary Lynn Dear

Dissertation

Submitted to the Faculty of the

Graduate School of Vanderbilt University

in partial fulfillment of the requirements

for the degree of

DOCTOR OF PHILOSOPHY

in

Biological Sciences

January 31, 2018

Nashville, Tennessee

Approved:

Todd Graham, Ph.D.
Kendal Broadie, Ph.D.
Katherine Friedman, Ph.D.
Barbara Fingleton, Ph.D.
Jared Nordman, Ph.D.

ACKNOWLEDGEMENTS

I would like to acknowledge my advisor, Kendal Broadie, and the entire Broadie laboratory, both past and present, for their endless support, engaging conversations, thoughtful suggestions and constant encouragement. I would also like to thank my committee members both past and present for playing such a pivotal role in my graduate career and growth as a scientist. I thank the Department of Biological Sciences for fostering my graduate education. I thank the entire protease community for their continued support, helpful suggestions and collaborative efforts that helped my project move forward. I would like to acknowledge Dr. Andrea Page-McCaw and her entire laboratory for helpful suggestions, being engaged in my studies and providing many tools that were invaluable to my project. I thank my parents, Leisa Justus and Raymond Dear, my brother Jake Dear and my best friend Jenna Kaufman. Words cannot describe how grateful I am for your support and encouragement. Most importantly, I would like to thank my husband, Jeffrey Thomas, for always believing in me, your unwavering support and for helping me endure all the ups and downs that come with graduate school. I am forever grateful and could not have done this without you.

ACKNOWLEDGEMENT OF FUNDING

This work was supported by the National Institutes of Health R01 MH096832 and R01 MH084989 to K.B.

PUBLICATIONS

Two classes of matrix metalloproteinases reciprocally regulate synaptogenesis. **Dear ML**, Dani N, Parkinson W, Zhou S, Broadie K. Development. 2016 Jan 1;143(1):75-87.

Synaptic roles for phosphomannomutase type 2 in a new Drosophila congenital disorder of glycosylation disease model. Parkinson WM, Dookwah M, **Dear ML**, Gatto CL, Aoki K, Tiemeyer M, Broadie K. Dis Model Mech. 2016 May 1;9(5):513-27.

Neuronal activity drives FMRP- and HSPG-dependent matrix metalloproteinase function required for rapid synaptogenesis. **Dear ML**, Shilts J, Broadie K. Sci. Signal. 2017 Nov 7;10:eaan3181.

TABLE OF CONTENTS

LIST OF FIGURES AND TABLES

Figures Page

Tables Page

LIST OF SUPPLEMENTARY MATERIAL

LIST OF ABBREVIATIONS

(ADAM)	a disintegrin and metalloprotease
(ADAMTS)	a disintegrin and metalloprotease with thrombospondin type I-like motifs
(Alk)	Anaplastic lymphoma kinase
(ANOVA)	Analysis of Variance
(AP-1)	Activator protein 1
(aPKC)	atypical Protein kinase C
(APP)	β-amyloid precursor protein
(Arm)	Armadillo
(Arr)	Arrow
(ASD)	autism spectrum disorder
(AZ)	Active zone
(BBB)	blood brain barrier
(BL)	basal lamina
(BM)	basement membrane
(BMP)	Bone morphogenic protein
(BMPR)	Bone morphogenic protein receptor
(BONCAT)	bio-orthogonal non-canonical amino acid tagging
(Brp)	Bruchpilot
(BSA)	Bovine Serum Albumin
($CaCl_2$)	calcium chloride
(CAM)	cell adhesion molecule
(CamKII)	Calcium/Calmodulin-dependent protein kinase
(Cas9)	CRISPR associated protein 9
(cat)	catalytic
(cGMP)	cyclic guanosine monophosphate
(CNS)	central nervous system
(Cow)	Carrier of Wingless
(CRISPR)	Clustered Regularly Interspaced Short Palindromic Repeats
(CS)	Chondroitin sulfate

(CSP)	Cysteine String Protein
(CSPG)	Chondroitin sulfate proteoglycan
(Dad)	Daughters against decapentaplegic
(Dally)	Division-abnormally delayed
(dblhet)	double heterozygous
(dblRNAi)	double *UAS-mmp1*^{RNAi}; *UAS-mmp2*$^{dsRNAi1794\text{-}1R\text{-}2}$
(dCask)	Calcium/Calmodulin Dependent Serine Protein Kinase
(DCV)	dense-core vesicle
(Dg)	Dystroglycan
(DGC)	Dystrophin-associated glycoprotein complex
(dGRIP)	glutamate receptor interacting protein
(dLAR)	Leukocyte common antigen-related
(DLG)	Discs-large
(Dlp)	Dally-like protein
(DNA)	deoxyribonucleic acid
(dpERK)	diphosphorylated extracellular signal-related kinase
(Dpp)	Decapentaplegic
(DQ-gelatin)	dye-quenched fluorogenic gelatin
(Drl)	Derailed
(DROP-1)	Proteoglycan-1
(DS)	Dermatan sulfate
(DSPG)	Dermatan sulfate proteoglycan
(dTRPA1)	Transient receptor potential cation channel A1
(Dvl)	Dishevelled
(Eag)	Ether a go-go
(ECM)	Extracellular matrix
(EDTA)	ethylenediaminetetraacetic acid
(EJC)	excitatory junctional current
(EJP)	excitatory junctional potential
(Elav)	Embryonic lethal abnormal vision
(ERK)	Extracellular signal-related kinase

(Evi/Wls/Srt) Evenness Interrupted/Wntless/Sprinter

(EXT1) Exostosin-1

(FACIT) Fibril-associated collagen with interrupted triple helix

(FAK) Focal adhesion kinase

(FGF) Fibroblast growth factor

(FISH) fluorescent *in situ* hybridization

(Fj) Four-jointed

(FMR1) fragile X mental retardation 1

(FMRP) Fragile X Mental Retardation Protein

(FNI) Frizzled nuclear import

(Frac) Faulty Attraction

(Frz2) Frizzled-2 receptor

(FUNCAT) fluorescent non-canonical amino acid tagging

(FXS) Fragile X syndrome

(Fz) Frizzled

(GAG) glycosaminoglycan

(Gbb) Glass Bottom Boat

(GF) growth factor

(GFP) Green fluorescent protein

(GlcNAc) *N*-Acetylglucosamine

(GlcNS) sulfated *N*-Acetylglucosamine

(GluR) Glutamate receptor

(GOF) gain-of-function

(GPI) glycosylphosphatidylinositol

(GSK-3β) Glycogen Synthase Kinase 3 Beta

(Hep) heparitinase

(HEPES) 4-(2-hydroxyethyl)-1-piperazineethanesulfonic acid

(Hh) Hedgehog

(hpx) hemopexin

(HRP) Horse Radish Peroxidase

(HS) Heparan sulfate

(Hs2st)	HS 2-O-sulfotransferases
(Hs6st)	HS 6-O-sulfotransferases
(HSPG)	Heparan sulfate proteoglycan
(Htl)	Heartless
(Htt)	huntingtin
(IM)	Interstitial matrix
(iTRAQ)	isobaric tags for relative and absolute quantitation
(JAK/STAT)	Janus kinase/signal transducers and activators of transcription
(Jeb)	Jelly-belly
(JNK)	c-Jun NH2-terminal kinase
(KCl)	potassium chloride
(KS)	Keratan sulfate
(Kul)	Kuzbanian-like
(Kuz)	Kuzbanian
(LamC)	Lamin C
(LanA)	Laminin A
(LGL)	Lethal (2) giant larvae
(LIMK)	LIM domain kinase 1
(LOF)	loss-of-function
(Loh)	Lonely heart
(LOX)	Lysyl oxidase
(LRP)	low density lipoprotein-receptor-related protein
(Mad)	Mothers against decapentaplegic
(MAP1B)	Microtubule Associated Protein 1B
(Mav)	Maverick
(MCC)	Manders' co-localization coefficient
(MDP-1)	Macrophage-Derived Proteoglycan-1
(Med)	Medea
(mEJC)	miniature EJC
(MES)	2-(N-morpholino)ethanesulfonic acid
(MetRS)	methionyl-tRNA synthetase

(MgCl2)	magnesium chloride
(mir-RNA)	micro-RNA
(Mmd)	Mind-meld
(Mmp)	Matrix metalloprotease
(MN)	Motorneuron
(MOPS)	3-(N-morpholino)propanesulfonic acid
(Mp)	Multiplexin
(mRNA)	messenger RNA
(MTG)	Mind-the-Gap
(NaCl)	sodium chloride
(NCAT)	non-canonical amino acid tagging
(NE)	nuclear envelope
(NLS)	nuclear localization signal
(NMJ)	Neuromuscular junction
(Nolo)	No-long nerve chord
(OE)	over-expression
(Par-6)	Partitioning-defective protein 6
(PBS)	Phosphate buffered saline
(Pcan)	Perlecan
(PDF)	pigment dispersing factor
(PFA)	paraformaldehyde
(PG)	Proteoglycan
(PI3K)	Phosphoinositide 3-kinase
(PKC)	Protein kinase C
(PKM)	Pyruvate kinase
(PLA)	proximity ligation assay
(pMad)	phosphorylated Mad
(PNS)	Peripheral nervous system
(Ppn)	Papilin
(Prc)	Pericardin
(PSD)	Postsynaptic density

(PTM)	posttranslational modification
(Puro)	Puromycylation
(Pxn)	Peroxidasin
(QC)	quantal content
(Rac1)	Ras-related C3 botulinum toxin substrate 1
(RECK)	reversion-inducing cysteine-rich protein domain with kazal motifs
(RIP)	RNA immunoprecipitation
(RNA)	ribonucleic acid
(RNAi)	RNA interference
(RNP)	ribonucleoprotein particle
(RTK)	receptor tyrosine kinase family
(Sax)	Saxophone
(SD)	standard deviation
(Sdc)	Syndecan
(SDS-PAGE)	sodium dodecyl sulfate polyacrylamide gel electrophoresis
(SEM)	standard error of the mean
(Sema-1a)	Semaphorin-1a
(serps)	serpins
(Sgg)	Shaggy
(Sh)	Shaker
(SILAC)	Stable Isotope Labeling with Amino acids in Cell culture
(Slmb)	Supernumerary limbs
(Sog)	Short gastrulation
(Sona aka Dimp)	Solo narae
(SP)	serine protease
(SPARC)	Secreted protein, acidic, cysteine-rich
(SSR)	subsynaptic reticulum
(Stl)	Stall
(Sulf)	Sulfatases
(Sulf1)	Sulfated
(SV)	Synaptic vesicle

(SWI/SNF)	SWItch/ Sucrose Non-Fermentable
(TACE)	TNF-α converting enzyme
(TAILS)	terminal amine isotopic labeling of substrates
(TBS)	tris-buffered saline
(TCA)	trichloroacetic acid
(TEM)	transmission electron microscopy
(TEVC)	two-electrode voltage clamp
(TG2)	Transglutaminase-2
(TGF-β)	Transforming growth factor
(TIMP)	Tissue inhibitor of metalloproteases
(Tkv)	Thickveins
(Tld)	Tolloid
(TNF-α)	Tumor necrosis factor-alpha
(Tok)	Tolkin
(tPA)	tissue plasminogen activator
(TRIBE)	targets of RNA-binding proteins identified by editing
(tRNA)	transfer RNA
(Trol)	Terribly reduced optic lobes
(ts)	temperature-sensitive
(Twit)	Target of Wit
(UAS)	Upstream Activation Sequence
(uPA)	urokinase plasminogen activator
(Upd)	Unpaired
(UTR)	untranslated region
(Vglut)	Vesicular glutamate transporter
(Vkg)	Viking
(VNC)	ventral nerve chord
(Wg)	Wingless
(Wit)	Wishful thinking
(Wnt)	Wingless-related integration site
(WT)	wild-type

CHAPTER I

INTRODUCTION

The extracellular matrix (ECM) and ECM-affiliated constituents comprise a complex glycoprotein network with fundamental roles in health and disease. The ECM regulates numerous important cellular functions including proliferation, adhesion, migration, differentiation and signaling communication. The synaptomatrix is a highly specialized and heavily glycosylated neural matrix that orchestrates coordinated neural development, but how this is regulated remains elusive. Extracellular proteases are critical regulators of ECM functions, cellular signaling, and cellular behavior. One family, the matrix metalloproteinases (Mmps), consists of secreted and membrane-anchored enzymes that might function as such key players in signaling networks regulating ECM- and non-ECM mediated biological processes. This thesis investigates the intersection of coordinated Mmp functions and synaptogenesis in normal neural development and disease.

The Extracellular Matrix

Characterizing the Extracellular Matrix

A substantial portion of tissues is extracellular, with ECM accounting for 50-70% of human body mass. The heavily-glycosylated ECM controls a wide variety of biological processes essential for all life. At the ultrastructural level, electron microscopy shows all cells are surrounded by developmentally dynamic and tissue-specific electron dense material (*1*). Early biochemical analyses described the ECM as a highly insoluble meshwork containing large structural proteins that are heavily cross-linked. Early molecular studies revealed that many ECM proteins contain characteristic, repetitive domains that are arranged in a highly characteristic manner. Multiple domains within a single ECM molecule permit multiple binding interactions to occur simultaneously (*2*). Genome sequencing paired with bioinformatics has shed light on the elaboration, diversification, and specialization of ECM molecules and domain functions throughout evolution (*2*, *3*). Recent advances in proteomic and genomic analyses has enabled researchers to begin organizing and categorizing ECM molecules (*3*, *4*), which account for 4% of the mammalian proteome and encompasses both ECM and ECM-affiliated proteins encoded by >1,000 genes ("the matrisome"; Fig. 1) (*4*). The core matrisome contains ~300 proteins with the most abundant including collagens, proteoglycans and non-collagenous glycoproteins.

Other matrisome components include ECM-associated factors such as ECM-modifying enzymes, growth factors (GF), and ECM-receptors, all of which increase the complexity and diversity of ECM functions (*4*). The ECM is synthesized by cells both proximal and distal within a given tissue. The ECM is produced locally by cells residing within the tissue and *en passant* by migratory cells (*5*). In some cases, secreted ECM diffuses over a long distance and is captured by the target tissue via cell-surface expressed ECM-receptors (*5*). Diversity in ECM composition is reflected in cell- and tissue-specific characteristics. Broadly speaking, mammals have two basic types of ECM; 1) basement membrane (BM or basal lamina (BL)) and 2) interstitial matrix (IM). The highly conserved BM forms a thin, sheet-like ECM layer ~100 nm thick at boundaries between the basal surface of epithelial and stromal cell layers forming connective tissues (*2*). In mesenchymal tissue, cells are clustered and grouped close together, but are not strictly adherent, and these cells secrete an IM which forms a variably hydrated, porous three-dimensional lattice filling the space surrounding cells (*2*).

The ECM was originally described as a passive, structural scaffold that simply filled intercellular space (*1*). It is now realized that along with scaffolding functions, the matrix has crucial, interactive roles in normal cell physiology, homeostasis and intercellular communication (*1*). Moreover, the ECM is a highly dynamic environment that is constantly remodeled, with tissue-specific developmental and spatio-temporal changes in composition and organization driving diverse ECM functions, including 1) serving as an adhesive substrate directing cell migration, 2) providing a structural support defining tissue boundaries, controlling cellular invasion events, maintaining tissue integrity and regulating elasticity, 3) sensing and transducing mechanical signals instructing differentiation and other cellular behaviors by cuing intracellular signaling and cytoskeletal machinery, 4) serving as a signaling reservoir sequestering and storing GFs, and 5) enabling context-specific, spatio-temporal signaling regulation by controlling the spatial distribution and bioavailability of ECM-bound molecules, regulating ligand-receptor interactions and establishing morphogen gradients (*4*, *6–9*). Numerous ECM molecules are encoded by essential genes with loss-of-function (LOF) resulting in lethality. The functional relevance of the ECM is further highlighted by the large number of human diseases attributed to matrix dysfunction (*10*).

The *Drosophila melanogaster* genetic model is an excellent system to interrogate the functional relevance of coordinated cell-matrix signaling driving tissue development and disease progression (*5*, *11*). Numerous core ECM constituents, ECM-associated molecules and ECM-dependent developmental processes are evolutionarily conserved between mammals and *Drosophila*, with less redundancy and compensation in this reductionist model (*3*, *5*, *11*). For example, *Drosophila* epithelial cells associate with an apical ECM (external, exoskeleton) and a basal ECM (internal, BM) (*5*, *11*). The exoskeleton contains cuticular ECM, rich in

chitin, which lines the apical surface of the epidermis, sensory organs and inner walls of trachea (respiratory organ) (*12*, *13*). Like bone matrices, the *Drosophila* exoskeletal matrix is quite rigid (*13*). Representative internal matrices include the tendon matrix located at muscle-epidermis attachment sites, specialized neuronal matrices, and BM/BL matrices lining the outer surfaces of all organs as well as the basal surface of the epidermis (*11*). A BL encases muscles and nerves, but this BL is excluded from interfacing motoneuron-muscle terminals at the neuromuscular junction (NMJ). The *Drosophila* NMJ contains a specialized, electron-dense and heavily glycosylated matrix termed the "synaptomatrix" (*11*, *14*, *15*). The synaptomatrix is unique with interspaced patterning that likely assists in compartmentalizing specialized neural signaling domains (*14*). Similar to mammals, *Drosophila* ECM constituents are produced by the epithelium, deposited locally by migratory cells, and secreted from distal or proximal tissue (*5*, *16*–*18*). Sources of *Drosophila* ECM include the fat body (analogous to adipose tissue/liver; long-range) and circulating haemocytes (analogous to blood cells/macrophages; local deposition) (*11*, *19*–*21*). The follicular epithelium of adult *Drosophila* females encases the germ cells in the developing ovary and is the only tissue known to secrete all of its own BM. *Drosophila* utilizes an open-circulatory system and internal organs are bathed in haemolymph (*22*). *Drosophila* tissues commonly used for assaying matrix-cell functions during development include imaginal discs, egg chamber, trachea, Malpighian tubes (kidney) and the nervous system. The following sections first introduce mammalian matrix biology followed by the corresponding *Drosophila* matrix biology.

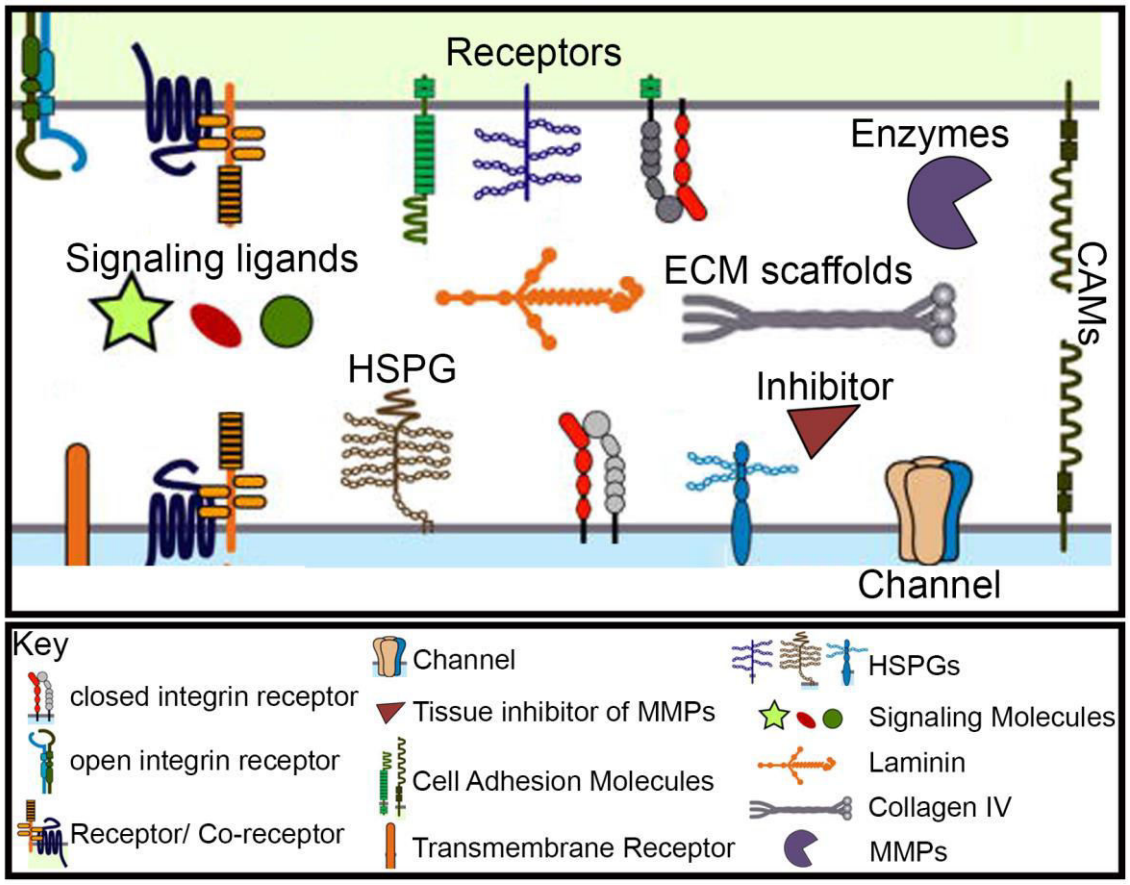

Figure 1

Figure 1: Components of the ECM and ECM-interacting molecules. Cartoon schematic shows examples of extracellular matrix (ECM) components and molecules that interface with the extracellular environment. These include ECM scaffolds such as Laminin and Collagen IV, ECM receptors such as integrin dimers, co-receptors, heparan sulfate proteoglycans (HSPGs), signaling ligands, transmembrane channels, cell adhesion molecules (CAMs), as well as enzymes and inhibitors such as matrix metalloproteinases (MMPs) and tissue inhibitor of MMPs (TIMPs).

Core Matrisome Components

Collagens

Major ECM constituents include collagen glycoproteins, proteoglycans, glycosaminoglycans (GAGs) and non-collagenous glycoproteins (*3*, *4*). Collagen is found in all metazoans, where it is the most abundant protein (*2*, *23*, *24*). All collagens are structurally defined by a triple helical organization composed of Gly-X-Y repeats where X is usually a proline and Y is usually a hydroxyproline (*24*). Collagens are considered the main scaffolding proteins of ECMs including bone, cartilage, BM and IM; however, not all of the 28 collagen members are part of the ECM proper. The mammalian core matrisome contains > 40 collagen subunits (*3*, *4*). Collagens are subdivided based on their supramolecular assemblies and can be more generally grouped as fibrillar or non-fibrillar (*24*). Fibrillar collagens (I-III, V, XI, XXIV and XXVII) are the most abundant collagens, and are prominently found in bone, skin, tendons, ligaments, and cartilage. The fibrillar collagens provide tensile strength and viscoelasticity to tissues with interstitial collagen I forming the major structural scaffold for tissues (*24*). Fibril-associated collagens with interrupted triple helices (FACIT) associate with fibrillar collagens and help organize collagen fibrils in the matrix. BM/BLs are more compact than IMs, consisting of non-fibrillar, network-forming collagens (IV, VIII, X) that link together matrix components and matrix-cell (*24*–*26*). Collagen IV is the main non-fibrillar collagen, and is instrumental for BM formation. BM-localized collagen XVIII contains both collagenous and proteoglycan domains as do collagens IX, XII, XIV and XV. Besides structural support roles, collagens interact with GFs in the matrix and function themselves as ligands. Proteolytic cleavage of collagen XVIII C-terminus produces endostatin, a bioactive signaling molecule (*24*, *27*). Mechanical force or ECM-collagen interactions can generate a conformational change in collagen, exposing cryptic functional sites. These so called “matricryptins” appear particularly relevant in BM signaling functions as most are derived from collagens associated with the BM (collagen IV, VIII, XVIII, XV and XIX). Transmembrane collagens (XIII, XVII, XXIII, and XXV) localize to the cell-surface and have roles in cell adhesion, differentiation and maintaining structural integrity. Similar to matricryptins, proteolytic cleavage and release of the extracellular domain (ectodomain shedding) can have signaling capabilities (*24*). Some collagens show strong developmental and tissue-specific expression, and thus have specialized biological functions. For example, collagen XXVI is specifically restricted to the extracellular space of reproductive organs (*28*). A recently identified collagen, collagen XXVIII, is almost exclusively expressed in the peripheral nervous system (PNS) surrounding glia (*29*). Collagens are subject to extensive posttranslational modifications (PTMs) that modify function, and additional

non-collagenous protein domains contribute to structural properties, specific binding affinities and dictate protein-protein interactions (*24*).

Drosophila lacks fibrillar collagens (*2*, *11*), however, collagen IV is well conserved with two genes encoding type IV collagens, Cg25C (Col4α1) and Viking (Vkg). These collagens are major BM components, required for tissue integrity and signaling interactions (*30*–*32*). Loss of *Drosophila* collagen IV function results in thin, fragile BMs and late embryonic lethality (*33*). Collagen IV metabolism and deposition are required for wound healing, organogenesis, embryonic neuromuscular adhesion and nervous system integrity (*33*–*37*). *Drosophila* contains another type IV-like collagen, Pericardin (Prc), involved in heart development and tissue morphogenesis (*38*, *39*). A homolog of collagen XV/XVIII, Multiplexin (Mp), is also present in *Drosophila* (*27*, *40*). Like mammalian collagen XVIII, Mp contains collagenous and non-collagenous domains, an N-terminal thrombospondin type 1 repeat domain, and a cleavable C-terminal endostatin domain with important signaling functions (*27*, *40*). Mp binds the secreted glycoprotein Slit, enhancing Slit signaling, and also localizes Wnt signaling ligands (*41*, *42*). Mp is required for synaptic homeostasis, calcium channel localization, calcium influx, neurotransmitter release at the NMJ synapse (*27*), motor axon pathfinding in the peripheral nervous system (*40*), as well as heart development (*37*, *41*).

Proteoglycans

The human genome encodes 43 distinct proteoglycans (PG) (*43*), and the core mammalian matrisome includes ~36 extracellular PGs, defined as glycoproteins with at least one covalently linked GAG chain (*3*, *4*). Both the core protein and GAG chains contribute to PG function, originally described as matrix “space-filler”, but that definition has dramatically expanded (*44*). Currently, PGs are reported to interact with over 200 GFs to modulate intercellular signaling. PG classification is based on cellular/subcellular localization, overall gene/protein homology and use of specific protein modules within the core proteins (*43*). GAGs are synthesized in the Golgi apparatus as long, unbranched carbohydrates composed of repeating disaccharide units that contain carboxyl, hydroxyl and sulfate groups (*45*). These chains are further modified by extracellular sulfatases and heparanase. The disaccharide units, consisting of either *N*-acetylgalactosamine or *N*-acetylglucosamine and uronic acid, are attached to serine residues of core proteins via a tetrasaccharide linker (*45*). GAGs are defined by carbohydrate composition and include chondroitin sulfate (CS), dermatan sulfate (DS), keratan sulfate (KS) and heparan sulfate (HS). GAGs contribute to the functional diversity of PGs since GAG attachment, composition, length and modifications vary from cell to cell and throughout development. CS is the most abundant GAG, and CSPGs are major matrix components in tissues such as bone

and cartilage. DSPGs are largely found in skin, vasculature and tendons. KS is commonly linked to core proteins that also contain CS and KS is primarily found in bone, cartilage and cornea. HSPGs are important BM and cell-surface molecules that can bind numerous ligands (*45–47*). GAG chains have a net negative charge lending to electrostatic interactions that sequester water, divalent cations and bind secreted molecules in the ECM. Matrix PGs are osmotically active and can create passageways between cells as well as regulate migration, invasion and signaling events (*43*, *47–50*). PGs are responsible for the hydrated gel-like properties of the IM and impart tissues with properties of high viscosity and low compressibility while maintaining rigidity. PGs can interact with various glycoproteins and the CSPGs and DSPGs are important for collagen organization (*43*, *51*). IM PGs display spatio-temporal diversity in both size and GAG composition which mainly includes CS, DS and KS. For example, neurocan is found in the central nervous system (CNS) during late embryogenesis and inhibits neurite outgrowth while brevican is produced by terminally differentiated neurons in the CNS (*43*, *52*, *53*). BM PGs include the HSPGs perlecan (Pcan), agrin and collagen XVIII as well as the CSPG leprecan. Pcan is the most common HSPG present in BMs and maintains tissue borders, functions in cell adhesion and modulates several GF morphogens (*44*, *54*). Pcan and agrin have numerous functions in the nervous system that are further discussed below. The membrane-tethered, ECM-associated HSPGs include 6 glypicans and 4 syndecans, which function as ECM-receptors as well as in signaling roles (*43*). It is important to note that similar to transmembrane collagens, membrane-tethered PGs are subject to ectodomain shedding which serves a range of signaling functions.

Biochemical analyses show that *Drosophila* GAGs consist of both CS and HS, which display spatio-temporal heterogeneity like mammals (*55*). *Drosophila* contains one Pcan homolog, *terribly reduced optic lobes* (*trol*) (*56–58*). Trol is a major constituent of the BM and interacts with ECM components and signaling GFs. Trol functions include matrix assembly and integrity, cell polarity, cell proliferation, tissue morphogenesis and GF signaling. An early biochemical study reported on a large proteoglycan, Macrophage-Derived Proteoglycan-1 (MDP-1), secreted exclusively from haemocytes and regulated by apoptosis with expression highly enriched in the developing nervous system (*59*). However, MDP-1 remains unannotated and its function remains unclear (FlyBase). Another biochemical study reports Proteoglycan-1 (DROP-1) as an HSPG expressed in the embryo; however, DROP-1 remains unannotated and follow-up studies have not yet been performed (FlyBase). Carrier of wingless (Cow) is a recently identified secreted HSPG with homology to Testican-2 and Testican-3 (*60*). Cow binds the Wnt-1 homolog Wingless (Wg) and this interaction stabilizes and promotes the extracellular Wg morphogen gradient in the developing wing disc (*60*). The *Drosophila* membrane-bound HSPGs include 2 glypican orthologues; Division-abnormally delayed (Dally) and Dally-like (Dlp), as well as a

single transmembrane Syndecan (Sdc). The glypicans are exclusively HS modified while Syndecan might exist as an exclusive HSPG or hybrid PG species containing HS modifications plus a single CS GAG attachment (*61*, *62*). These HSPGs also function as ECM-receptors as well as in signaling roles. As with mammals, *Drosophila* HSPGs have significant functions in the nervous system that are discussed in detail below.

Glycoproteins

The third group of abundant matrix molecules is the non-collagenous glycoproteins. The mammalian matrisome contains ~200 glycoproteins representing many protein families with a wide diversity of functions (*3*, *4*). Such glycoproteins include laminins, fibronectins, thrombospondins, nidogens and elastin. These molecules function to bridge ECM and/or ECM-affiliated components, serve as ligands signaling via ECM-receptors enabling matrix assembly and adhesion, and also function as a reservoir of GFs (*2*, *3*, *9*, *54*, *63*). ECM glycoproteins contain multiple domains that enable simultaneous protein interactions, and thus act as regulatory platforms coordinating various ECM functions. Laminins are cruciform-shaped heterotrimeric proteins composed of α-, β- and γ-subunits, that function as structural components of all BMs (*9*, *54*, *64*, *65*). Laminins interact with ECM receptors such as integrins and HSPGs to regulate tissue morphology, cell adhesion and cell migration via matrix-mediated signaling events. Fibronectins form dimers, bind GAGs, collagens and GFs, and similarly interact with ECM receptors to regulate cell adhesion, migration and differentiation. Thrombospondins are transiently expressed adapter molecules that associate with a variety of ECM molecules including fibronectin, laminin, PGs and collagens to guide ECM synthesis and tissue remodeling (*2*, *37*, *66*). Nidogens are ECM linker proteins ubiquitously expressed in BMs. Along with collagen, another main structural support glycoprotein is elastin. As the name implies, elastin imparts elasticity or flexibility on the ECM, permitting tissues to undergo repetitive mechanical stress without malforming or rupturing.

The *Drosophila* genome encodes two laminin α-chains, one β-subunit and one γ-subunit. Laminins have conserved roles in ECM assembly, BM integrity, adhesion and tissue morphogenesis (*11*). Disrupting Laminin-β function abolishes BM formation with reduced accumulation of Trol and Collagen IV (*67*). Laminin-A (LanA) is required for neuromuscular adhesion, and is regulated by Wnt signaling (*19*, *68*). Like mammals, *Drosophila* laminins interact with integrins and bind mammalian nidogen. *Drosophila* lacks fibronectin, consistent with the fact that the fibronectin domains 1 and 2 appeared recently in evolution and are largely restricted to chordates (*2*). Thrombospondins are evolutionarily conserved and are necessary for integrin-mediated cell adhesion at tendon-muscle attachment sites (*37*, *66*, *69*). Nidogen/entactin is a conserved BM linker molecule important for cell adhesion. Elasticity is clearly an important property for *Drosophila* morphogenesis and

tissue integrity, but elastin proteins remain poorly described (*70*). Tentative elastin genes include *elastin-like* and *resilin* with several uncharacterized cuticular and ECM proteins containing elastin-like motifs (*70*, *71*). Other conserved ECM glycoproteins include fibulins, BM-40/SPARC (secreted protein, acidic, cysteine-rich) and M-spondin (*11*). Many of these ECM glycoproteins are particularly enriched in the nervous system, and play prominent roles in many aspects of neural development.

Matrisome-Associated Molecules

ECM-cell interaction is reciprocal and bidirectionally coordinated. Cells both initiate or respond to extracellular cues by producing ECM and/or matrisome-associated molecules. Alterations in ECM composition or function are relayed back to the cell via ECM-receptors in a cyclical process signaling either homeostasis or instructing cellular behaviors (*7*, *72*, *73*). Matrisome-associated groups include ECM-affiliated molecules known or predicted to interact with the ECM (~176 in humans), ECM-regulators such as remodeling enzymes (~250 in humans), and other secreted factors including GFs and cytokines (~350 in humans) (*3*, *4*). However, any protein spanning the extracellular environment is probably integrated with the ECM. A particularly important sub-group consists of ECM-receptors, which permit cell-ECM signaling by integrating environmental cues and transducing downstream signaling events accordingly to direct changes in cellular behaviors. ECM receptor activation/deactivation provides critical cues coordinating cell survival, growth, proliferation and differentiation (*72*). Reciprocally, ECM-cell signaling mediates coordinated changes in ECM gene expression and/or ECM-receptor activity. ECM-receptor interactions are multifunctional, also serving as adhesive and physical connections controlling cell and tissue morphology, organization, polarity and migration. ECM receptors containing intra- and extracellular domains enable bidirectional signaling via both “inside-out” and “outside-in” cell-matrix regulatory functions. Well-described ECM-receptors include integrins, dystroglycan (Dg), PGs and GF-receptors.

Extracellular Matrix Receptors

The integrins make up the largest family of ECM-receptors and are the main cell adhesion receptors controlling cell migration (*72*, *74*, *75*). The integrins were the first ECM-receptors identified, and were named to highlight their importance for tissue integrity. Integrins bind the Arg-Gly-Asp (RGD) motif found in many ECM ligands, which include laminins, fibronectin, collagen IV, nidogen/entactin and thrombospondins. Integrins are composed of heterodimeric α- and β-subunits that assemble into distinct combinations with

differential ligand affinities, making integrin expression an important determinant of cell adhesion on a given matrix (*72*). Integrins respond to both biochemical and mechanical properties of an ECM and integrate both modalities through direct interactions with the cytoskeleton, which reciprocally regulate integrin conformations. The integrin-adhesion complex (or "integrin-adhesome") contains over 150 components that mediate signaling activities. Integrin and GF signaling display extensive cross-talk, and these pathways contain several points of convergence. A second transmembrane ECM-receptor, Dg, is the major non-integrin ECM-receptor; ubiquitously expressed but most well-studied in the context of the nervous system and skeletal muscle (*76*, *77*). Dg is a constituent of the dystrophin-associated glycoprotein complex (DGC) which stabilizes ECM-cell adhesion and forms a critical link between the matrix and cytoskeleton. Dg ligands include laminins, perlecan and agrin, and functional interactions strongly rely on proper glycosylation of both receptor and ligand (*76*, *78*, *79*). Dg is required for the initial anchoring of cell-BM, organizing the laminin matrix, preserving structural integrity of muscle and BM attachment, and influencing ECM metabolism. Laminin-dg binding activates Src-family signaling necessary for glial cell survival. In muscle, both laminin binding and mechanical force activate a dg-dependent signaling cascade leading to Ras-related C3 botulinum toxin substrate 1 (Rac1) activation and calcium immobilization. At the NMJ, the dg-agrin interactions enhance agrin function presumably by maintaining/stabilizing agrin in the extracellular space (*80–82*). Integrin- and Dg-dependent ECM receptor functions are likely cooperative.

Drosophila integrin heterodimers are constructed from 5 α-subunits and 2 β-subunits (*11*). Known ligands include laminins and an RGD-containing, secreted ECM molecule called Tiggrin (*19*, *20*, *83*). Fly integrins are involved in cell adhesion and migration, with prominent LOF phenotypes including defects in muscle attachment and morphology, and defects in epithelial tissue integrity, cell migration and tissue morphology. The *Drosophila* integrin-adhesome is conserved with fewer redundant components. Moreover, *Drosophila* and mammalian integrin signaling activate similar intracellular kinase pathways, suggesting conserved signal transduction. However, in contrast to vertebrates, cell fate and proliferation do not seem to have a strong requirement for integrin-mediated adhesion in flies (*84*). *Drosophila* Dg is likewise central to the DGC, connecting the ECM-cytoskeletal networks, and is ubiquitously expressed. Dg is required for cell-polarity in various cell types and facilitates muscle-matrix attachment (*57*, *85*, *86*). Dg ligands include laminins and Pcan, and glycosylation is an important posttranslational modification regulating Dg function. Dg is enriched in neural tissues with functions in scaffolding, maintaining the neural stem cell niche, and regulating intercellular communication and morphology (*11*, *85–88*).

Membrane-bound PGs also function as ECM-receptors and, like integrins, PGs detect, integrate and respond to many extracellular cues and exert spatio-temporal control of intra- and extracellular signaling (*44*). Mammals have 13 cell-surface PGs, including 7 transmembrane PGs and 6 glycosylphosphatidylinositol (GPI)-anchored glypicans (*43*). The extracellular ectodomains of these PGs are subject to proteolytic cleavage and subsequent membrane release which serves both extracellular and intracellular functional roles. The syndecan proteins (1-4) contain an extracellular ectodomain, transmembrane domain with a dimerization motif and intracellular C-terminal domain containing a PDZ-binding motif important for cytoskeletal anchoring (*43*). GAG attachments are prominently HS, but sometimes include CS, making syndecans hybrid species. Syndecans regulate cell adhesion, migration and proliferation by binding ECM molecules, largely through HS-interactions, establishing morphogen gradients, and cooperating with other cell-surface receptors. As the name implies, betaglycan/transforming growth factor β (TGFβ) type II receptor has high affinity for TGFβ GFs (*43*). Interestingly, TGFβ induces expression of the BM components collagen IV and HSPG perlecan highlighting bidirectional coordination of matrix-cell signaling (*89*–*91*). Betaglycan is another GAG hybrid containing a single HS and CS. The intracellular domain is contains several Ser/Thr residues subject to protein kinase C (PKC)-mediated phosphorylation, and also contains a PDZ domain that interacts with β-arrestin to stabilize betaglycan at the membrane and potentiate its activity (*43*). CSPG4/NG2 regulates fibroblast growth factor (FGF) ligand and receptor bioavailability and can bind other ECM molecules promoting PI3K-mediated cell survival and migration (*43*). Phosphacan/receptor-type protein tyrosine phosphatase β is a CSPG of particular importance in the nervous system. As a cell adhesion regulator, phosphacan interacts with neural-cell adhesion molecules, tenascin, contactin, and voltage-gated sodium channels to restrict neuronal migration during cortical development and promote neural stem cell self-renewal/ maintenance (*43*, *52*, *92*, *93*). The glypicans (1-6) are lipid-anchored and contain HS GAG chains juxtaposed in close proximity to the membrane. Glypican-dependent intracellular signal transduction is indirect and must be mediated through associated transmembrane receptors since glypicans are not directly connected to any intracellular components. Consequently, glypicans are poised to serve important roles as co-receptors with HS-bound ligands held near their membrane-bound receptors (*94*). Among many functions, the glypicans regulate ligand-receptor interactions, morphogen gradients and ECM-modifying enzymes. As a result, glypicans control a vast number of cell behaviors.

Drosophila contains a single transmembrane Sdc and two glypicans, Dally and Dlp (*11*, *62*, *95*, *96*). These PGs are categorized as exclusive HSPGs and hybrid HSPG/CSPG, respectively, with conserved GAG composition and structural arrangement (*55*, *62*). Perdido/Kon-tiki, is an ECM-associated transmembrane PG

similar to mammalian CSPG4/NG2 (*43*). Perdido/Kon-tiki genetically interacts with integrin receptors and is required for proper muscle development and muscle-tendon attachment. Numerous phenotypes associated with disruption of the HS-biosynthesis pathway highlight the conserved importance of HSPGs in *Drosophila* (*97–99*). Sdc is expressed in *Drosophila* embryonic tissues consistent with analogous mammalian syndecan expression patterns (*62*). Sdc is either a full HSPG or a hybrid PG bearing HS and an additional CS modification (*61*, *62*). The Sdc transmembrane and cytoplasmic protein domains are highly similar to vertebrates and the ectodomain is likewise subject to shedding (*62*). Sdc is required for visual-system assembly and has been predominantly studied in the nervous system. The two fly glypicans contain all 14 conserved cysteine residues and a globular head domain (*95*, *100*, *101*). Dally is analogous to the mammalian glypican 3/5 subfamily and Dlp is an orthologue of the glypican 1/2/4/6 subfamily (*94*). They are implicated in polyamine uptake, tissue patterning, and interact with several signaling pathways. Glypican-mediated signal regulation is highly context-dependent with HS-, core-protein and GPI-domain requirements. The glypicans regulate Wnt, FGF, bone morphogenic protein (BMP), hedgehog (Hh) and TGF-β transport, morphogen gradient formation, and signal transduction strength with spatio-temporal and tissue-specificity (*102–107*). HS chains are required for FGF signaling regulation, but only partially required for Hh, Wnt, and BMP signaling. In eye development, both glypicans regulate extracellular Unpaired (Upd) ligand abundance and Janus kinase/signal transducers and activators of transcription (JAK/STAT) signaling activity in an HS-dependent manner (*105*). The glypicans bind receptors at the membrane, and both Dlp and Sdc interact with the receptor phosphatase leukocyte common antigen-related (dLar) (*108*). Membrane-released Dally expands the range of Hh signaling activity, whilst Dlp transcytosis is necessary to activate full-strength Hh signaling (*109*, *110*). Dlp serves dual functions as both a positive and negative regulator of Wnt signaling dictated by the relative abundance of signaling ligand, receptor and co-receptor (*111*, *112*). These HSPGs, especially Dlp, also have well documented requirements in the context of the nervous system.

Extracellular Matrix Modifying Enzymes

The extracellular space is a highly dynamic environment with many enzymes at work re-modeling the ECM. Secreted and membrane-tethered ECM-regulators involved in remodeling the extracellular space include ECM cross-linkers and PG-modifiers, as well as proteases and their endogenous inhibitors (*23*). Once ECM components are deposited into the matrix they can be further organized and remodeled through additional PTMs such as cross-linking (*7*). For example, collagen is modified by an intricate series of PTMs both within and outside of the cell (*113*). Extracellular enzymatic cross-linking of fibrillar collagen modifies matrix stiffness and

stability. This necessarily changes matrix topology and mechanics which in turn, instruct cell behaviors (*113*). Following secretion and proteolytic procollagen processing, lysyl oxidase (LOX) initiates the covalent cross-linking of collagen fibrils via formation of reactive aldehydes (deamination) from lysine and hydroxylysine residues (*113*). Interestingly, BMP1/ Tolloid-like proteinase cleavage of both procollagen and pro-LOX zymogen are required for fibrillogenesis and activated LOX translocates to the nuclei regulating chromatin remodeling (*113*). Elastin fibril formation is likewise synthesized by these enzymes, providing structural integrity and stability to tissues under high mechanical stress. Peroxidasin mediates the formation of sulfilimine cross-linked collagen IV which is necessary for the sheet-like architecture and integrity of the BM (*114–116*). Transglutaminase-2 (TG2) is a promiscuous, multifunctional enzyme catalyzing covalent cross-linking, transamidation and deamidation of over 100 identified substrates (including itself) in both extracellular and intracellular compartments (*117*). Interestingly, TG2 possesses other enzymatic functions, including kinase activity at the cell surface, as well as non-enzymatic roles as an ECM co-receptor interacting with endostatin, integrins, HSPGs and MMPs (*117*). TG2 is an MMP proteolytic target and TG2 reciprocally regulates several MMPs at the transcriptional level (*117*). Thus, TG2 critically regulates cell adhesion, migration, scaffolding, tissue integrity and signal transduction (*117*).

Attempts to unravel mammalian LOX mechanisms led investigators to the *Drosophila* model which encodes only two LOX genes (dLOX-1 and dLOX-2), with conserved functions and differential spatio-temporal expression patterns (*118*). Indeed, dLOX-2 expression and catalytic activity is restricted to adults while dLOX-1 is the sole LOX functioning in the embryonic, larval and pupal stages (*118*). *Drosophila Lox* activity is still similarly required to regulate matrix stiffness (*118*, *119*). Integrin and dLOX activities are reciprocally regulated forming a positive feedback loop to maintain matrix rigidity necessary for glial cell migration (*119*). Other observed phenotypes in dLOX-1 manipulations include developmental delay and a significant shift in sex ratio attributable to dLOX-1 mediated gene regulation (*118*). Consistent with mammalian peroxidasin, *Drosophila* Peroxidasin (Pxn) catalyzes bromide-dependent sulfilimine cross-linking of collagen IV in the BM (*120*, *121*). Loss of Pxn function results in abnormal BM assembly with diminished tissue integrity caused by weakened Collagen IV scaffolds (*120*, *121*). *Drosophila* contains a single transglutaminase gene (*Tg*, TG) with two alternatively spliced isoforms (TG-A and TG-B) that display cross-linking activity (*122*, *123*). TG is important for morphogenesis, immune processes and intestinal homeostasis (*123*, *124*). TG helps form the fat body matrix via cross-linking chitin-binding proteins (*124*). A recent study provides strong evidence of calcium and exosome-dependent TG-A secretion via a non-canonical ER/Golgi-independent pathway (*123*). Four-jointed (Fj) is a Golgi-resident kinase that phosphorylates secreted cadherins and contains a signal peptidase site.

Though secretion is not essential to Fj function, similarities in its architecture enabled mammalian researchers to identify a family of secreted atypical kinases that phosphorylate several ECM proteins utilized for biomineralization (*125*). Therefore, matrix-enzymes also have important, conserved functions in *Drosophila* and *Drosophila* studies have helped shed light on mammalian functions.

A second group of critically important extracellular enzymes includes the HSPG-modifying sulfatases (Sulfs) and heparanase. Similar to collagen, HSPG biosynthesis and subsequent processive modification is an extremely intricate process involving more than 40 enzymes and giving rise to remarkable GAG complexity (*45*). Each HS chain contains between 20-400 repeating GAG units in which ~40-50% of the GlcNAc residues are first deacetylated and then sulfated (GlcNS), a process that sets the stage for a series of subsequent modifications. Accordingly, one HSPG could potentially contain several thousand sugar codes. With ~10^5-10^6 HSPGs present at the cell surface, these molecules are collectively one of nature's most information-rich biopolymers (*45*). HSPGs are further fine-tuned outside the cell by sulfate-modifying enzymes. The endosulfatases (Sulfs) remove specific sulfates from internal disaccharides in HS-GAGs and heparanase endoglycosidase releases HS from PGs in the extracellular space (*126*, *127*). Heparanase may also facilitate HSPG internalization or engage other cell surface receptors (*126*). Intracellular heparanase is mostly localized within endosomal and lysosomal compartments where it facilitates breakdown of internalized HSPGs (*126*). Modifying sulfation patterns and degrading HS regulate morphogenesis and context-dependent ligand functions via signaling complex and morphogen gradient formation, GF binding affinity, turnover and signal transduction. For example, Sulfs have been shown to promote Wnt signaling, restrict FGF signaling, and bidirectionally regulate BMP ligand-receptor interactions (*128*–*130*). Heparanase co-localizes with BM HSPGs such as Perlecan and HS cleavage reduces matrix cross-linking. Moreover, its activity not only alters PG structure and function but also releases bioactive HS and ligand-bound HS. Although somewhat controversial, endogenous lipases, such as Notum, are reported to release HSPG glypicans from the cell membrane (*131*, *132*). The function of Notum has recently been re-defined as a secreted carboxylesterase, deacylating Wnts to suppress signaling (*133*).

Though the heparanase homolog has not been identified, *Drosophila* contain one Sulf orthologue (*Sulf1*) with conserved enzymatic activity and substrate specificity (*134*–*136*). Sulf1 regulates Wnt, FGF, BMP and Hh signaling pathways in a context-dependent manner. In the wing disc, Sulf1 activity differentially affects Hh signaling in Hh-receiving vs. Hh-producing compartments (*137*). Both human and *Drosophila* Sulfs mediate Wnt-HSPG interactions and regulate Wnt morphogen gradient distribution (*130*, *134*). Moreover, Wnt signaling induces Sulf1 expression thereby stabilizing the Wnt gradient (*134*). However, Wnt-HSPG disruption

promotes Wnt signal transduction in mammals, but inhibits Wnt signaling in flies (*130*). An elegant study showed that both mammalian and *Drosophila* Sulf1 are intrinsically similar and context-specific differences in the fate of released Wnt influence downstream signaling activities (*130*). In vertebrates, HS-released Wnt enables receptor binding promoting intracellular signal transduction while in *Drosophila,* HS-released Wnt is rapidly degraded to reduce signaling (*130*). Notum was originally identified in *Drosophila* as a feedback inhibitor of Wnt/Wingless (Wg) activity that reciprocally regulates Notum expression (*138*). Moreover, structure/function analyses of both human and *Drosophila* Notum show a conserved mechanism in which HSPG glypicans bind Notum in close proximity to Wnt thereby facilitating the removal of a lipid moiety from the Wnt molecule essential for Wnt activity (*133*).

The third group of ECM-modifying enzymes includes a network of extracellular proteases that sits at the nexus of cell-ECM and cell-cell signaling (Fig. 6) (*7*). A protease is any enzyme that hydrolyzes either an internal peptide bond (endopeptidase) or terminal peptide bond (aminopeptidases and carboxypeptidases) in a protein substrate. Extracellular proteases modify signaling circuits and cell function and as such could be considered components of signaling pathways (*139*). Proteolytic activity is critical for development, with aberrant proteolysis underlying numerous disease states. Proteases are classified according to the catalytic residue or ligand used in the active site, and further grouped according to sequence and structural similarities (Fig. 6) (*140*). In humans, >450 proteases make up the cysteine, serine, threonine, aspartic and metallo protease classes. The degradome refers to all protease, protease-substrates, inhibitors and interactors related to the protease proteome (*141–143*). More than half of the degradome is secreted or membrane-anchored, thus ~225 proteases, balanced by numerous endogenous inhibitors, and ~300 extracellular constituents with various spatio-temporal expression and posttranslational modifications, converge to regulate a reciprocal ECM-cell signaling network (*4*, *23*, *139*, *140*). The most abundant proteases are the cysteine, serine, and metalloproteases. Proteolytic processes are interconnected and yield context-dependent protein-protein outputs and cell behaviors. Proteolysis is a special PTM with pleiotropic functional outputs and is necessarily tightly regulated. Regulation of proteases occurs at the level of transcription, translation, secretion, cellular and subcellular localization and turnover. Endogenous protease inhibitors reversibly or irreversibly restrict catalytic activity and most enzymes are produced as latent, inactive zymogens requiring pro-domain removal for activation.

Cysteine proteases are mostly intracellular with the notable exceptions of Cathepsin-B, Cathepsin-L, and Legumain, as well as the aggrecan-degrading, aspartyl-protease Cathepsin-D (*6*, *7*, *140*). In general, cathepsins function optimally in the acidic environment provided by intracellular lysosomal compartments,

but PGs within a local microenvironment might afford favorable conditions for secreted cathepsin activity. Conversely, serine proteases (SPs) prefer a more neutral environment, and numerous secreted or transmembrane SPs function in the ECM with roles in signal transduction, enzyme-activation and ECM degradation (*144*, *145*). Secreted elastase is capable of degrading fibronectin and elastin. A proteolytic cascade involving urokinase- and tissue plasminogen activators (uPA and tPA, respectively) converts plasminogen to plasmin, which then degrades laminin, fibrin and fibronectin. SPs can also activate other proteases such as ADAMTS (a disintegrin and metalloprotease with thrombospondin type I-like motifs) and MMPs. Other secreted SPs include chymotrypsin, trypsin, clotting factors and complement convertases, an important component of the immune system (*144*, *145*). SPs are irreversibly inhibited by endogenous serpins via a "suicide-trap" mechanism that utilizes SP-mediated serpin-cleavage. Members of the metalloprotease family are found in all kingdoms of life (*146*, *147*). Extracellular metzincin metalloproteases are master regulators of the extracellular space and intercellular signaling, orchestrating tissue growth, adhesion, remodeling and mediating cellular responses to extracellular cues (*141*, *148*, *149*). Numerous described roles include ECM degradation, molecular processing, cell-ECM and cell-cell signaling, cell adhesion, migration, and proliferation (*7*, *148*, *150*, *151*). Of particular note are the astacins, adamlysins (ADAM and ADAMTS) and matrixins (MMPs) (*7*, *151*). The astacins, including meprins and BMP-1/tolloid proteases, are involved in tissue morphogenesis, differentiation and matrix degradation (*152*). BMP-1/tolloid proteases do not degrade ECM, but rather process precursors and activate matrix molecules such as collagen, laminin, TGF-β, matricryptins and select PGs to regulate ECM assembly, maturation and mechanics (*7*, *152*, *153*). These zymogens (catalytically inactive enzymes) are activated by substrate-specific activators, or ADAMTS, and inhibited by the general scavenger α2-macroglobulin (*154*). The meprins, secreted and transmembrane, promote pro-MMP-9 activation and cleave ECM molecules such as collagen IV, nidogen and fibronectin. Meprins are inhibited by endogenous mannan-binding lectin and the transmembrane meprin is shed by ADAM-10 (*152*). The transmembrane adamlysins, ADAMs, are involved in ectodomain shedding, GF ligand and receptor processing, cell adhesion, differentiation, cell migration, and regulated intramembrane proteolysis (*150*, *155*). ADAMs contain a disintegrin domain mediating adhesion and cell-matrix interactions via integrin binding (*156*). The cysteine-rich domain promotes adhesion, binds fibronectin, and serves as a ligand for Sdc (*155*, *156*). The cytoplasmic domain serves various regulatory roles, adaptor functions, and signal transduction purposes (*155*). Pro-ADAM cleavage and activation occurs intracellularly and the released pro-domain can inhibit ADAM-9, 10 and 17 (*7*, *155*). ADAM and ADAMTS inhibition is mediated by TIMPs (tissue inhibitor of metalloproteases), RECK (reversion-inducing cysteine-rich protein domain with kazal motifs), and the general scavenger α2-

macroglobulin (*155*, *157*, *158*). Secreted ADAMTS proteases degrade ECM components and PGs, activate pro-proteinases, and regulate cell-matrix interactions (*150*, *151*, *155*). ADAMTS domain structure and composition follows that of the ADAMs but lacks transmembrane and cytoplasmic domains and instead contains thrombospondin type 1-like repeats (*147*, *155*, *159*, *160*). The matrixin/MMP group is discussed in more detail below.

Drosophila contains proteases from each of these catalytic groups. The cathepsins largely function within lysosomes, and are important for cuticular, exoskeletal molting and tissue remodeling during development. Similar to certain mammalian cathepsins, aspartic protease Cathepsin-D is secreted extracellularly and found in the haemolymph (*161*). SPs and SP-homologous proteases consist of 193 putative members, but with only ~12% characterized (FlyBase). Similar to mammals, many of these members are putative digestive enzymes; however, extracellular SP signaling requirements include roles in tissue patterning, immune response and wound healing (*162*, *163*). The type II transmembrane SP Stubble-stubbloid is required for epithelial tissue morphogenesis, with protease activity necessary for imaginal disc detachment and the intracellular domain coordinating signal transduction via cytoskeletal changes (*164*, *165*). Nudel, Gastrulation-defective, Snake and Easter SPs are part of a signaling cascade that activates Spatzle ligand and subsequent Toll signaling to establish dorsal-ventral patterning during embryogenesis (*163*, *166*). Thus, similar to mammals, *Drosophila* SPs function in proteolytic signaling cascades, latent protease activation and ECM breakdown, and are inhibited by endogenous Serpins (*162*, *167*). The *Drosophila* genome contains ~13-16 astacin family genes which remain largely uncharacterized, with the exception of seminal metalloprotease-1, Tolloid (Tld) and Tolkin (Tok) (*152*). Tld and Tok are members of the BMP1/tolloid-like family required for TGF-β-mediated dorsal-ventral axis determination during embryogenesis via interactions with the TGF-β (Dpp) inhibitor Short gastrulation (Sog) (*168*–*173*). Tld and Tok promote BMP diffusion and establish morphogen gradients in imaginal discs important for adult tissue morphogenesis. Tok also functions as a Procollagen C-endopeptidase. *Drosophila* has 12 adamlysins: 5 ADAMs and 7 ADAMTS family members. Like their mammalian counterparts, *Drosophila* ADAMs are sheddases and regulate tissue morphogenesis, cell fate and differentiation, and signaling pathways such as EGF and Notch (*37*, *174*, *175*). Kuzbanian (Kuz) and Kuzbanian-like (Kul) are similar to ADAM10, Meltrin/Neu3 is similar to ADAM12 and ADAM19 (*176*), Mind-meld (Mmd) is similar to ADAM11, and TACE (TNF-α converting enzyme) is similar to ADAM17/TACE (*177*). The *Drosophila* ADAMTS members are required for tissue morphogenesis and Wnt signaling, with particularly important roles in neural development. ADAMTS members include catalytically-inactive Lonely heart (Loh) (*38*) and No-long nerve chord (Nolo), and catalytically active Papilin (Ppn) (*178*, *179*), AdamTSA, Stall (Stl), Solo narae (Sona aka

Dimp), and uncharacterized CG4096 (FlyBase). As MMPs are central to this thesis work they will be discussed in further detail below.

The *Drosophila* Neuromuscular Junction as a Genetic Model Synapse

ECM mechanisms play important roles in nervous system development, maintenance, regeneration and disease (*11*, *73*, *180*, *181*), with key requirements at synaptic contact sites between presynaptic and postsynaptic partner cells. The *Drosophila* larval neuromuscular junction (NMJ) has long been a ground-breaking model synapse in which to study structural and functional neurodevelopment (*11*, *182*, *183*), providing insights into ECM-mediated signaling functions. Neuromuscular synaptogenesis requires the formation of an intercellular communicating junction between presynaptic motorneuron and postsynaptic target muscle which are separated by a specialized matrix (the "synaptomatrix") (*14*, *184*). This highly coordinated process is driven by a number of anterograde, retrograde and bi-directional *trans*-synaptic signaling molecules that necessarily traverse the heavily-glycosylated synaptomatrix in the ~20 nm extracellular synaptic cleft without a BM (*14*, *15*, *185*). Similar to primary excitatory synapses in the mammalian CNS, the *Drosophila* NMJ uses glutamate as the neurotransmitter, transducing this signal via juxtaposed ionotropic glutamate receptors (GluRs) contained within postsynaptic scaffolds, resembling mammalian postsynaptic densities (PSD) (*186*–*188*). In contrast, the vertebrate NMJ uses acetylcholine as the neurotransmitter across a much wider (~50-70 nm) cleft with a continuous BM (*188*). However, like vertebrate NMJs, the *Drosophila* NMJ contains elaborate postsynaptic membrane folds forming a subsynaptic reticulum (SSR) opening to synaptic clefts (*186*, *188*). Although *Drosophila* terminals lack BM, the muscle surface is covered by BM and BM integrity is important for neuromuscular adhesion (*19*, *34*). Many vertebrate ECM molecules, signaling pathways and synaptic machinery components are evolutionarily conserved at the *Drosophila* NMJ, with less functional redundancy, and numerous human neurological diseases have been effectively modeled using this synaptic system (*11*, *189*–*192*).

The NMJ System

The *Drosophila* neuromuscular system is mapped, displays stereotypical connectivity, is amenable to genetic manipulation, is easy to visualize, and is well suited for both electrophysiology and functional imaging. Each *Drosophila* abdominal hemisegment contains 36 motorneurons derived from 10 defined neuroblasts, and 30 muscles derived from 30 founder cells via myoblast fusion (Fig. 2) (*193*, *194*). In a highly stereotypical

fashion, axonal projections emanate from motorneuron (MN) soma located in the ventral nerve chord (VNC), fasciculate to form nerves, defasciculate at determined branch points, and synapse onto specific target muscle fibers in the periphery (Fig. 2) (*183*, *184*, *195*, *196*). By the end of embryogenesis, functional NMJs have formed, each consisting of a defined number of synaptic varicosities (boutons) housing presynaptic transmitter release machinery juxtaposed to postsynaptic receptor fields (*183*, *184*, *197*, *198*). Neurotransmitter release site active zones (AZs) contain electron-dense "T-bars" organizing docked synaptic vesicles (SVs), and localized voltage-gated calcium channels (Fig. 3) (*199*–*205*). Each bouton contains multiple spatially segregated AZs. Throughout the three larval instar growth stages, NMJs expand as synaptic boutons are added and AZ density increases, scaling consistently with the ~100-fold increase in muscle surface area. Thus, the larval NMJs display structural and functional matching defined as "synaptic homeostasis" (*182*, *206*). The NMJ is also highly dynamic and displays use-dependent structural growth and functional strengthening induced by higher motor activity or increased neural function ("activity-dependent plasticity") (*207*, *208*). Although structural and functional synaptogenesis are intimately linked, the mechanisms controlling these developmental processes are distinct and can be genetically uncoupled, indicating differential pathway regulation. Previous studies, in conjunction with work here, support the idea that NMJ development is regulated by dynamic interplay of multiple signaling pathways rather than through independent pathways (*209*). Importantly, ECM-receptors, cell adhesion molecules (CAMs), and HSPGs are potent regulators of synapse organization (*11*, *14*).

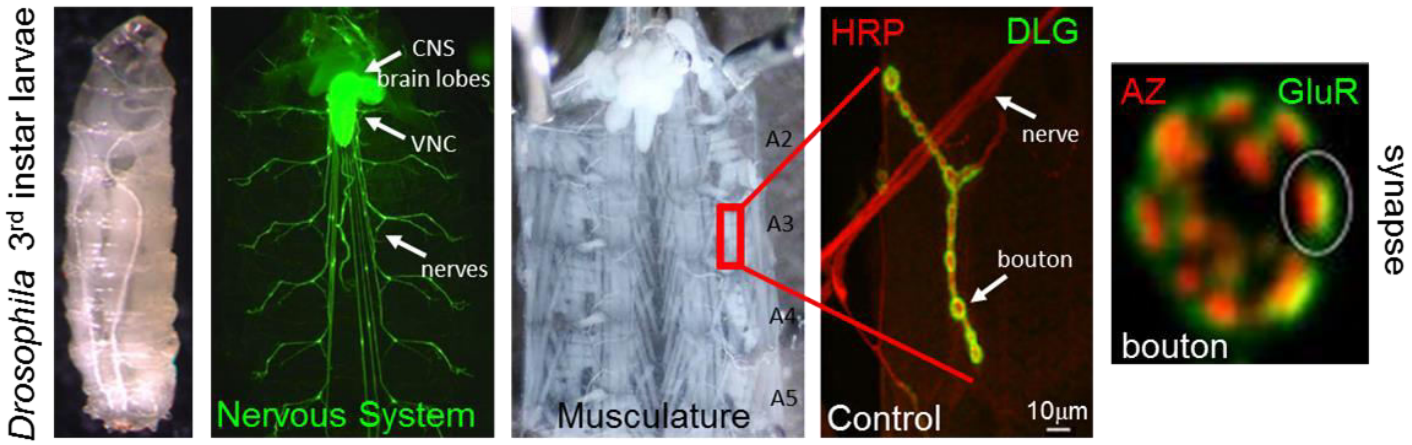

Figure 2

Figure 2: The *Drosophila* larval NMJ model synapse. (Left to right; anterior up in all images): Dorsal view of a *Drosophila* larva at the wandering 3rd instar stage. Fluorescent confocal image of the larval nervous system shown with *elav*-GAL4>UAS-mCD8::GFP (green). DIC (differential interference contrast) phase contrast image shows the repeating segmentation of unlabeled larval musculature from segments A2-A5. The red box outlines muscle 4 of segment A3. Confocal image of the NMJ innervation on muscle 4 from segment A3 shows the nerve bundle, defasciculating motoneuron axon (red, HRP) and postsynaptic density (green, anti-Discs large (DLG)). Note that a single NMJ is comprised of multiple boutons. Far right: confocal image of a single bouton showing presynaptic active zones (AZs as labeled by Bruchpilot (Brp), red) juxtaposed to postsynaptic glutamate receptor fields (GluR, green). A bouton is comprised of multiple spaced synapses (circled).

Structural Synaptogenesis

NMJ synaptic varicosity boutons connected by axonal processes resemble pearls on a string. Boutons are divided into three classes (type I, II, III) grouped by morphology, neurotransmitter type and degree of SSR elaboration (*195*, *199*). Each motorneuron arbor is comprised of only a single bouton type, but more than one motorneuron might innervate a specific NMJ or muscle at a distinct location. Type I boutons are glutamatergic, and are further broken down into the smaller Type Is and larger Type Ib classes, which are readily distinguishable based on the large bouton size and more extensive SSR in the Type Ib class (*195*). My work focuses on Type Ib NMJs formed on the dorsolateral longitudinal internal muscle 4, which contain Type I and II innervation, and the ventral internal longitudinal muscles 6/7 (*195*). NMJ expansion is via increases in branching and bouton number/size throughout the larval instar stages, with the most growth occurring in the 3rd instar stage (*210*). In the wandering 3rd instar stage (W3), immediately prior to pupation, different NMJ arbors display morphologically distinct branching patterns and a fairly stereotypical number of boutons (*182*, *195*). As such, NMJ area, branching, bouton number/size and clustering are all easily visualized and readily quantifiable; therefore, these parameters are commonly used as a direct readout for structural synaptogenesis. The Horse Radish Peroxidase (HRP) antibody recognizes an epitope produced by a neural-specific fucose modification present on membrane glycoproteins (*211*). Thus, HRP labeling is commonly used in imaging and structural studies to specifically visualize the presynaptic motorneuron membrane at the NMJ (*212*). NMJ expansion and synaptic growth via new bouton addition is achieved by *de novo* bouton formation from the axon, asymmetric budding or symmetric division of a pre-existing bouton (*210*). Other presynaptic structures observed during normal development include dynamic and transient filopodial-like protrusions called synaptopods, shed axonal membrane debris, immature ghost boutons, and developmentally-transient satellite boutons. Neural activity increases membrane shedding/debris and induces initial ghost bouton formation, which are either stabilized to form a differentiated, fully mature functional bouton or eliminated (*213*, *214*). Satellite boutons are small functional varicosities budding from a parent terminal bouton, and in some cases budding is observed from the axon in between two existing boutons (*210*). At wildtype NMJs, satellites form transiently and normal-sized parent terminal boutons only contain ~1-2 satellite buds at any given time. Excessive satellite bouton formation is commonly observed at overgrown mutant NMJs (*215*). Ghost boutons are likewise observed at low frequency, and are defined by the absence of postsynaptic machinery (*214*, *216*). The rare ghost bouton observed under normal conditions could either represent a new bouton that has yet to establish a postsynaptic compartment or a retracting bouton which has recently lost its postsynaptic machinery. Conversely, presynaptic retractions with intact postsynaptic densities that have yet to

be dismantled are called “footprints” and are also rarely observed (*217*). Overall, proper structural development requires a collaborative effort between both neuron and muscle with multiple processes regulating bouton formation, differentiation and maintenance.

Functional Synaptogenesis

Drosophila motoneurons express glutamate as an excitatory neurotransmitter released from SVs at AZs (*195*). Postsynaptic SSR elaborates only during the larval stages and houses glutamate receptors (GluRs) and voltage-gated ion channels necessary for neurotransmission. Apposition of presynaptic AZs and postsynaptic GluR clusters is critical for efficient glutamatergic signaling (Fig. 3) (*205*). Numerous scaffolding proteins organize and maintain the aforementioned pre- and postsynaptic functional machinery (*218*). The presynaptic scaffolding protein Bruchpilot (Brp) tethers SVs and calcium channels at AZs and Brp is critical for AZ integrity and neurotransmission (*200*, *205*). GluR function, mobility and clustering are modulated by postsynaptic scaffolds and auxiliary subunits (*86*, *222–227*). Discs large (DLG) is an important postsynaptic scaffold regulating GluR localization and SSR maturation (Fig. 2). Specifically, muscle cells contain ionotropic, non-NMDA-type GluR-tetrameric clusters with obligate GluRIIC/III, GluRIID and GluRIIE subunits, coupled to either a GlurIIA (A-type) or GluRIIB (B-type) subunit as the fourth component (*187*, *204*, *219–221*). Neurotransmission strength, synaptic plasticity, homeostatic properties and postsynaptic GluR composition are all tightly co-regulated (*221*, *228–232*). A-type and B-type receptors have different temporal expression patterns, channel kinetics, distinct functional properties and are independently regulated (*221*, *230*, *233*). A-type GluRs are enriched in newly formed postsynaptic sites and slowly desensitize (*228*, *230*). Reduced neurotransmission results in a compensatory increase in A-type GluRs (*228*, *231*). Functional neurotransmission can be measured via two-electrode voltage-clam (TEVC) electrophysiological recordings of the muscle response to SV release in either the presence (evoked) or absence (spontaneous) of an action potential (*183*). Since both pre- and postsynaptic machinery contribute to neurotransmission when measuring evoked excitatory junctional current or potential amplitudes (EJC or EJP), cell-type specific contributions are distinguished by measuring the parameters of spontaneous fusion. On the postsynaptic side, spontaneous/miniature EJC (mEJC) amplitude is thought to largely reflect postsynaptic GluR responsiveness to glutamate released from a single synaptic vesicle (*221*). A-type GluR properties are largely responsible for observed mEJC amplitudes (*221*). On the presynaptic side, the frequency of mEJC events reflects SV density or fusion probability with increased SV density/fusion rates yielding higher spontaneous release (*221*, *234*). Quantal content reflects how many SVs are released in response to evoked neurotransmission. Coordinated

structural and functional development is driven by anterograde, retrograde and bi-directional *trans*-synaptic signaling regulated by/in the extracellular space (Fig. 4). Wnt Wingless (Wg) signaling is of particular importance in both synaptogenesis and neurological disease states.

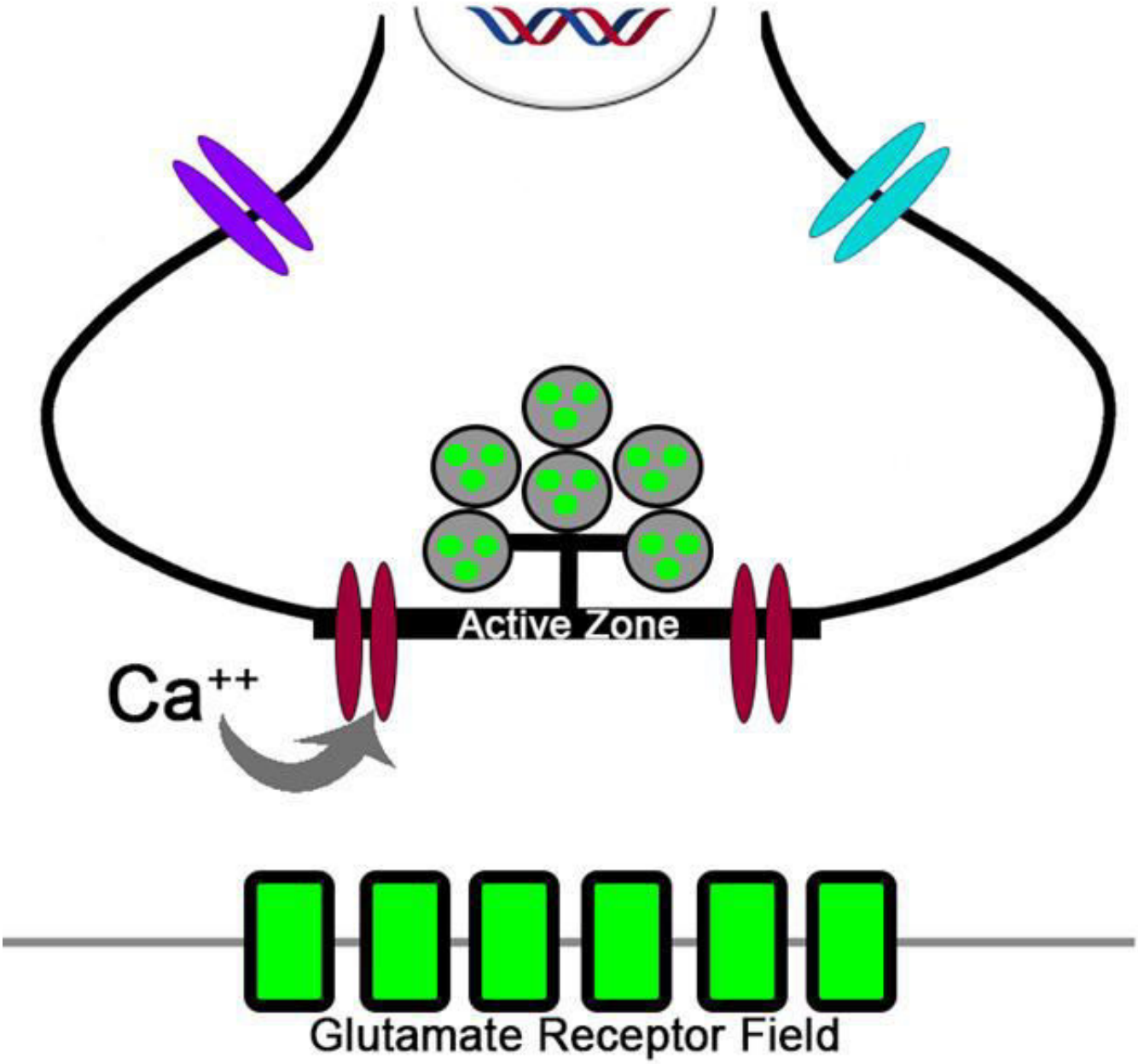

Figure 3

Figure 3: Cartoon schematic of a synapse at the *Drosophila* NMJ. The presynaptic active zone (AZ) is defined by an electron-dense T-bar (black) with docked glutamate-filled (green circles) synaptic vesicles (SV, grey) and localized voltage-gated calcium channels (maroon). On the postsynaptic side, glutamate receptor fields (green rectangles) cluster opposite the presynaptic AZs.

Wnt *Trans*-synaptic Signaling

Wingless-related integration site (Wnt) ligands are a family of secreted Cys-rich glycoproteins with well described roles as potent morphogens instructing many developmental processes (*235*, *236*). Several Wnt-receptors and co-receptors have been identified, including the Frizzled (Fz) receptors, low density lipoprotein-receptor-related protein (LRP) receptors, receptor tyrosine kinase (RTK) family members, and HSPG co-receptors (*111*, *237–239*). Canonical Wnt signaling results in β-catenin stabilization and subsequent transcriptional activation of target genes that modulate cell behavior and development in various tissues with differential Wnt-responsiveness (*238*). However, Wnts also stimulate several non-canonical signal transduction pathways which provide a variety of biological outcomes (*240*). Many of the Wnt-activated signaling pathways directing embryonic develop are re-purposed in essential processes during later developmental stages (*241*, *242*). Wnts are evolutionarily conserved and critically regulate several aspects of neural development in both vertebrates and invertebrates (*239*, *243*). Importantly, *trans*-synaptic Wnt signaling potently regulates structural and functional neuromuscular synaptogenesis and activity-dependent plasticity (Fig. 4) (*214*, *216*). Misregulated Wnt signaling underlies numerous disease state spanning from cancers to developmental neurological disorders and neurodegeneration (*244–247*). In mammals, the complexity of Wnt-signaling from 19 Wnts creates considerable challenges. In contrast, *Drosophila* has 7 Wnts, 5 Fz receptors and conserved modes of signal transduction, with a Nobel prize awarded for identifying Wnt-pathway components and mechanisms (*237*, *248*, *249*). Of particular relevance to this thesis, Wnt ligand and receptor expression are spatially restricted and temporally controlled, and signaling is further regulated by a range of extracellular Wnt modifiers (*237*, *250*, *251*).

Drosophila Wnt family members include the founding Wingless (Wnt1/Wg), Wnt2, Wnt3/5, Wnt4, Wnt6, Wnt10 and Wnt inhibitor of Dorsal (WntD/Wnt8) (*248*). To date only Wg, Wnt2 and Wnt3/5 have reported roles in neuromuscular synaptogenesis (Fig. 33). Anterograde Wnt5 signaling through Derailed is required for coordinated structural growth to keep pace with larval development. Autocrine Wnt5 activates an unknown mechanism regulating functional synaptogenesis (*252*). Retrograde Wnt2 signaling activates an unidentified pathway(s) required during early larval development to restrict branching and bouton growth, promote neurotransmission, and is later required in the 3rd instar stage to promote presynaptic molecular assembly (*253*). Biochemical studies show Wnt2 binds Fz, Fz2 and Fz3 with a similar binding affinity as Wg (*237*). During an attempt to identify the Wnt2 receptor(s) in these mechanisms it was discovered that Fz3 functions at the NMJ to restrict branching; however, the corresponding Wnt ligand remains elusive (*253*). Wg was first discovered in 1973 and is by far the most commonly studied Wnt in *Drosophila* with over 1,500 Wg-

publications compared to >150 for all other Wnt family members (FlyBase). A role for Wg in cell-cell communication was first hypothesized in 1989 in a study that revealed Wg is localized to both intra- and extracellular compartments and that extracellular Wg is present in the intercellular space (*254*). Wg receptors include Fz, Fz2 and Fz3 which transduce Wg activity via canonical and several non-canonical signaling pathways (*237*). Wg signaling restricts Fz2 expression and promotes Fz3 expression which in turn attenuates "low" Wg activity. Several secreted molecules including the Notum deacylase and ECM LanA are regulated by Wg activity, and in turn regulate Wg signaling (*68*, *138*). Wg signaling is implicated is a wide range of neurodevelopmental processes, and has well described functions at the NMJ where it is necessary for both pre- and postsynaptic structural and functional differentiation (*216*).

Components of the canonical Wnt pathway including Wg, Fz2, LRP/Arrow (Arr) and GSK-3β/Shaggy (Sgg) are all present at Type Ib NMJs, with the striking exception of β-catenin/ Armadillo (Arm) (*216*, *255*). The lack of Arm, in conjunction with rigorous genetic tests, indicates that Wg activates only non-canonical signaling pathways at the NMJ. Wg is expressed throughout larval NMJ development, Wg activity requires Porcupine-dependent lipidation and Dynamin/Shibire, and Wg transport and subsequent exosome release requires the type II transmembrane protein Evenness Interrupted/Wntless/Sprinter (Evi/Wls/Srt) (*216*, *256*). Wg is secreted from the presynaptic motoneuron and associated glia (*216*, *257*), and endocytosed by Fz2 receptors on both pre- and postsynaptic membranes (*216*). Restricting Wg loss to just the 3rd instar stage using a conditional temperature-sensitive (ts) wg^{ts} allele causes significant defects in NMJ growth with reduced bouton numbers and boutons formed that are either larger or badly misshapen. Muscle size is normal in these animals, suggesting defects are caused by uncoordinated synaptic growth. Interestingly, mutant animals retain microtubule features associated with dynamic growth even though structural expansion is halted (*216*). On the postsynaptic side, DLG expression is reduced and A-type GluRs are not clustered appropriately. Ultrastructural analysis of wg^{ts} mutants reveals a mixture of deficits: 1) terminal boutons are completely filled with SVs with reduced AZ T-bars and mitochondria, and 2) non-terminal boutons display misshapen AZ T-bars and enlarged postsynaptic pockets with pre- and postsynaptic membranes visibly detached and reduced SSR (*216*). Moreover, in some cases Fz2 overexpression phenocopies *wg* LOF, suggesting Wg-Fz2 positional cues are diluted; however, other studies report Fz2 overexpression reciprocally enhances NMJ growth (*216*, *258*).

On the postsynaptic side, anterograde Wg activity is transduced via a non-canonical Frizzled nuclear import pathway (FNI) to the muscle (Fig. 5) (*259*, *260*). Wg secreted from the neuron binds Fz2 receptor on the muscle surface triggering complex internalization (t< 5 minutes), the Fz2-C terminus is cleaved, and Evi-regulated, glutamate receptor interacting protein (dGRIP) drives Fz2-C trafficking to the muscle nuclei (t< 60

minutes) via a retrograde transport mechanism (*259*, *261*). Fz2-C terminus cleavage is necessary for Importin-dependent Fz2-C terminus import into postsynaptic nuclei where the C-terminal fragment localizes near transcriptionally active DNA (*259*, *260*). Presynaptic distal boutons and postsynaptic muscles contain dGRIP vesicles associated with the cytoskeleton and dGRIP promotes bouton growth in both cells; however, only postsynaptic dGRIP knockdown causes increased ghost bouton formation (*261*). Conversely, Evi functions in both cells to promote NMJ growth and restrict ghost bouton formation (*256*). Despite some overlap observed in cell-type requirements and sufficiency tests, postsynaptic FNI seems to be less important for Wg-dependent synaptic structural growth and more critical for postsynaptic differentiation and ghost bouton formation (*260*). Nuclear Fz2-C associates with ribonucleoprotein particles (RNPs) containing mRNA transcripts encoding postsynaptic proteins and together this complex shuttles from the nucleus to cytoplasm, presumably facilitating local protein synthesis in the muscle (*262*). RNP nuclear exit occurs via nuclear envelope (NE) budding regulated by atypical PKC-dependent phosphorylation of Lamin C (LamC) (*262*). Fz2-C containing RNPs localize with Pumilio and Bazooka/Par-3 proteins and a candidate approach to identify Fz2C-RNP-associated mRNA revealed 6 transcripts: *dcask*, *tkv*, *par-6*, *dpak*, *camkII*, and *magi* (*262*). Accordingly, loss of *LamC* results in NMJs that contain a reduced number of differentiated boutons, increased ghost bouton formation, increased mEJP frequency and amplitude, and increased A-type GluR volume and intensity, similar to phenotypes observed in Fz2 LOF and postsynaptic GOF conditions (*262*).

Autocrine Wg signaling via Fz2 involves LRP/Arrow, Dishevelled (Dsh) and GSK-3β/ Sgg and activates a transcription-independent, divergent canonical pathway (*255*). Sgg is enriched on the presynaptic side and is required in motorneurons to restrict NMJ expansion of synaptic bouton number and satellite formation via phosphorylation regulation of Futsch-dependent microtubule cytoskeleton dynamics (*255*, *263*, *264*). Functionally, both *sgg* LOF and Sgg overexpression display reduced neurotransmission strength, and Sgg restricts JNK-mediated AP-1 upregulation of transcriptional targets controlling synaptic structure and function (*263*). Loss of LRP/Arrow function at the NMJ causes reduced bouton numbers with larger areas and reduced microtubule Futsch loops (*255*). All phenotypes except for Futsch loops can be rescued by either pre- or postsynaptic Arrow re-expression, and proper Futsch loop formation similarly requires presynaptic Sgg and Dsh activities (*255*). No defects are observed following muscle knockdown of Dsh, suggesting Dsh is required in the motorneuron (*255*). Postsynaptic knockdown of the canonical Wg-responsive transcriptional regulator TCF/Pangolin causes gross defects in muscle morphology, but does not phenocopy *wg* LOF (*255*). In parallel, Fz2 physically interacts with the heterotrimeric Go protein to transduce Wg-Fz2 signaling via Sgg inhibition and local recruitment of Ankyrin, a membrane-cytoskeleton linker (*258*). Despite all this integration being

attributed to Wg ligand signaling, genetic interaction experiments have not yet been performed to fully interrogate the potential role of other Wnt ligands or receptors in these mechanisms. Moreover, contradictory reports of pre- and postsynaptic requirements and corresponding phenotypes make interpretations challenging.

Wg is also secreted from subperineurial glia in the periphery under the transcriptional control of Repo (*257*). Wg activity in this context also requires Porcupine-dependent Wg-lipidation for secretion and function (*257*). LOF and targeted RNAi studies show that glia-derived Wg regulates postsynaptic GluRIIA density with no observable difference in differentiated bouton number at the NMJ (*257*). Moreover, both neuronal- and glia-*Wg* knockdown result in functional defects including reduced neurotransmission, increased mEJP amplitude and reduced quantal content (*257*). However, Wg knockdown in glia, but not in neurons, shows a glia-specific requirement for Wg in restricting mEJP frequency (*257*). Nevertheless, both neuronal and glial Wg activities are clearly necessary for functional synaptogenesis, presumably signaling via the postsynaptic FNI pathway. The glia-specific homeodomain protein, Repo, further regulates the expression of several other Wnt pathway components including Fz, Pangolin, Slmb, Sgg, Arr, Drl and Wnt4, but potential requirements of these molecules in glia-mediated synaptogenesis have not yet been explored (*257*).

Bidirectional Wg signaling is required for use-dependent NMJ expansion (plasticity) that is independent from the NMJ expansion needed to match developmental growth (*214*). Acute increases in neural activity lead to structural and functional changes at the NMJ which include the formation of new undifferentiated boutons (ghost boutons), increased synaptopod dynamics, increased mEJP amplitude (Wg-independent), and increased mEJP frequency that remains potentiated for ~2-3 hours (*214*). Conversely, there are no observable changes in evoked EJP amplitude or quantal content following induced activity stimulation. Activity promotes Wg secretion and postsynaptic enrichment as well as enhancing FNI (*214*). Newly formed, undifferentiated ghost boutons form from existing presynaptic sites containing some AZs, synapsin and the SV-localized chaperone Cysteine String Protein (CSP) but completely lacking postsynaptic specializations. Activity-induced ghost boutons eventually acquire all the pre- and postsynaptic machinery that is necessary to form functional connections (*214*, *265*). Ghost bouton formation following spaced depolarization requires calcium, transcription, translation, presynaptic action potentials, Wg secretion, actin cytoskeleton rearrangement via Cortactin activation and Sgg inhibition (*214*). Ghost bouton formation induced using other activity paradigms have mixed requirements. Increased ghost bouton numbers observed in *importin* mutants are suppressed by either re-expression of postsynaptic Importin or Fz2 conjugated to a nuclear import signal, suggesting that FNI is indeed an important regulator of this process (*260*). Experiments assaying plasticity following spaced activity

in *wg* LOF or Sgg overexpression conditions show that removal of presynaptic Wg function negates ghost bouton formation and causes reduced mEJP frequency with a significant reduction in mEJP frequency potentiation (*214*). This is in stark contrast to the baseline increase in ghost bouton number reported for numerous conditions that perturb Wnt pathway signaling including Fz2 LOF and GOF, dGRIP LOF, Evi LOF, Wg LOF, Importin LOF, LamC LOF, aPKC LOF, Bazooka LOF and PKM LOF (*216*, *256*, *257*, *259*, *261*). Conversely, assaying plasticity following spaced activity in Wg overexpression, Sgg inhibition, or hyperexcitable conditions show that increasing Wg activity potentiates ghost bouton formation and mEJP frequency, partially by-passing the activity requirement to induce new bouton formation (*214*). This is also in stark contrast to the baseline decrease in ghost bouton number reported for conditions that enhance Wnt pathway signaling or chronic activity including Wg overexpression and eag^{1}, sh^{KS133} mutants (*214*). Therefore, both Wg LOF and GOF conditions as well as hyper- and hypoexcitable mutants display separable alterations in developmental and activity-dependent NMJ formation.

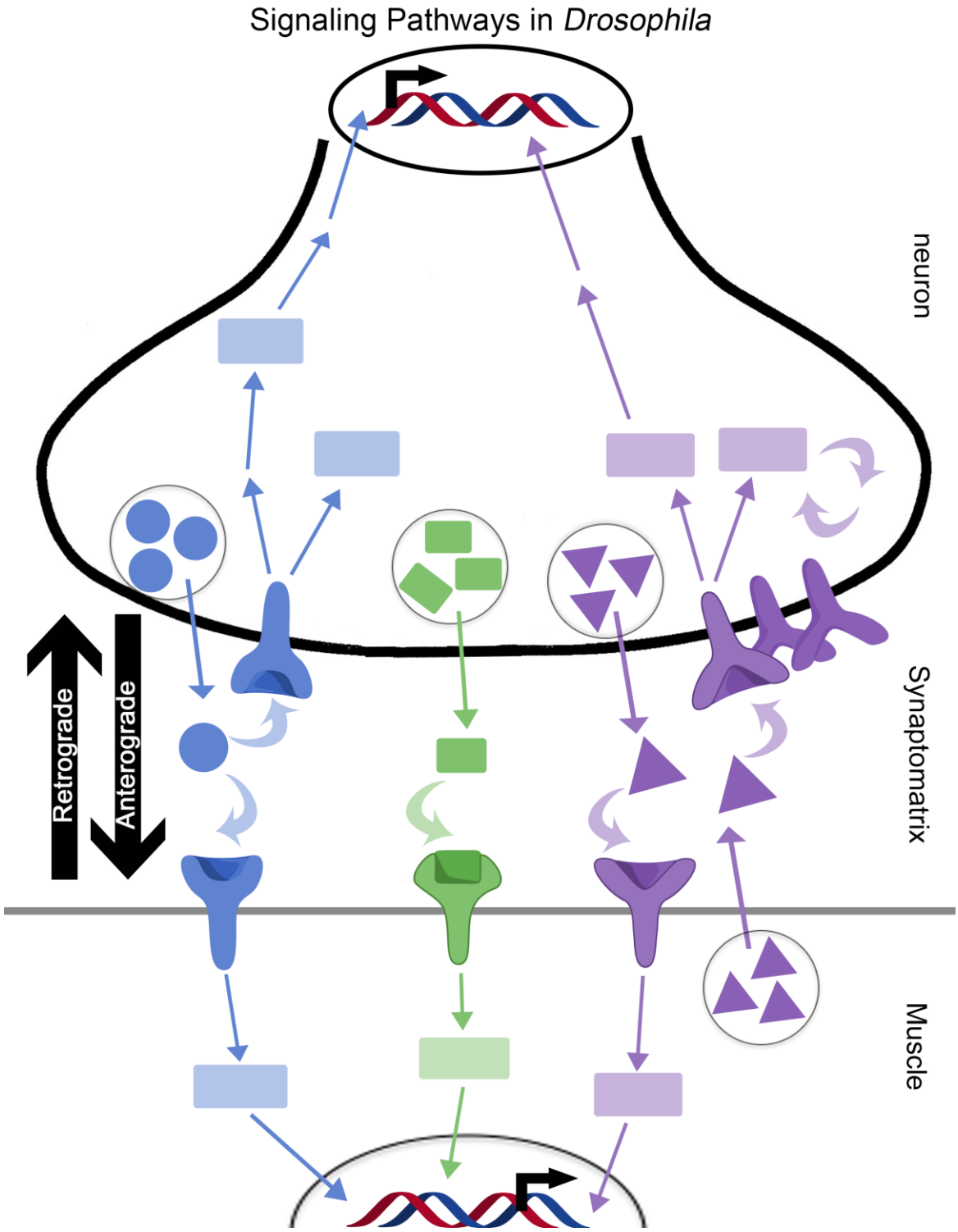

Figure 4

Figure 4: *Trans*-synaptic signaling pathways driving NMJ synaptogenesis. A variety of anterograde (neuron to muscle), retrograde (muscle to neuron), autocrine, and bi-directional signaling pathways interface with the synaptomatrix and drive structural and function development. Shapes within circles denote ligands, receptors are localized to cell surfaces, boxes represent protein components that transduce intracellular signaling and many pathways culminate in the nucleus to regulate gene transcription of pathway-responsive target genes. Specifically, Wnt Wingless (Wg) signaling pathways are shown in blue, BMP Glass bottom boat (Gbb) signaling pathways are shown in purple and Jelly belly (Jeb) to Anaplastic lymphoma kinase (Alk) signaling pathway is shown in green.

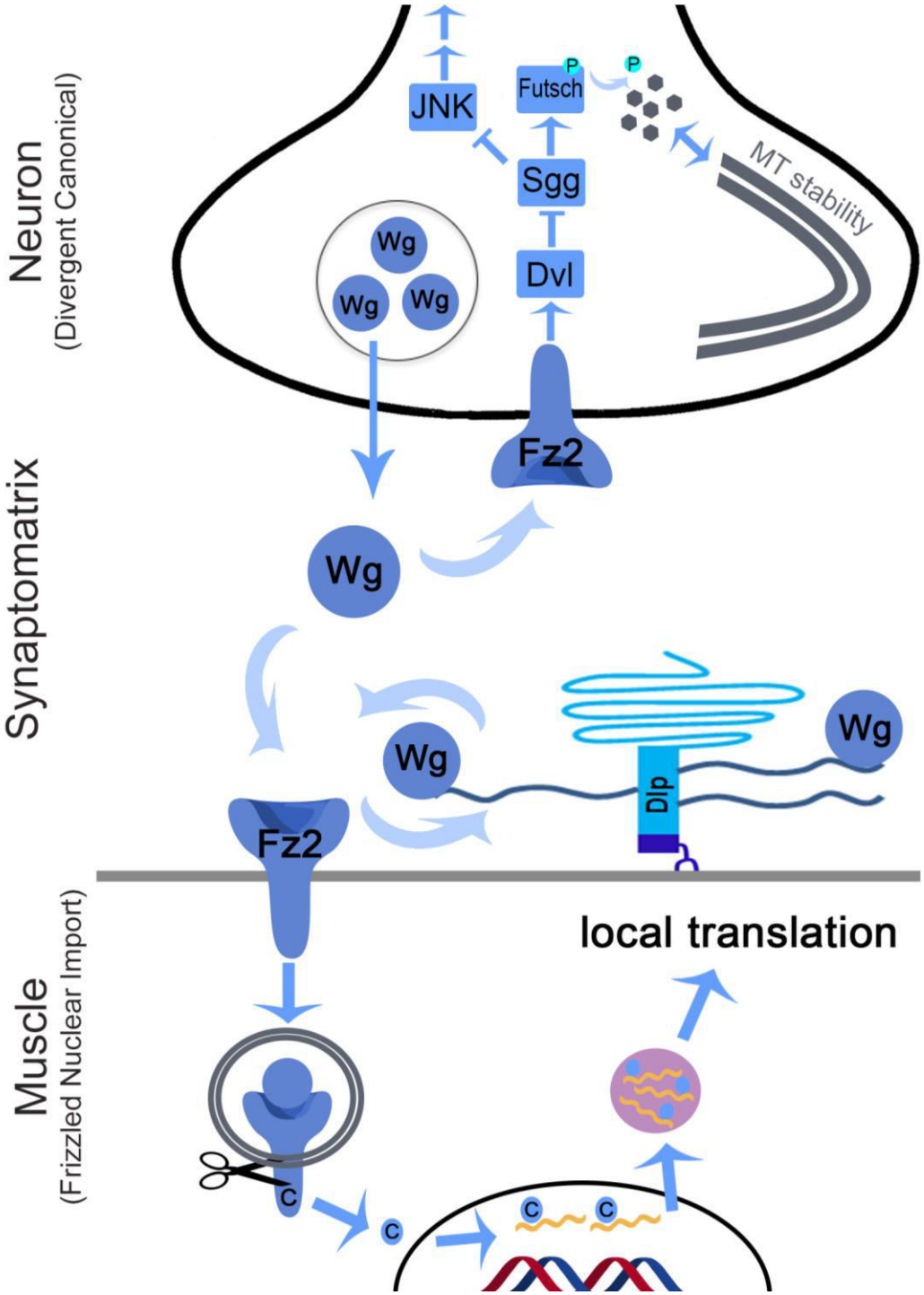

Figure 5

Figure 5: Cartoon schematic of the pre- and postsynaptic Wg-activated pathways at the NMJ. See text for complete details. In brief, Wnt/Wg signaling drives NMJ growth and synapse assembly via the HSPG co-receptor Dlp and Frizzled-2 (Fz2) cognate receptor. In the presynaptic divergent canonical pathway, autocrine Wg signaling functions through Dishevelled (Dvl), Glycogen synthetase kinase/Shaggy (Sgg), and MAP1b/Futsch to regulate microtubule stability. Sgg is a central node intersecting with many signaling pathways, such as JNK signaling. In the postsynaptic, anterograde Frizzled nuclear import (FNI) pathway, Fz2 is endocytosed following Wg activation, cleaved, transported into the muscle nuclei, where it associates with ribonucleoprotein (RNP) granules containing postsynaptic target transcripts and thereby drives local expression changes modulating synaptogenesis. According to the "Wg-exchange-factor model" Dlp functions as both a positive and negative regulator of Wg signaling. In this mechanism, a low Dlp:Frz2 ratio helps the Frz2 receptor obtain more Wg, whereas a high Dlp:Frz2 ratio prevents Frz2 from capturing Wg as Dlp competes and sequesters Wg away from Fz2.

Heparan Sulfate Proteoglycans in Synaptic Development

HSPGs are potent regulators of structural and functional synaptogenesis, with pleiotropic roles as extracellular signaling platforms for a wide variety of signaling molecules and ECM components (*14*, *108*, *266*, *267*). HSPGs are well poised to coordinate complex signaling driving synaptogenesis while maintaining context-dependent flexibility necessary for synapse maintenance. Synaptogenic HSPG-mediated molecular mechanisms are influenced by HS moieties, HS fine-tuning and the PG core protein (*17*, *98*, *267*, *268*). A large proportion of studies that implicate HSPGs in synaptogenesis broadly disrupt HSPG activity via acute enzymatic HS-removal, exogenous HS application, or by manipulating HSPG biosynthesis. Thus, detailed molecular mechanisms, specific core protein requirements, and particular HSPG contributions are less well understood. The conserved reductionist and genetically amenable *Drosophila* model system is well suited to interrogate the essential functions of HSPGs in synaptogenesis and coordinated signaling mechanisms.

Secreted HSPGs

The *Drosophila* genome encodes just two secreted HSPGs, Perlecan and Carrier of Wingless (Cow). In mammals, Agrin is an important secreted neural HSPG that clusters postsynaptic receptors and coordinates the formation of the NMJ by stabilizing and aligning pre- and postsynaptic specializations (*269–271*). Agrin is not present in *Drosophila*; however, Perlecan (*trol*; Pcan) and other HSPGs function to coordinate synaptogenesis, akin to the activities described for their mammalian counterpart (*11*, *14*, *268*). Moreover, *Drosophila* express the Mind-the-Gap (MTG) C-lectin, a presynaptically secreted organizer of the synaptomatrix required for postsynaptic differentiation (*272–274*). Cow requirements at the NMJ remain to be tested, but initial reports indicate likely Cow-dependent functions in the nervous system (*275*). Developmental transcriptome profiling and bioinformatics approaches identified Cow as a putative synaptic gene important for neural development and results from two separate genome-wide RNAi screens suggest Cow might play an important role in muscle morphogenesis and nociception (*276–278*). In a *Drosophila* model, Cow, Furin-1 and Anaplastic lymphoma kinase (Alk) were identified as candidate genes involved in attention-deficit/hyperactivity disorders, and this study revealed complex locomotor behavioral defects in *cow Minos*-insertion mutants (*275*).

Pcan regulates several molecular mechanisms via binding a variety of GFs in developmental-, tissue- and signaling-specific contexts (*56*, *279*). Timing of cell division in different neuroblast populations is strongly regulated by Pcan-dependent GF interactions requiring core protein and/or HS chains (*56*, *279–281*).

Specifically, Wg, Dpp, FGF and Hh actively signal in brain neuroblasts throughout larval development, but Pcan-dependent requirements in these signaling pathways reveal spatiotemporal differences (*56*). Pcan is a ligand for Dg, Dg abundance reciprocally regulates Pcan expression and distribution, and Pcan is an integral component of the neural lamella/BL encasing nerves and the blood brain barrier (BBB) (*36*, *282*, *283*). Pcan is also a guidance cue required for repulsive Sema-1a/PlexA mediated motorneuron axon guidance and defasciculation via integrin-dependent Focal adhesion kinase (FAK) signaling (*284*). In this context, Pcan removal suppresses Sema-1a gain-of-function (GOF) while disrupting HS biosynthesis enhances Sem-1a GOF (*284*). At the NMJ, muscle-derived Pcan balances bi-directional pre- vs. postsynaptic Wg activity via promoting muscle FNI which concurrently restricts the divergent, canonical autocrine pathway (*17*). Both Pcan core protein and HS chains regulate NMJ development. EM analysis shows Pcan is distributed in the external muscle BM, throughout the SSR, and in the synaptomatrix (*17*). Loss of *trol* causes NMJ defects from early larval stages that continue to worsen throughout development (*17*). *Trol* mutants display an HS-dependent reduction in muscle surface area with NMJs containing a similar number of boutons, suggesting a defect in coordinated growth scaling (*17*). Structurally, *trol* LOF causes irregular bouton clustering, increased satellite bouton (core-dependent) and ghost bouton formation, as well as increased Futsch loops associated with growth (*17*). Moreover, the SSR is densely packed with fewer layers, resulting in overall reduced SSR area, and postsynaptic pockets are visibly enlarged. Functional defects include deficits in peristalsis, A-type GluR expression and neurotransmission strength, indicating Pcan is required for proper functional differentiation (*17*). Total Wg levels are unchanged in *trol* LOF conditions but extracellular Wg levels, particularly in the postsynaptic domain, are significantly reduced (*17*). Similarly, acute HS removal via enzymatic digestion of GAG chains results in reduced extracellular Wg abundance while total Wg levels remain unchanged (*17*). Postsynaptic expression of Fz2-C-NLS in a *trol* null background is sufficient to restore FNI signaling and suppress most postsynaptic defects observed in *trol* mutants (*17*). However, this does not restore A-type GluR expression or neurotransmission defects, consistent with the idea that Wg regulates GluRIIA in an FNI-independent manner (*17*, *260*). The presynaptic satellite bouton number increase (but not ghost bouton number) is suppressed by single copy removal of *Wg*, Sgg overexpression or *Dsh* disruption, but not by removal of *gbb* (BMP) or *heartless* (*htl,* FGF), showing this defect is specific to increased presynaptic Wnt signaling in the *trol* mutants (*17*).

Membrane-tethered HSPGs

The membrane-tethered *Drosophila* HSPGs include two lipid-anchored glypicans, Dally and Dlp, as well as a single transmembrane Sdc. Sdc is reported as both an exclusively HS-bearing PG as well as a hybrid PG bearing predominantly HS-GAGs plus a single CS-GAG attachment (*61*, *62*). Interestingly, a targeted glycan screen suggests synaptogenic requirements for several genes involved in CS-GAG biosynthesis, but molecular mechanisms remain unexplored (*98*). Sdc promotes NMJ growth through interactions with dLAR, but little else is known regarding this molecular mechanism (*108*). Dally modulates a variety of neurodevelopmental processes, including differentiation (*95*), axon guidance (*284*), dendrite morphogenesis (*285*) and neurotoxicity (*286*). However, roles for Dally at the NMJ have not been described and have thus far Dally appears dispensable for synaptogenesis (*17*). In contrast, Dlp is a potent modifier of structural and functional synaptogenesis, with synaptic Dlp expression and/or localization misregulated in many mutant backgrounds (*98*, *108*, *266*, *287–289*). Importantly, disease-related synaptogenic defects are often ameliorated by correcting Dlp misexpression. Therefore, understanding how Dlp is regulated and functions in context-dependent molecular mechanisms are critically important in order to gain insight on human brain development and disease.

Dlp expression is largely restricted to the perisynaptic domain in a punctate pattern between neuron and muscle with small amounts of Dlp observed on the muscle surface (*98*, *108*, *267*). Dlp LOF results in increased evoked EJP amplitude with no change in spontaneous amplitude or frequency and a significant elevation in quantal content, likely caused by an increased number of AZs per bouton (*108*). Likewise, postsynaptic Dlp overexpression causes increased evoked EJC current amplitude, likely caused by increased AZ area (*108*, *266*). Dlp is limiting for AZ morphogenesis as *dlp* LOF causes an overall reduction in AZ area but a 2-fold increase in AZ number/bouton, while Dlp overexpression is sufficient to reciprocally increase AZ area (*108*). Dlp regulates AZ morphogenesis in the absence of any large changes in the abundance of pre- and postsynaptic molecular machinery components (*108*). This is accomplished by Dlp HS-chains engaging dLar with high affinity to inhibit intracellular dLar-phosphatase activity which instructs AZ morphogenesis (*108*). In terms of structural growth, *dlp* LOF mutants reportedly show no change in bouton number; however, pre- or postsynaptic Dlp overexpression is sufficient to reduce bouton number at NMJ m6/7 but, counterintuitively, increased bouton number at NMJ m4 is also observed in postsynaptic Dlp overexpression conditions (*108*, *266*).

HS Biosynthesis and HS-modifying Enzymes

Studies at the *Drosophila* NMJ show disruptions in HS-biosynthesis/modification enzymes have overlapping and non-overlapping correlates with single PG LOF phenotypes (*98*, *267*). Complementary structure/function studies that have integrated HS-biosynthesis and HS-modifications with individual and combinatorial PG-domain mutations have been particularly informative. Loss of HS sulfation sometimes has more severe consequences than disrupting HS chain length, suggesting although both chain length and subsequent modifications are important, aberrant HS sulfation interferes more with biological functions (*98*, *267*). The 2-O-sulfation and 6-O-sulfation modifications of sugar residues are catalyzed by HS 2-O- and 6-O-sulfotransferases (Hs2st and Hs6st), respectively. HS sulfation compensation is a common mechanism to both vertebrates and invertebrates, in which loss of one enzyme results in the upregulation of sulfate groups added by the other enzyme thereby ensuring the correct overall net negative charge on HSPGs (*135*). However, NMJ synaptogenic defects are still observed in the absence of *Hs6st* activity, suggesting that the location of specific sulfates, not just net charge, critically determines synaptic HSPG functions (*98*). Moreover, extracellular HS-modifying enzymes are regulated through feedback systems. For example, Wg signal transduction promotes *Sulf1* (Sulfated) expression and Sulf1 negatively regulates Wg (*134*, *290*). Roles for synaptic HS-GAG chains include modulating structural and functional differentiation, regulating extracellular ligand distribution and signaling efficacy, limiting activity-dependent endocytosis/SV recycling, and restricting autophagy (*267*). Some HSPG functions rely on dual core-protein and HS-GAG activities (*291*). For example, the increased ghost bouton phenotype caused by *trol* LOF is neither phenocopied nor enhanced by simply reducing HS modifications, suggesting an important role for the Pcan core protein. Conversely, overexpressing an unrelated HSPG (Dally) in the *trol* mutant background is sufficient to suppress the increased ghost bouton formation, suggesting an important role for HS chains (*17*). Reducing sulfation does not change GluRIIA levels at the NMJ, indicating GluRIIA is regulated independent of this HS interaction (*17*). It is clear that HSPGs fine-tune structural and functional synapse development by coordinating a variety of signaling events, including Wnt and BMP pathways, but many of the mechanistic details remain to be explored.

Matrix Metalloproteinases in Neural Development

Matrix metalloproteinases (MMPs) are members of the Metzincin superfamily of zinc-dependent proteases defined by a common HEXXHXXGXXH zinc-binding motif within the catalytic domain and an invariant downstream Met-turn which provides a hydrophobic base for the Zinc binding site (Fig. 6) (*146*, *147*).

The ~24 mammalian MMPs are secreted and membrane-tethered extracellular enzymes, classically described as ECM-remodeling enzymes that degrade structural ECM components. This interpretation has recently shifted following the identification of several other substrates, including receptors, cytokines, PGs, signaling molecules and many other targets (*141*, *151*). Thus, MMPs sit at a central node in the extracellular protease web and can directly or indirectly influence many intersecting pathways. With a potentially diverse substrate repertoire, as well as non-proteolytic functions, MMPs are critically important for extracellular remodeling and modulate a wide variety of biological processes (*7*, *141*, *148*, *151*, *292*). Canonical MMP domains include an N-terminal, self-inhibitory pro-domain maintaining enzymatic latency via a cysteine-switch, catalytic domain, and flexible linker region connected to the C-terminal hemopexin domain important for protein-protein interactions (Fig. 7) (*146*, *293*). The membrane-tethered MMPs contain either a C-terminal transmembrane domain and intracellular cytoplasmic tail or a GPI-anchor (*293*, *294*). Proteolytic MMP activities also generate bioactive molecules, reveal neo-epitopes, release, mobilize, activate, inhibit or sequester signaling ligands and/or receptors/co-receptors, and dictate cell-ECM as well as cell-cell interactions (*7*, *148*, *292*, *295–298*). The spatio-temporal enzymatic activity is tightly regulated at many levels, including reciprocal matrix regulation of MMP expression, localization, activation, internalization and inhibition (*299*). MMPs are produced as inactive zymogens requiring destabilization of an inhibitory Cys-switch for activation. Extracellular MMP activation is mediated by proteolytic cleavage of the pro-domain and environmental factors (*293*). MMPs containing a furin-consensus sequence are subject to intracellular activation, or partial activation requiring a subsequent proteolytic cleavage event (*293*, *296*). Enzymatic activity is balanced by endogenous inhibitors such as TIMPs, RECK and α2-macroglobulin, and other reported inhibitors include β-amyloid precursor protein (APP) and serine protease inhibitors (*158*, *293*). Thus, MMP and TIMP functions are largely coordinated by the MMP/TIMP axis as well as through elaborate feedback loops. The 4 mammalian TIMPs tightly bind MMPs in a 1:1 ratio via a non-covalent interaction that involves the N-terminal TIMP inhibitory domain wedging into the MMP-active cleft chelating the zinc ligand and displacing the water molecule required for catalysis (*293*, *300*, *301*). Besides MMPs, TIMPs inhibit ADAM and ADAMTS members and the TIMP C-terminal non-inhibitory domain can interact with MMP-Hpx domains as well as other molecules (*158*, *293*, *302*, *303*). Therefore, it is important to note that some TIMP-MMP interactions are non-inhibitory and actually promote MMP activation while other TIMP functions are independent of MMPs or protease interactions altogether (*158*, *292*, *303*, *304*).

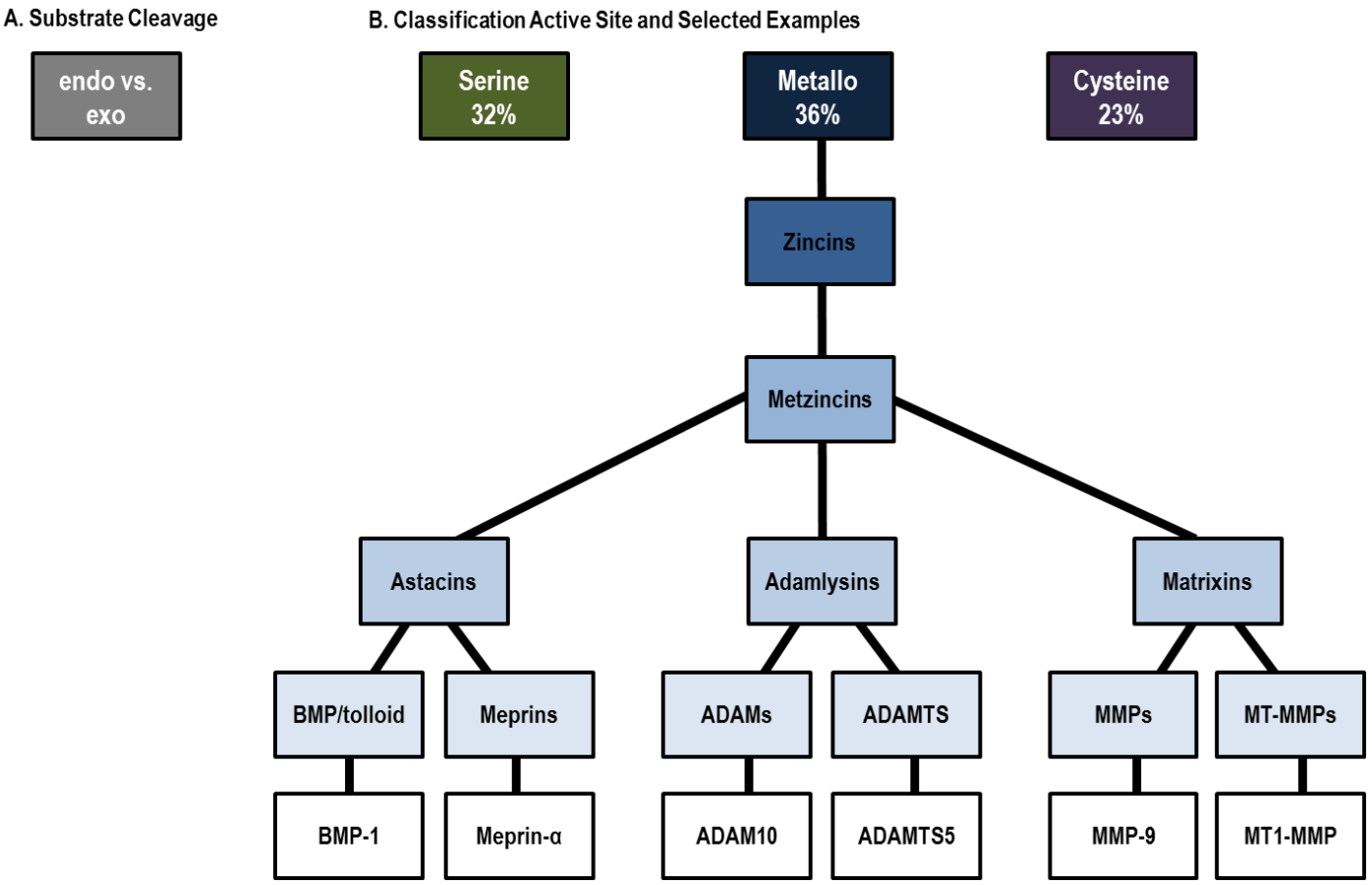

Figure 6

Figure 6: Mmps are members of the Metzincin superfamily of metalloproteinases. Proteases cleave internal peptide bonds (endo) or terminal peptide bonds (exo). MMPs are endopeptidases. Only three protease classes of the human degradome are shown with their percent make up. Serine proteases comprise ~32% of the degradome, metalloproteases comprise ~36% of the degradome and cysteine proteases comprise ~23% of the degradome. The classes are further divided as exemplified only for the metalloproteases. According to the MEROPS database, matrixins, which contain the matrix metalloproteinases (secreted or membrane-tethered, MT), are members of the metzincin super-family of zinc-dependent proteases (zincins). The metzincin super-family also includes the adamlysins and the astacins. MMP-9 is an example of a secreted MMP while MT1-MMP is an example of a membrane-tethered MMP. Two valuable resource centers for peptidase information include the following: the MEROPS database for peptidases and inhibitors (https://www.ebi.ac.uk/merops/) and the degradome database (http://degradome.uniovi.es).

There are just two *Drosophila* Mmps, secreted Mmp1 and GPI-anchored Mmp2 (Fig.7), inhibited by a single endogenous Timp (*305–307*). Note that *Drosophila* nomenclature uses “Mmp” and “Timp” whilst mammalian nomenclature or general references use “MMP” and “TIMP”. Alternative splicing enables one Mmp1 isoform to be GPI-modified, and both GPI-anchored Mmps can be shed from the membrane (*308*). The *Drosophila* Mmps display distinct and overlapping expression patterns and functions, as well as different substrate preferences (*305*, *306*, *308*, *309*). Mmp domain structure is conserved, as are biological functions. Both Mmp1 and Mmp2 contain the furin-like consensus sequence (RXK/RR) and are likely activated intracellularly (*305*, *306*, *308*). Like mammalian TIMPs, the *Drosophila timp* gene is nested within the *synapsin* gene and is most similar to mammalian TIMP-3 based off surface charge, sequence and functional properties (*301*, *302*, *307*, *309*, *310*). *Drosophila* studies show Timp is important in many tissues throughout larval and adult stages for balanced proteolytic activity with roles in vitality, fertility, tissue integrity, organ growth, adhesion, as well as ECM metabolism, remodeling and homeostasis (*307*, *309*, *311*, *312*). *In vivo* and *in vitro* studies reveal potent Timp inhibitory action against both Mmps and ADAMs (*302*, *309*). Importantly, mammalian MMPs are inhibited by *Drosophila* Timp and mammalian TIMPs reciprocally inhibit *Drosophila* Mmps (*302*). Mmps are not essential for viable *Drosophila* embryogenesis, but are critically important for tissue growth, remodeling, signaling and tissue homeostasis (*8*, *309*, *313*). *Drosophila* Mmps have direct and indirect roles in cell migration (*314*), wound healing (*35*), immune response (*315*), adhesion (*316*), autophagy (*317*, *318*) and signal transduction (*319–321*), as well as ECM deposition, remodeling and maintenance (*35*, *309*, *322*, *323*).

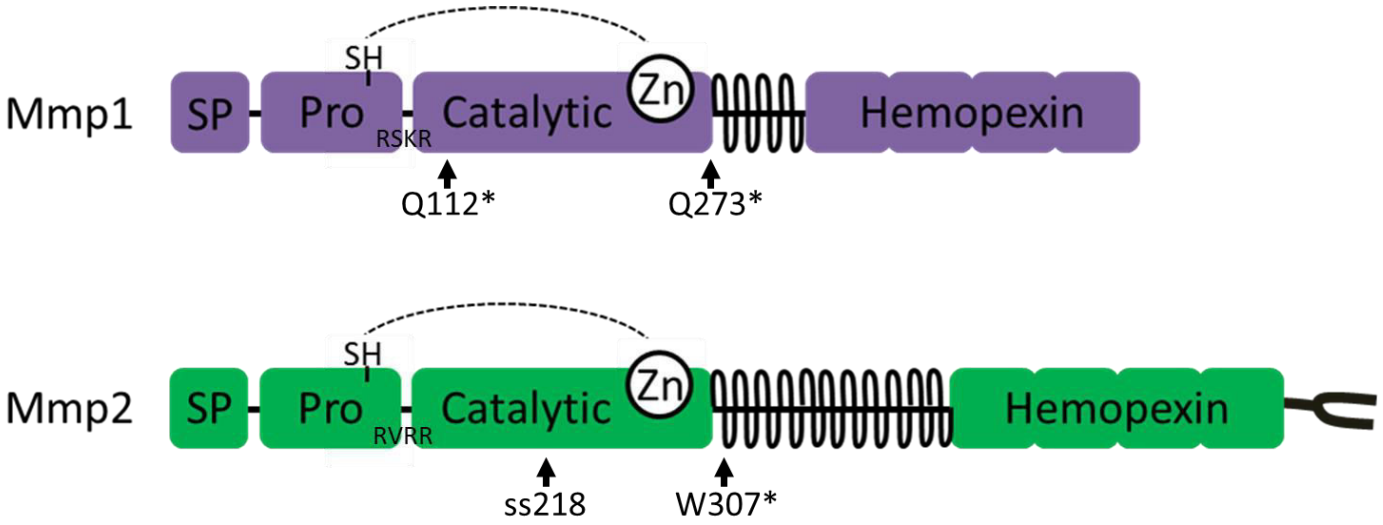

Figure 7

Figure 7: *Drosophila* Mmp structure and selected tools. Cartoon schematic of *Drosophila* Mmp1 (purple) shown as a secreted form and Mmp2 (green) shown with a GPI-anchor. Conserved domains include N-terminal cleavable signal peptide (SP) directing Mmps through the secretory pathway. The pro-domain maintains enzymatic latency through a cysteine-zinc interaction. The "cysteine-switch" must be destabilized for enzymatic activation. The cleavable Furin consensus sequence is shown for Mmp1 (RSKR) and Mmp2 (RVRR) which enables intracellular activation by pro-domain cleavage. The catalytic domains and zinc binding are shown. Flexible linker regions intersect the catalytic and hemopexin domains. Hemopexin domains consist of four-bladed propellers. Mmp2 C-terminal contains a GPI-anchor which tethers Mmp2 to the cell membrane. The location of Mmp point mutations used in this thesis is denoted by arrowheads. A full description detailing each mutation is included in the materials and methods section within chapters II and III.

Mmp functions in the nervous system are beginning to be described, with mammalian MMPs upregulated following increased neural stimulation and nerve injury (*324–327*). In the *Drosophila* embryonic nervous system, Mmp1 displays expression in midline glial cells and Mmp2 is more broadly expressed in both glia and neurons (*305*, *306*, *328*). During motoneuron outgrowth, Mmp2 activity is necessary to keep axons adherent within nerves bundles until they reach their target branch point and thus Mmp2 modulates appropriate axonal responsiveness to specific guidance cues (*328*). In this way, Mmp2 is not involved in motor axon extension but rather promotes correct targeting. In this mechanism, Mmp2-dependent cleavage is spatially restricted and acts on the ECM molecule Faulty Attraction (Frac) producing a signal for axons to stay bundled via non-canonical LIMK-dependent BMP signal transduction (*329*). However, this embryonic Mmp2 LOF phenotype does not persist and neuromuscular connectivity is not disrupted 3rd instar larvae (*330*). Peripheral nerves contain glia layers, which protect and support axon bundles, and both nerves and the CNS are encased by a dense neural lamella. Exogenous Mmp2 expression in specific glia phenocopies integrin LOF and is sufficient to degrade the neural lamella resulting in glial detachment and defects in VNC morphology (*36*). Interestingly, exogenous expression of wildtype Mmp2, dominant-negative inactive Mmp2, or Timp all result in a similar phenotype displaying elongated VNCs (*331*). During pupal metamorphosis, certain peripheral sensory neurons degrade their larval dendritic field and then regrow an adult dendritic field while axons remain intact. This dendrite-specific pruning event is triggered by environmental cues and requires the catalytic activities of both Mmps non-autonomously (*332*). In another context, Mmp2 is transiently upregulated in epithelial cells and modifies the Collagen-IV BM driving dendritic reshaping and directional elongation of dendrites in adult sensory neurons (*333*). Mmps both have distinct roles remodeling pigment dispersing factor (PDF) clock neurons in the *Drosophila* adult brain (*334*). The structure of PDF neurons oscillate, displaying more complex arbors during the day and less complex arbors at night (*334*). Mmp GOF in PDF neurons abolishes remodeling leading to less complex circuits and LOF has the opposite effect (*334*). In a complex mechanism, circadian regulation of electrical activity and Mmp1 expression, with subsequent cleavage of the PDF neuropeptide, modulates PDF signaling activity to regulate circadian structural plasticity (*334*). Thus, in the nervous system, Mmp expression is spatio-temporally regulated and substrates include ECM components, neuropeptides and signaling molecules, consistent with mammalian functions.

The importance of MMPs is further highlighted by the fact that aberrant MMP upregulation underlies numerous neurological disorders, including developmental and neurodegenerative disease states, as well as tumor invasiveness (*53*, *335–339*). A number of these neurological diseases have been effectively modeled in *Drosophila* and are likewise linked to Mmp dysfunction (*191*, *340–345*). Huntington's disease is a progressive

neurodegenerative disorder, with pathogenesis linked to proteolytic cleavage of huntingtin (Htt) protein (*340*). Similar to mammalian models, reducing *Drosophila* Mmp activity (*mmp2*/+) improves motor deficits and prevents retinal degeneration induced by exogenous Htt toxicity (*340*, *346*). Mmp2-dependent cleavage of tyrosyl-tRNA synthetase generates a signaling fragment recruiting macrophages to dying cells for clearance (*318*). Tyrosyl-tRNA synthetase dysfunction and MMP upregulation are both associated with Charcot-Marie-Tooth disease, a commonly inherited peripheral neuropathy also effectively modeled in *Drosophila* (*347*, *348*). In trachea and cell culture, *Drosophila* Mmp1 displays non-autonomous sheddase activity releasing the ectodomain of Ninjurin-A, a CAM known to be up-regulated following nerve injury in mammals (*316*). Importantly, both pharmacological and genetic Mmp inhibition, as well as HSPG reduction, remediates synaptogenic defects associated with the *Drosophila* model of Fragile X syndrome (FXS), the most common heritable monogenic cause of autism spectrum disorders (ASD) and intellectual disability (*266*, *342*, *349*). The FXS disease state is caused by loss of Fragile X Mental Retardation Protein (FMRP) function due to a CGG trinucleotide repeat expansion in the 5' untranslated region of the *FMR1* gene leading to hyper-methylation and gene silencing (*350*, *351*). Surprisingly, *Drosophila* FMRP co-removal in the *mmp1* LOF or Timp overexpression conditions reciprocally circumvents early lethality and non-neuronal phenotypes caused by Mmp inhibition (*342*). How MMP/FMRP pathways intersect remains elusive. FMRP is an mRNA and channel binding protein that regulates mRNA stability, trafficking, neuronal excitability and is most commonly described as a negative regulator of translation (*352–355*). FMRP is regulated by neural activity and phosphorylation and reciprocally modulates activity-dependent processes (*356–359*). FXS presents with a range of neurodevelopmental impairments observed in both humans and *Drosophila*. The fly model has been instrumental in dissecting the cellular and molecular underpinnings of FXS. Indeed, *Drosophila* and mammalian FMRP are evolutionarily conserved, loss of dFMRP leads to phenotypic consequences reminiscent of those observed in humans, and transgenic expression of human *FMR1* in the *Drosophila* FXS model corrects synaptogenic deficits (*357*, *360–362*), including structural overgrowth, circuit hyper-connectivity, accumulation of immature synapses and increased neuronal excitability (*362–370*). Behavioral phenotypes include hyperactivity, circadian arhythmicity, repetitive grooming, reduced courtship, and deficits in learning and memory (*371–380*). At the NMJ, FMRP modulates the microtubule cytoskeleton network and negatively regulates Futsch/MAP1B translation in motorneurons to restrict NMJ growth, branching, satellite and mature bouton number, and functional neurotransmission strength (*362*, *364*, *381*). On the postsynaptic side, FMRP regulates GluR composition with FXS NMJs containing a higher ratio of A-type to B-type GluRs, and larval locomotion is consistently increased in the FXS model (*370*, *382–384*). Interestingly, postsynaptic FMRP

restricts SV density and vesicle release in the presynaptic motorneuron, suggesting FMRP activity intersects with *trans*-synaptic signaling (*364*, *385*). Indeed, FMRP regulates *trans*-synaptic Wnt signaling driving coordinated structural and functional synaptogenesis in a mechanism mediated by HSPGs (*266*). Thus, HSPGs may provide the missing link between extracellular MMP dysfunction and FXS.

Clearly, Mmps have both beneficial roles important for normal neural development as well detrimental impacts in multiple disease pathologies. Therefore, in order to identify and design appropriate drug targets it is critical to understand the full scope of the Mmp network in both the context of development and disease (*386*). In the past, modest understanding of essential MMP functions and disease complexity, in conjunction with the challenges of MMP redundancy and compensation, have been associated with a global failure of MMP inhibitor (MMPI) clinical trials (*387*, *388*). It is now realized that removing even a single MMP can have far-reaching consequences on biological processes and other protease functions (*389*). There have been great advances in protease biology, but there is still a pressing need to better understand what these extracellular enzymes regulate and how they are controlled in the context of their *in vivo* pericellular environments (*299*). This thesis work takes advantage of the genetically amenable and much more manageable *Drosophila* model system, with only two Mmps and a single Timp, to collectively interrogate Mmp functions in both neural development and in the context of the FXS disease state (Fig. 8).

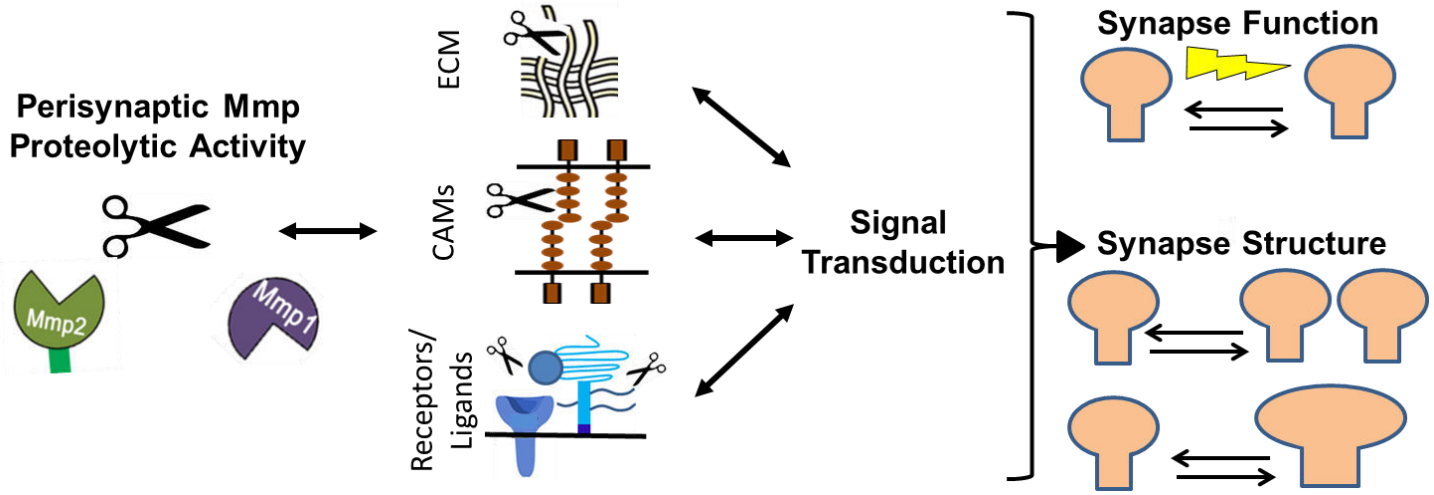

Figure 8

Figure 8: Overarching hypothesis. Mm1 (purple) and Mmp2 (green) are active within the synaptomatrix and cleave structural extracellular matrix components (ECM), cell adhesion molecules (CAMs), and/or ECM-associated receptors or ligands thereby influencing trans-synaptic signaling driving structural and/or functional synaptogenesis. Loss of Mmp activity will influence functional neurotransmission and/or synapse structure (synapse number or synapse size).

Thesis Outline

Part One

Part one of this thesis work investigates Mmp roles in structural and functional synaptogenesis. We use a battery of single *mmp* mutants, double *mmp* mutants and RNAi knock-down strategies to interrogate Mmp requirements for NMJ growth, functional neurotransmission, functional molecular assembly and ultrastructural development. I find that Mmp1 and Mmp2 normally serve to put the brakes on structural and functional development. I further test Mmp roles in Wnt/Wg trans-synaptic signaling and identify differential genetic interactions between both Mmps and the HSPG glypican Dlp. I find that Mmp control of synaptogenesis is through the differential regulation of Dlp. I create new antibody tools and, in conjunction with previously characterized tools, visualize all matrix metalloproteome components at the synapse and identify that Mmp1, Mmp2 and Timp expression is mutually co-regulated at the NMJ.

Part Two

Part two of this thesis work investigates Mmp1 and Mmp2 requirements for activity-dependent new bouton formation, the extracellular regulation of Mmp1 and Mmp2 expression through HSPG Dlp, and how neural activity regulates Mmp1 and Mmp2 expression and localization at the synapse. I find that Mmp1, but not Mmp2, is required for new bouton formation following elevated activity. I find that Mmp1 and Mmp2 are bi-directionally regulated following activity stimulation. Neural activity promotes Mmp1 expression and restricts Mmp2 abundance. Moreover, I find that extracellular Mmp1 localization is dependent upon the HSPG glypican, Dlp. I provide evidence that Dlp is likewise promoted by neural stimulation and regulates Mmp1 through a functional interaction requiring the HS GAG chains of Dlp. We also show that Dlp promotes proteolytic activity at the synapse. Finally, I extend these findings to the FXS disease state and find that both basal and activity-regulated Mmp1 expression are dependent upon FMRP in a mechanism mediated through Dlp.

References

1. R. O. Hynes, The Extracellular Matrix: Not Just Pretty Fibrils. *Science.* **326**, 1216–1219 (2009).
2. R. O. Hynes, The evolution of metazoan extracellular matrix. *J. Cell Biol.* **196**, 671–679 (2012).
3. R. O. Hynes, A. Naba, Overview of the matrisome-an inventory of extracellular matrix constituents and functions. *Cold Spring Harb. Perspect. Biol.* **4**, a004903 (2012).
4. A. Naba, K. R. Clauser, S. Hoersch, H. Liu, S. A. Carr, R. O. Hynes, The Matrisome: In Silico Definition and In Vivo Characterization by Proteomics of Normal and Tumor Extracellular Matrices. *Mol. Cell. Proteomics*. **11**, 14647–14665 (2012).
5. N. H. Brown, Extracellular matrix in development: Insights from mechanisms conserved between invertebrates and vertebrates. *Cold Spring Harb. Perspect. Biol.* **3**, a005082 (2011).
6. K. Kessenbrock, V. Plaks, Z. Werb, Matrix Metalloproteinases: Regulators of the Tumor Microenvironment. *Cell*. **141**, 52–67 (2010).
7. C. Bonnans, J. Chou, Z. Werb, Remodelling the extracellular matrix in development and disease. *Nat Rev Mol Cell Biol.* **15**, 786–801 (2014).
8. A. Page-McCaw, A. J. Ewald, Z. Werb, Matrix metalloproteinases and the regulation of tissue remodeling. *Nat Rev Mol Cell Biol.* **8**, 221–233 (2007).
9. R. O. Hynes, Q. Zhaot, Analysis The Evolution of Cell Adhesion. *J. Cell Biol.* **150**, 89–95 (2000).
10. F. Wiradjaja, T. DiTommaso, I. Smyth, Basement Membranes in Development and Disease. *Birth Defects Res. Part C-Embryo Today-Reviews*. **90**, 8–31 (2010).
11. K. Broadie, S. Baumgartner, A. Prokop, Extracellular matrix and its receptors in Drosophila neural development. *Dev. Neurobiol.* **71**, 1102–1130 (2011).
12. V. Hartenstein, Development of Drosophila larval sensory organs: spatiotemporal pattern of sensory neurones, peripheral axonal pathways and sensilla differentiation. *Development*. **102**, 869–886 (1988).
13. B. M. Glasheen, R. M. Robbins, C. Piette, G. J. Beitel, A. Page-McCaw, A matrix metalloproteinase mediates airway remodeling in Drosophila. *Dev. Biol.* **344**, 772–783 (2010).
14. N. Dani, K. Broadie, Glycosylated synaptomatrix regulation of trans-synaptic signaling. *Dev. Neurobiol.* **72**, 2–21 (2011).
15. J. Vautrin, The synaptomatrix: A solid though dynamic contact disconnecting transmissions from exocytotic events. *Neurochem. Int.* **57**, 85–96 (2010).
16. N. Denef, Y. Chen, S. D. Weeks, G. Barcelo, T. Schupbach, Crag is a novel regulator of epithelial

architecture and polarized deposition of basement membrane proteins in Drosophila. *Dev. Cell*. **14**, 354–364 (2008).

17. K. Kamimura, K. Ueno, J. Nakagawa, R. Hamada, M. Saitoe, N. Maeda, Perlecan regulates bidirectional Wnt signaling at the Drosophila neuromuscular junction. *J. Cell Biol.* **200**, 219–233 (2013).
18. Y. Matsubayashi, A. Louani, A. Dragu, B. J. Sanchez-Sanchez, E. Serna-Morales, L. Yolland, A. Gyoergy, G. Vizcay, R. A. Fleck, J. M. Heddleston, T. Chew, D. E. Siekhaus, B. M. Stramer, A Moving Source of Matrix Components Is Essential for De Novo Basement Membrane Formation. *Curr. Biol.* **27**, 3526–3534 (2017).
19. A. Prokop, M. D. Martin-Bermudo, M. Bate, N. H. Brown, Absence of PS integrins or laminin A affects extracellular adhesion, but not intracellular assembly, of hemiadherens and neuromuscular junctions in Drosophila embryos. *Dev. Biol.* **196**, 58–76 (1998).
20. F. J. Fogerty, L. I. Fessler, T. A. Bunch, Y. Yaron, C. G. Parker, R. E. Nelson, D. L. Brower, D. Gullberg, J. H. Fessler, Tiggrin, a novel Drosophila extracellular matrix protein that functions as a ligand for Drosophila alpha PS2 beta PS integrins. *Development*. **120**, 1747–1758 (1994).
21. D. Martin, S. Zusman, X. Li, E. L. Williams, N. Khare, S. DaRocha, R. Chiquet-Ehrismann, S. Baumgartner, wing blister, a new Drosophila laminin alpha chain required for cell adhesion and migration during embryonic and imaginal development. *J. Cell Biol.* **145**, 191–201 (1999).
22. J. H. Fessler, L. I. Fessler, DROSOPHILA EXTRACELLULAR MATRIX. *Annu. Rev. Cell Biol.* **5**, 309–339 (1989).
23. A. Naba, K. R. Clauser, H. Ding, C. A. Whittaker, S. A. Carr, R. O. Hynes, The extracellular matrix: Tools and insights for the “omics” era. *Matrix Biol.* **49**, 10–24 (2016).
24. S. Ricard-Blum, The Collagen Family. *Cold Spring Harb. Perspect. Biol.* **3**, a004978 (2011).
25. P. D. Yurchenco, Basement Membranes : Cell Scaffoldings and Signaling Platforms. *Cold Spring Harb Perspect Biol*. **3**, a004911 (2011).
26. W. P. Daley, K. M. Yamada, ECM-modulated cellular dynamics as a driving force for tissue morphogenesis. *Curr. Opin. Genet. Dev.* **23**, 408–414 (2013).
27. T. Wang, A. Hauswirth, A. Tong, D. Dickman, G. Davis, Endostatin is a Trans-Synaptic Signal for Homeostatic Synaptic Plasticity. *Neuron*. **83**, 616–629 (2014).
28. K. Sato, K. Yomogida, T. Wada, T. Yorihuzi, Y. Nishimune, N. Hosokawa, K. Nagata, Type XXVI collagen, a new member of the collagen family, is specifically expressed in the testis and ovary. *J. Biol. Chem.* **277**, 37678–37684 (2002).
29. S. Grimal, S. Puech, R. Wagener, S. Venteo, P. Carroll, A. Fichard-Carroll, Collagen XXVIII is a distinctive component of the peripheral nervous system nodes of ranvier and surrounds nonmyelinating glial cells.

Glia. **58**, 1977–1987 (2010).

30. B. Blumberg, A. J. Mackrell, J. H. Fessler, Drosophila basement-membrane procollagen alpha-1(IV).2. complete cDNA sequence, genomic structure, and general implications for supramolecular assemblies. *J. Biol. Chem.* **263**, 18328–18337 (1988).
31. G. P. Lunstrum, H. P. Bachinger, L. I. Fessler, K. G. Duncan, R. E. Nelson, J. H. Fessler, Drosophila basement membrane procollagen IV. I. Protein characterization and distribution. *J. Biol. Chem.* **263**, 18318–18327 (1988).
32. S. Yasothornsrikul, W. J. Davis, G. Cramer, D. A. Kimbrell, C. R. Dearolf, viking: identification and characterization of a second type IV collagen in Drosophila. *Gene*. **198**, 17–25 (1997).
33. C. Borchiellini, J. Coulon, Y. LeParco, The function of type IV collagen during Drosophila muscle development. *Mech. Dev.* **58**, 179–191 (1996).
34. A. Koper, A. Schenck, A. Prokop, Analysis of adhesion molecules and basement membrane contributions to synaptic adhesion at the drosophila embryonic NMJ. *PLoS One*. **7**, e36339 (2012).
35. L. J. Stevens, A. Page-McCaw, A secreted MMP is required for reepithelialization during wound healing. *Mol. Biol. Cell*. **23**, 1068–1079 (2012).
36. X. Xie, V. J. Auld, Integrins are necessary for the development and maintenance of the glial layers in the Drosophila peripheral nerve. *Development*. **138**, 3813–3822 (2011).
37. T. Volk, S. Wang, B. Rotstein, A. Paululat, Matricellular proteins in development: Perspectives from the Drosophila heart. *Matrix Biol.* **37**, 162–166 (2014).
38. M. Drechsler, A. C. Schmidt, H. Meyer, A. Paululat, The Conserved ADAMTS-like Protein Lonely heart Mediates Matrix Formation and Cardiac Tissue Integrity. *PLoS Genet.* **9**, e1003616 (2013).
39. A. Chartier, S. Zaffran, M. Astier, M. Sémériva, D. Gratecos, Pericardin, a Drosophila type IV collagen-like protein is involved in the morphogenesis and maintenance of the heart epithelium during dorsal ectoderm closure. *Development*. **129**, 3241–3253 (2002).
40. F. Meyer, B. Moussian, Drosophila multiplexin (Dmp) modulates motor axon pathfinding accuracy. *Dev. Growth Differ.* **51**, 483–498 (2009).
41. N. Harpaz, E. Ordan, K. Ocorr, R. Bodmer, T. Volk, Multiplexin Promotes Heart but Not Aorta Morphogenesis by Polarized Enhancement of Slit/Robo Activity at the Heart Lumen. *PLoS Genet.* **9**, e1003597 (2013).
42. R. Momota, I. Naito, Y. Ninomiya, A. Ohtsuka, Drosophila type XV/XVIII Collagen, Mp, is involved in Wingless distribution. *Matrix Biol.* **30**, 258–266 (2011).

43. R. V. Iozzo, L. Schaefer, Proteoglycan form and function: A comprehensive nomenclature of proteoglycans. *Matrix Biol.* **42**, 11–55 (2015).

44. T. Neill, L. Schaefer, R. Iozza, Decoding the matrix: Instructive roles of proteoglycan receptors. *Biochemistry*. **54**, 4583–4598 (2016).

45. L. Zhang, Glycosaminoglycan (GAG) biosynthesis and GAG-binding proteins. *Prog. Mol. Biol. Transl. Sci.* **93**, 1–17 (2010).

46. S. Ricard-Blum, Protein—glycosaminoglycan interaction networks: Focus on heparan sulfate. *Perspect. Sci.* **11**, 62–69 (2017).

47. S. Sarrazin, W. C. Lamanna, J. D. Esko, Heparan sulfate proteoglycans. *Cold Spring Harb. Perspect. Biol.* **3**, a004952 (2011).

48. M. C. Z. Meneghetti, A. J. Hughes, T. R. Rudd, H. B. Nader, A. K. Powell, E. A. Yates, M. A. Lima, Heparan sulfate and heparin interactions with proteins. *J. R. Soc. Interface*. **12**, 20150589 (2015).

49. Z. D. Shi, H. Wang, J. M. Tarbell, Heparan sulfate proteoglycans mediate interstitial flow mechanotransduction regulating MMP-13 expression and cell motility via FAK-ERK in 3D collagen. *PLoS One*. **6**, e15956 (2011).

50. F. Zhang, X. Liang, J. M. Beaudet, Y. Lee, R. J. Linhardt, The effects of metal ions on heparin/heparin sulfate-protein interactions. *J Biomed Technol Res*. **1**, 6000101 (2014).

51. R. V Iozzo, Matrix proteoglycans: From molecular design to cellular function. *Annu. Rev. Biochem.* **67**, 609–652 (1998).

52. R. U. Margolis, R. K. Margolis, Chondroitin sulfate proteoglycans as mediators of axon growth and pathfinding. *Cell Tissue Res.* **290**, 343–348 (1997).

53. I. M. Ethell, D. W. Ethell, Matrix metalloproteinases in brain development and remodeling: Synaptic functions and targets. *J. Neurosci. Res.* **85**, 2813–2823 (2007).

54. P. D. Yurchenco, P. S. Amenta, B. L. Patton, Basement membrane assembly, stability and activities observed through a developmental lens. *Matrix Biol.* **22**, 521–538 (2004).

55. H. Toyoda, A. Kinoshita-Toyoda, S. B. Selleck, Structural analysis of glycosaminoglycans in Drosophila and Caenorhabditis elegans and demonstration that tout-velu, a Drosophila gene related to EXT tumor suppressors, affects heparan sulfate in vivo. *J. Biol. Chem.* **275**, 2269–2275 (2000).

56. J. R. Lindner, P. R. Hillman, A. L. Barrett, M. C. Jackson, T. L. Perry, Y. Park, S. Datta, The Drosophila Perlecan gene trol regulates multiple signaling pathways in different developmental contexts. *BMC Dev. Biol.* **7**, 121 (2007).

57. M. Schneider, A. A. Khalil, J. Poulton, C. Castillejo-Lopez, D. Egger-Adam, A. Wodarz, W. M. Deng, S. Baumgartner, Perlecan and Dystroglycan act at the basal side of the Drosophila follicular epithelium to maintain epithelial organization. *Development*. **133**, 3805–3815 (2006).

58. M. V Friedrich, M. Schneider, R. Timpl, S. Baumgartner, Perlecan domain V of Drosophila melanogaster. Sequence, recombinant analysis and tissue expression. *Eur. J. Biochem.* **267**, 3149–3159 (2000).

59. M. Hortsch, A. Olson, S. Fishman, S. N. Soneral, Y. Marikar, R. Dong, J. R. Jacobs, The expression of MDP-1, a component of Drosophila embryonic basement membranes, is modulated by apoptotic cell death. *Int. J. Dev. Biol.* **42**, 33–42 (1998).

60. Y.-H. Chang, Y. H. Sun, Carrier of Wingless (Cow), a Secreted Heparan Sulfate Proteoglycan, Promotes Extracellular Transport of Wingless. *PLoS One*. **9**, e111573 (2014).

61. B. Chanana, P. Steigemann, H. Jackle, G. Vorbruggen, Reception of Slit requires only the chondroitin-sulphate-modified extracellular domain of Syndecan at the target cell surface. *Proc. Natl. Acad. Sci. U. S. A.* **106**, 11984–11988 (2009).

62. J. Spring, S. E. Painesaunders, R. O. Hynes, M. Bernfield, Drosophila Syndecan - conservation of a cell-surface heparan-sulfate proteoglycan. *Proc. Natl. Acad. Sci. U. S. A.* **91**, 3334–3338 (1994).

63. K. J. Hamill, K. Kligys, S. B. Hopkinson, J. C. R. Jones, Laminin deposition in the extracellular matrix: a complex picture emerges. *J. Cell Sci.* **122**, 4409–4417 (2009).

64. B. L. Patton, Laminins of the neuromuscular system. *Microsc. Res. Tech.* **51**, 247–261 (2000).

65. J. W. Dean, S. Chandrasekaran, M. L. Tanzer, A biological role of the carbohydrate moieties of laminin. *J. Biol. Chem.* **265**, 12553–12562 (1990).

66. A. Subramanian, B. Wayburn, T. Bunch, T. Volk, Thrombospondin-mediated adhesion is essential for the formation of the myotendinous junction in Drosophila. *Development*. **134**, 1269–1278 (2007).

67. J. M. Urbano, C. N. Torgler, C. Molnar, U. Tepass, A. López-Varea, N. H. Brown, J. F. de Celis, M. D. Martin-Bermudo, Drosophila laminins act as key regulators of basement membrane assembly and morphogenesis. *Development*. **136**, 4165–4176 (2009).

68. P.-I. Tsai, M. Wang, H.-H. Kao, Y.-J. Cheng, Y.-J. Lin, R.-H. Chen, C.-T. Chien, Activity-dependent retrograde laminin A signaling regulates synapse growth at Drosophila neuromuscular junctions. *Proc. Natl. Acad. Sci. U. S. A.* **109**, 17699–17704 (2012).

69. K. W. Adolph, A thrombospondin homologue in Drosophila melanogaster: cDNA and protein structure. *Gene*. **269**, 177–184 (2001).

70. B. Bullard, W. A. Linke, K. Leonard, Varieties of elastic protein in invertebrate muscles. *J. Muscle Res.*

Cell Motil. **23**, 435–447 (2002).

71. R. S. Cornman, The distribution of GYR- and YLP-like motifs in drosophila suggests a general role in cuticle assembly and other protein-protein interactions. *PLoS One*. **5**, e12536 (2010).
72. S. H. Kim, J. Turnbull, S. Guimond, Extracellular matrix and cell signalling: The dynamic cooperation of integrin, proteoglycan and growth factor receptor. *J. Endocrinol.* **209**, 139–151 (2011).
73. A. Dityatev, C. I. Seidenbecher, M. Schachner, Compartmentalization from the outside: the extracellular matrix and functional microdomains in the brain. *Trends Neurosci.* **33**, 503–512 (2010).
74. I. Delon, N. H. Brown, Integrins and the actin cytoskeleton. *Curr. Opin. Cell Biol.* **19**, 43–50 (2007).
75. N. De Franceschi, H. Hamidi, J. Alanko, P. Sahgal, J. Ivaska, Integrin traffic - the update. *J. Cell Sci.* **128**, 839–52 (2015).
76. P. T. Martin, Dystroglycan glycosylation and its role in matrix binding in skeletal muscle. *Glycobiology*. **13**, 55R--66R (2003).
77. M. D. Henry, K. P. Campbell, Dystroglycan: An extracellular matrix receptor linked to the cytoskeleton. *Curr. Opin. Cell Biol.* **8**, 625–631 (1996).
78. E. L. McDearmon, A. C. Combs, J. M. Ervasti, Core 1 glycans on alpha-dystroglycan mediate laminin-induced acetylcholine receptor clustering but not laminin binding. *J. Biol. Chem.* **278**, 44868–44873 (2003).
79. J. E. Hewitt, Abnormal glycosylation of dystroglycan in human genetic disease. *Biochim. Biophys. Acta-Molecular Basis Dis.* **1792**, 853–861 (2009).
80. W. A. Grow, M. Ferns, H. Gordon, A mechanism for acetylcholine receptor clustering distinct from agrin signaling. *Dev. Neurosci.* **21**, 436–443 (1999).
81. N. Parkhomovskiy, P. T. Martin, alpha-galactosidase stimulates acetylcholine receptor aggregation in skeletal muscle cells via PNA-binding carbohydrates. *Biochem. Biophys. Res. Commun.* **270**, 899–902 (2000).
82. J. Sugiyama, D. C. Bowen, Z. W. Hall, Dystroglycan binds nerve and muscle agrin. *Neuron*. **13**, 103–115 (1994).
83. Y. Inoue, S. Hayashi, Tissue-specific laminin expression facilitates integrin-dependent association of the embryonic wing disc with the trachea in Drosophila. *Dev. Biol.* **304**, 90–101 (2007).
84. M. Narasimha, N. H. Brown, Novel functions for integrins in epithelial morphogenesis. *Curr. Biol.* **14**, 381–385 (2004).
85. H. R. Shcherbata, A. S. Yatsenko, L. Patterson, V. D. Sood, U. Nudel, D. Yaffe, D. Baker, H. Ruohola-Baker,

Dissecting muscle and neuronal disorders in a Drosophila model of muscular dystrophy. *Embo J.* **26**, 481–493 (2007).

86. L. Bogdanik, B. Framery, A. Froelich, B. Franco, D. Mornet, J. Bockaert, S. J. Sigrist, Y. Grau, M. L. Parmentier, Muscle Dystroglycan Organizes the Postsynapse and Regulates Presynaptic Neurotransmitter Release at the Drosophila Neuromuscular Junction. *PLoS One*. **3**, e2084 (2008).
87. M. Schneider, S. Baumgartner, Differential expression of Dystroglycan-spliceforms with and without the mucin-like domain during Drosophila embryogenesis. *Fly (Austin).* **2**, 29–35 (2008).
88. M. M. Kucherenko, M. Pantoja, A. S. Yatsenko, H. R. Shcherbata, K. A. Fischer, D. V. Maksymiv, Y. I. Chernyk, H. Ruohola-Baker, Genetic modifier screens reveal new components that interact with the Drosophila Dystroglycan-Dystrophin complex. *PLoS One*. **3**, e2418 (2008).
89. Y. G. Shi, J. Massague, Mechanisms of TGF-beta signaling from cell membrane to the nucleus. *Cell*. **113**, 685–700 (2003).
90. M. Lyon, G. Rushton, J. T. Gallagher, The interaction of the transforming growth factor-beta s with heparin heparan sulfate is isoform-specific. *J. Biol. Chem.* **272**, 18000–18006 (1997).
91. C. C. Rider, Heparin/heparan sulphate binding in the TGF-beta cytokine superfamily. *Biochem. Soc. Trans.* **34**, 458–460 (2006).
92. J. Garwood, O. Schnädelbach, A. Clement, K. Schütte, A. Bach, A. Faissner, DSD-1-proteoglycan is the mouse homolog of phosphacan and displays opposing effects on neurite outgrowth dependent on neuronal lineage. *J. Neurosci.* **19**, 3888–3899 (1999).
93. P. Maurel, U. Rauch, M. Flad, R. K. Margolis, R. U. Margolis, Phosphacan, a chondroitin sulfate proteoglycan of brain that interacts with neurons and neural cell-adhesion molecules, is an extracellular variant of a receptor-type protein tyrosine phosphatase. *Proc. Natl. Acad. Sci. U. S. A.* **91**, 2512–2516 (1994).
94. J. Filmus, M. Capurro, J. Rast, Glypicans. *Genome Biol.* **9**, 224 (2008).
95. H. Nakato, T. A. Futch, S. B. Selleck, THE DIVISION ABNORMALLY DELAYED (DALLY) GENE - A PUTATIVE INTEGRAL MEMBRANE PROTEOGLYCAN REQUIRED FOR CELL-DIVISION PATTERNING DURING POSTEMBRYONIC DEVELOPMENT OF THE NERVOUS-SYSTEM IN DROSOPHILA. *Development*. **121**, 3687–3702 (1995).
96. G. H. Baeg, X. Lin, N. Khare, S. Baumgartner, N. Perrimon, Heparan sulfate proteoglycans are critical for the organization of the extracellular distribution of Wingless. *Development*. **128**, 87–94 (2001).
97. X. H. Lin, N. Perrimon, Role of heparan sulfate proteoglycans in cell-cell signaling in Drosophila. *Matrix*

Biol. **19**, 303–307 (2000).

98. N. Dani, M. Nahm, S. Lee, K. Broadie, A Targeted Glycan-Related Gene Screen Reveals Heparan Sulfate Proteoglycan Sulfation Regulates WNT and BMP Trans-Synaptic Signaling. *PLoS Genet.* **8**, e1003031 (2012).
99. T. E. Haerry, T. R. Heslip, J. L. Marsh, M. B. Oconnor, Defects in glucuronate biosynthesis disrupt wingless signaling in Drosophila. *Development*. **124**, 3055–3064 (1997).
100. J. Filmus, S. B. Selleck, Glypicans: proteoglycans with a surprise. *J. Clin. Invest.* **108**, 497–501 (2001).
101. T. Rozario, D. W. DeSimone, The Extracellular Matrix In Development and Morphogenesis: A Dynamic View. *Dev. Biol.* **341**, 126–140 (2010).
102. C. Han, D. Yan, T. Y. Belenkaya, X. J. Lin, Drosophila glypicans Dally and Dally-like shape the extracellular Wingless morphogen gradient in the wing disc. *Development*. **132**, 667–679 (2005).
103. Y. Hayashi, S. Kobayashi, H. Nakato, Drosophila glypicans regulate the germline stem cell niche. *J. Cell Biol.* **187**, 473–480 (2009).
104. L. Hufnagel, J. Kreuger, S. M. Cohen, B. I. Shraiman, On the role of glypicans in the process of morphogen gradient formation. *Dev. Biol.* **300**, 512–522 (2006).
105. Y. Zhang, J. You, W. Ren, X. Lin, Drosophila glypicans Dally and Dally-like are essential regulators for JAK/STAT signaling and Unpaired distribution in eye development. *Dev. Biol.* **375**, 23–32 (2013).
106. G. H. Baeg, E. M. Selva, R. M. Goodman, R. Dasgupta, N. Perrimon, The Wingless morphogen gradient is established by the cooperative action of Frizzled and Heparan Sulfate Proteoglycan receptors. *Dev. Biol.* **276**, 89–100 (2004).
107. S. M. Jackson, H. Nakato, M. Sugiura, A. Jannuzi, R. Oakes, V. Kaluza, C. Golden, S. B. Selleck, dally, a Drosophila glypican, controls cellular responses to the TGF-beta-related morphogen, Dpp. *Development*. **124**, 4113–4120 (1997).
108. K. G. Johnson, A. P. Tenney, A. Ghose, A. M. Duckworth, M. E. Higashi, K. Parfitt, O. Marcu, T. R. Heslip, J. L. Marsh, T. L. Schwarz, J. G. Flanagan, D. Van Vactor, The HSPGs Syndecan and dallylike bind the receptor phosphatase LAR and exert distinct effects on synaptic development. *Neuron*. **49**, 517–531 (2006).
109. A. Gallet, L. Staccini-Lavenant, P. P. Thérond, Cellular Trafficking of the Glypican Dally-like Is Required for Full-Strength Hedgehog Signaling and Wingless Transcytosis. *Dev. Cell*. **14**, 712–725 (2008).
110. K. L. Ayers, A. Gallet, L. Staccini-Lavenant, P. P. Therond, The Long-Range Activity of Hedgehog Is Regulated in the Apical Extracellular Space by the Glypican Dally and the Hydrolase Notum. *Dev. Cell*.

18, 605–620 (2010).

111. Y. Wu, T. Y. Belenkaya, X. Lin, Dual roles of drosophila glypican dally-like in Wingless/Wnt signaling and distribution. *Methods Enzymol.* **480**, 33–50 (2010).
112. D. Yan, Y. Wu, Y. Feng, S.-C. Lin, X. Lin, The Core Protein of Glypican Daily-Like Determines Its Biphasic Activity in Wingless Morphogen Signaling. *Dev. Cell*. **17**, 470–481 (2009).
113. M. Yamauchi, M. Sricholpech, Lysine post-translational modifications of collagen. *Essays Biochem.* **52**, 113–33 (2012).
114. E. Lazar, G. Sirokmany, H. A. Kovacs, E. Klement, K. F. Medzihradszky, M. Geiszt, Structure-function analysis of peroxidasin provides insight into the mechanism of collagen IV crosslinking. *Free Radic Biol Med*. **83**, 273–282 (2015).
115. Z. Péterfi, A. Donkó, A. Orient, A. Sum, A. Prókai, B. Molnár, Z. Veréb, E. Rajnavölgyi, K. J. Kovács, V. Müller, A. J. Szabó, M. Geiszt, Peroxidasin is secreted and incorporated into the extracellular matrix of myofibroblasts and fibrotic kidney. *Am. J. Pathol.* **175**, 725–35 (2009).
116. M. Soudi, M. Paumann-Page, C. Delporte, K. F. Pirker, M. Bellei, E. Edenhofer, G. Stadlmayr, G. Battistuzzi, K. Z. Boudjeltia, P. G. Furtmüller, P. Van Antwerpen, C. Obinger, Multidomain human peroxidasin 1 is a highly glycosylated and stable homotrimeric high spin ferric peroxidase. *J. Biol. Chem.* **290**, 10876–10890 (2015).
117. M. V. Nurminskaya, A. M. Belkin, Cellular functions of tissue transglutaminase. *Int. Rev. Cell Mol. Biol.* **294**, 1–97 (2013).
118. J. Molnar, Z. Ujfaludi, S. F. T. Fong, J. A. Bollinger, G. Waro, B. Fogelgren, D. M. Dooley, M. Mink, K. Csiszar, Drosophila lysyl oxidases Dmloxl-1 and Dmloxl-2 are differentially expressed and the active DmLOXL-1 influences gene expression and development. *J. Biol. Chem.* **280**, 22977–22985 (2005).
119. S. N. Kim, A. Jeibmann, K. Halama, H. T. Witte, M. Walte, T. Matzat, H. Schillers, C. Faber, V. Senner, W. Paulus, C. Klambt, ECM stiffness regulates glial migration in Drosophila and mammalian glioma models. *Development*. **141**, 3233–3242 (2014).
120. G. Bhave, C. F. Cummings, R. M. Vanacore, C. Kumagai-Cresse, I. A. Ero-Tolliver, M. Rafi, J. S. Kang, V. P. Pedchenko, L. I. Fessler, J. H. Fessler, B. G. Hudson, Peroxidasin Forms Sulfilimine Chemical Bonds Using Hypohalous Acids In Tissue Genesis. *Nat. Chem. Biol.* **8**, 784–790 (2012).
121. A. S. McCall, C. F. Cummings, G. Bhave, R. Vanacore, A. Page-Mccaw, B. G. Hudson, Bromine is an essential trace element for assembly of collagen IV scaffolds in tissue development and architecture. *Cell*. **157**, 1380–1392 (2014).

122. T. Shibata, S. Kawabata, Pluripotency and a secretion mechanism of Drosophila transglutaminase. *J. Biochem.* (2017), doi:10.1093/jb/mvx059.

123. T. Shibata, J. Hadano, D. Kawasaki, X. Dong, S. Kawabata, Drosophila TG-A transglutaminase is secreted via an unconventional Golgi-independent mechanism involving exosomes and two types of fatty acylations. *J. Biol. Chem.* **292**, 10723–10734 (2017).

124. T. Shibata, S. Ariki, N. Shinzawa, R. Miyaji, H. Suyama, M. Sako, N. Inomata, T. Koshiba, H. Kanuka, S. I. Kawabata, Protein crosslinking by transglutaminase controls cuticle morphogenesis in Drosophila. *PLoS One*. **5**, e13477 (2010).

125. V. S. Tagliabracci, J. L. Engel, J. Wen, S. E. Wiley, A. Carolyn, L. N. Kinch, J. Xiao, N. V Grishin, J. E. Dixon, Secreted Kinase Phosphorylated Extracellular Proteins That Regulate Biomineralization. *Science.* **336**, 1150–1153 (2012).

126. V. Vreys, G. David, Mammalian heparanase : what is the message ? *J. Cell. Mol. Med.* **11**, 427–452 (2007).

127. X. B. Ai, A. T. Do, M. Kusche-Gullberg, U. Lindahl, K. Lu, C. P. Emerson, Substrate specificity and domain functions of extracellular heparan sulfate 6-O-endosulfatases, QSulf1 and QSulf2. *J. Biol. Chem.* **281**, 4969–4976 (2006).

128. W. C. Lamanna, M. A. Frese, M. Balleininger, T. Dierks, Sulf loss influences N-, 2-O-, and 6-O-sulfation of multiple heparan sulfate proteoglycans and modulates fibroblast growth factor signaling. *J. Biol. Chem.* **283**, 27724–27735 (2008).

129. C. R. Holst, H. Bou-Reslan, B. B. Gore, K. Wong, D. Grant, S. Chalasani, R. A. Carano, G. D. Frantz, M. Tessier-Lavigne, B. Bolon, D. M. French, A. Ashkenazi, Secreted Sulfatases Sulf1 and Sulf2 Have Overlapping yet Essential Roles in Mouse Neonatal Survival. *PLoS One*. **2**, e575 (2007).

130. A. Kleinschmit, M. Takemura, K. Dejima, P. Y. Choi, H. Nakato, Drosophila heparan sulfate 6-o-endosulfatase sulf1 facilitates wingless (Wg) protein degradation. *J. Biol. Chem.* **288**, 5081–5089 (2013).

131. D. R. Taylor, N. M. Hooper, GPI-Anchored Proteins in Health and Disease. *Protein Rev.* **13**, 39–55 (2011).

132. A. Traister, W. Shi, J. Filmus, Mammalian Notum induces the release of glypicans and other GPI-anchored proteins from the cell surface. *Biochem. J.* **410**, 503–11 (2008).

133. S. Kakugawa, P. F. Langton, M. Zebisch, S. Howell, Y. Liu, T. Feizi, G. Bineva, N. O. Reilly, A. P. Snijders, Y. Jones, J. Vincent, Notum deacylates Wnts to suppress signalling activity. *Nature*. **519**, 187–192 (2015).

134. A. Kleinschmit, T. Koyama, K. Dejima, Y. Hayashi, K. Kamimura, H. Nakato, Drosophila heparan sulfate 6-O endosulfatase regualtes Wingless morphogen gradient formation. *Dev. Biol.* **345**, 204–214 (2010).

135. K. Dejima, A. Kleinschmit, M. Takemura, P. Y. Choi, A. Kinoshita-Toyoda, H. Toyoda, H. Nakato, The role of drosophila heparan sulfate 6-O-endosulfatase in sulfation compensation. *J. Biol. Chem.* **288**, 6574–6582 (2013).

136. K. Kamimura, T. Koyama, H. Habuchi, R. Ueda, M. Masu, K. Kimata, H. Nakato, Specific and flexible roles of heparan sulfate modifications in Drosophila FGF signaling. *J. Cell Biol.* **174**, 773–778 (2006).

137. A. Wojcinski, H. Nakato, C. Soula, B. Glise, DSulfatase-1 fine-tunes Hedgehog patterning activity through a novel regulatory feedback loop. *Dev. Biol.* **358**, 168–180 (2011).

138. O. Gerlitz, K. Basler, Wingful, an extracellular feedback inhibitor of Wingless. *Genes Dev.* **16**, 1055–1059 (2002).

139. C. M. Overall, C. P. Blobel, In search of partners: linking extracellular proteases to substrates. *Nat. Rev. Mol. Cell Biol.* **8**, 245–257 (2007).

140. N. Fortelny, J. H. Cox, R. Kappelhoff, A. E. Starr, P. F. Lange, P. Pavlidis, C. M. Overall, Network Analyses Reveal Pervasive Functional Regulation Between Proteases in the Human Protease Web. *PLoS Biol.* **12**, e1001869 (2014).

141. D. Rodríguez, C. J. Morrison, C. M. Overall, Matrix metalloproteinases: What do they not do? New substrates and biological roles identified by murine models and proteomics. *Biochim. Biophys. Acta - Mol. Cell Res.* **1803**, 39–54 (2010).

142. P. Schlage, U. auf dem Keller, Proteomic approaches to uncover MMP function. *Matrix Biol.* **44–46**, 232–238 (2015).

143. U. Eckhard, G. Marino, G. S. Butler, C. M. Overall, Positional proteomics in the era of the human proteome project on the doorstep of precision medicine. *Biochimie*. **122**, 110–118 (2016).

144. S. Patel, A critical review on serine protease: Key immune manipulator and pathology mediator. *Allergol Immunopathol (Madr)*. **45**, 579–591 (2017).

145. E. Di Cera, Serine Proteases. *IUBMB Life*. **61**, 510–515 (2009).

146. F. X. Gomiz-Rüth, Catalytic domain architecture of metzincin metalloproteases. *J. Biol. Chem.* **284**, 15353–15357 (2009).

147. N. M. Hooper, Families of zinc metalloproteases. *FEBS Lett.* **354**, 1–6 (1994).

148. D. Singh, S. K. Srivastava, T. K. Chaudhuri, G. Upadhyay, Multifaceted role of matrix metalloproteinases (MMPs). *Front. Mol. Biosci.* **2**, 19 (2015).

149. M. Fanjul-Fernández, A. R. Folgueras, S. Cabrera, C. López-Otín, Matrix metalloproteinases: Evolution, gene regulation and functional analysis in mouse models. *Biochim. Biophys. Acta - Mol. Cell Res.* **1803**,

3–19 (2010).

150. L. Sevenich, J. A. Joyce, Pericellular proteolysis in cancer. *Genes Dev.* **28**, 2331–2347 (2014).

151. P. Lu, K. Takai, V. M. Weaver, Z. Werb, Extracellular matrix degradation and remodeling in development and disease. *Cold Spring Harb Perspect Biol*. **3**, a005058 (2011).

152. E. E. Sterchi, W. Stocker, J. S. Bond, Meprins, membrane-bound and secreted astacin metalloproteinases. *Mol Asp. Med*. **29**, 309–328 (2008).

153. S. Vadon-Le Goff, D. J. S. Hulmes, C. Moali, BMP-1/tolloid-like proteinases synchronize matrix assembly with growth factor activation to promote morphogenesis and tissue remodeling. *Matrix Biol.* **44–46**, 14–23 (2015).

154. J. Gaffney, I. Solomonov, E. Zehorai, I. Sagi, Multilevel regulation of matrix metalloproteinases in tissue homeostasis indicates their molecular specificity in vivo. *Matrix Biol.* **44–46**, 191–199 (2015).

155. D. F. Seals, S. A. Courtneidge, The ADAMs family of metalloproteases: Multidomain proteins with multiple functions. *Genes Dev.* **17**, 7–30 (2003).

156. H. Yi, J. Gruszczynska-Biegala, D. Wood, Z. Zhao, A. Zolkiewska, Cooperation of the metalloprotease, disintegrin, and cysteine-rich domains of ADAM12 during inhibition of myogenic differentiation. *J. Biol. Chem.* **280**, 23475–23483 (2005).

157. M. Kashiwagi, M. Tortorella, H. Nagase, K. Brew, TIMP-3 Is a Potent Inhibitor of Aggrecanase 1 (ADAM-TS4) and Aggrecanase 2 (ADAM-TS5). *J. Biol. Chem.* **276**, 12501–12504 (2001).

158. G. Murphy, Tissue inhibitors of metalloproteinases. *Genome Biol.* **12**, 233 (2011).

159. C. Streuli, Extracellular matrix remodelling and cellular differentiation. *Curr. Opin. Cell Biol.* **11**, 634–640 (1999).

160. M. Tortorella, M. Pratta, R. Q. Liu, I. Abbaszade, H. Ross, T. Burn, E. Arner, The thrombospondin motif of Aggrecanase-1 (ADAMTS-4) is critical for aggrecan substrate recognition and cleavage. *J. Biol. Chem.* **275**, 25791–25797 (2000).

161. C. Karlsson, A. M. Korayem, C. Scherfer, O. Loseva, M. S. Dushay, U. Theopold, Proteomic analysis of the Drosophila larval hemolymph clot. *J. Biol. Chem.* **279**, 52033–52041 (2004).

162. R. A. Patterson, M. T. Juarez, A. Hermann, R. Sasik, G. Hardiman, W. McGinnis, Serine Proteolytic Pathway Activation Reveals an Expanded Ensemble of Wound Response Genes in Drosophila. *PLoS One*. **8**, e61773 (2013).

163. D. S. Schneider, Y. Jin, D. Morisato, K. V Anderson, A processed form of the Spätzle protein defines dorsal-ventral polarity in the Drosophila embryo. *Development*. **120**, 1243–1250 (1994).

164. A. S. Hammonds, J. W. Fristrom, Mutational analysis of stubble-stubbloid gene structure and function in drosophila leg and bristle morphogenesis. *Genetics*. **172**, 1577–1593 (2006).

165. L. F. Appel, M. Prout, R. Abu-Shumays, A. Hammonds, J. C. Garbe, D. Fristrom, J. Fristrom, The Drosophila Stubble-stubbloid gene encodes an apparent transmembrane serine protease required for epithelial morphogenesis. *Proc. Natl. Acad. Sci. U. S. A.* **90**, 4937–4941 (1993).

166. R. Chasan, Y. Jin, K. V Anderson, Activation of the easter zymogen is regulated by five other genes to define dorsal-ventral polarity in the Drosophila embryo. *Development*. **115**, 607–616 (1992).

167. J. H. Han, H. Y. Zhang, G. S. Min, D. Kemler, C. Hashimoto, A novel Drosophila serpin that inhibits serine proteases. *FEBS Lett.* **468**, 194–198 (2000).

168. A. Sawala, C. Sutcliffe, H. L. Ashe, Multistep molecular mechanism for Bone morphogenetic protein extracellular transport in the Drosophila embryo. *Proc. Natl. Acad. Sci.* **109**, 11222–11227 (2012).

169. K. Yu, S. Srinivasan, O. Shimmi, B. Biehs, K. E. Rashka, D. Kimelman, M. B. O'Connor, E. Bier, E. Bier, Processing of the Drosophila Sog protein creates a novel BMP inhibitory activity. *Development*. **127**, 2143–2154 (2000).

170. A. L. Finelli, T. Xie, C. A. Bossie, R. K. Blackman, R. W. Padgett, The tolkin gene is a tolloid/BMP-1 homologue that is essential for Drosophila development. *Genetics*. **141**, 271–281 (1995).

171. T. Nguyen, J. Jamal, M. J. Shimell, K. Arora, M. B. O'Connor, Characterization of tolloid-related-1: a BMP-1-like product that is required during larval and pupal stages of Drosophila development. *Dev Biol.* **166**, 569–586 (1994).

172. M. Serpe, M. B. O'Connor, The metalloprotease tolloid-related and its TGF-beta-like substrate Dawdle regulate Drosophila motoneuron axon guidance. *Development*. **133**, 4969–4979 (2006).

173. L. A. Raftery, V. Twombly, K. Wharton, W. M. Gelbart, Genetic screens to identify elements of the decapentaplegic signaling pathway in Drosophila. *Genetics*. **139**, 241–254 (1995).

174. S. Albrecht, S. Wang, A. Holz, A. Bergter, A. Paululat, The ADAM metalloprotease Kuzbanian is crucial for proper heart formation in Drosophila melanogaster. *Mech. Dev.* **123**, 372–387 (2006).

175. H. Meyer, M. Panz, S. Albrecht, M. Drechsler, S. Wang, M. Hüsken, C. Lehmacher, A. Paululat, Drosophila metalloproteases in development and differentiation: The role of ADAM proteins and their relatives. *Eur. J. Cell Biol.* **90**, 770–778 (2011).

176. H. Meyer, T. Von Ohlen, M. Panz, A. Paululat, The disintegrin and metalloprotease Meltrin from Drosophila forms oligomers via its protein binding domain and is regulated by the homeobox protein VND during embryonic development. *Insect Biochem. Mol. Biol.* **40**, 814–823 (2010).

177. M. L. Moss, S. L. Jin, M. E. Milla, D. M. Bickett, W. Burkhart, H. L. Carter, W. J. Chen, W. C. Clay, J. R. Didsbury, D. Hassler, C. R. Hoffman, T. a Kost, M. H. Lambert, M. a Leesnitzer, P. McCauley, G. McGeehan, J. Mitchell, M. Moyer, G. Pahel, *et al.*, Cloning of a disintegrin metalloproteinase that processes precursor tumour-necrosis factor-alpha. *Nature*. **385**, 733–736 (1997).

178. J. H. Fessler, I. Kramerova, A. Kramerov, Y. Chen, L. I. Fessler, Papilin, a novel component of basement membranes, in relation to ADAMTS metalloproteases and ECM development. *Int. J. Biochem. Cell Biol.* **36**, 1079–1084 (2004).

179. I. A. Kramerova, Papilin in development. **5485**, 5475–5485 (2000).

180. S. Soleman, M. A. Filippov, A. Dityatev, J. W. Fawcett, Targeting the neural extracellular matrix in neurological disorders. *Neuroscience*. **253**, 194–213 (2013).

181. A. Dityatev, M. Schachner, The extracellular matrix and synapses. *Cell Tissue Res.* **326**, 647–654 (2006).

182. K. Menon, R. Carrillo, K. Zinn, Development and Plasticity of Drosophila Larval Neuromuscular Junction. *Dev. Biol.* **2**, 647–670 (2013).

183. H. Keshishian, K. Broadie, A. Chiba, M. Bate, The drosophila neuromuscular junction: a model system for studying synaptic development and function. *Annu. Rev. Neurosci.* **19**, 545–575 (1996).

184. K. S. Broadie, M. Bate, Development of the embryonic neuromuscular synapse of drosophila-melanogaster. *J. Neurosci.* **13**, 144–166 (1993).

185. H. T. Wu, W. C. Xiong, L. Mei, To build a synapse: signaling pathways in neuromuscular junction assembly. *Development*. **137**, 1017–1033 (2010).

186. A. Prokop, Organization of the efferent system and structure of neuromuscular junctions in Drosophila. *Int. Rev. Neurobiol.* **75**, 71–90 (2006).

187. L. Y. Jan, Y. N. Jan, L-glutamate as an excitatory transmitter at Drosophila larval neuromuscular junction. *J. Physiol.* **262**, 215–236 (1976).

188. B. L. Patton, Basal lamina and the organization of neuromuscular synapses. *J. Neurocytol.* **32**, 883–903 (2003).

189. L. Reiter, L. Potocki, S. Chien, M. Gribskov, E. Bier, A Systematic Analysis of Human Disease-Associated Gene Sequences In Drosophila melanogaster. *Genome Res.*, 1114–1125 (2001).

190. A. Salzberg, H. J. Bellen, Invertebrate versus vertebrate neurogenesis: Variations on the same theme? *Dev Genet*. **18**, 1–10 (1996).

191. C. L. Gatto, K. Broadie, Drosophila modeling of heritable neurodevelopmental disorders. *Curr. Opin. Neurobiol.* **21**, 834–841 (2011).

192. B. Ugur, K. Chen, H. J. Bellen, *Drosophila* tools and assays for the study of human diseases. *Dis. Model. Mech.* **9**, 235–244 (2016).

193. M. Landgraf, T. Bossing, G. M. Technau, M. Bate, The origin, location, and projections of the embryonic abdominal motorneurons of Drosophila. *J. Neurosci.* **17**, 9642–9655 (1997).

194. a Schmid, a Chiba, C. Q. Doe, Clonal analysis of Drosophila embryonic neuroblasts: neural cell types, axon projections and muscle targets. *Development*. **126**, 4653–4689 (1999).

195. J. Johansen, M. E. Halpern, K. M. Johansen, H. Keshishian, stereotypic morphology of glutamatergic synapses on identified muscle-cells of drosophila larvae. *J. Neurosci.* **9**, 710–725 (1989).

196. J. Johansen, M. E. Halpern, H. Keshishian, AXONAL GUIDANCE AND THE DEVELOPMENT OF MUSCLE-FIBER SPECIFIC INNERVATION IN DROSOPHILA EMBRYOS. *J. Neurosci.* **9**, 4318–4332 (1989).

197. M. Bate, K. Broadie, Wiring by fly - the neuromuscular system of the drosophila embryo. *Neuron*. **15**, 513–525 (1995).

198. K. S. Broadie, Synaptogenesis in Drosophila- coupling genetics and electrophysiology. *J. Physiol.* **88**, 123–139 (1994).

199. C. Feeney, S. Karunanithi, J. Pearce, C. Govind, H. Atwood, Motor nerve terminals on abdominal muscles in larval flesh flies, Sarcophaga bullata: comparisons with Drosophila. *J Comp Neurol*. **402**, 197–209 (1998).

200. D. A. Wagh, T. M. Rasse, E. Asan, A. Hofbauer, I. Schwenkert, H. Dürrbeck, S. Buchner, M. C. Dabauvalle, M. Schmidt, G. Qin, C. Wichmann, R. Kittel, S. J. Sigrist, E. Buchner, Bruchpilot, a protein with homology to ELKS/CAST, is required for structural integrity and function of synaptic active zones in Drosophila. *Neuron*. **49**, 833–844 (2006).

201. I. A. Meinertzhagen, C. K. Govind, B. A. Stewart, J. M. Carter, H. L. Atwood, Regulated spacing of synapses and presynaptic active zones at larval neuromuscular junctions in different genotypes of the flies Drosophila and Sarcophaga. *J. Comp. Neurol.* **393**, 482–492 (1998).

202. A. Prokop, M. Landgraf, E. Rushton, K. Broadie, M. Bate, Presynaptic development at the Drosophila neuromuscular junction: Assembly and localization of presynaptic active zones. *Neuron*. **17**, 617–626 (1996).

203. A. A. Long, E. Kim, H. T. Leung, E. Woodruff, L. An, R. W. Doerge, W. L. Pak, K. Broadie, Presynaptic calcium channel localization and calcium-dependent synaptic vesicle exocytosis regulated by the fuseless protein. *J. Neurosci.* **28**, 3668–3682 (2008).

204. S. B. Marrus, A. DiAntonio, Preferential localization of glutamate receptors opposite sites of high

presynaptic release. *Curr. Biol.* **14**, 924–931 (2004).

205. W. Fouquet, D. Owald, C. Wichmann, S. Mertel, H. Depner, M. Dyba, S. Hallermann, R. J. Kittel, S. Eimer, S. J. Sigrist, Maturation of active zone assembly by Drosophila Bruchpilot. *J. Cell Biol.* **186**, 129–145 (2009).

206. L. S. Gramates, V. Budnik, Assembly and maturation of the Drosophila larval neuromuscular junction. *Int. Rev. Neurobiol.* **43**, 93–100 (1999).

207. S. J. Sigrist, D. F. Reiff, P. R. Thiel, J. R. Steinert, C. M. Schuster, Experience-dependent strengthening of Drosophila neuromuscular junctions. *J. Neurosci.* **23**, 6546–6556 (2003).

208. C. M. Schuster, G. W. Davis, R. D. Fetter, C. S. Goodman, Genetic Dissection of Structural and Functional Components of Synaptic Plasticity. II. Fasciclin II Controls Presynaptic Structural Plasticity. *Neuron*. **17**, 655–667 (1996).

209. I. U. Haussmann, K. White, M. Soller, Erect wing regulates synaptic growth in Drosophila by integration of multiple signaling pathways. *Genome Biol.* **9**, R73 (2008).

210. K. Zito, D. Parnas, R. D. Fetter, E. Y. Isacoff, C. S. Goodman, Watching a synapse grow: Noninvasive confocal imaging of synaptic growth in Drosophila. *Neuron*. **22**, 719–729 (1999).

211. D. Rendic, M. Sharrow, T. Katoh, B. Overcarsh, K. Nguyen, J. Kapurch, K. Aoki, I. B. H. Wilson, M. Tiemeyer, Neural-specific alpha 3-fucosylation of N-linked glycans in the Drosophila embryo requires Fucosyltransferase A and influences developmental signaling associated with O-glycosylation. *Glycobiology*. **20**, 1353–1365 (2010).

212. L. Y. Jan, Y. N. Jan, Antibodies to horseradish-peroxidase as specific neuronal markers in drosophila and in grasshopper embryos. *Proc. Natl. Acad. Sci. United States Am. Sci.* **79**, 2700–2704 (1982).

213. Y. Fuentes-Medel, M. A. Logan, J. Ashley, B. Ataman, V. Budnik, M. R. Freeman, Glia and muscle sculpt neuromuscular arbors by engulfing destabilized synaptic boutons and shed presynaptic debris. *PLoS Biol.* **7**, e1000184 (2009).

214. B. Ataman, J. Ashley, M. Gorczyca, P. Ramachandran, W. Fouquet, S. J. Sigrist, V. Budnik, Rapid activity-dependent modifications in synaptic structure and function require bidirectional Wnt signaling. *Neuron*. **57**, 705–718 (2008).

215. K. Menon, R. Carrillo, K. Zinn, Development and Plasticity of the Drosophila Larval Neuromuscular Junction. *Wiley Interdiscip. Rev. Dev. Biol.* **2**, 647–670 (2013).

216. M. Packard, E. S. Koo, M. Gorczyca, J. Sharpe, S. Cumberledge, V. Budnik, The Drosophila Wnt, wingless, provides an essential signal for pre- and postsynaptic differentiation. *Cell*. **111**, 319–330 (2002).

217. B. A. Eaton, R. D. Fetter, G. W. Davis, Dynactin is necessary for synapse stabilization. *Neuron*. **34**, 729–741 (2002).

218. B. Ataman, V. Budnik, U. Thomas, Scaffolding Proteins at the Drosophila Neuromuscular Junction. *Int. Rev. Neurobiol.* **75**, 181–216 (2006).

219. D. E. Featherstone, E. Rushton, J. Rohrbough, F. Liebl, J. Karr, Q. Sheng, C. K. Rodesch, K. Broadie, An essential Drosophila glutamate receptor subunit that functions in both central neuropil and neuromuscular junction. *J. Neurosci.* **25**, 3199–3208 (2005).

220. G. Qin, T. Schwarz, R. J. Kittel, A. Schmid, T. M. Rasse, D. Kappei, E. Ponimaskin, M. Heckmann, S. J. Sigrist, Four Different Subunits Are Essential for Expressing the Synaptic Glutamate Receptor at Neuromuscular Junctions of Drosophila. *J. Neurosci.* **25**, 3209–3218 (2005).

221. A. DiAntonio, S. A. Petersen, M. Heckmann, C. S. Goodman, Glutamate receptor expression regulates quantal size and quantal content at the Drosophila neuromuscular junction. *J. Neurosci.* **19**, 3023–3032 (1999).

222. T. H. Han, P. Dharkar, M. L. Mayer, M. Serpe, Functional reconstitution of Drosophila melanogaster NMJ glutamate receptors. *Proc. Natl. Acad. Sci. U. S. A.* **112**, 6182–7 (2015).

223. K. Chen, D. E. Featherstone, Discs-large (DLG) is clustered by presynaptic innervation and regulates postsynaptic glutamate receptor subunit composition in Drosophila. *BMC Biol.* **3**, 1 (2005).

224. A. Fukui, M. Inaki, G. Tonoe, H. Hamatani, M. Homma, T. Morimoto, H. Aburatani, A. Nose, Lola regulates glutamate receptor expression at the Drosophila neuromuscular junction. *Biol. Open*. **1**, 362–375 (2012).

225. H. G. Lee, N. Zhao, B. K. Campion, M. M. Nguyen, S. B. Selleck, Akt regulates glutamate receptor trafficking and postsynaptic membrane elaboration at the Drosophila neuromuscular junction. *Dev. Neurobiol.* **73**, 723–743 (2013).

226. E. S. Heckscher, R. D. Fetter, K. W. Marek, S. D. Albin, W. Davis, NF-κB, I-κB and IRAK Control Glutamate Receptor Density at the Drosophila NMJ. *Neuron*. **55**, 859–873 (2007).

227. J. Staples, K. Broadie, The cell polarity scaffold Lethal Giant Larvae regulates synapse morphology and function. *J. Cell Sci.* **126**, 1992–2003 (2013).

228. A. Schmid, S. Hallermann, R. J. Kittel, O. Khorramshahi, A. M. J. Frolich, C. Quentin, Activity-dependent site-specific changes of glutamate receptor composition in vivo. *Nat. N*. **11**, 659–666 (2008).

229. C. A. Frank, J. Pielage, G. W. Davis, A Presynaptic Homeostatic Signaling System Composed of the Eph Receptor , Ephexin , Cdc42 , and Ca V 2 . 1 Calcium Channels. *Neuron*. **61**, 556–569 (2009).

230. A. DiAntonio, Glutamate receptors at the Drosophila neuromuscular junction. *Int. Rev. Neurobiol.* **75**, 165–179 (2006).

231. G. Davis, G. Goodman, Synapse-specific control of synaptic efficacy at the terminals of a single neuron. *Nature*. **392**, 82–86 (1998).

232. G. W. Davis, A. DiAntonio, S. A. Petersen, C. S. Goodman, Postsynaptic PKA controls quantal size and reveals a retrograde signal that regulates presynaptic transmitter release in Drosophila. *Neuron*. **20**, 305–315 (1998).

233. S. A. Petersen, R. D. Fetter, J. N. Noordermeer, C. S. Goodman, A. DiAntonio, Genetic analysis of glutamate receptors in Drosophila\rreveals a retrograde signal regulating presynaptic\rtransmitter release. *Neuron*. **19**, 1237–1248 (1997).

234. R. J. Kittel, S. Hallermann, S. Thomsen, C. Wichmann, S. J. Sigrist, M. Heckmann, Active zone assembly and synaptic release. *Biochem. Soc. Trans.* **34**, 939–941 (2006).

235. T. Tabata, Morphogens, their identification and regulation. *Development*. **131**, 703–712 (2004).

236. G. P. Solis, A. M. Lüchtenborg, V. L. Katanaev, Wnt secretion and gradient formation. *Int. J. Mol. Sci.* **14**, 5130–5145 (2013).

237. C. Wu, R. Nusse, Ligand Receptor Interactions in the Wnt Signaling Pathway in Drosophila. *J. Biol. Chem.* **277**, 41762–41769 (2002).

238. K. Saito-diaz, T. W. Chen, X. Wang, C. a Thorne, H. a Wallace, A. Page-mccaw, E. Lee, The way Wnt works: Components and mechanism. *Growth Factors*. **31**, 1–31 (2013).

239. C. Korkut, V. Budnik, WNTs tune up the neuromuscular junction. *Nat. Rev. Neurosci.* **10**, 627–634 (2009).

240. R. van Amerongen, Alternative Wnt pathways and receptors. *Cold Spring Harb. Perspect. Biol.* **4**, a007914 (2012).

241. V. Y. Poon, S. Choi, M. Park, Growth factors in synaptic function. *Front. Synaptic Neurosci.* **5**, 6 (2013).

242. G. Marques, Morphogens and synaptogenesis in Drosophila. *J. Neurobiol.* **64**, 417–434 (2005).

243. K. M. Cadigan, R. Nusse, Wnt signaling: a common theme in animal development. *Genes Dev.* **11**, 3286–3305 (1997).

244. C. A. Oliva, J. Y. Vargas, N. C. Inestrosa, Wnts in adult brain: from synaptic plasticity to cognitive deficiencies. *Front. Cell. Neurosci.* **7**, 224 (2013).

245. V. Kwan, B. K. Unda, K. K. Singh, Wnt signaling networks in autism spectrum disorder and intellectual disability. *J. Neurodev. Disord.* **8**, 45 (2016).

246. T. Zhan, N. Rindtorff, M. Boutros, Wnt signaling in cancer. *Oncogene*. **36**, 1461–1473 (2017).

247. G. V De Ferrari, R. T. Moon, The ups and downs of Wnt signaling in prevalent neurological disorders. *Oncogene*. **25**, 7545–7553 (2006).

248. M. Llimargas, P. a Lawrence, Seven Wnt homologues in Drosophila: a case study of the developing tracheae. *Proc. Natl. Acad. Sci. U. S. A.* **98**, 14487–14492 (2001).

249. C. Nüsslein-Volhard, E. Wieschaus, Mutations affecting segment number and polarity in Drosophila. *Nature*. **287**, 795–801 (1980).

250. T. Malinauskas, E. Y. Jones, Extracellular modulators of Wnt signalling. *Curr. Opin. Struct. Biol.* **29**, 77–84 (2014).

251. D. Kopke, S. Lima, C. Alexandre, K. Broadie, Notum coordinates synapse development via extracellular regulation of Wingless trans-synaptic signaling. *Development*. **144**, 3499–3510 (2017).

252. F. L. W. Liebl, Y. P. Wu, D. E. Featherstone, J. N. Noordermeer, L. Fradkin, H. Hing, Derailed regulates development of the Drosophila neuromuscular junction. *Dev. Neurobiol.* **68**, 152–165 (2008).

253. F. L. W. Liebl, C. McKeown, Y. Yao, H. K. Hing, Mutations in Wnt2 Alter Presynaptic Motor Neuron Morphology and Presynaptic Protein Localization at the Drosophila Neuromuscular Junction. *PLoS One*. **5**, e12778 (2010).

254. M. van den Heuvel, R. Nusse, P. Johnston, P. Lawrence, Distribution of the wingless gene product in Drosophila embryos: a protein involved in cell-cell communication. *Cell*. **59**, 739–749 (1989).

255. C. Miech, H. U. Pauer, X. He, T. L. Schwarz, Presynaptic Local Signaling by a Canonical Wingless Pathway Regulates Development of the Drosophila Neuromuscular Junction. *J. Neurosci.* **28**, 10875–10884 (2008).

256. C. Korkut, B. Ataman, P. Ramachandran, J. Ashley, R. Barria, N. Gherbesi, V. Budnik, Trans-Synaptic Transmission of Vesicular Wnt Signals through Evi/Wntless. *Cell*. **139**, 393–404 (2009).

257. K. S. Kerr, Y. Fuentes-Medel, C. Brewer, R. Barria, J. Ashley, K. C. Abruzzi, A. Sheehan, O. E. Tasdemir-Yilmaz, M. R. Freeman, V. Budnik, Glial wingless/Wnt regulates glutamate receptor clustering and synaptic physiology at the Drosophila neuromuscular junction. *J. Neurosci.* **34**, 2910–2920 (2014).

258. A. Luchtenborg, G. P. Solis, D. Egger-adam, A. Koval, C. Lin, M. G. Blanchard, S. Kellenberger, V. L. Katanaev, Heterotrimeric Go protein links Wnt-Frizzled signaling with ankyrins to regulate the neuronal microtubule cytoskeleton. *Development*. **141**, 3399–3409 (2014).

259. D. Mathew, B. Ataman, J. Chen, Y. Zhang, S. Cumberledge, V. Budnik, Wingless Signaling at Synapses Is Through Cleavage and Nuclear Import of Receptor DFrizzled2. *Science*. **310**, 1344–1347 (2005).

260. T. J. Mosca, T. L. Schwarz, The nuclear import of Frizzled2-C by Importins-beta 11 and alpha 2 promotes postsynaptic development. *Nat. Neurosci.* **13**, 935–943 (2010).

261. B. Ataman, J. Ashley, D. Gorczyca, M. Gorczyca, D. Mathew, C. Wichmann, S. J. Sigrist, V. Budnik, Nuclear trafficking of Drosophila Frizzled-2 during synapse development requires the PDZ protein dGRIP. *Proc. Natl. Acad. Sci. U. S. A.* **103**, 7841–7846 (2006).

262. S. D. Speese, J. Ashley, V. Jokhi, J. Nunnari, R. Barria, Y. Li, B. Ataman, A. Koon, Y.-T. Chang, Q. Li, M. J. Moore, V. Budnik, Nuclear envelope budding enables large ribonucleoprotein particle export during synaptic Wnt signaling. *Cell*. **149**, 832–846 (2012).

263. A. L. Franciscovich, A. A. V Mortimer, A. A. Freeman, J. Gu, S. Sanyal, Overexpression Screen in Drosophila Identifies Neuronal Roles of GSK-3 beta/shaggy as a Regulator of AP-1-Dependent Developmental Plasticity. *Genetics*. **180**, 2057–2071 (2008).

264. B. Franco, L. Bogdanik, Y. Bobinnec, A. Debec, J. R. L. Bockaert, M. L. Parmentier, Y. Grau, Shaggy, the homolog of glycogen synthase kinase 3, controls neuromuscular junction growth in Drosophila. *J. Neurosci.* **24**, 6573–6577 (2004).

265. A. Vasin, L. Zueva, C. Torrez, D. Volfson, J. T. Littleton, M. Bykhovskaia, Synapsin regulates activity-dependent outgrowth of synaptic boutons at the Drosophila neuromuscular junction. *J. Neurosci.* **34**, 10554–10563 (2014).

266. S. H. Friedman, N. Dani, E. Rushton, K. Broadie, Fragile X mental retardation protein regulates trans-synaptic signaling in Drosophila. *Dis. Model. Mech.* **6**, 1400–1413 (2013).

267. Y. Ren, C. A. Kirkpatrick, J. M. Rawson, M. Sun, S. B. Selleck, Cell Type-Specific Requirements for Heparan Sulfate Biosynthesis at the Drosophila Neuromuscular Junction: Effects on Synapse Function, Membrane Trafficking, and Mitochondrial Localization. *J. Neurosci.* **29**, 8539–8550 (2009).

268. K. Kamimura, N. Maeda, Heparan sulfate proteoglycans in Drosophila neuromuscular development. *Biochim. Biophys. Acta - Gen. Subj.* **1861**, 2442–2446 (2017).

269. S. T. Ngo, P. G. Noakes, W. D. Phillips, Neural agrin: A synaptic stabiliser. *Int. J. Biochem. Cell Biol.* **39**, 863–867 (2007).

270. P. T. Martin, J. R. Sanes, Integrins mediate adhesion to agrin and modulate agrin signaling. *Development*. **124**, 3909–3917 (1997).

271. B. G. Wallace, THE MECHANISM OF AGRIN-INDUCED ACETYLCHOLINE-RECEPTOR AGGREGATION. *Philos. Trans. R. Soc. London Ser. B-Biological Sci.* **331**, 273–280 (1991).

272. E. Rushton, J. Rohrbough, K. Broadie, Presynaptic secretion of mind-the-gap organizes the synaptic

extracellular matrix-integrin interface and postsynaptic environments. *Dev. Dyn.* **238**, 554–571 (2009).

273. E. Rushton, J. Rohrbough, K. Deutsch, K. Broadie, Structure-function analysis of endogenous lectin mind-the-gap in synaptogenesis. *Dev. Neurobiol.* **72**, 1161–1179 (2012).

274. J. Rohrbough, E. Rushton, E. Woodruff, T. Fergestad, K. Vigneswaran, K. Broadie, Presynaptic establishment of the synaptic cleft extracellular matrix is required for post-synaptic differentiation. *Genes Dev.* **21**, 2607–2628 (2007).

275. P. D. Rohde, L. S. Madsen, S. M. Neumann Arvidson, V. Loeschcke, D. Demontis, T. N. Kristensen, Testing candidate genes for attention-deficit/hyperactivity disorder in fruit flies using a high throughput assay for complex behavior. *Fly (Austin).* **10**, 25–34 (2016).

276. F. Pazos Obregón, C. Papalardo, S. Castro, G. Guerberoff, R. Cantera, Putative synaptic genes defined from a Drosophila whole body developmental transcriptome by a machine learning approach. *BMC Genomics*. **16**, 694 (2015).

277. G. G. Neely, A. Hess, M. Costigan, A. C. Keene, S. Goulas, M. Langeslag, R. S. Griffin, I. Belfer, F. Dai, S. B. Smith, L. Diatchenko, V. Gupta, C.-P. Xia, S. Amann, S. Kreitz, C. Heindl-Erdmann, S. Wolz, C. V Ly, S. Arora, *et al.*, A Genome-wide Drosophila Screen for Heat Nociception Identifies alpha 2 delta 3 as an Evolutionarily Conserved Pain Gene. *Cell*. **143**, 628–638 (2010).

278. F. Schnorrer, C. Schönbauer, C. C. H. Langer, G. Dietzl, M. Novatchkova, K. Schernhuber, M. Fellner, A. Azaryan, M. Radolf, A. Stark, K. Keleman, B. J. Dickson, Systematic genetic analysis of muscle morphogenesis and function in Drosophila. *Nature*. **464**, 287–291 (2010).

279. Y. Park, C. Rangel, M. M. Reynolds, M. C. Caldwell, M. Johns, M. Nayak, C. J. R. Welsh, S. McDermott, S. Datta, Drosophila Perlecan modulates FGF and Hedgehog signals to activate neural stem cell division. *Dev. Biol.* **253**, 247–257 (2003).

280. A. Voigt, R. Pflanz, U. Schafer, H. Jackle, Perlecan participates in proliferation activation of quiescent Drosophila neuroblasts. *Dev. Dyn.* **224**, 403–412 (2002).

281. S. Datta, Control of proliferation activation in quiescent neuroblasts of the Drosophila central nervous system. *Development*. **121**, 1173–1182 (1995).

282. A. S. Yatsenko, A. K. Marrone, H. R. Shcherbata, miRNA-based buffering of the cobblestone-lissencephaly-associated extracellular matrix receptor dystroglycan via its alternative 3'-UTR. *Nat. Commun.* **5**, 4906 (2014).

283. M. K. DeSalvo, S. J. Hindle, Z. M. Rusan, S. Orng, M. Eddison, K. Halliwill, R. J. Bainton, The Drosophila surface glia transcriptome: Evolutionary conserved blood-brain barrier processes. *Front. Neurosci.* **8**,

346 (2014).

284. J. Y. Cho, K. Chak, B. J. Andreone, J. R. Wooley, A. L. Kolodkin, The extracellular matrix proteoglycan perlecan facilitates transmembrane semaphorin-mediated repulsive guidance. *Genes Dev.* **26**, 2222–2235 (2012).

285. W. B. Grueber, B. Ye, C.-H. Yang, S. Younger, K. Borden, L. Y. Jan, Y.-N. Jan, Projections of Drosophila multidendritic neurons in the central nervous system: links with peripheral dendrite morphology. *Development*. **134**, 55–64 (2007).

286. P. Merlo, B. Frost, S. Peng, Y. J. Yang, P. J. Park, M. Feany, P53 Prevents Neurodegeneration By Regulating Synaptic Genes. *Proc. Natl. Acad. Sci.* **111**, 18055–18060 (2014).

287. P. P. Jumbo-Lucioni, W. M. Parkinson, D. L. Kopke, K. S. Broadie, Coordinated movement, neuromuscular synaptogenesis and trans-synaptic signaling defects in Drosophila galactosemia models. *Hum. Mol. Genet.* **25**, 3699–3714 (2016).

288. P. Jumbo-Lucioni, W. Parkinson, K. Broadie, Overelaborated synaptic architecture and reduced synaptomatrix glycosylation in a Drosophila classic galactosemia disease model. *Dis. Model. Mech.* **7**, 1365–1378 (2014).

289. W. M. Parkinson, M. Dookwah, M. L. Dear, C. L. Gatto, K. Aoki, M. Tiemeyer, K. Broadie, Synaptic roles for phosphomannomutase type 2 in a new Drosophila congenital disorder of glycosylation disease model. *Dis. Model. Mech.* **9**, 513–527 (2016).

290. J. You, T. Belenkaya, X. Lin, Sulfated Is a Negative Feedback Regulator of Wingless in Drosophila. *Dev. Dyn.* **240**, 640–648 (2011).

291. C. A. Kirkpatrick, S. M. Knox, W. D. Staatz, B. Fox, D. M. Lercher, S. B. Selleck, The function of a Drosophila glypican does not depend entirely on heparan sulfate modification. *Dev. Biol.* **300**, 570–582 (2006).

292. M. Sternlicht, Z. Werb, How matrix metalloproteinases regulate cell behavior. *Annu Rev Cell Biol*. **17**, 463–516 (2001).

293. H. Nagase, R. Visse, G. Murphy, Structure and function of matrix metalloproteinases and TIMPs. *Cardiovasc. Res.* **69**, 562–573 (2006).

294. G. Murphy, H. Nagase, Localizing matrix metalloproteinase activities in the pericellular environment. *FEBS J.* **278**, 2–15 (2011).

295. G. Giannelli, J. Falk-Marzillier, O. Schiraldi, W. G. Stetler-Stevenson, V. Quaranta, Induction of cell migration by matrix metalloprotease-2 cleavage of laminin-5. *Science.* **277**, 225–228 (1997).

296. C. J. Malemud, Matrix metalloproteinases (MMPs) in health and disease: an overview. *Front. Biosci.* **11**, 1696 (2006).

297. S. Schenk, E. Hintermann, M. Bilban, N. Koshikawa, C. Hojilla, R. Khokha, V. Quaranta, Binding to EGF receptor of a laminin-5 EGF-like fragment liberated during MMP-dependent mammary gland involution. *J. Cell Biol.* **161**, 197–209 (2003).

298. P. Chen, L. E. Abacherli, S. T. Nadler, Y. Wang, Q. Li, W. C. Parks, MMP7 shedding of syndecan-1 facilitates re-epithelialization by affecting alpha(2)beta(1) integrin activation. *PLoS One*. **4**, e6565 (2009).

299. K. Yamamoto, G. Murphy, L. Troeberg, Extracellular regulation of metalloproteinases. *Matrix Biol.* **44–46**, 255–263 (2015).

300. V. Arpino, M. Brock, S. E. Gill, The role of TIMPs in regulation of extracellular matrix proteolysis. *Matrix Biol.* **44–46**, 247–254 (2015).

301. K. Brew, H. Nagase, The tissue inhibitors of metalloproteinases (TIMPs): An ancient family with structural and functional diversity. *Biochim Biophys Acta*. **1803**, 55–71 (2010).

302. S. Wei, Z. Xie, E. Filenova, K. Brew, Drosophila TIMP Is a Potent Inhibitor of MMPs and TACE: Similarities in Structure and Function to TIMP-3. *Biochemistry*. **42**, 12200–12207 (2003).

303. W. G. Stetler-stevenson, The tumor microenvironment: regulation by MMP- independent effects of tissue inhibitor of metalloproteinases-2. *Cancer Metastasis Rev.* **27**, 57–66 (2008).

304. C. S. Moore, S. J. Crocker, An Alternate Perspective on the Roles of TIMPs and MMPs in Pathology. *AJPA*. **180**, 12–16 (2011).

305. E. Llano, A. M. Pendas, P. Aza-Blanc, T. B. Kornberg, C. Lopez-Otin, Dm1-MMP, a matrix metalloproteinase from Drosophila with a potential role in extracellular matrix remodeling during neural development. *J. Biol. Chem.* **275**, 35978–35985 (2000).

306. E. Llano, G. Adam, A. M. Pendás, V. Quesada, L. M. Sánchez, I. Santamaría, S. Noselli, C. López-Otín, Structural and enzymatic characterization of Drosophila Dm2-MMP, a membrane-bound matrix metalloproteinase with tissue-specific expression. *J. Biol. Chem.* **277**, 23321–23329 (2002).

307. T. A. Godenschwege, N. Pohar, S. Buchner, E. Buchner, Inflated wings, tissue autolysis and early death in tissue inhibitor of metalloproteinases mutants of Drosophila. *Eur. J. Cell Biol.* **79**, 495–501 (2000).

308. K. LaFever, X. Wang, P. Page-McCaw, G. Bhave, A. Page-McCaw, Both Drosophila matrix metalloproteinases have released and membrane-tethered forms but have different substrates. *Sci. Rep.* **7**, 44560 (2017).

309. A. Page-McCaw, J. Serano, J. M. Sante, G. M. Rubin, Drosophila matrix metalloproteinases are required

for tissue remodeling, but not embryonic development. *Dev. Cell*. **4**, 95–106 (2003).

310. N. Pohar, T. A. Godenschwege, E. Buchner, Invertebrate tissue inhibitor of metalloproteinase: structure and nested gene organization within the synapsin locus is conserved from Drosophila to human. *Genomics*. **57**, 293–296 (1999).
311. J. R. Pearson, F. Zurita, L. Tomás-Gallardo, A. Díaz-Torres, M. del C. Díaz de la Loza, K. Franze, M. D. Martín-Bermudo, A. González-Reyes, ECM-Regulator timp Is Required for Stem Cell Niche Organization and Cyst Production in the Drosophila Ovary. *PLoS Genet.* **12**, e1005763 (2016).
312. J. J. Kiger, J. Natzle, D. Kimbrell, M. Paddy, K. Kleinhesselink, M. Green, Tissue Remodeling During Maturation Of The Drosophila Wing. *Dev Biol.* **301**, 178–191 (2007).
313. A. Page-McCaw, Remodeling the model organism: Matrix metalloproteinase functions in invertebrates. *Semin. Cell Dev. Biol.* **19**, 14–23 (2008).
314. Q. S. Raza, J. L. Vanderploeg, J. R. Jacobs, Matrix Metalloproteinases are required for membrane motility and lumenogenesis during Drosophila heart development. *PLoS One*. **12**, e0171905 (2017).
315. R. L. Schmidt, F. M. Rinaldo, S. E. Hesse, M. Hamada, Z. Ortiz, D. T. Beleford, A. Page-mccaw, J. L. Platt, A. H. Tang, Cleavage of PGRP-LC receptor in the Drosophila IMD pathway in response to live bacterial infection in S2 cells. *Self. Nonself.* **2**, 125–141 (2011).
316. S. Zhang, G. M. Dailey, E. Kwan, B. M. Glasheen, G. E. Sroga, A. Page-McCaw, An MMP liberates the Ninjurin A ectodomain to signal a loss of cell adhesion. *Genes Dev.* **20**, 1899–1910 (2006).
317. S. Broderick, X. Wang, N. Simms, A. Page-McCaw, Drosophila Ninjurin A Induces Nonapoptotic Cell Death. *PLoS One*. **7**, e44567 (2012).
318. S. Casas-tinto, F.-N. Lolo, E. Moreno, Active JNK-dependent secretion of Drosophila Tyrosyl-tRNA synthetase by loser cells recruits haemocytes during cell competition. *Nat. Commun.* **6**, 10022 (2015).
319. Q. Wang, M. Uhlirova, D. Bohmann, Spatial Restriction of FGF Signaling by a Matrix Metalloprotease Controls Branching Morphogenesis. *Dev. Cell*. **18**, 157–164 (2010).
320. X. Wang, A. Page-McCaw, A matrix metalloproteinase mediates long-distance attenuation of stem cell proliferation. *J. Cell Biol.* **206**, 923–936 (2014).
321. J. Schleede, S. S. Blair, The Gyc76C Receptor Guanylyl Cyclase and the Foraging cGMP-Dependent Kinase Regulate Extracellular Matrix Organization and BMP Signaling in the Developing Wing of Drosophila melanogaster. *PLoS Genet.* **11**, e1005576 (2015).
322. A. Guha, L. Lin, T. Kornberg, Regulation of Drosophila matrix metalloprotease Mmp2 is essential for wing imaginal disc:trachea association and air sac tubulogenesis. *Dev Biol.* **335**, 317–326 (2009).

323. B. M. Glasheen, A. T. Kabra, A. Page-McCaw, Distinct functions for the catalytic and hemopexin domains of a Drosophila matrix metalloproteinase. *Proc. Natl. Acad. Sci. U. S. A.* **106**, 2659–2664 (2009).

324. S. M. Reinhard, K. Razak, I. M. Ethell, A delicate balance: role of MMP-9 in brain development and pathophysiology of neurodevelopmental disorders. *Front. Cell. Neurosci.* **9**, 280 (2015).

325. T. V. Bilousova, D. A. Rusakov, D. W. Ethell, I. M. Ethell, Matrix metalloproteinase-7 disrupts dendritic spines in hippocampal neurons through NMDA receptor activation. *J. Neurochem.* **97**, 44–56 (2006).

326. A. Szklarczyk, J. Lapinska, M. Rylski, R. D. G. McKay, L. Kaczmarek, Matrix metalloproteinase-9 undergoes expression and activation during dendritic remodeling in adult hippocampus. *J. Neurosci.* **22**, 920–930 (2002).

327. V. Nagy, O. Bozdagi, G. W. Huntley, The extracellular protease matrix metalloproteinase-9 is activated by inhibitory avoidance learning and required for long-term memory. *Learn. Mem.* **14**, 655–664 (2007).

328. C. M. Miller, A. Page-McCaw, H. T. Broihier, Matrix metalloproteinases promote motor axon fasciculation in the Drosophila embryo. *Development*. **135**, 95–109 (2008).

329. C. M. Miller, N. Liu, A. Page-McCaw, H. T. Broihier, Drosophila Mmp2 Regulates the Matrix Molecule Faulty Attraction (Frac) to Promote Motor Axon Targeting in Drosophila. *J. Neurosci.* **31**, 5335–5347 (2011).

330. F. Meyer, H. Aberle, At the next stop sign turn right: the metalloprotease Tolloid-related 1 controls defasciculation of motor axons in Drosophila. *Development*. **133**, 4035–4044 (2006).

331. S. Meyer, I. Schmidt, C. Klambt, Glia ECM interactions are required to shape the Drosophila nervous system. *Mech. Dev.* **133**, 105–116 (2014).

332. C. T. Kuo, L. Y. Jan, Y. N. Jan, Dendrite-specific remodeling of Drosophila sensory neurons requires matrix metalloproteases, ubiquitin-proteasome, and ecdysone signaling. *Proc. Natl. Acad. Sci. U. S. A.* **102**, 15230–15235 (2005).

333. K. I. Yasunaga, T. Kanamori, R. Morikawa, E. Suzuki, K. Emoto, Dendrite Reshaping of Adult Drosophila Sensory Neurons Requires Matrix Metalloproteinase-Mediated Modification of the Basement Membranes. *Dev. Cell*. **18**, 621–632 (2010).

334. A. Depetris-Chauvin, Á. Fernández-Gamba, E. A. Gorostiza, A. Herrero, E. M. Castaño, M. F. Ceriani, Mmp1 Processing of the PDF Neuropeptide Regulates Circadian Structural Plasticity of Pacemaker Neurons. *PLoS Genet.* **10**, e1004700 (2014).

335. G. W. Huntley, Synaptic circuit remodelling by matrix metalloproteinases in health and disease. *Nat. Rev. Neurosci.* **13**, 743–757 (2012).

336. T. V Bilousova, L. Dansie, M. Ngo, J. Aye, J. R. Charles, D. W. Ethell, I. M. Ethell, Minocycline promotes dendritic spine maturation and improves behavioural performance in the fragile X mouse model. *J. Med. Genet.* **46**, 94–102 (2009).

337. P. Michaluk, M. Wawrzyniak, P. Alot, M. Szczot, P. Wyrembek, K. Mercik, N. Medvedev, E. Wilczek, M. De Roo, W. Zuschratter, D. Muller, G. M. Wilczynski, J. W. Mozrzymas, M. G. Stewart, L. Kaczmarek, J. Wlodarczyk, M. Asahi, K. Asahi, J. C. Jung, *et al.*, Influence of matrix metalloproteinase MMP-9 on dendritic spine morphology. *J. Cell Sci.* **124**, 3369–3380 (2011).

338. H. Sidhu, L. E. Dansie, P. W. Hickmott, D. W. Ethell, I. M. Ethell, Genetic removal of matrix metalloproteinase 9 rescues the symptoms of fragile X syndrome in a mouse model. *J. Neurosci.* **34**, 9867–9879 (2014).

339. K. Lepeta, K. J. Purzycka, K. Pachulska-Wieczorek, M. Mitjans, M. Begemann, B. Vafadari, K. Bijata, R. W. Adamiak, H. Ehrenreich, M. Dziembowska, L. Kaczmarek, A normal genetic variation modulates synaptic MMP-9 protein levels and the severity of schizophrenia symptoms. *EMBO*. **9**, 1100–1116 (2017).

340. J. P. Miller, J. Holcomb, I. Al-ramahi, M. De Haro, J. Gafni, N. Zhang, E. Kim, M. Sanhueza, C. Torcassi, S. Kwak, R. E. Hughes, L. M. Ellerby, Matrix Metalloproteinases are Modifiers of Huntingtin Proteolysis and Toxicity in Huntington's Disease. *Neuron*. **67**, 199–212 (2010).

341. R. D. Read, W. K. Cavenee, F. B. Furnari, J. B. Thomas, A Drosophila Model for EGFR-Ras and PI3K-Dependent Human Glioma. *PLoS Genet.* **2**, e1000374 (2009).

342. S. S. Siller, K. Broadie, Neural circuit architecture defects in a Drosophila model of Fragile X syndrome are alleviated by minocycline treatment and genetic removal of matrix metalloproteinase. *Dis. Model. Mech.* **4**, 673–685 (2011).

343. C. A. Doll, K. Broadie, Impaired activity-dependent neural circuit assembly and refinement in autism spectrum disorder genetic models. *Front. Cell. Neurosci.* **8**, 30 (2014).

344. M. Uhlirova, D. Bohmann, JNK- and Fos-regulated Mmp1 expression cooperates with Ras to induce invasive tumors in Drosophila. *EMBO J.* **25**, 5294–5304 (2006).

345. W. O. Miles, N. J. Dyson, J. A. Walker, Modeling tumor invasion and metastasis in Drosophila. *Dis. Model. Mech.* **4**, 753–761 (2011).

346. M. Jimenez-sanchez, W. Lam, M. Hannus, B. Sönnichsen, A. Fleming, A. Tarditi, F. Menzies, T. E. Dami, C. Xu, E. Gonzalez-couto, G. Lazzeroni, F. Heitz, L. Massai, V. P. Satagopam, G. Marconi, C. Caramelli, A. Nencini, M. Andreini, G. L. Sardone, *et al.*, siRNA screen identifies QPCT as a druggable target for Huntington ' s disease. *Nat. Chem. Biol.* **11**, 347–354 (2015).

347. A. Misko, T. Ferguson, L. Notterpek, Matrix metalloproteinase mediated degradation of basement membrane proteins in Trembler J neuropathy nerves. *J. Neurochem.* **83**, 885–894 (2002).

348. E. Storkebaum, R. Leit, I. Bosmans, T. Ooms, A. Jacobs, P. Van Dijck, X. Yang, P. Schimmel, K. Norga, V. Timmerman, P. Callaerts, A. Jordanova, Dominant mutations in the tyrosyl-tRNA synthetase gene recapitulate in Drosophila features of human Charcot – Marie – Tooth neuropathy. *Proc Natl Acad Sci USA*. **106**, 11782–11787 (2009).

349. S. S. Siller, K. Broadie, Matrix metalloproteinases and minocycline: Therapeutic avenues for fragile X syndrome. *Neural Plast.* **2012**, 43–47 (2012).

350. K. B. Garber, J. Visootsak, S. T. Warren, Fragile X syndrome. *Eur.J Hum.Genet.* **16**, 666–672 (2008).

351. A. J. Verkerk, M. Pieretti, J. S. Surtcliffe, Y.-H. Fu, D. P. Kuhl, A. Pizzuti, O. Reiner, S. Richards, M. F. Victoria, F. Zhang, B. E. Eussen, G.-J. B. van Ommen, L. A. Bionden, G. J. Riggins, J. L. Chastain, C. B. Kunst, H. Galjaard, C. T. Caskey, D. L. Nelson, *et al.*, Identification of a Gene (FMR-1) Containing a CGG Repeat Coincident with a Breakpoint Cluster Region Exhibiting Length Variation in Fragile X Syndrome. *Cell*. **65**, 905–914 (1991).

352. E. Chen, M. R. Sharma, X. Shi, R. K. Agrawal, S. Joseph, Fragile X Mental Retardation Protein Regulates Translation by Binding Directly to the Ribosome. *Mol. Cell*. **54**, 407–417 (2014).

353. L. Ferron, Fragile X Mental Retardation Protein controls Ion Channel Expression and Activity. *J. Physiol.* **594**, 5861–5867 (2016).

354. J. C. Darnell, S. J. Van Driesche, C. Zhang, K. Y. S. Hung, A. Mele, C. E. Fraser, E. F. Stone, C. Chen, J. J. Fak, S. W. Chi, D. D. Licatalosi, J. D. Richter, R. B. Darnell, FMRP stalls ribosomal translocation on mRNAs linked to synaptic function and autism. *Cell*. **146**, 247–261 (2011).

355. G. J. Bassell, S. T. Warren, Fragile X Syndrome: Loss of Local mRNA Regulation Alters Synaptic Development and Function. *Neuron*. **60**, 201–214 (2008).

356. M. C. Siomi, K. Higashijima, A. Ishizuka, H. Siomi, Casein Kinase II Phosphorylates the Fragile X Mental Retardation Protein and Modulates Its Biological Properties Casein Kinase II Phosphorylates the Fragile X Mental Retardation Protein and Modulates Its Biological Properties. *Mol. Cell. Biol.* **22**, 8438–8447 (2002).

357. R. L. Coffee, A. J. Williamson, C. M. Adkins, M. C. Gray, T. L. Page, K. Broadie, In vivo neuronal function of the fragile X mental retardation protein is regulated by phosphorylation. *Hum. Mol. Genet.* **21**, 900–915 (2012).

358. A. Schenck, B. Bardoni, C. Langmann, N. Harden, J. L. Mandel, A. Giangrande, CYFIP/Sra-1 controls

neuronal connectivity in Drosophila and links the Rac1 GTPase pathway to the fragile X protein. *Neuron*. **38**, 887–898 (2003).

359. X. Wang, Y. Mu, M. Sun, J. Han, Bidirectional regulation of fragile X mental retardation protein phosphorylation controls rhodopsin homoeostasis. *J. Mol. Cell Biol.* **9**, 104–116 (2017).
360. L. Wan, T. C. Dockendorff, T. A. Jongens, G. Dreyfuss, Characterization of dFMR1, a Drosophila melanogaster homolog of the fragile X mental retardation protein. *Mol. Cell. Biol.* **20**, 8536–8547 (2000).
361. R. L. Coffee, C. R. Tessier, E. A. Woodruff, K. Broadie, Fragile X mental retardation protein has a unique, evolutionarily conserved neuronal function not shared with FXR1P or FXR2P. *Dis. Model. Mech.* **3**, 471–485 (2010).
362. Y. Q. Zhang, A. M. Bailey, H. J. G. Matthies, R. B. Renden, M. A. Smith, S. D. Speese, G. M. Rubin, K. Broadie, Drosophila fragile X-related gene regulates the MAP1B homolog Futsch to control synaptic structure and function. *Cell*. **107**, 591–603 (2001).
363. J. Morales, P. R. Hiesinger, A. J. Schroeder, K. Kume, P. Verstreken, F. R. Jackson, D. L. Nelson, B. A. Hassan, Drosophila Fragile X Protein, DFXR, Regulates Neuronal Morphology and Function in the Brain. *Neuron*. **34**, 961–972 (2002).
364. C. L. Gatto, K. Broadie, Temporal requirements of the fragile X mental retardation protein in the regulation of synaptic structure. *Development*. **135**, 2637–2648 (2008).
365. C. A. Doll, K. Broadie, Activity-dependent FMRP requirements in development of the neural circuitry of learning and memory. *Development*. **142**, 1346–1356 (2015).
366. C. A. Doll, K. Broadie, Neuron class-specific requirements for Fragile X Mental Retardation Protein in critical period development of calcium signaling in learning and memory circuitry. *Neurobiol. Dis.* **89**, 76–87 (2016).
367. A. Lee, W. Li, B. A. Bogert, K. Su, F. B. Gao, Control of dendritic development by the Drosophila fragile X-related gene involves the small GTPase Rac1. *Development*. **130**, 5543–5552 (2003).
368. C. I. Michel, R. Kraft, L. L. Restifo, Defective Neuronal Development in the Mushroom Bodies of Drosophila Fragile X Mental Retardation 1 Mutants. *J. Neurosci.* **24**, 5798–5809 (2004).
369. L. Pan, Y. Q. Zhang, E. Woodruff, K. Broadie, The Drosophila Fragile X Gene Negatively Regulates Neuronal Elaboration and Synaptic Differentiation. *Curr. Biol.* **14**, 1863–1870 (2004).
370. L. Pan, K. S. Broadie, Drosophila fragile X mental retardation protein and metabotropic glutamate receptor a convergently regulate the synaptic ratio of ionotropic glutamate receptor subclasses. *J.*

Neurosci. **27**, 12378–12389 (2007).

371. T. C. Dockendorff, H. S. Su, S. M. J. McBride, Z. Yang, C. H. Choi, K. K. Siwicki, A. Sehgal, T. A. Jongens, Drosophila lacking dfmr1 activity show defects in circadian output and fail to maintain courtship interest. *Neuron*. **34**, 973–984 (2002).

372. S. B. Inoue, M. Shimoda, I. Nishinokubi, M. C. Siomi, M. Okamura, A. Nakamura, S. Kobayashi, N. Ishida, H. Siomi, A role for the Drosophila fragile X-related gene in circadian output. *Curr. Biol.* **12**, 1331–1335 (2002).

373. F. V Bolduc, K. Bell, H. Cox, K. Broadie, T. Tully, Excess protein synthesis in Drosophila Fragile X mutants impairs long-term memory. *Nat. Neurosci.* **11**, 1143–1145 (2008).

374. P. Banerjee, B. P. Schoenfeld, A. J. Bell, C. H. Choi, P. Michael, P. Hinchey, M. Kollaros, J. H. Park, S. M. J. Mcbride, C. Dockendorff, Short and long-term memory are modulated by mulyiple isoforms of the fragile X mental retardation protein. *J. Neurosci.* **30**, 6782–6792 (2010).

375. F. V. Bolduc, D. Valente, A. T. Nguyen, P. P. Mitra, T. Tully, An assay for social interaction in Drosophila fragile X mutants. *Fly (Austin).* **4**, 216–225 (2010).

376. J. M. Tauber, P. A. Vanlandingham, B. Zhang, Elevated levels of the vesicular monoamine transporter and a novel repetitive behavior in the Drosophila model of fragile X syndrome. *PLoS One*. **6**, e27100 (2011).

377. A. K. Kanellopoulos, O. Semelidou, A. G. Kotini, M. Anezaki, E. M. C. Skoulakis, Learning and memory deficits consequent to reduction of the fragile X mental retardation protein result from metabotropic glutamate receptor-mediated inhibition of cAMP signaling in Drosophila. *J. Neurosci.* **32**, 13111–13124 (2012).

378. I. P. Sudhakaran, J. Hillebrand, A. Dervan, S. Das, E. E. Holohan, J. Hulsmeier, M. Sarov, R. Parker, K. VijayRaghavan, M. Ramaswami, FMRP and Ataxin-2 function together in long-term olfactory habituation and neuronal translational control. *Proc. Natl. Acad. Sci.* **111**, 99–108 (2014).

379. B. Z. Kacsoh, J. Bozler, S. Hodge, M. Ramaswami, G. Bosco, A novel paradigm for nonassociative long-term memory in Drosophila: Predator-induced changes in oviposition behavior. *Genetics*. **199**, 1143–1157 (2015).

380. C. H. Choi, B. P. Schoenfeld, E. D. Weisz, A. J. Bell, D. B. Chambers, J. Hinchey, R. J. Choi, P. Hinchey, M. Kollaros, M. J. Gertner, N. J. Ferrick, A. M. Terlizzi, N. Yohn, E. Koenigsberg, D. A. Liebelt, R. S. Zukin, N. H. Woo, M. R. Tranfaglia, N. Louneva, *et al.*, PDE-4 Inhibition Rescues Aberrant Synaptic Plasticity in Drosophila and Mouse Models of Fragile X Syndrome. *J. Neurosci.* **35**, 396–408 (2015).

381. A. Yao, S. Jin, X. Li, Z. Liu, X. Ma, J. Tang, Y. Q. Zhang, Drosophila FMRP regulates microtubule network formation and axonal transport of mitochondria. *Hum. Mol. Genet.* **20**, 51–63 (2011).

382. R. Kashima, P. L. Redmond, P. Ghatpande, S. Roy, T. B. Kornberg, T. Hanke, S. Knapp, G. Lagna, A. Hata, Hyperactive locomotion in a Drosophila model is a functional readout for the synaptic abnormalities underlying fragile X syndrome. *Sci. Signal.* **10**, 8133 (2017).

383. K. Xu, B. A. Bogert, W. Li, K. Su, A. Lee, F. B. Gao, The fragile X-related Gene Affects the Crawling Behavior of Drosophila Larvae by Regulating the mRNA Level of the DEG/ENaC Protein Pickpocket1. *Curr. Biol.* **14**, 1025–1034 (2004).

384. B. R. Jakubowski, R. A. Longoria, G. T. Shubeita, A high throughput and sensitive method correlates neuronal disorder genotypes to Drosophila larvae crawling phenotypes. *Fly (Austin).* **6**, 303–308 (2012).

385. L. Pan, E. Woodruff, P. Liang, K. Broadie, Mechanistic relationships between Drosophila fragile X mental retardation protein and metabotropic glutamate receptor A signaling. *Mol. Cell. Neurosci.* **37**, 747–760 (2008).

386. R. E. Vandenbroucke, C. Libert, Is there new hope for therapeutic matrix metalloproteinase inhibition? *Nat. Rev. Drug Discov.* **13**, 904–927 (2014).

387. L. M. Coussens, B. Fingleton, L. M. Matrisian, Matrix metalloproteinase inhibitors and cancer: trials and tribulations. *Science.* **295**, 2387–2392 (2002).

388. M. Pavlaki, S. Zucker, Matrix metalloproteinase inhibitors (MMPIs): The beginning of phase I or the termination of phase III clinical trials. *Cancer Metastasis Rev.* **22**, 177–203 (2003).

389. U. auf dem Keller, A. Prudova, U. Eckhard, B. Fingleton, C. Overall, Systems-level analysis of proteolytic events in increased vascular permeability and complement activation in skin inflammation. *Sci. Signal.* **6**, 2 (2013).

CHAPTER II

TWO CLASSES OF MATRIX METALLOPROTEINASES RECIPROCALLY REGULATE SYNAPTOGENESIS

This paper has been published under the same title in *Development*, 2016

Mary Lynn Dear, Neil Dani, William Parkinson, Scott Zhou and Kendal Broadie

Department of Biological Sciences,
Kennedy Center for Research on Human Development,
Vanderbilt University, Nashville, TN 37232 USA

Neil Dani performed the electrophysiology experiments. William Parkinson performed the ultrastructural transmission electron microscopy studies and corresponding quantification. Scott Zhou assisted Mary Lynn Dear with dissections and antibody work-up. Mary Lynn Dear performed all other studies and quantifications.

Summary

Synaptogenesis requires orchestrated intercellular communication between synaptic partners, with *trans*-synaptic signals necessarily traversing the extracellular synaptomatrix separating presynaptic and postsynaptic cells. Extracellular matrix metalloproteinases (Mmps) regulated by secreted tissue inhibitors of metalloproteinases (Timps), cleave secreted and membrane-associated targets to sculpt the extracellular environment and modulate intercellular signaling. Here, we test the roles of Mmp at the neuromuscular junction (NMJ) model synapse in the reductionist *Drosophila* system, which contains just two Mmps (secreted Mmp1 and GPI-anchored Mmp2) and one secreted Timp. We found that all three matrix metalloproteome components co-dependently localize in the synaptomatrix and show that both Mmp1 and Mmp2 independently restrict synapse morphogenesis and functional differentiation. Surprisingly, either dual knockdown or simultaneous inhibition of the two Mmp classes together restores normal synapse development, identifying a reciprocal suppression mechanism. The two Mmp classes co-regulate a Wnt *trans*-synaptic signaling pathway modulating structural and functional synaptogenesis, including the GPI-anchored heparan sulfate proteoglycan (HSPG) Wnt co-receptor Dally-like protein (Dlp), cognate receptor Frizzled-2 (Frz2) and Wingless (Wg) ligand. Loss of either Mmp1 or Mmp2 reciprocally misregulates Dlp at the synapse, with normal signaling restored by co-removal of both Mmp classes. Correcting Wnt co-receptor Dlp levels in both Mmp mutants prevents structural and functional synaptogenic defects. Taken together, these results identify an Mmp mechanism that fine-tunes HSPG co-receptor function to modulate Wnt signaling to coordinate synapse structural and functional development.

Introduction

Development of a communicating junction between a presynaptic neuron and its postsynaptic target requires coordinated signaling between synaptic partner cells. Bidirectional *trans*-synaptic signals modulate synaptogenesis by traversing a specialized extracellular environment (the 'synaptomatrix'; (*1*, *2*)). Matrix metalloproteinases (Mmps) are a conserved family of secreted and membrane-anchored extracellular proteases that regulate developmental processes by cleaving membrane proteins, secreted signaling ligands and extracellular matrix (ECM) components to inhibit, activate, sequester, release or expose cryptic sites, thereby sculpting the extracellular environment and modulating intercellular signaling (*3*–*5*). Mammalian Mmps have known roles in neurogenesis, axon guidance, dendritic development, synaptic plasticity and

behavioral outputs, but mechanisms remain elusive and roles in synaptogenesis are under-studied (*6*). In mice, 24 Mmps regulated by four Timps make genetic studies challenging, with extensive functional redundancy and compensation (*4*). By contrast, the *Drosophila* genome encodes just one secreted Mmp (Mmp1), one membrane Mmp (GPI-anchored Mmp2) and one secreted Timp. In lieu of mammalian studies, which show that extracellular proteases play central roles determining synapse structure, function and number (reviewed in (*7*–*9*)), we took advantage of the reductionist *Drosophila* model to genetically dissect the complete, integrated mechanism of the matrix metalloproteome in synaptic development.

Drosophila Mmps display canonical structure and function, with a cleavable prodomain that modulates enzyme latency, a zinc-dependent catalytic domain and hemopexin domain (*10*–*12*). *Drosophila* Timp resembles mammalian Timps in structure and function. *Drosophila* Timp inhibits mammalian Mmps and mammalian Timps inhibit *Drosophila* Mmps, demonstrating an evolutionarily conserved function (*10*, *13*). Like the roles of mouse Mmps in neurodevelopment, *Drosophila* Mmps have been shown to regulate embryonic axonogenesis, BMP-dependent motor axon pathfinding and dendritic remodeling in larval sensory neurons (*14*–*17*). Importantly, mammalian Mmps are upregulated in neurological disorders (*6*), including multiple sclerosis (*18*), epilepsy (*19*, *20*) and Fragile X syndrome (FXS), the most common heritable determinant of intellectual disability and autism spectrum disorders (*21*). Similar to the mouse FXS model (*22*, *23*), the *Drosophila* FXS disease model exhibits Mmp dysfunction as an underlying cause of neurodevelopmental phenotypes (*24*, *25*). Neural defects in the *Drosophila* FXS model, including impairments in both morphological and functional synaptic differentiation (*26*) are remediated by pharmacological or genetic Mmp inhibition (*25*).

In the *Drosophila* FXS disease model, synaptogenic defects have been causally linked to heparan sulfate proteoglycan (HSPG) Dally-like protein (Dlp) co-receptor misregulation of the Wnt Wingless (Wg) trans-synaptic signaling that drives synaptogenesis (*27*). Does the function of Mmp intersect with this established synaptogenic mechanism? The findings in this study support the model that synapse development requires a precise balance of Mmp activities from both presynaptic and postsynaptic partner cells. The results also show that the two Mmps (secreted Mmp1 and GPI-anchored Mmp2) bidirectionally regulate Dlp to modulate Wg *trans*-synaptic signaling. Both Mmp functions inhibit structural and functional synaptogenesis, suggesting that Dlp can act as both a positive and negative regulator of synapse development.

Materials and Methods

Drosophila Stocks

All strains were maintained on standard medium at 25°C. The Mmp mutants used included: point mutant null *mmp1*^{Q112*}, P-element deletion null *mmp1*^{2} and point mutant hypomorph *mmp1*^{Q273*}; point mutant null *mmp2*^{W307*}, deficiency null *mmp2*$^{Df(2R)Uba1-Mmp2}$, point mutant hypomorph *mmp2*^{W621*} and 3′ splice-site genetic-null *mmp2*^{ss218} (*12*, *28*). The double heterozygous (dblhet) genotype was *mmp1*$^{Q112*/+}$; *mmp2*$^{W307*/+}$. The *timp*-null deficiency was *timp*^{1}*syn*^{28} (*29*). Knockdown studies used UAS-*mmp1*^{RNAi}, UAS-*mmp2*^{RNAi} (*30*) and UAS-*mmp2*$^{dsRNAi1794-1R-2}$ (NIG-Fly). Pan-neuronal *elav-Gal4*, motoneuron-specific *D42-Gal4*, pan-muscle *24B-Gal4* and ubiquitous *UH1-Gal4* drivers were obtained from the Bloomington *Drosophila* Stock Center (Indiana University). *24B-Gal4* and *elav-Gal4* were recombined in a dual driver line. Double inhibition studies included *UAS-timp* (*12*) overexpression (OE) and double *UAS-mmp1*^{RNAi}; *UAS-mmp2*$^{dsRNAi1794-1R-2}$ (dblRNAi). *UAS-dlp* (*31*) and *dlp*^{A187} deletion (*32*) were used in Dlp modulation studies. Genetic controls included *w*^{1118} and Gal4 drivers crossed into the *w*^{1118} background.

Antibody Production

Constructs for Mmp2 and Timp were optimized and ordered from GenArt. His-tagged Mmp2 and MBP-tagged Timp proteins were recombinantly expressed in E. coli and purified in the Vanderbilt Antibody and Protein Resource core (VAPR). The Mmp2 antigen was 162 amino acids immediately following the furin cleavage site (F186-Q298), which spans the catalytic domain included in all predicted isoforms:

MFSKYVLATLLALFAQSMCIQELSLPPEGSHSTAATRSKKAKTAISEDIMYNYLMQFDY
LPKSDLETGALRTEDQLKEAIRSLQSFGNITVTGEIDSATARLIQKPRCGVGDRRSADSFS
PDNLYHEIGSNVRVRRFALQGPKWSRTDLTWSMVNRSMPDASKVERMVQTALDV
WANHSKLTFREVYSDQADIQILFARRAHGDGYKFDGPGQVLAHAFYPGEGRGGDA
HFDADETWNFDGESDDSHGTNFLNVALHELGHSLGLAHSAIPDAVMFPWYQNNEV
AGNLPDDDRYGIQQLYGTKEKTWGPYKPQTTTTTTTTTTMRAMIYRADKPAYWPWN
NPSNNPNNDRNRARERQEEERRRQEKERRRQEEERRHQEEERRRQVEERQRQEEERWR
QEQERQEEENRRRKIEHKSQWERNPSKERNRPRERQEMERRRQEQERQEQERQEQEDR
RRERERDRQLEWERRNRNGAREPVTPTANTTPRPTNKPYPTVHRQHHHHNKPRKPKPD
SCMTYYDAISIIRGELFIFRGPYLWRIGTSGLYNGYPTEIRRHWSALPENLTKVDAVYEN
KQRQIVFFIGREYYVFNSVMLAPGFPKPLASLGLPPTLTHIDASFVWGHNNRTYMTSGTL

YWRIDDYTGQVELDYPRDMSIWSGVGYNIDAAFQYLDGKTYFFKNLGYWEFNDDRMK
VAHARAKLSARRWMQCARSANEVDDEQRWTASLVSEGEETGRSGSRELRINHFILSILL
LAIANWRS

The following codon optimized Mmp2 sequence was used:
TTTGCACTGCAGGGTCCGAAATGGTCACGTACCGATCTGACCTGGTCAATGGTTAAT
CGTAGCATGCCGGATGCAAGCAAAGTTGAACGTATGGTTCAGACCGCACTGGATGT
TTGGGCAAATCATTCAAAACTGACCTTTCGTGAAGTGTATAGCGATCAGGCAGATAT
TCAGATTCTGTTTGCACGTCGTGCACATGGTGATGGTTACAAATTTGATGGTCCGGG
TCAGGTTCTGGCACATGCATTTTATCCGGGTGAAGGTCGTGGCGGAGATGCACATTT
TGATGCAGATGAAACCTGGAATTTTGATGGTGAAAGTGATGATAGCCATGGCACCA
ATTTTCTGAATGTTGCCCTGCATGAACTGGGTCATAGCCTGGGTCTGGCCCATAGCG
CAATTCCGGATGCAGTTATGTTTCCGTGGTATCAGAATAATGAAGTTGCAGGTAATC
TGCCGGATGATGATCGTTATGGTATTCAGCAG

The Timp antigen was 113 amino acids (P32-N144) as shown below:
MDLRKHLGLLTLLLVAVFAFYGRPADACSCMPSHPQTHFAQADYVVQLRVLRKSDTI
EPGRTTYKVHIKRTYKATSEARRMLRDGRLSTPQDDAMCGINLDLGKVYIVAGRM
PTLNICSYYKEYTRMTITERHGFSGGYAKATNCTVTPCFGERCFKGRNYADTCKWSP
FGKCETNYSACMPHKVQTVNGVISRCRWRRTQLYRKCMSNP

The following codon optimized Timp sequence was used:
CCGAGTCATCCGCAGACCCATTTTGCACAGGCAGATTATGTTGTTCAGCTGCGTGTT
CTGCGTAAAAGCGATACCATTGAACCGGGTCGTACCACCTATAAAGTTCATATTAAA
CGCACGTATAAAGCGACCAGCGAAGCACGTCGTATGCTGCGTGATGGTCGTCTGAG
CACACCGCAGGATGATGCAATGTGTGGTATTAATCTGGATCTGGGCAAAGTGTATAT
TGTTGCAGGTCGTATGCCGACCCTGAATATTTGTAGCTATTACAAAGAATACACCCG
CATGACCATTACCGAACGTCATGGTTTTAGCGGTGGTTATGCAAAAGCAACCAAT
Rabbit polyclonal antibodies were raised against both sequences (Cocalico Biologicals, Inc.) and column affinity purified (VAPR).

Western Blot Analyses

SDS-PAGE Western blots were performed as previously described (*33*). The neuromusculature or brain/ventral nerve cord (CNS) was isolated from dissected larvae, and equal amounts of tissue were homogenized in buffer (67mM NaCl, 2M urea, 1mM EDTA, 1.3% SDS, Tris pH 8.0, Roche protease inhibitor cocktail) and centrifuged (20 min, 16kxg). Equal volumes of 2X NuPage sample buffer (Invitrogen) were added to supernatant and heated at 60°C for 15 mins with (Mmp1 and Mmp2) or without (Timp) 5% β-mercaptoethanol. Samples were loaded onto Bis-Tris SDS gels (Invitrogen), electrophoresed in 1X MES buffer (Mmp1 and Mmp2) or 1X MOPS (Timp) and transferred to nitrocellulose membranes (Biorad). Membranes were blocked for 1 hr at RT in either 2% BSA (Mmp1), 2% milk (Mmp2), or Odyssey blocking buffer (Timp) diluted TBS-T (10 mM Tris pH 8, 150 mM NaCl, 0.05% Tween 20). Primary antibodies were diluted in block, incubated overnight at 4°C and washed 6X in TBS-T for 5 mins the following day. All secondary antibodies were diluted 1:5000 in block, incubated for 1 hr at RT, washed 6X for 5 mins in TBS-T, and visualized using the Licor Odyssey Infrared Imaging System. Primary antibody concentrations used: mouse anti-tubulin (1:1000; DSHB 12G10), mouse α-Mmp1 catalytic cocktail (1:1:1 at 1:100; DSHB, 3B8D12/ 3A6B4/ 5H7B11), rabbit anti-Mmp2 (1:1k, this study) and rabbit anti-Timp (1:2k, this study). Secondary antibodies (all raised in goat) used: anti-mouse680 (Invitrogen), anti-mouse800 (Rockland), anti-rabbit680 (Invitrogen) and anti-rabbit800 (Rockland).

Immunocytochemistry Imaging

Larval NMJ preparations were processed with (permeabilized) or without (extracellular labeling) detergent, incubated overnight in primary antibodies, including; mouse anti-Mmp1 (1:10; DSHB), rabbit anti-Mmp2 (1:1000; this study), rabbit anti-Timp (1:500; this study), rabbit anti-HRP (1:200; Sigma, P7899), goat anti-HRP (1:200; Jackson Laboratories, 123-165-021), mouse anti-DLG (1:200; DSHB), mouse anti-GluRIIA (1:100; DHSB), rabbit anti-GluRIIB (1:1000, (*34*)), rabbit anti-GluRIID (1:500; (*34*)), mouse anti-Brp (1:100; DHSB), mouse anti-Wg (1:2; DSHB), rabbit anti-DFz2-C (1:500; (*35*)) and mouse anti-Dlp (1:5; DSHB). Preparations fixed in ice-cold methanol for 5 mins (GluRIIA/B) or 4% PFA for 10 min at RT (all other labels) were processed with 0.1% Triton X-100 (permeabilized) or without detergent (extracellular labeling). Primary antibodies were incubated overnight at 4°C and then washed 3X for 10 mins. Secondary antibodies were incubated for 2 hr at RT, then washed 3X for 10 mins. Primary antibodies used: rabbit anti-HRP (1:200; Sigma P7899), Cy3-conjugated goat anti-HRP (1:250; Jackson Laboratories 123-165-021), Cy5-conjugated goat anti-HRP (1:200; Jackson Laboratories 123-605-021), mouse anti-Mmp1 (1:1:1 at 1:10; DSHB, 3B8D12/3A6B4/5H7B11), rabbit anti-Mmp2 (1:1000; this study), rabbit anti-Timp (1:500; this study), mouse anti-GluRIIA (1:100; DHSB,

8B4D2(MH2B)), rabbit anti-GluRIIB (1:1000; (*34*, *36*)), rabbit anti-GluRIID (1:500; (*34*)), mouse anti-Brp (1:100; DHSB, NC82), mouse anti-DLG (1:200; DSHB, DLG1), mouse anti-Wg (1:2; DSHB, 4D4), rabbit anti-DFz2-C (1:500; (*35*)), and mouse anti-Dlp (1:5; DSHB, 13G8). Secondary antibodies (all 1:500; Invitrogen) used: goat anti-mouse (488, 568) and goat anti-rabbit (488, 568). Samples were mounted in Fluoromount-G (Electron Microscopy Sciences). Entire NMJ Z-stack images were acquired with a Zeiss LSM 510 META laser-scanning confocal using 63X Plan Apo oil immersion objective. For intensity comparisons, images were obtained with the same settings and quantified using NIH ImageJ software.

Electrophysiology

Two-electrode voltage-clamp (TEVC) records were made in 128 mM NaCl, 2 mM KCl, 4 mM $MgCl_2$, 1.0 mM $CaCl_2$, 70 mM sucrose and 5 mM HEPES at pH 7.1. Recording electrodes of >15 MΩ (1 mm outer diameter; World Precision Instruments) were used to record from muscle six voltage-clamped (V_{hold}, −60 mV) with an Axoclamp2B amplifier (Molecular Devices) in the episodic recording configuration. Evoked EJC records were made with nerve stimulation using glass suction electrodes at supra-threshold voltages (50% above threshold) for 0.5 ms at 0.2 Hz. Spontaneous mEJC records were obtained following cutting of the segmental nerves. Records were acquired with Clampex (Molecular Devices) and analyzed using Clampfit 9.0.

Electron Microscopy

Larvae were dissected and fixed in 4% PFA+0.1% glutaraldehyde for 1 h, then post-fixed in 1% osmium tetroxide for 1 h. Preparations were dehydrated in an ethanol, propylene oxide and resin infiltration series. Muscle 6/7 was dissected free and placed in a resin block. Ultrathin (40 nm) sections were made (Leica Ultracut UCT ultramicrotome), collected on Formvar-coated grids, and imaged using a Phillips CM10 transmission electron microscope at 80 kV. Imaging was done with a 4 megapixel AMT CCD camera. Bouton area was defined by the greatest cross-sectional area containing an electron-dense T-bar active zone.

Statistical Measurements

All analyses were done on stage- or size-matched animals. All images were projected in Zeiss LSM Image Examiner. Type IB synaptic boutons were defined as HRP- and DLG-positive varicosities ≥2 µm in diameter (*37*). Bouton volume was determined using the Volumest plugin in ImageJ (*38*). Intensity measurements were made with HRP signal delineated *z*-stack areas of maximum projection. Dlp area measurements were quantified as fluorescent signal area normalized to HRP area calculated in ImageJ. The Zeiss LSM line profile

function was used for line scan quantification through boutons. GluR and Brp puncta measurements were normalized to bouton volume for five boutons per NMJ. Images for display were exported to Adobe Photoshop. Data presented as means±s.e.m. Statistical comparisons were performed using Instat3 software (GraphPad Software). Mann–Whitney *U*-tests were used for nonparametric comparisons. ANOVA tests were used for data sets of ≥3 comparisons followed by appropriate post-hoc analyses. Raw data values and sample sizes are listed in Tables S1-S3 (supplemental materials are located in the Appendix).

Results

Mmp1 and Mmp2 both regulate synapse morphogenesis

We first asked whether the two *Drosophila* Mmps affect morphological synaptogenesis at the well-characterized glutamatergic neuromuscular junction (NMJ). Each NMJ terminal contains a fairly stereotypical array of synaptic boutons, each containing large synaptic vesicle reserves and multiple active zone release sites (*39*). To test Mmp requirements in NMJ structural development, we assayed a wide range of single mutant, double mutant and targeted transgenic conditions (Fig. 9, Table S1A). Both *mmp1* and *mmp2* loss-of-function (LOF) mutants displayed a significant, 25-40% increase in synaptic bouton number (Fig. 9A,B, 'single *mmp* LOF') compared with matched genetic controls, indicating that Mmp1 and Mmp2 both restrict synaptic structural development. In addition, only *mmp1* mutant boutons were significantly smaller in size (Fig. 9A, Table S1B). Surprisingly, both Mmp heterozygotes (*mmp1*/+ and *mmp2*/+) similarly show a striking increase in bouton number, comparable in magnitude to the Mmp homozygous mutants (Fig. S1D, Table S1A). Ubiquitous (*UH1*) mmp^{RNAi} for both Mmp classes produced similar increases in bouton number compared with LOF mutants (Fig. 9B, cell-targeted mmp^{RNAi}), with measured protein knockdown levels that were also comparable to the corresponding mutants (Fig. S7).

To test for stronger effects, we wanted to assay simultaneous removal of Mmp1 and Mmp2. However, Mmp double mutants are early larval lethal and the few animals that survive to early third instar are much smaller than matched controls. We therefore used double $mmp1^{RNAi}$; $mmp2^{RNAi}$ knockdown (*UH1>mmp1+2*^{RNAi}) and Timp overexpression (*UH1>Timp*), as two independent means of blocking the functions of both Mmps simultaneously. Both Mmp blocking conditions individually display 100% penetrant late larval/early pupal lethality; together they represent the most severe double Mmp LOF conditions available for these studies. Astonishingly, neither *UH1>mmp1+2*^{RNAi} nor *UH1>Timp* resulted in the predicted additive effect but, unexpectedly, displayed architecturally normal NMJs (Fig. 9A; Table S1A). In the first

test, *UH1>mmp1+2^{RNAi}* produced NMJ bouton numbers that were comparable to the control and were significantly reduced compared with the supernumerary boutons present in both single RNAi conditions (Fig. 9B, 'double *mmp* inhibition'). Likewise, *UH1>Timp* NMJ architecture closely resembled matched genetic controls (Fig. 9A), with only a subtle 10% reduction in synaptic bouton number (Fig. 9B, 'double inhibition'). Moreover, double *mmp* heterozygotes (*mmp2$^{W307*/+}$, mmp1$^{Q112*/+}$*; dblhet) also showed no significant difference in bouton number compared with controls, and thus suppressed the overgrowth characterizing both single *mmp* heterozygotes alone (Fig. 9B, 'double inhibition', Table S1A). Consistently, postsynaptic Timp overexpression (*24B>Timp*) was sufficient to suppress the elevated bouton number in both single *mmp* heterozygotes back to control levels (Fig. S1B,C). Collectively, these results indicate a co-suppressive interplay between the two Mmp classes and strongly suggest that the Mmp ratio is a critically important determinant of synapse structure.

To further test this interaction, we sought to genetically reduce Mmp levels in a dose-dependent manner (Fig. 9B, 'double inhibition', Table S1A). Using the *mmp* double heterozygote condition as a baseline, we sequentially removed additional *mmp* gene copies (Fig. 9B, 'double inhibition'). The Mmp imbalance caused by removal of *mmp1* (*mmp2$^{W307*/+}$, mmp1$^{Q112*/Q112*}$*) resulted in a ~40% increase in synaptic bouton number and the converse removal of *mmp2* (*mmp2$^{W307*/Df}$, mmp1$^{Q112*/+}$*) significantly reduced bouton number (Fig. 9B, 'double inhibition'). These results support an Mmp suppression model, and indicate that development of NMJs requires a precise balance of Mmp1:Mmp2 activities. Consistent with the interpretation that Mmp balance is crucial, all rescue attempts with UAS-*mmp* transgenes resulted in lethality.

To dissect the tissue-specific requirements for NMJ structural development, we used cell-targeted RNAi to knock down Mmp classes singly (*mmp^{RNAi}*) and in combination (*mmp1+2^{RNAi}*) in either neurons (*elav*) or muscles (*24B*; also known as *how*) (see Table S3A for knockdown levels). Consistent with the model, reducing each single Mmp class alone either presynaptically or postsynaptically caused a significant increase in synaptic bouton number (Fig. 9B, 'cell-targeted *mmp^{RNAi}*'). Importantly, the double *mmp1+2^{RNAi}* phenotype within either muscle or neuron was stronger than either single *mmp^{RNAi}* alone (Fig. S1A,C; Table S1A). Conversely, simultaneous knockdown in neurons and muscles of each Mmp alone using a novel combined driver (*elav,24B>mmp^{RNAi}*) caused a robust increase in bouton differentiation, which also failed to occur in the *elav,24B>mmp1+2^{RNAi}* double knockdown condition (Fig. S1A,C, Table S1A). These results clearly show that proper NMJ differentiation requires both Mmp classes in both pre- and postsynaptic cells, and indicate that Mmp1+2 (neuron): Mmp1+2 (muscle) ratios across both cell types must be balanced for proper structural morphogenesis.

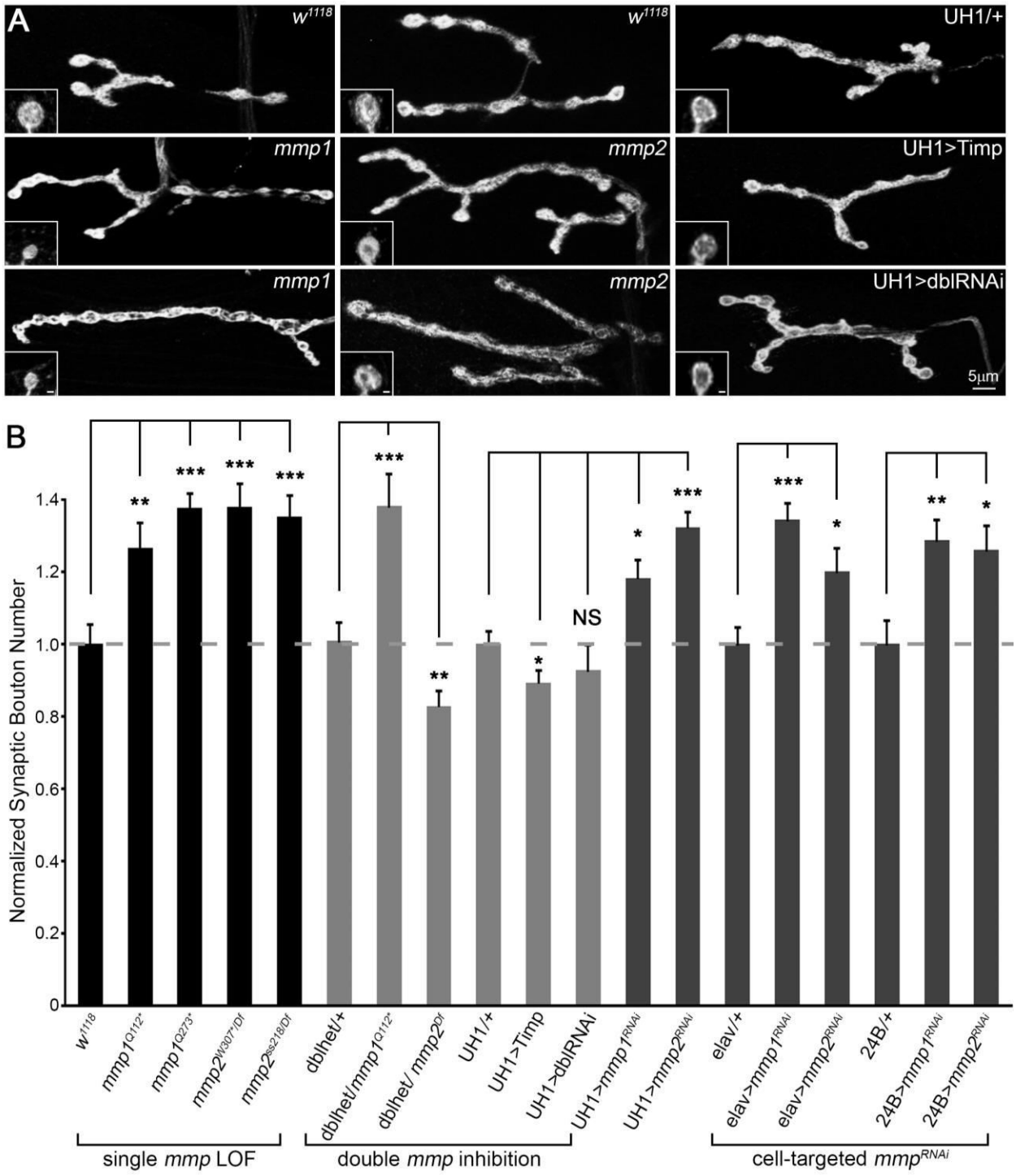

Figure 9

Figure 9: Mmp1 and Mmp2 repress NMJ structural development. (A) Black and white images of NMJs co-labeled for synaptic markers HRP and DLG in *mmp1* (middle row: $mmp1^{Q112*}$ and bottom row: $mmp1^{Q273*}$), *mmp2* (middle row: $mmp2^{W307*/Df}$ and bottom row: $mmp2^{ss218/Df}$) and two double *mmp* inhibition conditions [*UH1>Timp* and *UH1>mmp1+2*^{RNAi} (*UH1>dblRNAi*)], compared with controls (top row). Insets show high magnification single boutons. Scale bars: 1 µm. **(B)** Quantified bouton number for denoted genotypes normalized to genetic controls. Genotypes clustered by single *mmp*loss-of-function (LOF; left), double inhibition (middle) and cell-targeted RNAi knockdown in neurons (*elav*) or muscle (*24B*) for both genes (right). Double inhibition includes double *mmp1,mmp2* heterozygous condition (dblhet), *UH1>Timp* and *UH1>mmp1+2*^{RNAi} (dblRNAi). See Fig. S1 for additional genotypes. See Table S1A for raw data values and sample sizes.

Mmp1 and Mmp2 both regulate differentiation of synapse function

Structural and functional synaptic development occurs simultaneously, but they are regulated independently by distinct molecular mechanisms. To test how Mmps might contribute to NMJ functional development, nerve stimulation evoked excitatory junction currents (EJCs) were quantified as a measure of neurotransmission strength (Fig. 10, Table S2A). Both Mmp1 and Mmp2 negatively regulate functional differentiation, resulting in clearly elevated neurotransmission in all single Mmp mutants (Fig. 10A). The range of Mmp single mutants showed highly significant 25-65% increased EJC amplitudes compared with matched genetic controls (Fig. 10B, 'single *mmp* LOF', Table S2A). Conversely, *UH1>Timp* showed significantly reduced neurotransmission. Similarly, *UH1>mmp1+2*^{RNAi} completely suppressed the elevated EJC amplitudes characterizing both single *UH1>mmp*^{RNAi} conditions, with neurotransmission significantly reduced ~25% compared with controls (Fig. 10A,B). These results suggest that Mmp1 and Mmp2 might also co-suppress NMJ functional differentiation. Postsynaptic, but not presynaptic, targeted *mmp* knockdown of both classes caused significantly increased EJC amplitudes, indicating that Mmp1 and Mmp2 are required only from the muscle for functional regulation (Fig. 10B, 'cell-targeted *mmp*^{RNAi}'). However, both Mmps function extracellularly and homeostatic mechanisms between synaptic partners act trans-synaptically; thus, the underlying mechanism regulating neurotransmission strength might not be cell-autonomous (*40*).

To further investigate how Mmps regulate functional differentiation, we next assayed spontaneous neurotransmission by quantifying miniature EJC (mEJC) frequency and amplitude as measures of pre- and postsynaptic machinery, respectively (Fig. S2, Table S2B) (*41*). Presynaptically, we found that *mmp2* LOF mutants exhibited a robust ~80% increase in mEJC frequency (Fig. S2A,B). Postsynaptically, *mmp1* LOF mutants showed a significant ~30% increase in mEJC amplitude, whereas *mmp2* LOF mutants displayed a ~15% decrease in mEJC amplitude (Fig. S2A,B). Importantly, there were no detectable changes in mEJC amplitude or frequency in UH1>*mmp1+2*^{RNAi} double knockdown animals (Fig. S2). In calculating quantal content to measure the level of synaptic vesicle release, *mmp2*mutants had a ~twofold increase, whereas *mmp1* mutants showed no significant change compared with controls (Fig. S2B). In the *UH1>mmp1+2*^{RNAi} double loss condition, quantal content was decreased by ~35%. It is noted that there are inconsistencies between Mmp LOF mutant and *mmp*^{RNAi} mEJC phenotypes (Table S2B). Nevertheless, the results clearly demonstrate that Mmp1 and Mmp2 regulate different aspects of NMJ functional development.

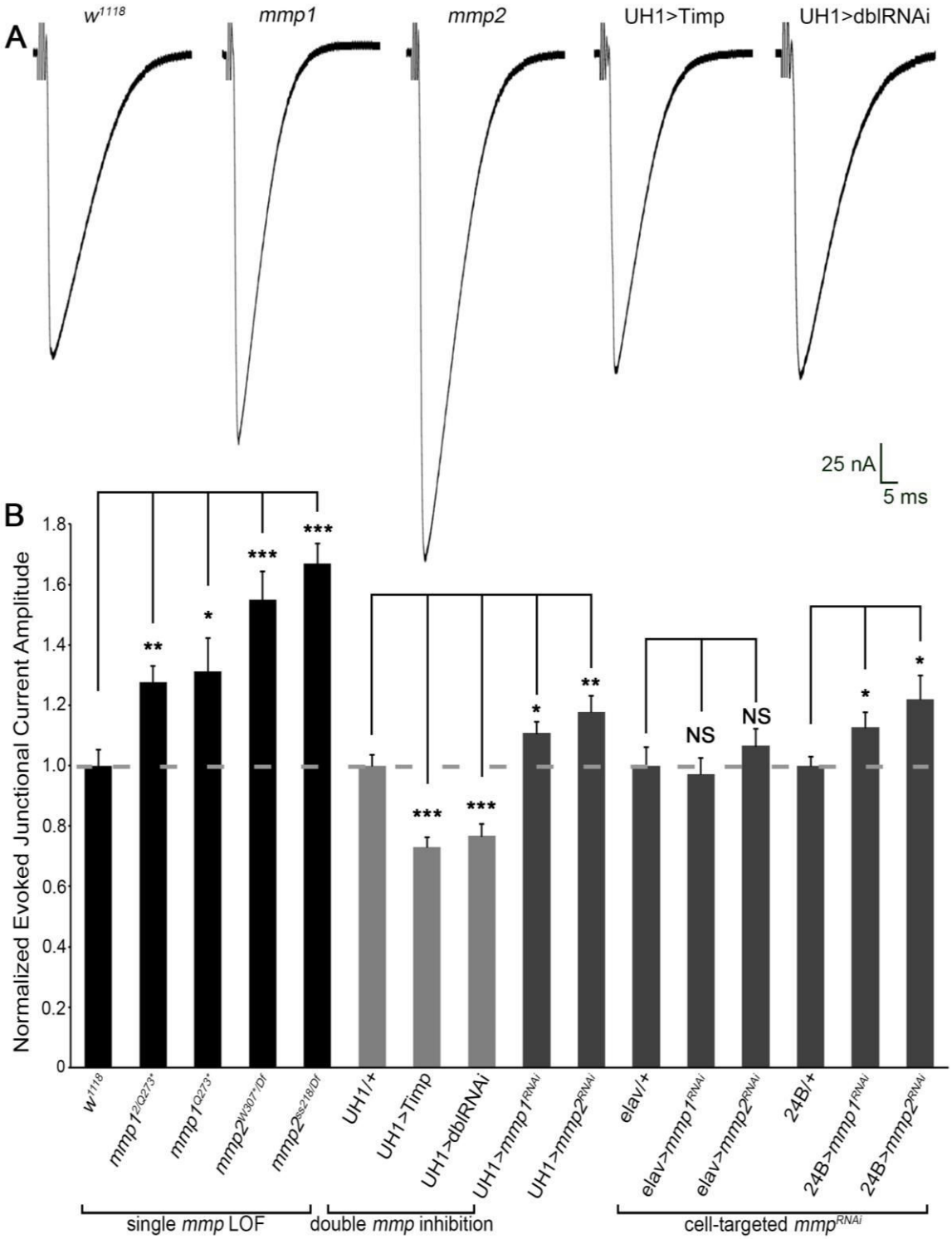

Figure 10

Figure 10: Mmp1 and Mmp2 repress functional differentiation of the NMJ.
(A) NMJ electrophysiology two-electrode voltage-clamp (TEVC) records showing motor nerve stimulation evoked excitatory junctional currents (EJCs) from genetic control (w^{1118}), $mmp1^{2/Q273*}$, $mmp2^{ss218/}Df$, *UH1>Timp* and *UH1>mmp1+2*^{RNAi} (dblRNAi). **(B)** Quantified EJC amplitudes for denoted genotypes normalized to genetic controls. See Fig. S2 for mEJC analyses. See Table S2 for raw data values and sample sizes. **P*<0.05, ***P*<0.01, ****P*<0.001; NS, not significant.

Mmp1 and Mmp2 both regulate synapse molecular assembly

NMJ function is regulated by the number and composition of postsynaptic glutamate receptors (GluRs) juxtaposing presynaptic active zone glutamate release sites (*39*). Since both evoked and spontaneous neurotransmission are altered in Mmp mutants, we next tested how the two Mmp classes might regulate molecular synaptic assembly by quantifying both presynaptic Bruchpilot (Brp) containing active zones (*42*) and postsynaptic GluR domains (*43*). On the presynaptic side, both *mmp1* and *mmp2* LOF mutants had significantly more Brp-containing active zones (puncta/μm^3) compared with matched controls (Fig. S3C, Table S2C). On the postsynaptic side, *mmp1* LOF mutants had more domains containing the essential GluRIID subunit (*43*) measured as puncta/μm^3, whereas *mmp2* LOF mutants showed a smaller, non-significant increase in GluR puncta density (Fig. S3, Table S2C). No defects were detected in the apposition between synaptic compartments in either *mmp1* or *mmp2* mutants, as all Brp-positive active zones juxtaposed a GluRIID cluster (Table S2C). Importantly, no defects in either presynaptic active zones or postsynaptic GluR domains were detected in *UH1>mmp1+2^{RNAi}* animals (Fig. S3).

Each GluR tetramer contains either a GluRIIA or GluRIIB variable subunit modulated by distinct regulatory mechanisms (*34*, *44*). Subunit selection dictates distinct receptor functional properties (*43*); for example, A-type GluRs mediate increased postsynaptic sensitivity and B-Type GluRs rapidly desensitize. The *mmp2* LOF mutants displayed significantly more GluRIIA puncta/μm^3, although the overall fluorescence signal intensity was slightly decreased (Fig. S4, Table S3C). Conversely, *mmp1* mutants showed a non-significant increase in GluRIIA puncta/μm^3, with overall signal intensity significantly increased compared with controls (Fig. S4, Table S3C). For GluRIIB, both *mmp1* and *mmp2* mutants showed significantly increased puncta/μm^3, with signal intensity decreased in the *mmp1* mutants alone (Fig. S5, Table S3C). These GluR alterations likely confer the increased functional neurtransmission properties characterizing the Mmp LOF mutants (Fig. 10, Fig. S2) (*36*). These results show that Mmp1 and Mmp2 have distinct roles negatively regulating synaptic molecular assembly.

Drosophila NMJ synaptic ultrastructure is particularly well-characterized, with functionally and spatially defined synaptic vesicle pools organized around presynaptic active zones (containing an electron-dense T-bar) and the muscle subsynaptic reticulum (SSR) molded into elaborate membrane folds (*45*, *46*). We therefore next examined Mmp roles in NMJ ultrastructural development using transmission electron microscopy (TEM), with the prediction that *mmp2* mutants would show presynaptic defects aligning with the previously observed functional phenotypes (Fig. 11, Table S1B). As Mmps have well established roles in ECM degradation, we were surprised to find that synaptic ultrastructure were largely normal in both Mmp mutants, with no detectable

deficits in: (1) the architecture of the active zone or T-bar; (2) the appearance or width of the synaptic cleft; and (3) SSR folding or density (Fig. 11A; Table S1B). Similar to bouton volume confocal measurements, bouton cross-sectional area was significantly reduced by ~50% in *mmp1* mutants (Fig. 11A,B). The *mmp2* LOF mutants had significantly increased synaptic vesicle number/density (Fig. 11A,B), agreeing with elevated mEJC frequency (Fig. S2). Synaptic vesicle density at the active zone (<250 nm from T-bar; (*47*)) and in the reserve domain (250-500 nm from T-bar; (*48*)) was elevated in *mmp2* single mutants, with a similar non-significant trend in *mmp1* mutants (Fig. 11A,B). Again, these phenotypes were not present in *UH1>mmp1+2*^{RNAi} animals. Lack of any gross abnormalities in the matrix or SSR suggest that Mmps at the synapse function in the synaptomatrix to actively modulate intercellular signaling interactions between neurons and muscle, rather than permissive proteases degrading physical barriers, such as structural ECM components.

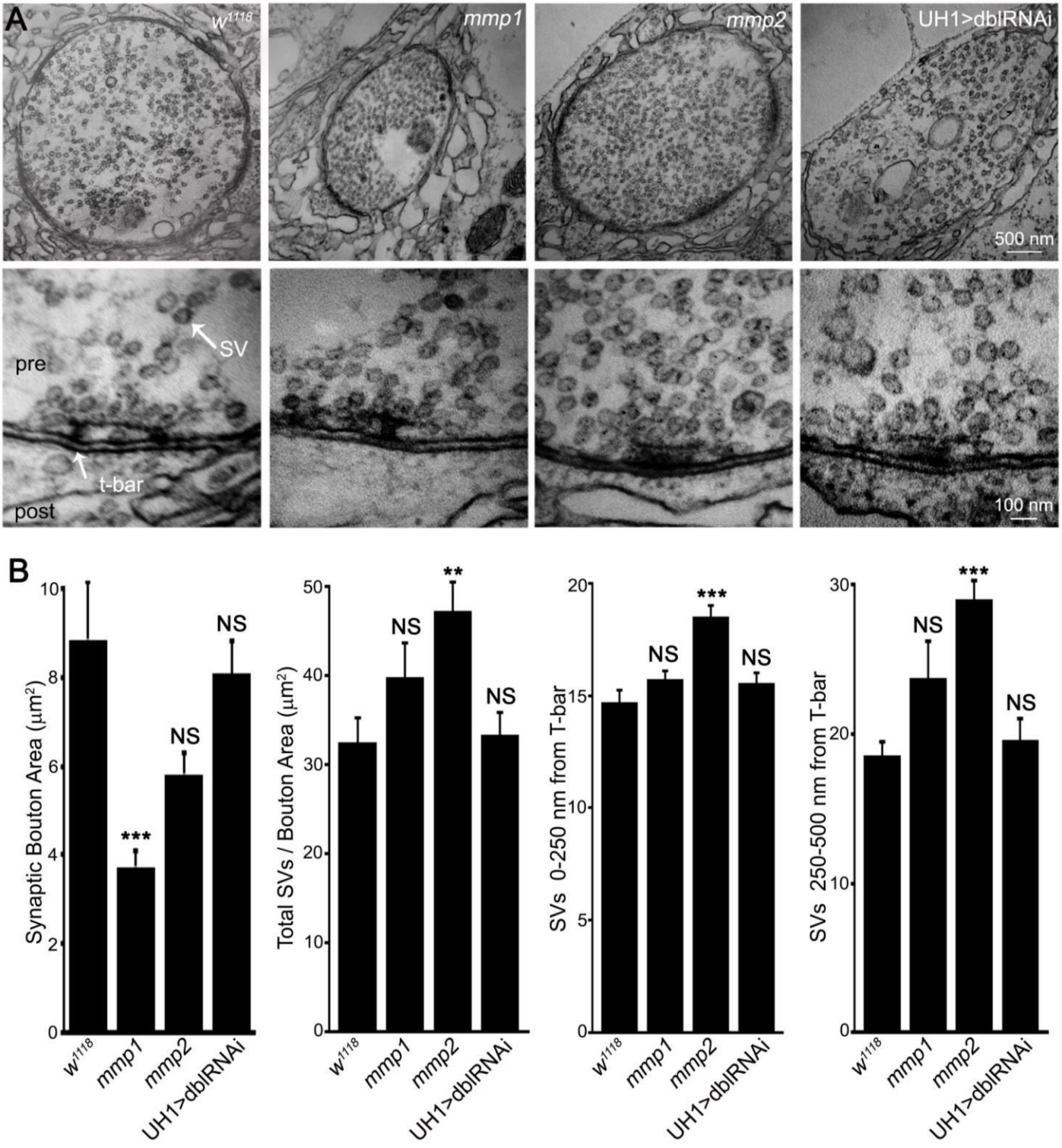

Figure 11

Figure 11: Mmp1 and Mmp2 modulate synaptic ultrastructural development.

(A) Transmission electron microscopy (TEM) images of NMJ boutons (low magnification, top) and presynaptic active zones (high magnification, bottom) in control (w^{1118}), $mmp1^{Q112*/Q273*}$, $mmp2^{ss218/Df}$ and *UH1>mmp1+2*^{RNAi} (dblRNAi). **(B)** Quantification of ultrastructural bouton area, synaptic vesicle (SV) number/bouton area, and SV number within 0-250 and 250-500 nm of active zone T-bars. See Table S1B for data values and sample sizes. See Figs S3-S5 for analyses of pre- and postsynaptic molecular components. ***P*<0.01, ****P*<0.001; NS, not significant.

Mmp1, Mmp2 and Timp co-dependently localize to the NMJ synaptomatrix

Our working model proposes that Mmp1, Mmp2 and their Timp inhibitor all co-localize extracellularly to the NMJ synapse. We therefore next examined expression of this three-component matrix metalloproteome in wild-type and mutant backgrounds. Prior efforts have produced Mmp1 antibodies (*12*, *49*), which we previously used to reveal localization of Mmp1 to the NMJ (*25*) as confirmed here (Fig. S6A, Fig. S7A,D). Two Mmp2 antibodies exist that work on western blots (*28*, *50*), but neither is effective for immunocytochemistry. No *Drosophila* Timp antibody has been reported. We therefore generated new antibodies against both *Drosophila* Mmp2 and Timp that work for both immunocytochemistry and western blot analyses (Fig. 12, Figs. S6-S8).

Western blot studies showed that the antibody against Mmp2 specifically recognized a ~90 kDa band in larvae of the predicted Mmp2 molecular mass, as well as three weaker bands (~120, 85 and 76 kDa) in isolated neuromusculature (Fig. 12G, Fig. S6B). The antibody against Timp specifically recognized a ~28 kDa band at the predicted Timp molecular mass, which increased with *UH1>*Timp and was absent in *timp*-null mutants (Fig. S6C). In tissue immunocytochemistry, Mmp1, Mmp2 and Timp labeling were all dramatically reduced in respective single LOF mutants as well as with single *UH1>mmp*^{RNAi} conditions (Fig. S7, Table S3A,B). Importantly, *UH1>mmp1+2*^{RNAi} eliminated Mmp1 and Mmp2 expression at the NMJ (Fig. S7A,B), comparable to quantified protein levels at corresponding single *UH1>mmp*^{RNAi} and genetic LOF mutant NMJs (Fig. S7D,E). As previously described (*25*), detergent-free immunohistochemistry showed that Mmp1 localized to the extracellular space within the perisynaptic domain at the NMJ and was particularly enriched around synaptic boutons (Fig. S7A, Fig. S8A). Similarly, extracellularly labeled Mmp2 had a closely overlapping expression pattern, but was more restricted to the bouton surface, as predicted for a membrane-tethered protein (Fig. S7B, Fig. S8B). Finally, detergent-free labeling showed that Timp was highly enriched at the NMJ surrounding boutons in the extracellular synaptomatrix, albeit with a slightly more diffuse pattern, as predicted for a smaller secreted protein (Fig. S7C, Fig. S8C). Thus, all three proteins of the tripartite matrix metalloproteome overlap at the NMJ synapse.

With these new antibody tools and knowledge of Mmp1, Mmp2 and Timp expression at the synapse, we next addressed interactive changes (Fig. 12, Table S3A,B). Under detergent-free conditions, all three proteins were examined for extracellular expression in the respective Mmp LOF mutant and *UH1>Timp*conditions. First, imaging for Mmp1 expression using the antibodies specific for the catalytic domain (*12*, *49*) revealed significant increases in Mmp1 levels in *mmp2* LOF mutants and, conversely, significant decreases in Mmp1 at *UH1>Timp* NMJs (Fig. 12A,B, Table S3A). By contrast, Mmp2 was significantly

decreased in *mmp1* LOF mutants and also moderately decreased at *UH1>Timp* NMJs (Fig. 12C,D; Table S3A). Local Timp levels within the HRP-labeled NMJ terminal were unchanged in both *mmp1* and *mmp2* mutants, but the perisynaptic spatial domain of Timp expression was dramatically increased at *mmp2* LOF synapses (Fig. 12E, Table S3B). These immunocytochemistry results suggest that Mmp1 positively regulates Mmp2 levels, whereas Mmp2 negatively regulates both Mmp1 levels and localization of Timp.

To test whether changes were locally restricted or ubiquitous, we performed western blots on neuromusculature lysates. In agreement with imaging results, Mmp1 levels were increased in *mmp2*LOF lysates (Fig. 12F). By contrast, Mmp1 levels were strongly increased in *UH1>Timp* neuromusculature and in whole larvae (Fig. 12F, Fig. S6A). These differences may be due to Timp binding the Mmp1 catalytic domain to sterically hinder antibody accessibility (Fig. 12F, Fig. S6A). Mmp2 levels were also not noticeably decreased in *mmp1* LOF lysates, suggesting that these changes are locally restricted to the NMJ synapse (Fig. 12G). Similar to tissue immunocytochemistry results, Timp levels were comparable between mutants and controls (Fig. 12H). Taken together, these results reveal strong cross-talk between Mmp1, Mmp2 and Timp at the NMJ synapse, raising the possibility that tripartite complex interactions could contribute, at least in part, to the observed suppression mechanism.

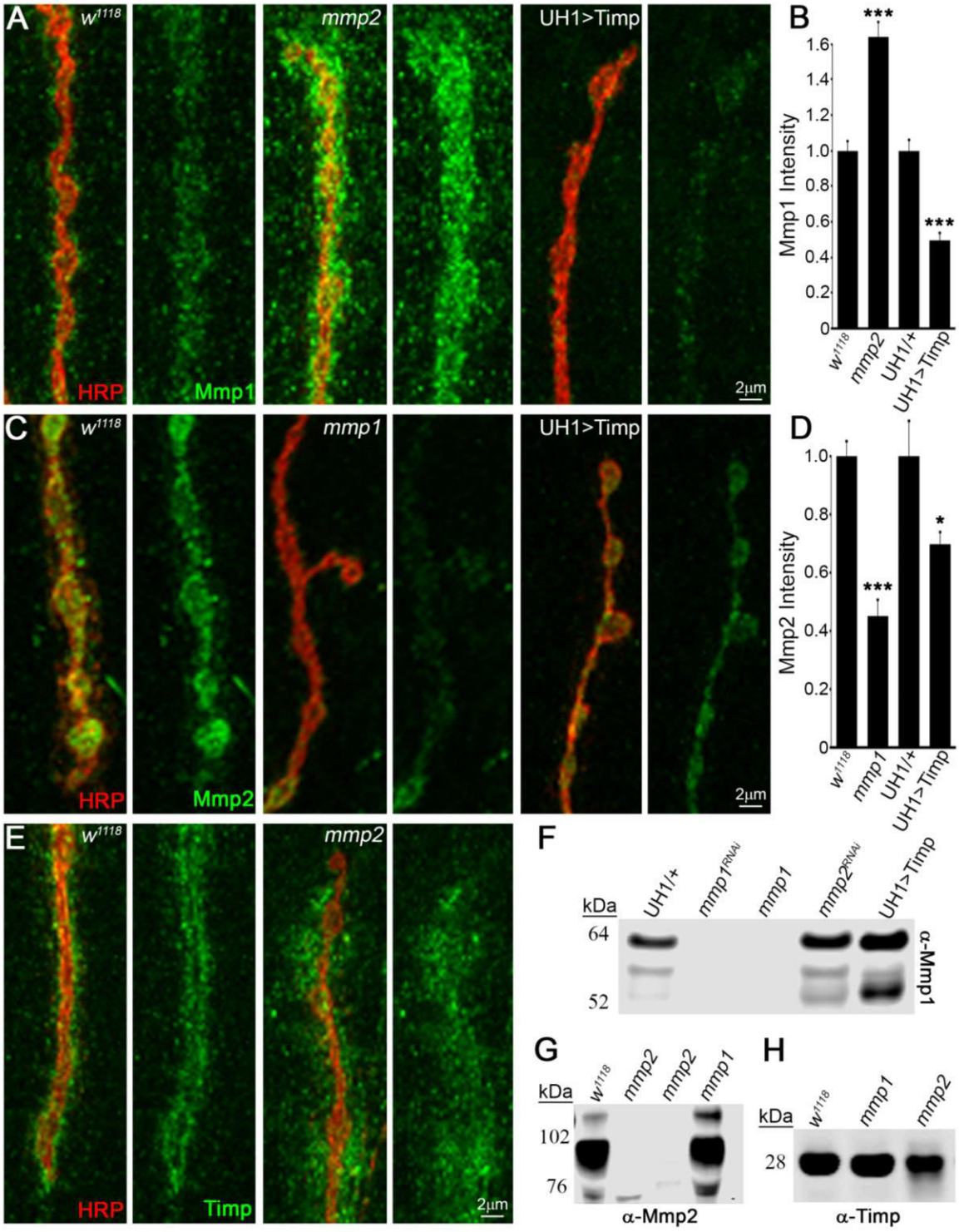

Figure 12

Figure 12: Mmp1, Mmp2 and Timp exhibit co-dependent synaptic localization.
(A) NMJ extracellular Mmp1 (green) relative to synaptic marker HRP (red) in control w^{1118}, $mmp2^{ss218/Df}$ and *UH1>Timp*. **(B)** Quantified fluorescent intensities normalized to controls (w^{1118}, *UH1/+*). **(C)** Extracellular Mmp2 (green) and HRP (red) in w^{1118}, $mmp1^{Q112*/Q273*}$ and *UH1>Timp*. **(D)** Quantified fluorescent intensities normalized to controls (w^{1118}, *UH1/+*). **(E)** Extracellular Timp (green) and HRP (red) in w^{1118} and $mmp2^{ss218/Df}$. Western blots of **(F)** Mmp1 (neuromusculature), **(G)** Mmp2 (whole tissue) and (H) Timp (neuromusculature). Genotypes: $mmp1^{Q112*/Q273*}$ (F-H), $mmp2^{W307*}$ and $mmp2^{W621*}$ (G) and $mmp2^{ss218/Df}$ (H). Further antibody characterization in Figs S6-S8. See Table S3 for raw data values and sample sizes. **P*<0.05, ****P*<0.001.

Mmp1 and Mmp2 restrict Wnt trans-synaptic signaling

Extracellular regulation of trans-synaptic signaling is important for modulating both structural and functional synaptic development (*2*, *33*, *41*, *45*). Both Mmp classes reside within the synaptomatrix, where they are perfectly positioned to participate in this mechanism and the LOF phenotypes are consistent with increased Wnt trans-synaptic signaling at the NMJ. Wnt signaling driving NMJ growth and synapse assembly involves the Wg ligand, HSPG co-receptor Dlp and Frizzled2 (Frz2) receptor (*27*, *51*). In the Frizzled nuclear import (FNI) pathway, Frz2 is endocytosed following Wg activation, cleaved, transported into the muscle nuclei, where it associates with RNP granules containing synaptic transcripts and thereby drives expression changes modulating synapse structure and function (*35*, *52*). This pathway is specifically misregulated in the *Drosophila* FXS disease model (*27*) and associated NMJ synaptogenic phenotypes are remediated by either genetic or pharmacological inhibition of Mmp (*25*). Therefore, we tested whether this well-characterized Wnt mechanism is impacted by removal of Mmp.

At wild-type NMJs, the extracellular Wg ligand was localized to a dynamic subset of synaptic boutons (Fig. 13A). In *mmp1* LOF mutants, overall Wg levels at the NMJ were significantly decreased by ~40% (Fig. 13A,C, Table S3C). Because Mmps can facilitate signal localization, we assayed whether the percentage of Wg-expressing boutons was altered at *mmp1* mutant NMJs. Consistent with total abundance of Wg, *mmp1* mutants showed ~50% reduction in Wg-expressing boutons compared with matched controls (Fig. 13C, Table S3C). These results were replicated by *UH1>mmp1*^{RNAi}, but there were no significant changes in either *mmp2* LOF mutants or *UH1>mmp1+2*^{RNAi} animals (Fig. 13A,C, Table S3C). However, trans-synaptic FNI signal transduction via Frz2 receptor cleavage and FrzC2 intracellular trafficking to the muscle nuclei was increased in both Mmp single mutants. Importantly, this defect was not apparent in the *UH1>mmp1+2*^{RNAi} condition (Fig. 13B,D, Table S3C). It seems counter-intuitive that Wg was decreased in *mmp1* mutants alone, although both *mmp1* and *mmp2* mutants showed increased Wg signal transduction (FNI), yet there are multiple precedents for this observation at the *Drosophila* NMJ (*27*, *41*). Negative feedback is one possibility. In any case, the data are consistent with previous work showing that elevated Wg trans-synaptic signaling induces synaptic bouton formation (as in *mmp1* and *mmp2* mutants) and increases mEJC frequency (as in *mmp2* mutants) (*53*), strongly reminiscent of the respective Mmp mutant phenotypes (Fig. 9, Fig. S2).

A recent report has shown that *Drosophila* Mmp2 directly cleaves the Wg HSPG co-receptor Dlp, in a mechanism that spatially tunes Wg signaling in developing ovary stem cells (*54*). This function provides a putative mechanism for Mmp misregulation of Wg trans-synaptic signaling during NMJ synaptogenesis,

because Dlp is also an established Wg co-receptor and potent regulator of intercellular signaling at the developing synapse (*27*, *41*, *55*). Consistent with this hypothesis, Dlp was strongly reduced in *mmp1* LOF mutants (Fig. 14A, Table S3C). Moreover, there was also a strong defect in synaptic Dlp spatial distribution in both Mmp LOF mutants (Fig. 14B), which is consistent with known roles of Mmp in spatially regulating target proteins (*50*, *54*). First, a line scan through single synaptic boutons, with the intensity profile of Dlp (green) compared with the synaptic membrane marker HRP (red in Fig. 14B,C), showed that Dlp and HRP signals largely overlap in genetic controls, with a slight extension of Dlp beyond the HRP-marked membrane (Fig. 14C, left). By contrast, *mmp1* mutants showed strong reduction of the Dlp domain and *mmp2* LOF mutants showed strongly expanded Dlp domain (Fig. 14C, green arrows). Second, Dlp area outside the HRP-marked synaptic domain, normalized to NMJ area to account for terminal size, also showed that the spatial distribution of Dlp was reciprocally regulated by Mmp1 and Mmp2. Dlp area decreased ∼40% in *mmp1* LOF mutants and increased almost twofold in *mmp2* LOF mutants (Fig. 14, Table S3C). Importantly, Dlp spatial misregulation was not detected in the *UH1>mmp1+2*^{RNAi} condition (Fig. 14, Table S3C).

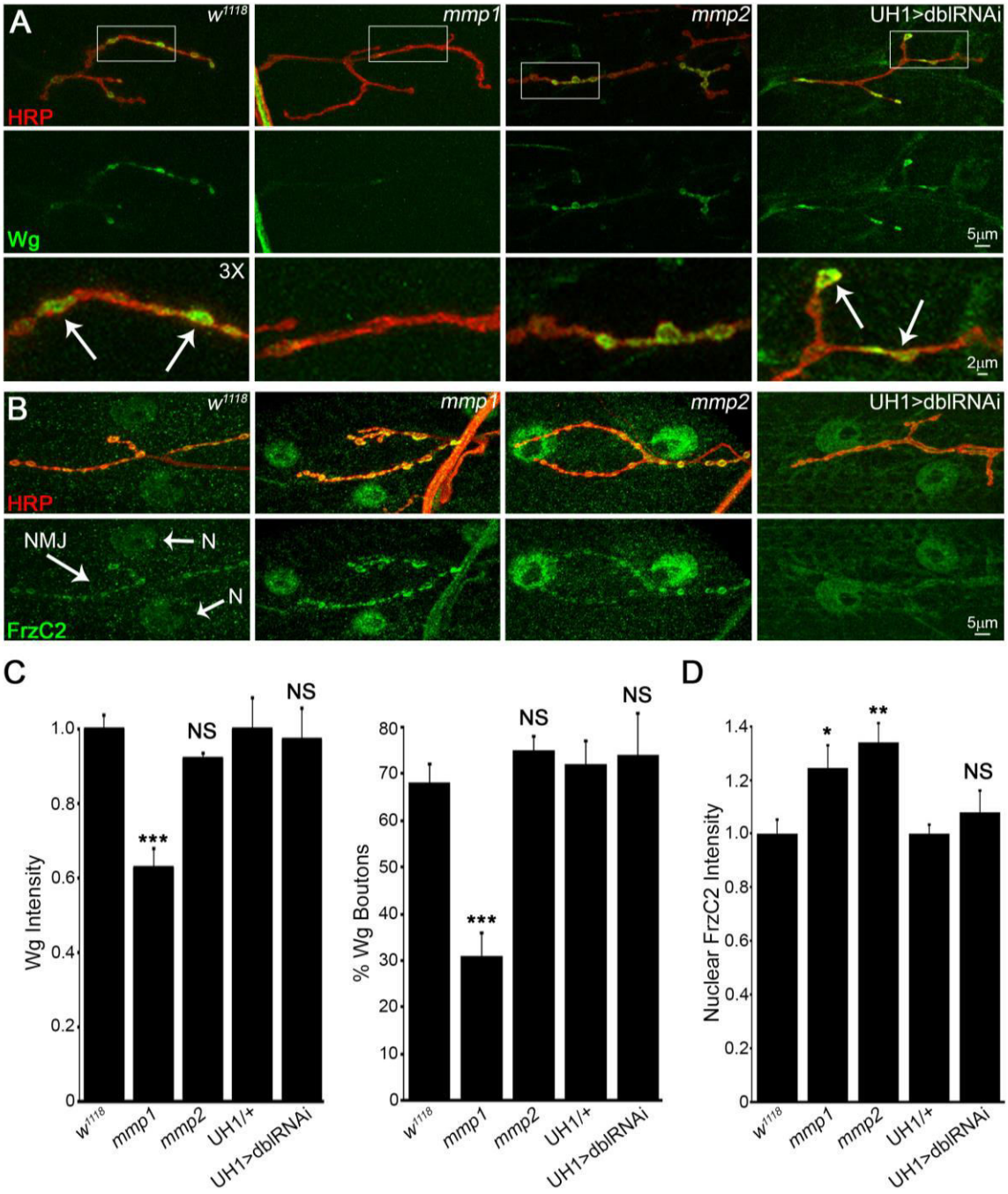

Figure 13

Figure 13: Mmp1 and Mmp2 restrict Wnt trans-synaptic signal transduction.

(A) NMJs labeled for extracellular Wg ligand (green) relative to synaptic HRP (red) in control (w^{1118}), $mmp1^{Q112*/Q273*}$, $mmp2^{ss218/Df}$ and *UH1>mmp1+2*^{RNAi} (dblRNAi). White boxes are enlarged 3× in bottom panels. Arrows indicate Wg-expressing boutons. **(B)** NMJs labeled for Frizzled 2 receptor C-terminus (Fz2-C, green) and HRP (red) in the same genotypes. Synaptic terminal (NMJ, arrow) and muscle nuclei (N, arrows) labeled in control. **(C)** Quantified Wg intensity (left) and percentage of Wg-expressing boutons (right) within HRP synaptic domain. **(D)** Quantified nuclear Fz2-C intensity in above genotypes. See Table S3C for raw data values and sample sizes. **P*<0.05, ***P*<0.01, ****P*<0.001; NS, not significant.

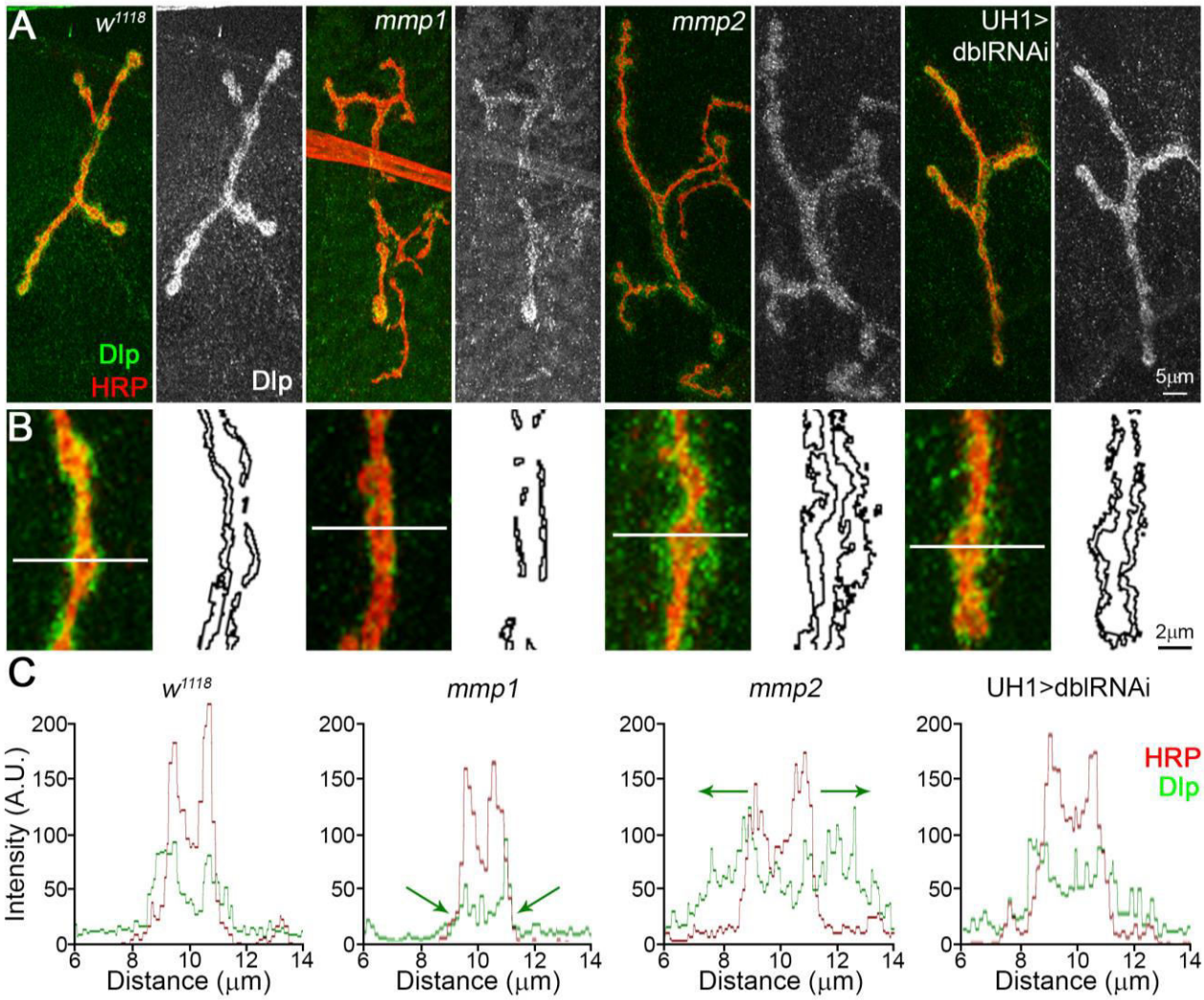

Figure 14

Figure 14: Mmp1 and Mmp2 reciprocally regulate Wnt HSPG co-receptor Dlp.
(A) NMJs labeled for Dlp (green) and HRP synaptic marker (red) in w^{1118}, $mmp1^{Q112*/Q273*}$, $mmp2^{ss218/Df}$ and *UH1>mmp1+2*^{RNAi} (dblRNAi). Black and white images show Dlp. **(B)** Higher magnification images of Dlp (green) at synaptic boutons (red). Skeleton outlines of Dlp area beyond HRP-masked NMJ are shown at the right. **(C)** Line-scan (line in panel B) of Dlp spatial expression (green) relative to HRP synaptic membrane marker (red). Arrows indicate Dlp spatial restriction in *mmp1* and expansion in *mmp2* mutants. See Table S3C for raw data values and sample sizes.

Restoring Wnt co-receptor Dlp levels in Mmp mutants prevents synaptogenic defects

Our working model proposes that the two Mmp classes, balanced by Timp inhibition and reciprocal co-suppression, mediate synaptomatrix control of Wnt trans-synaptic signaling at the level of the Dlp co-receptor to coordinate structural and functional development of the NMJ. If this hypothesis is correct, the altered Dlp levels and/or spatial distribution should be causative for the synaptogenic defects in both classes of Mmp mutants. To test this prediction, we created lines to compensate for changes in Dlp levels in each Mmp mutant, and then tested for correction of both structural and functional defects (Fig. 15, Tables S1A, S2A, 'Dlp modulation'). In *mmp1* LOF mutants, Dlp was significantly reduced in the postsynaptic compartment and therefore, we transgenically increased Dlp expression in the muscle (*mmp1*$^{Q112*/Q273*}$*; 24B>UAS-dlp*). Conversely, in *mmp2* mutants, Dlp was spatially expanded and therefore, we removed one *dlp* gene copy to reduce levels (*mmp2*$^{W307*/Df}$*; dlp*$^{A187/+}$). In both *mmp1* and *mmp2* mutants, correcting Dlp expression toward normal levels suppressed the synaptic morphogenesis defects (Fig. 15A, Table S1A). Quantification of the number of synaptic boutons showed that *mmp1* supernumerary boutons were completely prevented by elevated levels of postsynaptic Dlp (Fig. 15B). Likewise, the elevated number of synaptic boutons in *mmp2* mutants was completely prevented by reducing Dlp levels with the *dlp*/+ heterozygote (Fig. 15B). Next, EJC recordings to assay neurotransmission strength in both *mmp1* and *mmp2* mutants showed that correcting Dlp levels reduced the elevated transmission in both cases (Fig. 15C, Table S2A). Quantification of EJC amplitude showed that postsynaptic Dlp expression in *mmp1* mutants prevented the elevated transmission and reversed the phenotype to cause significantly reduced transmission (Fig. 15D). In *mmp2* mutants, reduction of the Dlp levels restored EJC amplitude towards the control level, showing a significant reduction from the mutant level, with no significant difference remaining compared with the control (Fig. 15D). Thus, both increased NMJ structural development and elevated neurotransmission strength in both classes of Mmp mutant were rectified by manipulating Dlp expression back towards wild-type levels.

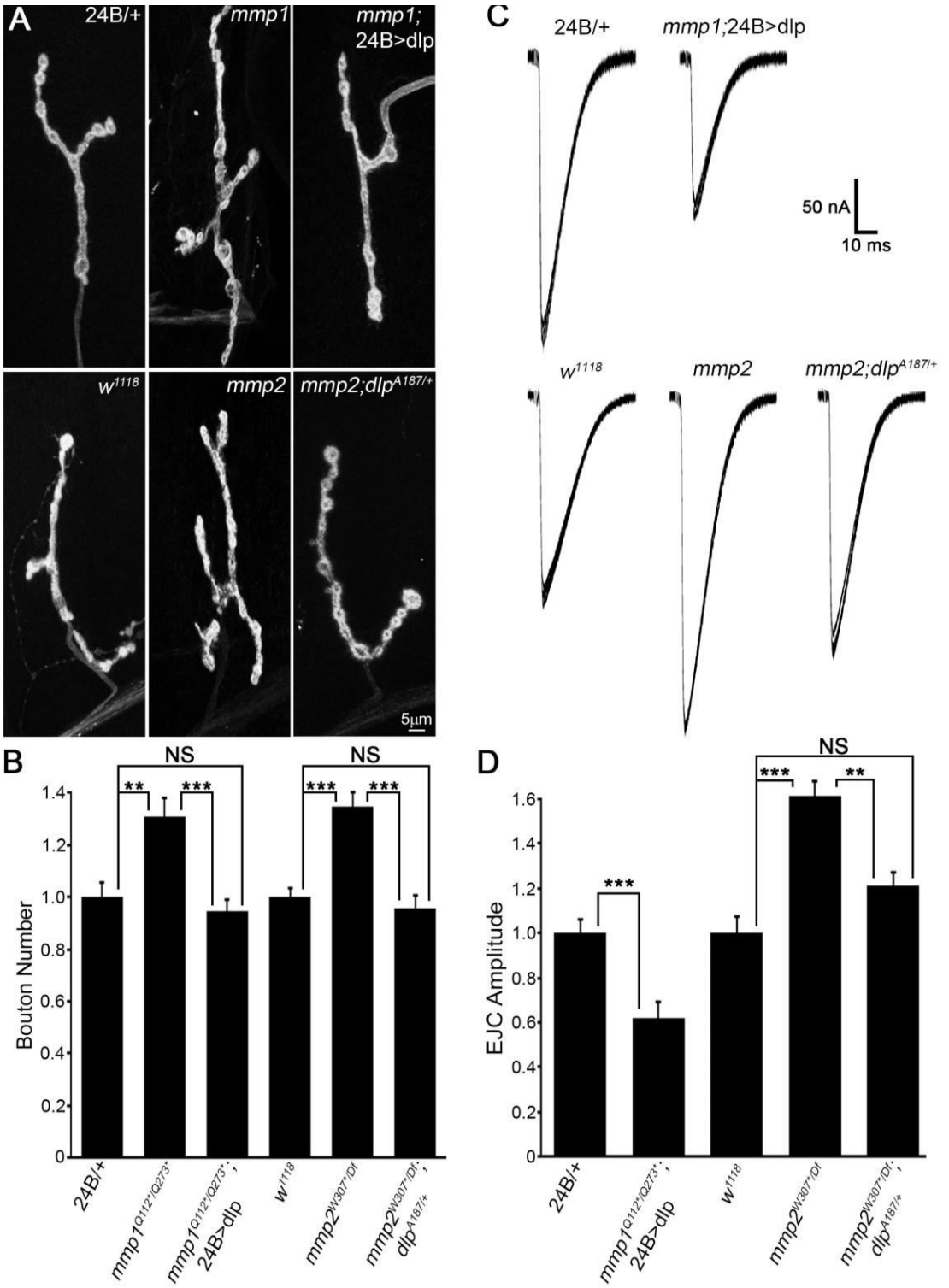

Figure 15

Figure 15: Restoring Dlp levels in Mmp mutants prevents defects in NMJ structure or function.

(A) NMJs labeled for HRP and DLG. Top row: *24B/+* transgenic control, *mmp1*$^{Q112*/Q273*}$ and *mmp1*$^{Q112*/Q273*}$*; 24B>UAS-dlp*. Bottom row: *w*^{1118} genetic control, *mmp2*$^{W307*/Df}$ and *mmp2*$^{W307*/Df}$*; dlp*$^{A187/+}$. (B) Quantified bouton number normalized to controls for above genotypes. (C) EJC traces recorded from denoted genotypes. Top row: *24B/+* transgenic control (left) and *mmp1*$^{Q112*/Q273*}$*; 24B>UAS-dlp*(right). Bottom row: *w*^{1118} genetic control, *mmp2*$^{W307*/Df}$ and *mmp2*$^{W307*/Df}$*; dlp*$^{A187/+}$. (D) Quantified EJC amplitudes normalized to controls for above genotypes. See Table S1A for raw data values and sample sizes. ***P*<0.01, ****P*<0.001; NS, not significant.

Discussion

A large number of Mmps are expressed in the mammalian nervous system, with roles in neurodevelopment, plasticity and neurological disease (*56*). Understanding how each Mmp individually and combinatorially functions is hindered by genetic redundancy and compensatory mechanisms. We have therefore exploited the *Drosophila* system to analyze a matrix metalloproteome containing just one member of each conserved component: one secreted Mmp, one membrane-tethered Mmp and one Timp (*4*, *10–12*, *49*). We found that both Mmp classes attenuate structural and functional synaptic development, with electrophysiological, ultrastructural and molecular roles in both presynaptic and postsynaptic cells. A surprising discovery is that the Mmp classes suppress each other's requirements at the synapse. From discrete activities to redundancy, cooperation and now reciprocal suppression, studies continue to reveal how Mmps interact to regulate developmental processes (*15*, *28*, *54*). This study shows that the two Mmp classes play separable yet interactive roles in sculpting NMJ development. During the writing of this manuscript, a genomic Mmp2 rescue line was produced (*54*), which will be critical in further testing this interactive mechanism. It will be interesting to determine whether the Mmp suppressive mechanism is used in other developmental contexts, other intercellular signaling pathways and in mammalian models. Mammalian Mmp9 regulates synapse architecture and also postsynaptic glutamate receptor expression and/or localization (*20*, *57*, *58*). Likewise, mammalian Mmp7 regulates both presynaptic properties and postsynaptic glutamate receptor subunits (*59*, *60*). Thus, the dual roles of Mmps in pre- and postsynaptic compartments appear to be evolutionarily conserved.

Previous work demonstrated that Mmp1 and Mmp2 both regulate motor axon pathfinding in *Drosophila*embryos, albeit to different degrees and here, double Mmp mutants still exhibited defasciculated nerve bundles that separate prematurely (*15*). Consistently, both Mmp single mutants display excessive terminal axon branching at the postembryonic NMJ, but here the defect is fully alleviated by the removal of both Mmps. To our knowledge, other studies have either not identified, or not tested, a similar Mmp interaction, suggesting that reciprocal suppression might be specific to synaptogenesis. However, there are numerous reports that highlight the importance of Mmp and Timp balance. Mmp:Timp ratios can influence protease activation, localization, substrate specificity and Timp signaling and are commonly used as predictive clinical correlates in disease pathology (*61–63*). At the *Drosophila* NMJ, a similar reciprocal suppression interaction between *pgant* glycosyltransferases involved in *O*-linked glycosylation regulates synaptogenesis via integrin-tenascin trans-synaptic signaling (*45*). A recent study reported that *pgant* activity protects substrates

from Furin-mediated proteolysis, which is a protease responsible for processing or activating *Drosophila* Mmp1 and Mmp2 (*64*). Thus, Mmp proteolytic and glycan mechanisms could converge within the NMJ synaptomatrix to regulate trans-synaptic signaling.

New antibody tools produced here provide the means to interrogate an entire matrix metalloproteome, and will be important for testing Mmp and Timp functions throughout *Drosophila*. Many Mmps are both developmentally and activity regulated, with highly context-dependent functions (*57*, *65*, *66*). Our future work will temporally dissect this mechanism at the developing NMJ and investigate how activity might regulate Mmp localization and function. It will be informative to correlate synaptogenic Mmp requirements with Mmp enzymatic activity by using *in situ* zymography assays, although non-enzymatic roles are certainly also possible. Lack of ultrastructure defects in Mmp mutant NMJs suggests that *Drosophila* Mmps have primarily instructive functions at the synapse, rather than broad proteolytic roles in ECM degradation. Consistently, *Drosophila* Mmp2 instructs motor axon pathfinding via a BMP intercellular signaling mechanism (*16*). Conversely, Mmp2 functions permissively in basement membrane degradation while shaping dendritic arbors (*17*). Because synaptic bouton size is reduced in *mmp1* mutants, Mmp1 activity might degrade a prohibitive physical barrier at the NMJ. However, our results indicate a primary Mmp role in regulating intercellular signaling during synaptic development.

HSPG co-receptors of *trans*-synaptic ligands are key modulators of NMJ synaptogenesis (*27*, *41*, *55*, *67*) and HSPGs are also established substrates of both mammalian and *Drosophila* Mmps (*3*, *54*). Mmp1 and Mmp2 differentially regulate the HSPG Dlp co-receptor to restrict the Wnt Wg trans-synaptic signaling driving structural and functional NMJ development (*35*, *51*, *52*). How might both increased and decreased levels of the Dlp co-receptor yield increased FNI pathway signal transduction? Regulation of Wnt signaling interactions ligands, co-receptors and receptors is managed at many levels (*68*). The 'Wg exchange factor model' (*69*) provides a mechanistic framework for understanding the suppressive interactions of Mmp. In this mechanism, a low Dlp:Frz2 ratio helps the Frz2 receptor obtain more Wg, whereas a high Dlp:Frz2 ratio prevents Frz2 from capturing Wg as Dlp competes and sequesters Wg away from Frz2. Importantly, however, Dlp exhibits a context-dependent, bimodal role as both activator and repressor (*70*). Indeed, our previous studies show these mechanisms are a key driving force in Wg signal transduction at the *Drosophila* NMJ (*27*, *41*). In *mmp1* mutants, Wg and Dlp are both reduced, resulting in a low Dlp:Frz2 ratio and elevated FNI. In *mmp2* mutants, Dlp is spatially diffuse and Frz2 is increased, similarly resulting in a low Dlp:Frz2 ratio and elevated FNI. Balance is reset with Mmp co-removal because neither form of Mmp-induced HSPG tuning occurs. In this regard, it might be predicted that Dlp reduction in *mmp2* mutants would only further increase

FNI and therefore structural and functional defects. However, *mmp2*$^{W307*/Df}$;*dlp*$^{A187/+}$ NMJs are indistinguishable from controls. It is therefore likely that absolute Dlp levels are the important driving factor in synaptogenesis and/or that Dlp exhibits bimodal functions in synaptic development.

Interestingly, a recent mouse study showed the Mmp3 hemopexin domain promotes Wnt signaling by inhibiting a negative Wnt regulator, raising the possibility that Mmps can act as molecular switches (or in feedback loops) dictating Wnt transduction (*71*). Another study suggests that Wnt signaling can directly mediate co-regulation of heparanase and Mmps (*72*). Indeed, both neural activity and intercellular signaling can stimulate Mmp-dependent ectodomain shedding of plasma membrane target proteins, thereby directly regulating the surface abundance of HSPGs and receptors, as well as other Mmps, which thus reciprocally modulate intra- and extracellular organization (*6*, *73*, *74*). From this model, the spatial arrangement of Dlp could be affected by co-regulated sheddase activity that is differentially altered in *mmp1* and *mmp2* mutants. Specifically, Mmp2 could shed Dlp, resulting in an increased area of Dlp expression in *mmp2* mutants and loss of Mmp2 regulation by Mmp1 could result in aberrant Dlp restriction in *mmp1*mutants, with Mmp co-removal remediating the Dlp domain thereby restoring normal Wnt trans-synaptic signaling. Our future work will test the reciprocal impacts of Wnt signaling on Mmp expression and/or function in the context of synaptic development.

Emerging evidence suggests HSPG glycosaminoglycan (GAG) chains function as allosteric regulators of Mmps, with GAG content or composition influencing the localization and substrate specificity of Mmp (*75*). Indeed, studies from our lab and others show that Wg signaling is sensitive to perturbations in HSPG chain biosynthesis and HS modifying enzymes, which modulate both NMJ structure and function (*39*, *41*, *76*, *77*). It is easy to envision how tissue- and development-stage-specific HS modifications could coordinate HSPG/Mmp-dependent functions, thereby differentially regulating diverse signaling events, which enable context-specific responses instructed by the extracellular environment. Future work will examine how dual inputs of the HSPG co-receptor function and how Mmp proteolytic cleavage coordinates Wnt trans-synaptic signaling during synaptogenesis, particularly in the context of our Fragile X syndrome (FXS) disease model (*78*, *79*). Given that both Mmp loss or Mmp inhibition Mmp (*25*) and correction of HSPG elevation (*27*) independently alleviate synaptic defects in the FXS disease state, the overlapping mechanism provides an exciting avenue to therapeutic interventions for FXS and, potentially, related intellectual disability and autism spectrum disorders.

References

1. J. Vautrin, The synaptomatrix: A solid though dynamic contact disconnecting transmissions from exocytotic events. *Neurochem. Int.* **57**, 85–96 (2010).
2. N. Dani, K. Broadie, Glycosylated synaptomatrix regulation of trans-synaptic signaling. *Dev. Neurobiol.* **72**, 2–21 (2011).
3. K. Kessenbrock, V. Plaks, Z. Werb, Matrix Metalloproteinases: Regulators of the Tumor Microenvironment. *Cell*. **141**, 52–67 (2010).
4. A. Page-McCaw, A. J. Ewald, Z. Werb, Matrix metalloproteinases and the regulation of tissue remodeling. *Nat Rev Mol Cell Biol.* **8**, 221–233 (2007).
5. M. Sternlicht, Z. Werb, How matrix metalloproteinases regulate cell behavior. *Annu Rev Cell Biol*. **17**, 463–516 (2001).
6. G. W. Huntley, Synaptic circuit remodelling by matrix metalloproteinases in health and disease. *Nat. Rev. Neurosci.* **13**, 743–757 (2012).
7. S. M. Reinhard, K. Razak, I. M. Ethell, A delicate balance: role of MMP-9 in brain development and pathophysiology of neurodevelopmental disorders. *Front. Cell. Neurosci.* **9**, 280 (2015).
8. T. Shinoe, Y. Goda, Tuning synapses by proteolytic remodeling of the adhesive surface. *Curr. Opin. Neurobiol.* **December 2**, 148–155 (2015).
9. T. Wójtowicz, J. W. Mozrzymas, Diverse impact of acute and long-term extracellular proteolytic activity on plasticity of neuronal excitability. *J. Neurosci. Res.* **93**, 1330–1344 (2015).
10. E. Llano, A. M. Pendas, P. Aza-Blanc, T. B. Kornberg, C. Lopez-Otin, Dm1-MMP, a matrix metalloproteinase from Drosophila with a potential role in extracellular matrix remodeling during neural development. *J. Biol. Chem.* **275**, 35978–35985 (2000).
11. E. Llano, G. Adam, A. M. Pendás, V. Quesada, L. M. Sánchez, I. Santamaría, S. Noselli, C. López-Otín, Structural and enzymatic characterization of Drosophila Dm2-MMP, a membrane-bound matrix metalloproteinase with tissue-specific expression. *J. Biol. Chem.* **277**, 23321–23329 (2002).
12. A. Page-McCaw, J. Serano, J. M. Sante, G. M. Rubin, Drosophila matrix metalloproteinases are required for tissue remodeling, but not embryonic development. *Dev. Cell*. **4**, 95–106 (2003).
13. S. Wei, Z. Xie, E. Filenova, K. Brew, Drosophila TIMP Is a Potent Inhibitor of MMPs and TACE: Similarities in Structure and Function to TIMP-3. *Biochemistry*. **42**, 12200–12207 (2003).
14. C. T. Kuo, L. Y. Jan, Y. N. Jan, Dendrite-specific remodeling of Drosophila sensory neurons requires

matrix metalloproteases, ubiquitin-proteasome, and ecdysone signaling. *Proc. Natl. Acad. Sci. U. S. A.* **102**, 15230–15235 (2005).

15. C. M. Miller, A. Page-McCaw, H. T. Broihier, Matrix metalloproteinases promote motor axon fasciculation in the Drosophila embryo. *Development*. **135**, 95–109 (2008).
16. C. M. Miller, N. Liu, A. Page-McCaw, H. T. Broihier, Drosophila Mmp2 Regulates the Matrix Molecule Faulty Attraction (Frac) to Promote Motor Axon Targeting in Drosophila. *J. Neurosci.* **31**, 5335–5347 (2011).
17. K. I. Yasunaga, T. Kanamori, R. Morikawa, E. Suzuki, K. Emoto, Dendrite Reshaping of Adult Drosophila Sensory Neurons Requires Matrix Metalloproteinase-Mediated Modification of the Basement Membranes. *Dev. Cell*. **18**, 621–632 (2010).
18. S. M. Agrawal, L. Lau, V. W. Yong, MMPs in the central nervous system: Where the good guys go bad. *Semin. Cell Dev. Biol.* **19**, 42–51 (2008).
19. E. Pollock, M. Everest, A. Brown, M. O. Poulter, Metalloproteinase inhibition prevents inhibitory synapse reorganization and seizure genesis. *Neurobiol. Dis.* **70**, 21–31 (2014).
20. G. M. Wilczynski, F. A. Konopacki, E. Wilczek, Z. Lasiecka, A. Gorlewicz, P. Michaluk, M. Wawrzyniak, M. Malinowska, P. Okulski, L. R. Kolodziej, W. Konopka, K. Duniec, B. Mioduszewska, E. Nikolaev, A. Walczak, D. Owczarek, D. C. Gorecki, W. Zuschratter, O. P. Ottersen, *et al.*, Important role of matrix metalloproteinase 9 in epileptogenesis. *J. Cell Biol.* **180**, 1021–1035 (2008).
21. C. L. Gatto, K. Broadie, Drosophila modeling of heritable neurodevelopmental disorders. *Curr. Opin. Neurobiol.* **21**, 834–841 (2011).
22. T. V Bilousova, L. Dansie, M. Ngo, J. Aye, J. R. Charles, D. W. Ethell, I. M. Ethell, Minocycline promotes dendritic spine maturation and improves behavioural performance in the fragile X mouse model. *J. Med. Genet.* **46**, 94–102 (2009).
23. H. Sidhu, L. E. Dansie, P. W. Hickmott, D. W. Ethell, I. M. Ethell, Genetic removal of matrix metalloproteinase 9 rescues the symptoms of fragile X syndrome in a mouse model. *J. Neurosci.* **34**, 9867–9879 (2014).
24. S. S. Siller, K. Broadie, Matrix metalloproteinases and minocycline: Therapeutic avenues for fragile X syndrome. *Neural Plast.* **2012**, 43–47 (2012).
25. S. S. Siller, K. Broadie, Neural circuit architecture defects in a Drosophila model of Fragile X syndrome are alleviated by minocycline treatment and genetic removal of matrix metalloproteinase. *Dis. Model. Mech.* **4**, 673–685 (2011).

26. C. A. Doll, K. Broadie, Impaired activity-dependent neural circuit assembly and refinement in autism spectrum disorder genetic models. *Front. Cell. Neurosci.* **8**, 30 (2014).
27. S. H. Friedman, N. Dani, E. Rushton, K. Broadie, Fragile X mental retardation protein regulates trans-synaptic signaling in Drosophila. *Dis. Model. Mech.* **6**, 1400–1413 (2013).
28. Q. Jia, Y. Liu, H. Liu, S. Li, Mmp1 and Mmp2 cooperatively induce Drosophila fat body cell dissociation with distinct roles. *Sci. Rep.* **4**, 7535 (2014).
29. T. A. Godenschwege, N. Pohar, S. Buchner, E. Buchner, Inflated wings, tissue autolysis and early death in tissue inhibitor of metalloproteinases mutants of Drosophila. *Eur. J. Cell Biol.* **79**, 495–501 (2000).
30. M. Uhlirova, D. Bohmann, JNK- and Fos-regulated Mmp1 expression cooperates with Ras to induce invasive tumors in Drosophila. *EMBO J.* **25**, 5294–5304 (2006).
31. G. H. Baeg, X. Lin, N. Khare, S. Baumgartner, N. Perrimon, Heparan sulfate proteoglycans are critical for the organization of the extracellular distribution of Wingless. *Development*. **128**, 87–94 (2001).
32. C. Han, T. Y. Belenkaya, B. Wang, X. Lin, Drosophila glypicans control the cell-to-cell movement of Hedgehog by a dynamin-independent process. *Development*. **131**, 601–611 (2004).
33. W. Parkinson, M. L. Dear, E. Rushton, K. Broadie, N-glycosylation requirements in neuromuscular synaptogenesis. *Development*. **140**, 4970–4981 (2013).
34. K. Chen, D. E. Featherstone, Discs-large (DLG) is clustered by presynaptic innervation and regulates postsynaptic glutamate receptor subunit composition in Drosophila. *BMC Biol.* **3**, 1 (2005).
35. D. Mathew, B. Ataman, J. Chen, Y. Zhang, S. Cumberledge, V. Budnik, Wingless Signaling at Synapses Is Through Cleavage and Nuclear Import of Receptor DFrizzled2. *Science*. **310**, 1344–1347 (2005).
36. S. B. Marrus, A. DiAntonio, Preferential localization of glutamate receptors opposite sites of high presynaptic release. *Curr. Biol.* **14**, 924–931 (2004).
37. C. L. Gatto, K. Broadie, Temporal requirements of the fragile X mental retardation protein in the regulation of synaptic structure. *Development*. **135**, 2637–2648 (2008).
38. C. A. Doll, K. Broadie, Activity-dependent FMRP requirements in development of the neural circuitry of learning and memory. *Development*. **142**, 1346–1356 (2015).
39. K. Menon, R. Carrillo, K. Zinn, Development and Plasticity of Drosophila Larval Neuromuscular Junction. *Dev. Biol.* **2**, 647–670 (2013).
40. G. Davis, M. Muller, Homeostatic control of presynaptic neurotransmitter release. *Annu Rev Physiol*. **77**, 251–270 (2015).
41. N. Dani, M. Nahm, S. Lee, K. Broadie, A Targeted Glycan-Related Gene Screen Reveals Heparan Sulfate

Proteoglycan Sulfation Regulates WNT and BMP Trans-Synaptic Signaling. *PLoS Genet.* **8**, e1003031 (2012).

42. D. A. Wagh, T. M. Rasse, E. Asan, A. Hofbauer, I. Schwenkert, H. Dürrbeck, S. Buchner, M.-C. Dabauvalle, M. Schmidt, G. Qin, C. Wichmann, R. Kittel, S. J. Sigrist, E. Buchner, Bruchpilot, a protein with homology to ELKS/CAST, is required for structural integrity and function of synaptic active zones in Drosophila. *Neuron*. **49**, 833–844 (2006).
43. G. Qin, T. Schwarz, R. J. Kittel, A. Schmid, T. M. Rasse, D. Kappei, E. Ponimaskin, M. Heckmann, S. J. Sigrist, Four Different Subunits Are Essential for Expressing the Synaptic Glutamate Receptor at Neuromuscular Junctions of Drosophila. *J. Neurosci.* **25**, 3209–3218 (2005).
44. A. DiAntonio, S. A. Petersen, M. Heckmann, C. S. Goodman, Glutamate receptor expression regulates quantal size and quantal content at the Drosophila neuromuscular junction. *J. Neurosci.* **19**, 3023–3032 (1999).
45. N. Dani, H. Zhu, K. Broadie, Two Protein N-Acetylgalactosaminyl Transferases Regulate Synaptic Plasticity by Activity-Dependent Regulation of Integrin Signaling. *J. Neurosci.* **34**, 13047–13065 (2014).
46. A. A. Long, C. T. Mahapatra, E. A. Woodruff, J. Rohrbough, H.-T. Leung, S. Shino, L. An, R. W. Doerge, M. M. Metzstein, W. L. Pak, K. Broadie, The nonsense-mediated decay pathway maintains synapse architecture and synaptic vesicle cycle efficacy. *J. Cell Sci.* **123**, 3303–3315 (2010).
47. J. Rohrbough, E. Rushton, E. Woodruff, T. Fergestad, K. Vigneswaran, K. Broadie, Presynaptic establishment of the synaptic cleft extracellular matrix is required for post-synaptic differentiation. *Genes Dev.* **21**, 2607–2628 (2007).
48. R. Mohrmann, H. J. Matthies, E. Woodruff, K. Broadie, Stoned B Mediates Sorting of Integral Synaptic Vesicle Proteins. *Neuroscience*. **153**, 1048–1063 (2008).
49. B. M. Glasheen, A. T. Kabra, A. Page-McCaw, Distinct functions for the catalytic and hemopexin domains of a Drosophila matrix metalloproteinase. *Proc. Natl. Acad. Sci. U. S. A.* **106**, 2659–2664 (2009).
50. Q. Wang, M. Uhlirova, D. Bohmann, Spatial Restriction of FGF Signaling by a Matrix Metalloprotease Controls Branching Morphogenesis. *Dev. Cell*. **18**, 157–164 (2010).
51. M. Packard, E. S. Koo, M. Gorczyca, J. Sharpe, S. Cumberledge, V. Budnik, The Drosophila Wnt, wingless, provides an essential signal for pre- and postsynaptic differentiation. *Cell*. **111**, 319–330 (2002).
52. S. D. Speese, J. Ashley, V. Jokhi, J. Nunnari, R. Barria, Y. Li, B. Ataman, A. Koon, Y.-T. Chang, Q. Li, M. J. Moore, V. Budnik, Nuclear envelope budding enables large ribonucleoprotein particle export during synaptic Wnt signaling. *Cell*. **149**, 832–846 (2012).

53. B. Ataman, J. Ashley, M. Gorczyca, P. Ramachandran, W. Fouquet, S. J. Sigrist, V. Budnik, Rapid activity-dependent modifications in synaptic structure and function require bidirectional Wnt signaling. *Neuron*. **57**, 705–718 (2008).

54. X. Wang, A. Page-McCaw, A matrix metalloproteinase mediates long-distance attenuation of stem cell proliferation. *J. Cell Biol.* **206**, 923–936 (2014).

55. K. G. Johnson, A. P. Tenney, A. Ghose, A. M. Duckworth, M. E. Higashi, K. Parfitt, O. Marcu, T. R. Heslip, J. L. Marsh, T. L. Schwarz, J. G. Flanagan, D. Van Vactor, The HSPGs Syndecan and dallylike bind the receptor phosphatase LAR and exert distinct effects on synaptic development. *Neuron*. **49**, 517–531 (2006).

56. H. Fujioka, Y. Dairyo, K. I. Yasunaga, K. Emoto, Neural functions of matrix metalloproteinases: Plasticity, neurogenesis, and disease. *Biochem. Res. Int.* **2012**, 789083 (2012).

57. M. Dziembowska, J. Wlodarczyk, MMP9: a novel function in synaptic plasticity. *Int. J. Biochem. Cell Biol.* **44**, 709–713 (2012).

58. P. Michaluk, L. Mikasova, L. Groc, R. Frischknecht, D. Choquet, L. Kaczmarek, Matrix Metalloproteinase-9 Controls NMDA Receptor Surface Diffusion through Integrin 1 Signaling. *J. Neurosci.* **29**, 6007–6012 (2009).

59. A. Szklarczyk, K. Conant, D. F. Owens, R. Ravin, R. D. McKay, C. Gerfen, Matrix metalloproteinase-7 modulates synaptic vesicle recycling and induces atrophy of neuronal synapses. *Neuroscience*. **149**, 87–98 (2007).

60. A. Szklarczyk, O. Ewaleifoh, J.-C. Beique, Y. Wang, D. Knorr, N. Haughey, T. Malpica, M. P. Mattson, R. Huganir, K. Conant, MMP-7 cleaves the NR1 NMDA receptor subunit and modifies NMDA receptor function. *FASEB J.* **22**, 3757–3767 (2008).

61. H. Nagase, R. Visse, G. Murphy, Structure and function of matrix metalloproteinases and TIMPs. *Cardiovasc. Res.* **69**, 562–573 (2006).

62. C. S. Moore, S. J. Crocker, An Alternate Perspective on the Roles of TIMPs and MMPs in Pathology. *AJPA*. **180**, 12–16 (2011).

63. F. Romi, G. Helgeland, N. E. Gilhus, Serum levels of matrix metalloproteinases: Implications in clinical neurology. *Eur. Neurol.* **67**, 121–128 (2012).

64. L. Zhang, Z. A. Syed, I. van Dijk Härd, J.-M. Lim, L. Wells, K. G. Ten Hagen, O-glycosylation regulates polarized secretion by modulating Tango1 stability. *Proc. Natl. Acad. Sci. U. S. A.* **111**, 7296–7301 (2014).

65. D. L. Benson, G. W. Huntley, Building and remodeling synapses. *Hippocampus*. **22**, 954–968 (2012).

66. I. M. Ethell, D. W. Ethell, Matrix metalloproteinases in brain development and remodeling: Synaptic functions and targets. *J. Neurosci. Res.* **85**, 2813–2823 (2007).

67. K. Kamimura, K. Ueno, J. Nakagawa, R. Hamada, M. Saitoe, N. Maeda, Perlecan regulates bidirectional Wnt signaling at the Drosophila neuromuscular junction. *J. Cell Biol.* **200**, 219–233 (2013).

68. R. van Amerongen, Alternative Wnt pathways and receptors. *Cold Spring Harb. Perspect. Biol.* **4**, a007914 (2012).

69. D. Yan, Y. Wu, Y. Feng, S.-C. Lin, X. Lin, The Core Protein of Glypican Daily-Like Determines Its Biphasic Activity in Wingless Morphogen Signaling. *Dev. Cell*. **17**, 470–481 (2009).

70. Y. Wu, T. Y. Belenkaya, X. Lin, in *Methods in Enzymology*, M. Fukuda, Ed. (Elsevier Inc., 2010), vol. 480, pp. 33–50.

71. K. Kessenbrock, G. J. P. Dijkgraaf, D. A. Lawson, L. E. Littlepage, P. Shahi, U. Pieper, Z. Werb, A Role for matrix metalloproteinases in regulating mammary stem cell function via the Wnt signaling pathway. *Cell Stem Cell*. **13**, 300–313 (2013).

72. E. Zcharia, J. Jia, X. Zhang, L. Baraz, U. Lindahl, T. Peretz, I. Vlodavsky, J. P. Li, Newly generated heparanase knock-out mice unravel co-regulation of heparanase and matrix metalloproteinases. *PLoS One*. **4**, e5181 (2009).

73. L. E. Dansie, I. M. Ethell, Casting a Net on Dendritic Spines: The Extracellular Matrix and its Receptors. *Dev. Neurobiol.* **71**, 956–981 (2011).

74. L. Tian, M. Stefanidakis, L. Ning, P. Van Lint, H. Nyman-Huttunen, C. Libert, S. Itohara, M. Mishina, H. Rauvala, C. G. Gahmberg, Activation of NMDA receptors promotes dendritic spine development through MMP-mediated ICAM-5 cleavage. *J. Cell Biol.* **178**, 687–700 (2007).

75. A. Tocchi, W. C. Parks, Functional interactions between matrix metalloproteinases and glycosaminoglycans. *FEBS J.* **280**, 2332–2341 (2013).

76. F. Reichsman, L. Smith, S. Cumberledge, Glycosaminoglycans can modulate extracellular localization of the wingless protein and promote signal transduction. *J. Cell Biol.* **135**, 819–827 (1996).

77. Y. Ren, C. A. Kirkpatrick, J. M. Rawson, M. Sun, S. B. Selleck, Cell Type-Specific Requirements for Heparan Sulfate Biosynthesis at the Drosophila Neuromuscular Junction: Effects on Synapse Function, Membrane Trafficking, and Mitochondrial Localization. *J. Neurosci.* **29**, 8539–8550 (2009).

78. R. L. Coffee, C. R. Tessier, E. A. Woodruff, K. Broadie, Fragile X mental retardation protein has a unique, evolutionarily conserved neuronal function not shared with FXR1P or FXR2P. *Dis. Model. Mech.* **3**, 471–485 (2010).

79. C. R. Tessier, K. Broadie, The Fragile X Mental Retardation Protein Developmentally Regulates the Strength and Fidelity of Calcium Signaling in Drosophila Mushroom Body Neurons. *Neurobiol. Dis.* **41**, 147–159 (2011).

CHAPTER III

NEURONAL ACTIVITY DRIVES FMRP- AND HSPG-DEPENDENT MATRIX METALLOPROTEINASE FUNCTION REQUIRED FOR RAPID SYNAPTOGENESIS

This paper has been published under the same title in *Science Signaling*, 2017

Mary Lynn Dear, Jarrod Shilts and Kendal Broadie

Department of Biological Sciences, Vanderbilt University, Nashville, TN, USA
Department of Cell & Developmental Biology, Vanderbilt Medical Center, Nashville, TN, USA
Vanderbilt Brain Institute, Vanderbilt University and Medical Center, Nashville, TN, USA

Jarrod Shilts performed zymography assays and Mary Lynn Dear performed all other experiments and all quantification.

Summary

Matrix metalloproteinase (MMP) functions modulate synapse formation and activity-dependent plasticity, with MMP dysfunction implicated in the Fragile X syndrome (FXS) disease state. *Drosophila* studies show that Mmps genetically interact with the heparan sulfate proteoglycan (HSPG) glypican co-receptor Dally-like protein (Dlp) to restrict *trans*-synaptic Wnt signaling, and that synaptogenic defects in this FXS disease model are alleviated by both Mmp inhibition and Dlp genetic reduction. Here, we employed the *Drosophila* neuromuscular junction (NMJ) glutamatergic synapse to test activity-dependent Dlp and Mmp intersections in the context of the FXS disease state. We found rapid, activity-dependent synaptic bouton formation is completely dependent upon secreted Mmp1. Acute neuronal stimulation reduced Mmp2, but increased both Mmp1 and Dlp. We found acute activity enhanced Dlp and Mmp1 co-localization at the synapse, and that Dlp function bidirectionally controlled Mmp1 abundance. We found Dlp is required for activity-dependent Mmp1 enhancement, with Dlp glycosaminoglycan (GAG) chains mediating this interaction. In parallel, we found Dlp bidirectionally regulates proteolytic activity surrounding synapses. In the FXS model, we found restricting Dlp prevents Mmp1 elevation. Moreover, we found that activity-dependent Mmp1 enhancement is lost in the FXS disease state, but could be completely restored by reducing synaptic Dlp. This mechanistic axis from neuronal activity to HSPG-dependent Mmp regulation drives activity-dependent synaptogenesis, and provides a causative mechanism for FXS synaptogenic defects.

Introduction

Developing and maintaining proper synaptic connectivity requires tightly coordinated intercellular signaling across the synaptic cleft between pre- and postsynaptic cells. This feat is achieved through selective expression of a range of cell adhesion molecules and secreted ligands within the highly specialized extracellular synaptomatrix that separates synaptic partners (*1*, *2*). This cellular interface is highly adaptable (plastic), sculpted by use (activity), and constantly remodeled by secreted enzymes molding the dynamic environment (*3*–*6*). A principal challenge is to understand exactly how these extracellular forces are regulated to control activity-dependent synaptic development. A core family of secreted proteases, matrix metalloproteinases (MMPs), occupy a key nexus of coordinated cell-cell and cell-matrix signaling to modulate synaptic architecture and neurotransmission strength (*7*–*9*). Conserved MMP domains include N-terminal secretory signal sequence, the cleavable pro-domain, zinc-binding catalytic site and the closely linked C-

terminal hemopexin domain (*10*). Changes in MMP function regulate synaptogenesis and mediate activity-dependent remodeling, and MMP dysfunction is implicated in numerous neurological disorders including autism, epilepsy, addiction and schizophrenia (*11*–*15*). Thus, MMP-dependent control of the extracellular synaptomatrix interface appears critical for normal synaptic development, and is implicated in a wide range of synaptic disease states.

The *Drosophila* glutamatergic neuromuscular junction (NMJ) synapse has proven an excellent model to interrogate synaptomatrix questions, with conserved extracellular mechanisms and well defined activity-dependent synaptogenic processes (*2*, *16*–*18*). Compared to challenges of testing the 24 MMPs in mammalian models, *Drosophila* has just 2 MMPs, secreted Mmp1 and glycosylphosphatidylinositol (GPI)-anchored Mmp2 (*19*–*21*); although one Mmp1 isoform is also GPI-anchored (*22*). Both Mmps regulate motor neuron axon defasciculation, with the matrix molecule Faulty Attraction (Frac) identified as an Mmp2 substrate promoting motor axon targeting (*23*, *24*). Both Mmps also regulate synaptogenesis in multiple contexts, including reshaping dendritic arbors (*25*, *26*) and axonal terminals (*27*). At the NMJ, these two Mmps coordinate structural and functional synaptogenesis by heparan sulfate proteoglycan (HSPG) dependent regulation of Wnt Wingless (Wg) *trans*-synaptic signaling (*7*). In the *Drosophila* Fragile X syndrome (FXS) disease model, aberrant HSPG- and Mmp-dependent Wg signaling is causative for synaptogenic defects (*28*). This common intellectual disability and autism spectrum disorder is caused by loss of Fragile X Mental Retardation Protein (FMRP), an mRNA-binding translational regulator of activity-dependent synaptogenesis (*29*–*31*). Both HSPGs and Mmps are putative FMRP targets misregulated in the *Drosophila* FXS model (*28*, *29*, *32*, *33*).

HSPGs are particularly intriguing extracellular regulators of activity-dependent MMP localization and function (*34*, *35*). The diverse, multi-functional HSPGs can be fully secreted, membrane-tethered or transmembrane, and consist of a core protein plus heparan sulfate (HS) glycosaminoglycan (GAG) chains. HSPGs are known to function as extracellular signaling platforms linking secreted ligands, receptors and proteases, and MMPs can also proteolytically cleave HSPGs in a reciprocal HSPG-Mmp relationship (*34*, *36*–*39*). HSPGs are potent regulators of activity-dependent synaptic development and plasticity (*40*–*43*). The ~17 HSPGs in mammals present considerable experimental challenges, but the *Drosophila* genome encodes just 5 HSPGs in total, with only 3 synaptic HSPGs (*38*, *40*, *41*). At the NMJ, the secreted HSPG Perlecan mediates Wg signaling directionality, and serves to restrict synaptic structural growth (*44*), the transmembrane HSPG Syndecan conversely promotes synaptic development (*41*), whereas the GPI-anchored HSPG Dally-like Protein (Dlp) serves as a critical biphasic regulator of Wg signaling to modulate synaptogenesis (*40*, *45*, *46*). This *trans*-synaptic Wg signaling drives activity-dependent synaptogenesis, promoting both structural growth and

functional strengthening (*47*–*50*). Activity-induced Wg signaling mediates rapid, new synaptic bouton formation (*47*), but a Dlp co-receptor role in this synaptogenic mechanism has not been explored.

Given the role of neuronal activity in controlling FMRP abundance and function (*51*–*54*), with known requirements in activity-dependent synaptogenesis (*28*, *55*–*60*), we hypothesized a downstream mechanistic link between membrane-anchored glypican Dlp and the Mmps driving activity-induced synapse modulation. In testing this hypothesis, we found that Mmp1, but not Mmp2, is absolutely required for rapid, activity-dependent synaptic bouton formation. Using both acute transgenic and ionic depolarization paradigms, we found that Mmp1 is increased in response to heightened activity, with both FMRP and Dlp required for this activity-dependent mechanism. Conversely, Mmp2 is reduced following activity stimulation. We found that Dlp co-localization with Mmp1 is enhanced by activity, and that Dlp induces Mmp1 synaptic localization with heightened co-localization in use-activated synapses. We found both FMRP and Dlp are absolutely required for this activity-dependent Mmp1 enhancement, with the FMRP requirement by-passed by genetically reducing Dlp abundance in the FXS disease model. Overall, these results show that the HSPG glypican Dlp is a direct, positive regulator of basal and activity-dependent Mmp1 abundance at the synapse. This work also reveals that inappropriate Mmp1 regulation in the FXS disease state can be rectified by reducing Dlp, thereby identifying a potential means to correct neuropathological synaptic defects.

Materials and Methods

Drosophila Genetics

All stocks were maintained on standard medium at 25°C, except for lines used to manipulate neuronal activity with dTRPA1 (see below). The following Gal4 driver lines were obtained from the Bloomington *Drosophila* Stock Center (BDSC; Bloomington, Indiana): pan-neuronal driver *elav-Gal4* (#8760), selective neuronal driver *CcapR-Gal4* (#39292), glutamatergic neuron driver *vglut-Gal4* (#26160) and muscle-specific driver *24B-Gal4* (#1767). The dual neuron and muscle driver *elav-Gal4, 24B-Gal4* was created using standard genetic recombination (*61*). For the dTRPA1 studies, *vglut-Gal4* or *CcapR-Gal4* were crossed to the warmth-activated *UAS-dTRPA1* (BDSC, #26263) cation channel transgene to stimulate activity within motor neurons (*62*–*66*). Genetic lines used to manipulate Mmps include; 1) $mmp1^{Q112*}$ (BDSC #59380) genetic null loss of function allele, 2) $mmp1^{Q273*}$ hypomorphic allele caused by a point mutation early stop codon, 3) $UAS\text{-}mmp1^{RNAi}$ (*67*), 4) $mmp2^{W307*}$ genetic null loss of function allele, and 5) chromosomal deficiency *Df(2R)BSC132* (BDSC #9410) that removes the entire *mmp2* gene (*21*, *68*). Standard recombination was used to create *vglut-Gal4*,

mmp1^{Q112*} and *vglut-Gal4, mmp2*^{W307*}, and *UAS-dTRPA1*, *mmp1*^{Q112*} and *UAS-dTRPA1, Df(2R)BSC132* lines, which were then crossed to generate *vglut-Gal4> UAS-dTRPA1*, *mmp1*^{Q112*} */mmp1*^{Q112*} and *vglut-Gal4> UAS-dTRPA1*, *mmp2*^{W307*}*/Df(2R)BSC132*, respectively. The genetic lines used to manipulate Dlp expression include; 1) *dlp*^{A187}*,* a 26-nucleotide reading frame shift deleting the GAG attachment domain, GPI-anchor and part of the cysteine-rich region (*69*), 2) *UAS-dlp*^{RNAi} (Vienna *Drosophila* Resource Center (VDRC), #10299), 3) wildtype *UAS-dlp*^{WT} (BDSC, #9160; (*70*), and 4) *UAS-dlp*$^{-HS}$, with all 5 GAG attachment sites (Ser^{625}, Ser^{629}, Ser^{631}, Ser^{643} and Ser^{686}) mutated to alanines (*46*, *71*). The Dlp::GFP line used was *y*^{1},*w**;*dlp*$^{MI04217\text{-}GFSTF.1}$ (BDSC, #60540; (*72*, *73*) containing an *EGFP-FlAsH-StrepII-TEV-3xFlag* insertion within a *dlp* coding intron, shared by both annotated transcripts, resulting in expression of Dlp tagged with internal GFP tag incorporated into the endogenous *dlp* locus. The *dfmr1*^{50M} deletion allele is a full loss of function null mutant (*74*). Standard genetic recombination was used to generate *dlp*^{A187}, *dfmr1*^{50M}/TM6, Hu-GFP (*28*), which was subsequently crossed to *dfmr1*^{50M}/TM6, Tb to produce *dlp*$^{A187/+}$, *dfmr1*^{50M}*/*^{50M} animals. Genetic controls included the *w*^{1118} genetic background, as well as *Gal4* drivers alone crossed into the *w*^{1118} background.

Activity Manipulations

A high [K^+] depolarization paradigm was performed for 10 minutes using 90mM KCl in 1.8 mM $CaCl_2$ saline (*75*). Unstimulated controls received a 10-minute mock treatment with standard physiological saline (see below). For dTRPA1 studies, the pan-motor neuron driver *vglut-Gal4* (BDSC #26160, *OK371*) (*76–78*) or selective neuronal driver *CcapR-Gal4* (BDSC #39292 (*79–81*)), were crossed to warmth-activated *UAS-dTRPA1* cation channel transgene (BDSC, #26263) to stimulate activity (*62–66*). Animals were raised at the dTRPA1-restrictive temperature (18°C) until the wandering 3rd instar stage, then transferred to pre-temperature treated apple juice agar plates for 1-hour at the dTRPA1-permissive temperature (30°C). Controls included *vglut-Gal4/+* or *CcapR-Gal4/+* (+/- temperature shift), *vglut-Gal4/+*, *mmp1*^{Q112*}*/ mmp1*^{Q112*} or *vglut-Gal4/+, mmp2*^{w307*}*/Df(2R)BSC132* (+/- temperature shift), *vglut-Gal4>UAS-dTRPA1* and *CcapR-Gal4>UAS-dTRPA1* (no temperature shift), and *vglut-Gal4>UAS-dTRPA1*, *mmp1*^{Q112*}*/mmp1*^{Q112*} or *vglut-Gal4> UAS-dTRPA1*, *mmp2*^{w307*} */Df(2R)BSC132* (no temperature shift).

Immunocytochemistry Confocal Imaging

Imaging was performed on wandering 3rd instars at muscle 4 and 6/7 NMJs. Staged larvae were dissected in physiological saline (in mM: 128 NaCl, 2 KCl, 4 $MgCl_2$, 70 sucrose, 5 HEPES, and 0 $CaCl_2$ pH 7.2), fixed with 4% paraformaldehyde (4% PFA + 4% sucrose in phosphate buffered saline (PBS)) for 15 minutes, washed 3X with

PBS, and then incubated with primary antibodies diluted in PBS overnight at 4°C. Preparations were then washed 3X with PBS, incubated with secondary antibodies diluted in PBS for 2 hours at room temperature, washed 3X with PBS, and then mounted in Fluoromount-G (Electron Microscopy Sciences). For co-localization studies, a 1-hour blocking step (0.5% Bovine Serum Albumin (BSA) in PBS) was used, with primary and secondary antibody incubations containing 0.5% BSA in PBS. Primary antibodies included: Alexa-Fluor 488 conjugated goat α-HRP (1:200; Jackson Laboratories 123-545-021), Cy3-conjugated goat α-HRP (1:250; Jackson Laboratories 123-165-021), Cy5-conjugated goat α-HRP (1:200; Jackson Laboratories 123-605-021), rabbit α-GFP (Abcam, ab290), rabbit α -Mmp2 (1:500), mouse α-Mmp1 (1:1:1 at 1:10; DSHB, 3B8D12, 3A6B4, 5H7B11), mouse α-DLG (1:200; DSHB, DLG1) and mouse α-Dlp (1:5; DSHB, 13G8). Secondary antibodies included (all 1:500; Invitrogen): goat α-mouse (488, 568), donkey α-mouse 555, donkey α-rabbit 488 and goat α-rabbit (488, 568). All labeling was performed detergent-free (extracellular labeling only (*82*, *83*)), except for structural studies using mouse α-DLG, which required addition of 0.1% Triton X-100 to both primary and secondary antibody incubations. NMJ *Z*-stacks were acquired with a Zeiss LSM 510 META laser-scanning confocal using 40x/1.4 (ghost boutons) and 63x/1.4 (all other experiments) Plan Apochromat oil immersion objectives.

Synaptic *In Situ* Zymography

NMJ in situ zymography assays were performed as previously described (*33*, *84*). Briefly, live larval preparations were dissected exposing the neuromusculature in physiological saline, and then immediately submerged in the zymography buffer (50 mM Tris-HCl, 150 mM NaCl, 5 mM $CaCl_2$, 0.2 mM NaN_3, pH 7.6) containing 500 µg/ml of fluorescein-conjugate DQ porcine gelatin (Molecular Probes by Life Technologies, D-12054). Preparations were incubated for 45 minutes at room temperature, kept stationary and protected from light. Preparations were then briefly rinsed 3X in PBS, fixed in 4% PFA in PBS for 30 minutes, and washed again 3X in PBS. Preparations were then incubated with Cy3-conjugated goat α-HRP (1:250; Jackson Laboratories 123-165-021) for 1 hour at room temperature. Preparations were finally washed again 3X in PBS and mounted in Fluoromount-G (Electron Microscopy Sciences). NMJ Z-stacks were acquired with a Zeiss LSM 510 META laser-scanning confocal microscope using a 488 nm argon laser to excite the fluorescein substrate, and imaged with a 63x/1.4 Plan Apo oil immersion objective.

Quantification and Statistical Analyses

All experiments were independently performed at least 3 times, with all comparisons performed blind. All analyses were done on staged and sized-matched animals. For each trial, 3-5 animals per condition were assayed, with NMJs from both left and right segments (A3-A4) analyzed. For all intensity comparisons, images were obtained with the same confocal settings and quantified in parallel using NIH ImageJ software (*85*). Intensity measurements were made with the HRP signal delineated from *Z*-stack areas of maximum projections. Muscle intensity was taken from areas adjacent to the HRP-marked NMJ, and subsequently subtracted from the NMJ intensity measurement. NMJ and background region selection excluded regions that overlapped with obstructions, such as trachea. For high [K^+] stimulation studies involving multiple genotypes, each stimulated condition was normalized to its own unstimulated genotype control. Confocal settings were maintained constant for unstimulated and stimulated conditions within each genotype. All cross-compared genotypes within each experiment were processed together and imaged at the same time. Ghost boutons were quantified as HRP-positive and DLG-negative varicosities emanating from the main NMJ arbor. DLG-negative was defined as <2 standard deviations below the mean. Contrast and brightness were applied uniformly using ImageJ. Co-localization analyses were performed using ZEN image processing software (Zeiss). Single slices (<1 μm) from the middle of a Z-stack were analyzed for each NMJ. Measurements of full width at half maximum (FWHM) for axial resolution were $FWHM_{488}$: 840nm and $FWHM_{555}$: 880nm. HRP was used as a guide to create an ROI. Thresholds were manually set based on background intensity values. Manders' overlap coefficients and weighted Manders' co-localization coefficients were used (*86*). All images were filtered and processed in parallel in ImageJ before being exported to Adobe Photoshop. ImageJ versions used were 1.46r, 1.51h and 1.51p (*85*, *87*). All reported statistical comparisons were always performed using Instat3 software (GraphPad Software). Mann-Whitney U tests and ANOVAs (Kruskal-Wallis) were used for all the nonparametric comparisons. ANOVA tests were used for all data sets of ≥3 comparisons, followed by appropriate post hoc analyses as stated in the figure legends. All data are presented in figures as mean±SEM, and N represents the total number of NMJs analyzed from at least 3 independent replicates. Significance is indicated in figures by *p<0.05, **p<0.01 and ***p<0.001.

Results

Mmp1 is required for rapid activity-dependent synaptic bouton formation

At the *Drosophila* NMJ, presynaptic bouton formation occurs rapidly in response to acute neuronal stimulation (*47*). The initial, immature, transitional "ghost boutons" contain synaptic vesicles and presynaptic markers, such as membrane marker Horse Radish Peroxidase (HRP), but are largely devoid of presynaptic active zones and postsynaptic markers, such as Discs Large (DLG) (*47*, *88–90*). Activity-dependent ghost boutons develop into mature boutons, and thus represent the immediate read-out for activity-dependent synaptogenesis (*47*, *90*, *75*). To acutely increase activity, we targeted the temperature-dependent dTRPA1 (Transient receptor potential cation channel A1) to motor neurons (*vglut-Gal4>UAS-dTRPA1*) (*62–66*), and then assayed new ghost bouton formation following a transient 1-hour temperature increase (Fig. 16). We used the $mmp1^{Q112*}$ genetic null allele to remove Mmp1 function, and the $mmp2^{W307*}$ genetic null allele in trans to chromosomal deficiency *Df(2R)BSC132* to remove Mmp2 function (*21*, *68*). In each *mmp* mutant condition ($mmp^{-/-}$), we compared four genotypes at both restrictive (18°C) and permissive (30°C) temperatures (8 conditions total): the driver controls (*vglut-Gal4*/+), experimental animals (*vglut-Gal4>UAS-dTRPA1*), *mmp* driver controls (*vglut-Gal4*/+, $mmp^{-/-}$) and experimental mutants (*vglut-Gal4>UAS-dTRPA1,* $mmp^{-/-}$). Representative images and data summaries are shown in Figure 1, as well as Supplemental Figures 1 and 2.

Unstimulated controls (*vglut-Gal4*/*+*) or transgenic experimental animals reared at the dTRPA1-restrictive temperature (*vglut-Gal4>UAS-dTRPA1*) display very few ghost boutons (Fig. 16A,B; Fig. S17A,B; Fig. S10A,B), consistent with previous reports (*47*, *88–90*). In contrast, shifting *vglut-Gal4>UAS-dTRPA1* animals to a dTRPA1-permissive temperature resulted in a significant increase in activity-dependent ghost bouton formation (Fig. 16A,B; Fig. S10B,C). We did not observe any difference in ghost bouton number after shifting *vglut-Gal4*/+ driver controls to the dTRPA1-permissive temperature, confirming the temperature shift did not contribute to synaptogenesis. We next tested the Mmp1 requirement for ghost bouton formation. In all non-stimulated conditions, ghost bouton number was completely indistinguishable between *vglut-Gal4*/+ control, *vglut-Gal4>UAS-dTRPA1*, *vglut-Gal4*/+, $mmp1^{Q112*}/mmp1^{Q112*}$ null, and the *vglut-Gal4>UAS-dTRPA1,* $mmp1^{Q112*}/mmp1^{Q112*}$ animals (Fig S1A,B). Following acute neuronal stimulation, we did not detect any increase in ghost bouton formation in the absence of Mmp1 (Fig. 16A,B). There was no detectable difference between the *mmp1* null driver control and the *mmp1* null dTRPA1 stimulated conditions. As a result, the *mmp1* null stimulated condition (*vglut-Gal4>UAS-dTRPA1,* $mmp1^{Q112*}/mmp1^{Q112*}$) had significantly reduced bouton numbers compared with the wildtype stimulated condition (*vglut-Gal4>UAS-dTRPA1*; Fig. 16A,B).

We next tested whether Mmp2 is similarly required for activity-dependent ghost bouton formation (Fig. S10). In all non-stimulated conditions, ghost bouton number was indistinguishable between *vglut-Gal4*/+, *vglut-Gal4>UAS-dTRPA1*, *vglut-Gal4*/+,*mmp2*^{W307*}/*Df(2R)BSC132* null and the *vglut-Gal4>UAS-dTRPA1, mmp2*^{W307*}/*Df(2R)BSC132* animals (Fig S2A,B). Following acute neuronal stimulation, we found a significant increase in ghost bouton formation in both the *vglut-Gal4>UAS-dTRPA1* (control) and *vglut-Gal4>UAS-dTRPA1, mmp2*^{W307*}/*Df(2R)BSC132* (mutant) conditions, with no significant difference detected between the groups (Fig. S10C,D). Consistently, activity-dependent ghost bouton formation in the *mmp2* null dTRPA1 stimulated condition was significantly increased relative to both the driver (*vglut-Gal4*/+) and the *mmp2* null (*vglut-Gal4*/+, *mmp2*^{w307*}/*Df(2R)BSC132*) stimulated controls (Fig. S10C,D). Together, these results show that Mmp2 is not detectably involved in ghost bouton formation, whereas Mmp1 is absolutely required for this activity-dependent synaptic bouton formation.

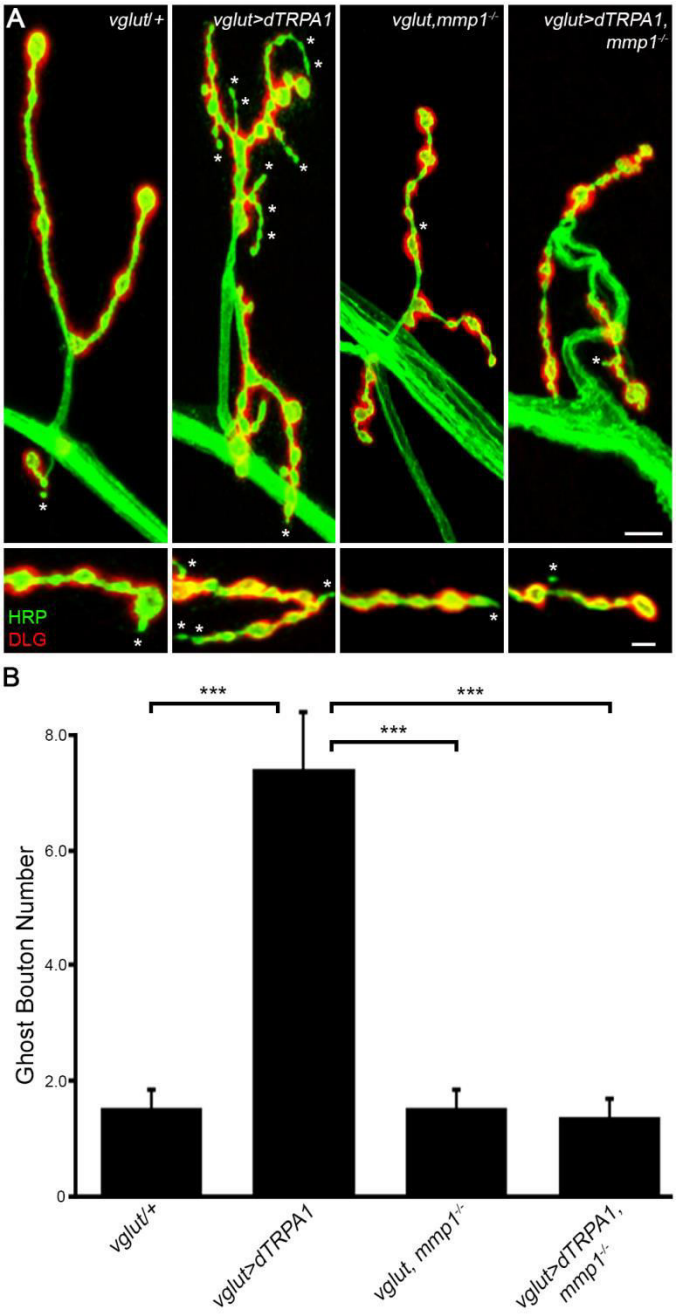

Figure 16

Figure 16: Mmp1 is required for rapid activity-dependent synaptic bouton formation. (**A**) NMJs co-labeled for HRP and DLG after dTRPA1 stimulation in the 4 genotypes shown. White stars mark ghost boutons. Scale bar: 5 μm. Higher magnification images of synaptic boutons are shown below. Scale bar: 2 μm. **(B)** Quantified ghost bouton number per terminal after dTRPA1 stimulation: *vglut-Gal4*/+ (N=28, 1.54±0.30), *vglut-Gal4>UAS-dTRPA1* (N=20, 7.4±0.97), *vglut-Gal4, mmp1^{Q112*}/mmp1^{Q112*}* (N=24, 1.54±0.34) and *vglut-Gal4>UAS-dTRPA1, mmp1^{Q112*}/mmp1^{Q112*}* (N=24, 1.38±0.33). Data show mean ± SEM from 3 replicates, with N = separate NMJs. Significance was determined by nonparametric ANOVA (Kruskal-Wallis) and Dunn's multiple comparisons post-test (***p<0.001). Non-significant (p>0.05) comparisons are not represented for 1) *vglut-Gal4*/+ vs. *vglut-Gal4, mmp1^{Q112*}/mmp1^{Q112*}* and 2) *vglut-Gal4*/+ vs. *vglut-Gal4>UAS-dTRPA1, mmp1^{Q112*}/mmp1^{Q112*}* and 3) *vglut-Gal4, mmp1^{Q112*}/mmp1^{Q112*}* vs. *vglut-Gal4>UAS-dTRPA1, mmp1^{Q112*}/mmp1^{Q112*}*. See Fig. S17 for temperature controls.

Co-localized Mmp1 and Dlp exhibit positive activity-dependent regulation

We next tested whether activity regulates synaptic Mmps using both genetic and ionic stimulation paradigms (*75*, *62*, *91*, *92*). We labeled Mmp1 with well-characterized antibodies, using detergent-free conditions to mark extracellular protein (*7*, *21*, *82*, *83*, *93*). Mmp1 abundance and spatial distribution were both increased by stimulation (Fig. 17). First, we again used dTRPA1 to transgenically increase activity, and found stimulation caused a significant >40% increase in Mmp1 compared to matched controls (*vglut-Gal4*/+; Fig. 17A,B). We repeated tests with a more restricted Gal4 driver (*CcapR-Gal4*), which expresses dTRPA1 in only a subset of motor neurons to provide an additional internal control (Fig. S11). *CcapR-Gal4* drives in the RP3 motor neuron innervating muscle 6 and 7 (NMJ m6/7), but is excluded from the motor neuron innervating muscle 4 (NMJ m4). At the dTRPA1-restrictive temperature (18^{o}C) we found no difference in Mmp1 between driver controls (*CcapR-Gal4/+*) and *CcapR-Gal4>UAS-dTRPA1* conditions at either NMJ m6/7 or m4 (Fig. S11A,B). Mmp1 was significantly increased by >50% at NMJ m6/7 following the heat-induced dTRPA1 channel activation (30^{o}C) in *CcapR-Gal4>UAS-dTRPA1* compared to the *CcapR-Gal4/+* driver control (Fig. S11C,D). However, there was no change in Mmp1 abundance at NMJ m4 following dTRPA1 neuronal stimulation, consistent with the restricted *CcapR-Gal4>UAS-dTRPA1* expression pattern (Fig. S11C,D).

Following the dTRPA1 transgenic trials, we tested Mmp1 abundance and distribution after depolarizing synaptic terminals with KCl (high [K^+]) for varying time periods (2-60 mins). We found that synaptic Mmp1 was highly increased after just 10 minutes of acute stimulation (Fig. 17A,B), and therefore used this rapid stimulation paradigm for the remainder of our studies (*75*). Similar to the above dTRPA1 results, this acute depolarizing stimulation caused a highly significant >50% increase in Mmp1 at the synapse relative to unstimulated controls (Fig. 17A,B). Although Mmp2 had no detectable role in activity-dependent bouton formation (Fig. S10), we also tested whether Mmp2 is regulated by neuronal activity. We labeled extracellular Mmp2 under detergent-free conditions utilizing our previously characterized polyclonal antibody (*7*), and quantified Mmp2 abundance at the synapse before and after the ionic depolarization paradigm (Fig. S12). In contrast to Mmp1, synaptic Mmp2 was significantly decreased by ~35% following acute, high [K^+] stimulation (Fig. S12A,B). Together, these results demonstrate that elevated neuronal activity causes concurrent strong Mmp1 increase and Mmp2 reduction at the synapse. Consistent with previous studies, the loss of Mmp2 may be a secondary consequence of elevated Mmp1 function (*7*). The specific increase in Mmp1 supports its requirement in activity-dependent synaptic bouton formation.

We previously established a strong genetic interaction between Dlp and both Mmps at the NMJ (*7*). We therefore next tested whether Dlp is similarly regulated by activity (Fig. S13). Dlp was labeled with a well-

characterized antibody (*28*, *41*, *94*), as well as a transgenic green fluorescent protein (GFP) tag in the endogenous *dlp* locus (Dlp::GFP) (*72*, *73*). Following an acute increase in activity, NMJs displayed an immediate and striking increase in synaptic Dlp intensity (Fig. S13A). With high [K^+] depolarization, GFP labeling showed a significant >60% increase in Dlp::GFP and Dlp labeling consistently revealed a significant >60% increase compared to the unstimulated control condition (Fig. S13B). These results indicate that activity induces rapid upregulation of Dlp at the synapse. In unstimulated terminals, both Mmp1 and Dlp appeared in concurrent domains in a dynamic subset of synaptic boutons (Fig. 18A; arrows), with overlap but also with spatial separation of the two proteins. Upon acute stimulation, both proteins were significantly increased within the same synaptic subdomains (Fig. 18A, top panels; arrows), and the incidence of co-localization became much greater (Fig. 18A, bottom panels; asterisks). Given that HSPGs bind and localize MMPs in other contexts (*34*, *36*, *39*), we hypothesized that activity stimulates the co-localization of Dlp and Mmp1 at the synapse, with GPI-tethered Dlp serving to capture and localize the secreted Mmp1.

To test for this co-regulation, we triple-labeled unstimulated and high [K^+] stimulated Dlp::GFP terminals with antibodies against GFP, Mmp1 and HRP. In parallel comparisons, we confirmed a significant ~50% increase in Dlp and Mmp1 after stimulation compared to unstimulated controls (Fig. 18A,B). Moreover, acute stimulation increased the spatial overlap between Dlp and Mmp1, with specificity confirmed by multiple antibody and imaging controls (Fig. 18C and Fig. S14). We assessed co-occurrence with Manders' co-localization coefficient (MCC) measurements (*95*, *86*). Upon stimulation, the Mmp1:Dlp MCC significantly increased over 2-fold compared to unstimulated controls (Fig. 18C). Likewise, the Dlp:Mmp1 MCC showed a similar significant increase in stimulated terminals (Fig. 18C). Thus, with acute stimulation both Dlp::GFP and Mmp1 MCC values were similarly increased compared to unstimulated controls, demonstrating a rapid activity-dependent recruitment of both proteins to co-localized synaptic domains. These results suggest four possible interpretations; 1) Dlp and Mmp1 have unrelated activity-dependent increases within the same dynamic synaptic domains, 2) secreted Mmp1 drives the activity-dependent Dlp increase, 3) membrane-tethered Dlp drives the activity-dependent Mmp1 increase, recruiting Mmp1 to synaptic subdomains, or 4) Dlp and Mmp1 activity-dependent increases are reciprocally co-dependent.

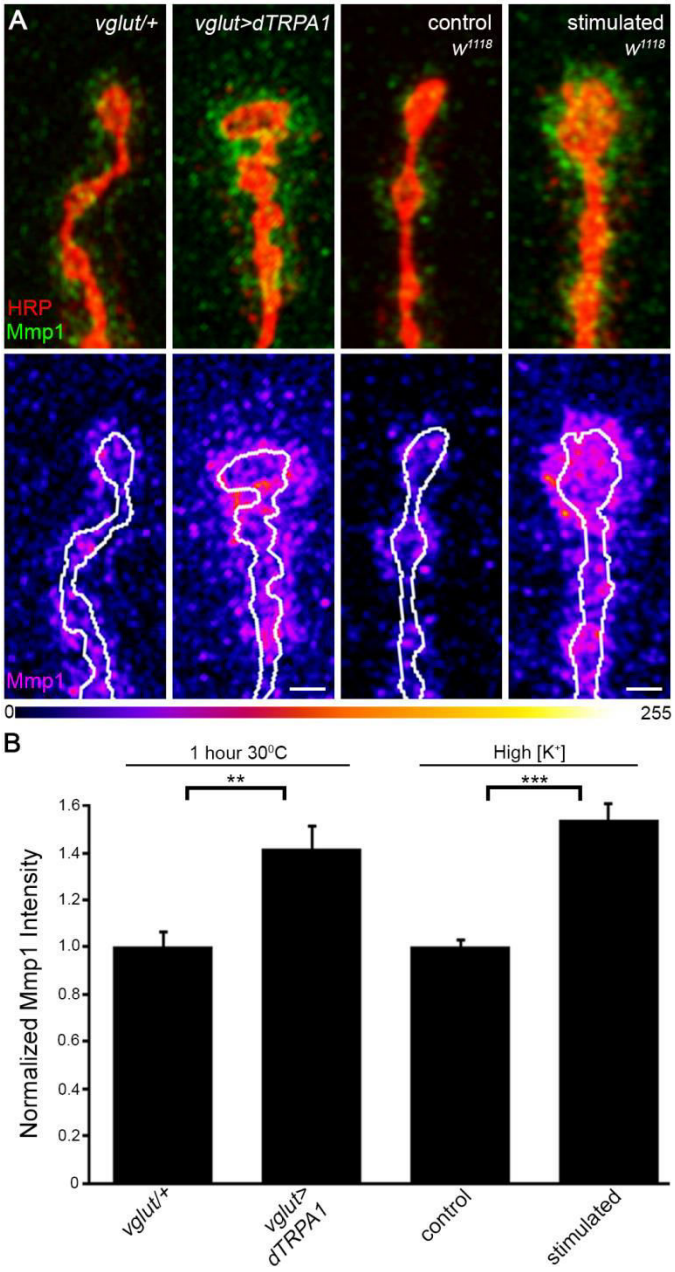

Figure 17

Figure 17: Synaptic Mmp1 is rapidly increased following acute neuronal stimulation. (A) Images of NMJs following the denoted activity stimulation, co-labeled with HRP and Mmp1 in the 3 genotypes shown. Heat map shows Mmp1 alone (scale below) with white HRP bouton outline. Scale bar: 2 μm. (B) Quantification of synaptic Mmp1 intensity normalized to matched controls in: *vglut-Gal4*/+ (N=10, 1.0±0.07) vs. *vglut-Gal4>UAS-dTRPA1* (N=13, 1.42±0.1) and w^{1118} control (unstimulated, N=56, 1.0±0.03) vs. w^{1118} stimulated (high [K^+], N=57, 1.54±0.07). Significance determined by Unpaired t-test with Welch correction (dTRPA1) or Mann-Whitney U-Test (High [K^+]), indicated by **p<0.01 and ***p<0.001. Data show mean ± SEM from 3 replicates for each experiment, with N = separate NMJs. See Fig. S11 for additional controls.

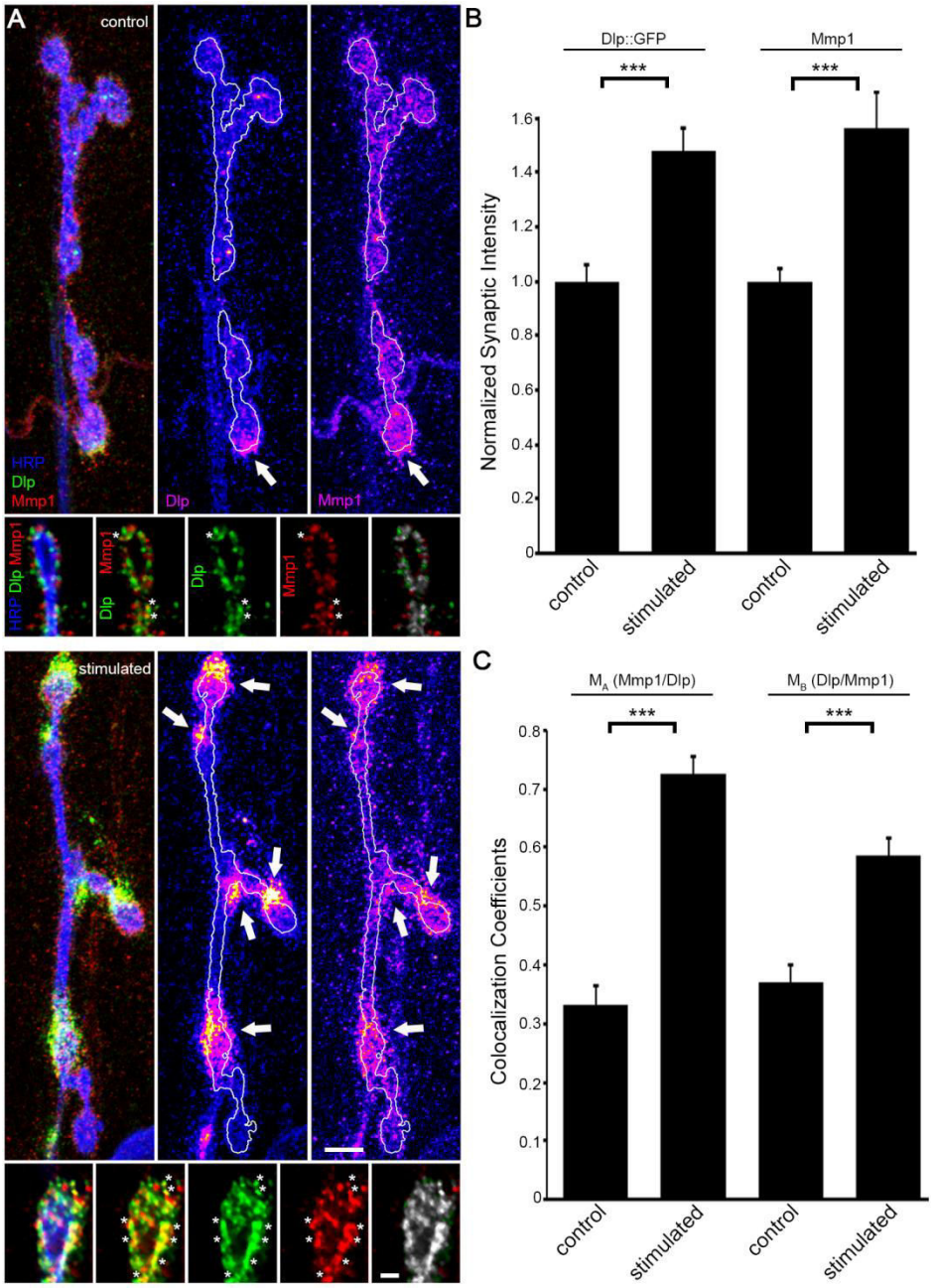

Figure 18

Figure 18: Mmp1 and Dlp co-localization in synaptic subdomains is increased by acute activity. (A) Images of Dlp::GFP NMJs labeled with HRP, GFP and Mmp1 under basal conditions or following high [K^+] stimulation. Dlp::GFP and Mmp1 signals are shown as a heat map with HRP synaptic outlines in white. Arrows point to overlapping Dlp::GFP and Mmp1 signals. Scale bar: 5 μm. Higher magnification images show single optical sections. Scale bar: 1 μm. Asterisks denote overlapping Dlp::GFP and Mmp1, shown pseudo-colored in white. **(B)** Quantification of both Dlp::GFP and Mmp1 fluorescence intensities normalized to unstimulated controls. Dlp::GFP: control (N=20, 1.0±0.06) vs. stimulated (N=19, 1.48±0.09) and Mmp1: control (N=20, 1.0±0.05) vs. stimulated (N=19, 1.56±0.14). Significance determined by Unpaired t-test with Welch correction, indicated by ***p<0.001. **(C)** Quantification of Manders' co-localization coefficients. M_A (Mmp1/Dlp::GFP) in basal control (N=27, 0.33±0.03) and after stimulation (N=27, 0.72±0.03). M_B (Dlp::GFP/Mmp1) in basal control (N=27, 0.37±0.03) and after stimulation (N=27, 0.59±0.03). Significance determined by Unpaired t-test (M_A) or Mann-Whitney U-Test (M_B), indicated by ***p<0.001. Data show mean ± SEM from 3 replicates; N represents NMJ number. See Figs. S13 and S14 for further controls.

Dlp localizes Mmp1 in synaptic domains and bidirectionally promotes Mmp1 intensity

To first test the hypothesis that Dlp regulates Mmp1, we altered synaptic Dlp expression and quantified Mmp1 abundance. At the *Drosophila* NMJ, Dlp serves as a Wg co-receptor in a mechanism dependent on HS-GAG sulfation state, and Dlp also binds the receptor phosphatase dLAR through HS-GAG chains to modulate synaptogenesis (*40*, *41*). Complete loss of *dlp* is embryonic lethal, so we used $dlp^{A187/+}$ heterozygotes and dlp^{RNAi} (*68*, *69*). To reduce Dlp at the NMJ, we targeted dlp^{RNAi} to both pre- (*elav-Gal4*) and postsynaptic (*24B-Gal4*) cells (*elav-Gal4, 24B-Gal4>UAS-*dlp^{RNAi}). Both $dlp^{A187/+}$ and dlp^{RNAi} significantly reduced synaptic Dlp abundance by >45% (Fig. S15A,B). In parallel, $dlp^{A187/+}$ significantly reduced Mmp1 intensity by >30% compared to background controls (Fig. 19A,B), and dlp^{RNAi} likewise significantly decreased Mmp1 intensity by >20% compared to Gal4 driver controls (Fig. 19A,B). To conversely test whether Dlp overexpression reciprocally increases Mmp1, we postsynaptically overexpressed wild-type Dlp (*24B-Gal4>UAS-*dlp^{WT}; (*70*)). Excess Dlp caused a significant >50% increase in synaptic Mmp1 (Fig. 19C,D). Moreover, the expanded Dlp domain caused a striking increase in perisynaptic Mmp1 localization (Fig. 19C). Taken together, these results indicate that Dlp positively regulates Mmp1 intensity and spatial distribution at the synapse.

HSPG interactions are often mediated through HS-GAG chain binding, which can anchor interactors in close proximity, influencing both diffusion and clustering (*96*, *97*). In addition, however, HSPG core proteins also have well-characterized binding functions (*38*, *46*, *98*, *99*, *71*). Therefore, we next sought to test whether Dlp-dependent Mmp1 regulation is mediated through the Dlp core protein, HS-GAG chains, or both. To test Dlp HS-GAG chain requirements, we overexpressed a HS-deficient Dlp (*UAS-*dlp^{-HS}), in which all 5 serine GAG attachment sites have been mutated to alanine (*46*). We reasoned if the Dlp-Mmp1 interaction is mediated by the Dlp core protein, then overexpressing HS-deficient Dlp should phenocopy the synaptic Mmp1 increase caused by overexpressing wild-type Dlp (Fig. 19C,D). We confirmed that the *24B-Gal4>UAS-*dlp^{-HS} overexpression was comparable to the *24B-Gal4>UAS-*dlp^{WT} condition, with very high synaptic expression in both cases (Fig. S15C). However, in stark contrast to the striking Mmp1 increase with wild-type Dlp overexpression, Dlp^{-HS} overexpression did not cause any change in synaptic Mmp1 abundance compared to Gal4 driver control (*24B-Gal4*/+, Fig. 19C,D). When the activity-induced Mmp1 increase caused by wild-type Dlp were compared to Dlp^{-HS}, there was a significant decrease (Fig. 19C,D). These results strongly suggest that Dlp promotes synaptic Mmp1 localization through HS-GAG chain interaction.

Despite the lack of Mmp2 involvement in this synaptogenic mechanism, we also tested whether synaptic Mmp2 may be regulated by Dlp, independently or downstream of the Mmp1 changes. Dlp is a direct

Mmp2 proteolytic substrate (*68*) and Mmp1 and Mmp2 are reciprocally co-regulated at the NMJ synapse under both basal conditions and following neuronal stimulation (Fig. 17; Figs. S11 and S12; (*7*)). To test whether Dlp regulates synaptic Mmp2, we again used $dlp^{A187/+}$ heterozygotes to reduce Dlp and postsynaptic Dlp overexpression (*24B-Gal4>UAS-*dlp^{WT}) to increase Dlp, respectively (Fig. S15). We quantified Mmp2 abundance at the NMJ compared to matched controls under both conditions (Fig. S16). We did not observe any change in synaptic Mmp2 in the $dlp^{A187/+}$ heterozygous condition compared to w^{1118} genetic background control (Fig. S16A,B). Postsynaptic Dlp overexpression caused a subtle ~10% decrease in Mmp2 abundance at the NMJ (Fig. S16A,B). These data show that Dlp has a minor influence on synaptic Mmp2, but functions as a strong, bidirectional regulator of Mmp1 at the synapse.

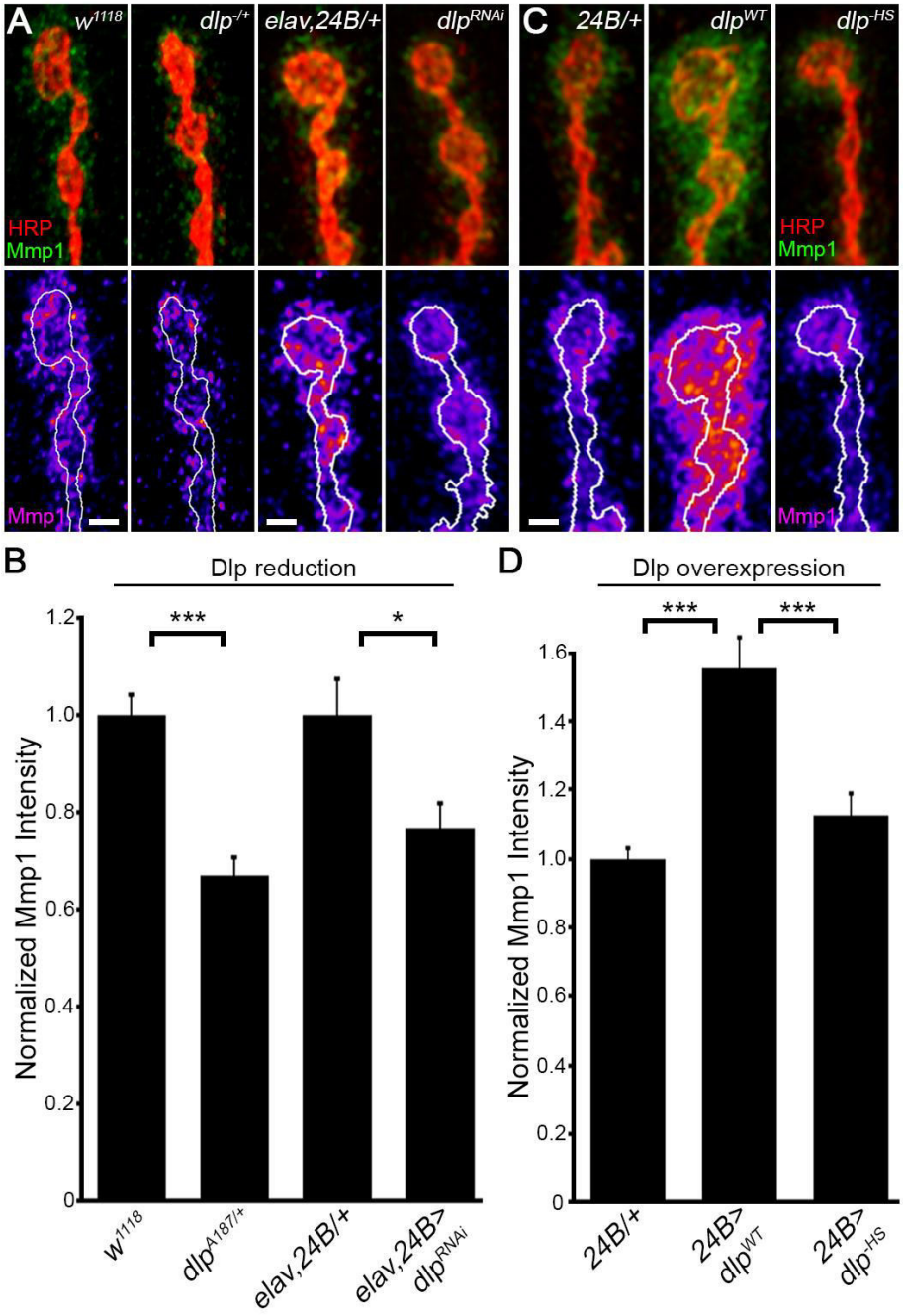

Figure 19

Figure 19: Synaptic Dlp positively and bidirectionally regulates secreted Mmp1 abundance. (A,C) Images of NMJs from the denoted *dlp* reduction (A) and overexpression (C) conditions compared to matched controls co-labeled with HRP and Mmp1. Mmp1 signal intensity is shown as a heat map with HRP synaptic outlines in white. Scale bars: 2 μm. **(B)** Quantification of Mmp1 fluorescence intensity normalized to matched genetic controls: w^{1118} (N=34, 1.0±0.04) vs. $dlp^{A187/+}$ (N=37, 0.67±0.04), and *elav-Gal4,24B-Gal4/+* control (N=28, 1.0±0.07) vs. *elav-Gal4,24B-Gal4>UAS-*dlp^{RNAi} knockdown (N=32, 0.77±0.05). Significance determined by Mann-Whitney U-Test, indicated by ***p<0.001 and *p<0.05. **(D)** Quantification of Mmp1 intensity normalized to controls: *24B-Gal4/+* (N=51, 1.0±0.03), *24B-Gal4>UAS-*dlp^{WT} (N=42, 1.55±0.09), and *24B-Gal4>UAS-*dlp^{-HS} (N=34, 1.13±0.06). Significance determined by nonparametric ANOVA (Kruskal-Wallis) with Dunn's multiple comparisons post-test, indicated by ***p<0.001. The non-significant (p>0.05) comparison for *24B-Gal4/+* vs. *24B-Gal4>UAS-*dlp^{-HS} is not shown. Data show mean ± SEM from at least 3 independent replicates for each experiment, with N representing NMJ number. See Fig. S15 for Dlp in the genetic manipulations.

Dlp is required for the rapid, activity-dependent increase of synaptic Mmp1

Since Dlp and Mmp1 are both increased by acute neuronal activity, and Dlp regulates synaptic Mmp1 abundance, we next hypothesized that Dlp is required for the activity-induced Mmp1 increase at the synapse. To test this hypothesis, we genetically manipulated Dlp and quantified Mmp1 after acute high [K^+] depolarization (Fig. 20). Supporting the above results, we found an activity-dependent Mmp1 increase in both w^{1118} background and Gal4 driver controls, with significant increases in all comparisons. Reducing Dlp abolished any detectable Mmp1 increase in response to the acute activity stimulation (Fig. 20A,B). Indeed, we found instead a small ~15% decrease in synaptic Mmp1 abundance in the stimulated $dlp^{A187/+}$ heterozygotes relative to unstimulated $dlp^{A187/+}$ controls (Fig. 20B). The dlp^{RNAi} condition yielded very similar results, with a small, non-significant ~12% reduction in synaptic Mmp1 following the high [K^+] stimulation (Fig. 20B). Conversely, the activity-stimulated Mmp1 abundance was significantly increased a further ~65% with Dlp overexpression (Fig. 20C,D). The basal amount of Mmp1 at the synapse was increased by Dlp overexpression (Fig. 19), yet there was still a strong increase in synaptic Mmp1 following acute depolarizing stimulation, consistent with Dlp promoting the activity-dependent Mmp1 elevation. Taken together, these results show that Dlp is required for the activity-dependent Mmp1 increase at the synapse.

Previous work has established that HS-GAG chains often mediate Dlp functions and binding interactions (*41*, *46*, *70*). We therefore next tested whether a HS-GAG chain deficient Dlp (*UAS-*dlp^{-HS}) interferes with the activity-dependent synaptic Mmp1 induction (Fig. 20C,D). Although the endogenous Dlp with intact HS-GAG chains was still present, we hypothesized that the HS-GAG chain deficient Dlp should dominantly dampen activity-induced Mmp1 elevation. Following acute high [K^+] depolarizing stimulation, we observed increased synaptic Mmp1 in both *24B-Gal4*/+ driver control and *24B-Gal4>UAS-*dlp^{WT} overexpression conditions, with a significant increase in both conditions (Fig. 20C,D). However, the synaptic Mmp1 abundance in the activity-stimulated *24B-Gal4>UAS-*dlp^{-HS} synapses was only slightly increased (by 19%) compared to the matched unstimulated controls, a much weaker albeit still significant response (Fig. 20C,D). In sharp contrast, the activity-induced Mmp1 increase was significantly reduced at *24B-Gal4>UAS-*dlp^{-HS} NMJ synapses compared with the wild-type Dlp overexpression condition (19% vs. ~65%, respectively). Taken together, these results support the conclusion that both basal and activity-induced Mmp1 regulation by Dlp at the synapse are directly mediated through HS-GAG chain binding interactions in the extracellular space.

At NMJs lacking Mmp1 (*mmp1* null mutants), basal Dlp abundance is reduced and Dlp is more spatially restricted, thus Mmp1 reciprocally serves as a positive regulator of synaptic Dlp (*7*). We consistently found above that Dlp is required for the activity-dependent Mmp1 increase at the synapse (Fig. 20). However, there

still might be a reciprocal Mmp1 requirement for the activity-dependent increase in Dlp abundance. To test for this putative co-regulation, we next genetically reduced Mmp1 abundance using two independent approaches and then quantified Dlp intensity following acute high [K^+] depolarization (Fig. S17). Consistent with above results, control animals displayed a significant >30% increase in synaptic Dlp following the acute stimulation (Fig. S17A,B). Using the combinatorial pre- and postsynaptic *mmp1*^{RNAi} knockdown (*elav-Gal4, 24B-Gal4>UAS-mmp1*^{RNAi}), synaptic Mmp1 was reduced by ~70%, yet we still observed the significant increase in Dlp following depolarizing stimulation (Fig. S17C,D). We validated these results in a *trans*-heteroallelic *mmp1* mutant condition (*mmp1*^{Q112*}/*mmp1*^{Q273*}) and again observed a similar, maintained >30% increase in synaptic Dlp following acute stimulation (Fig. S17A,B). These results indicate that Mmp1 is not reciprocally required for the activity-dependent Dlp increase at the synapse. Taken together, the data suggest that Mmp1 is downstream of Dlp in this activity-dependent mechanism.

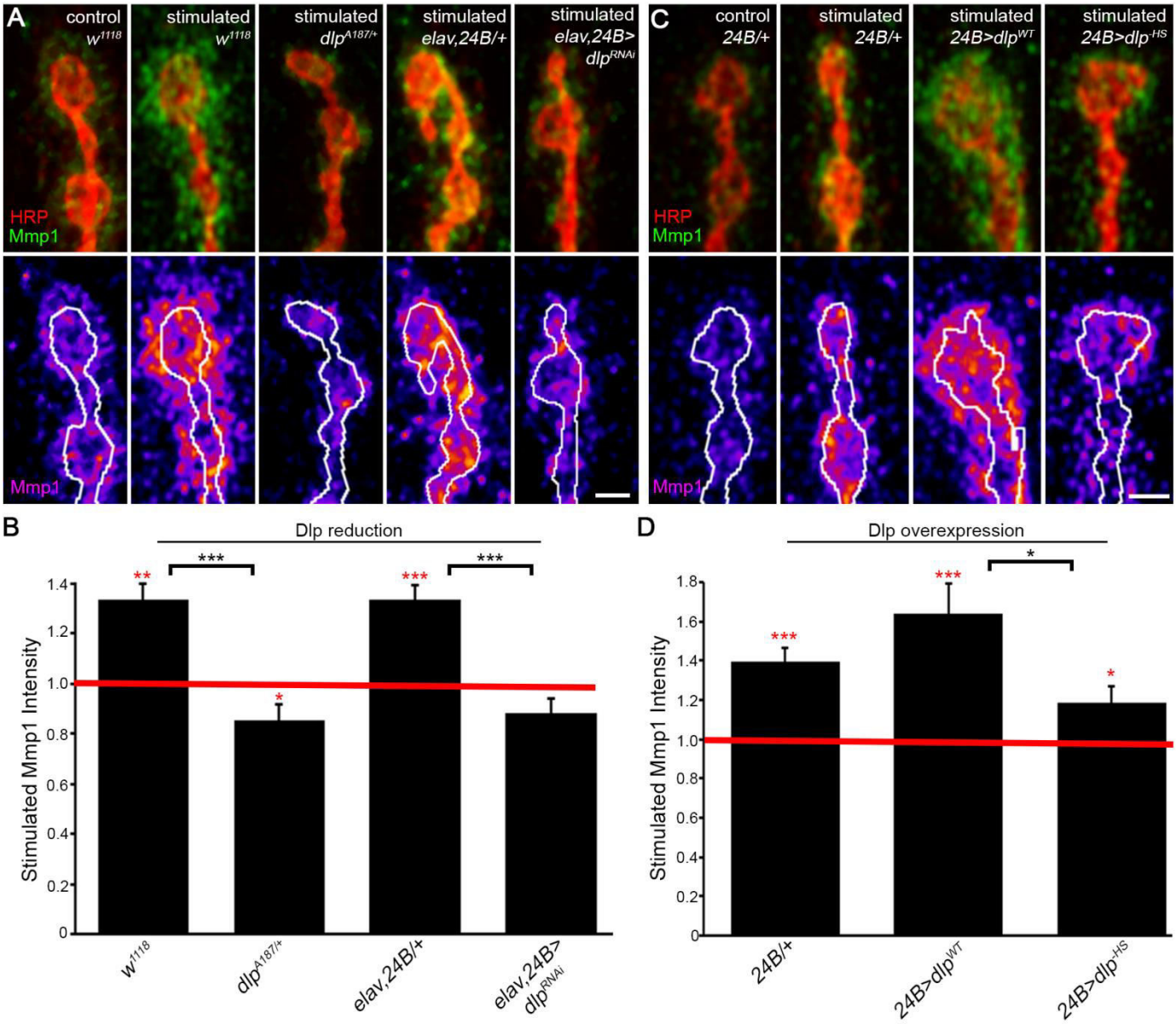

Figure 20

Figure 20: Dlp is required for the activity-dependent synaptic Mmp1 regulation. (A,C) Images show NMJs from the indicated *dlp* reduction (A) or overexpression (C) conditions treated with or without high [K^+] co-labeled for HRP and Mmp1. Heat maps show Mmp1 intensity with white HRP outlines. Scale bars: 2 μm. **(B,D)** Quantified Mmp1 fluorescence intensity from stimulated conditions (bar graphs) normalized to unstimulated controls (red lines). **(B)** w^{1118} control (N=17, 1.0±0.08) vs. w^{1118} stimulated (N=19, 1.34±0.06); $dlp^{A187/+}$ control (N=19, 1.0±0.03) vs. $dlp^{A187/+}$ stimulated (N=21, 0.85±0.06); *elav-Gal4,24B-Gal4/+* control (N=26, 1.0±0.04) vs. *elav-Gal4,24B-Gal4/+* stimulated (N=24, 1.34±0.06) and *elav-Gal4,24B-Gal4>UAS-dlp*^{RNAi} control (N=25, 1.0±0.06) vs. *elav-Gal4,24B-Gal4>UAS-dlp*^{RNAi} stimulated (N=18, 0.88±0.06). **(D)** *24B-Gal4/+* control (N=21, 1.0±0.06) vs. *24B-Gal4/+* stimulated (N=18, 1.39±0.07); *24B-Gal4>UAS-dlp*^{WT} control (N=21, 1.0±0.03) vs. *24B-Gal4>UAS-dlp*^{WT} stimulated (N=16, 1.64±0.16); and *24B-Gal4>UAS-dlp*$^{-HS}$ control (N=23, 1.0±0.05) vs. *24B-Gal4>UAS-dlp*$^{-HS}$ stimulated (N=13, 1.19±0.08). (B,D) For stimulated vs. unstimulated pair-wise comparisons (red), significance determined by Mann-Whitney U-Tests and across genotypes (black) by Unpaired t-tests (B) or nonparametric ANOVA (Kruskal-Wallis; D) with Dunn's multiple comparisons post-test, indicated by *p<0.05, **p<0.01, and ***p<0.001. Non-significant (p>0.05) comparisons: stimulated vs. unstimulated *elav-Gal4,24B-Gal4>UAS-dlp*^{RNAi} (B), stimulated *24B-Gal4/+* vs. stimulated *24B-Gal4>UAS-dlp*^{WT} (D), and stimulated *24B-Gal4/+* vs. stimulated *24B-Gal4>UAS-dlp*$^{-HS}$ (D) are not shown. Data show mean ± SEM from 3 independent replicates, with N = separate NMJs.

Synaptic Dlp bidirectionally determines proteolytic function at the NMJ

After discovering that synaptic Mmp abundance and distribution are dependent on Dlp (Figs. 19, 20), we next assayed whether these changes correlate with synaptic proteolytic activity. We used in situ zymography at the NMJ to measure the metalloproteinase-dependent conversion of a dye-quenched fluorogenic gelatin (DQ-gelatin), and quantified fluorescence changes in both the *dlp* reduction and overexpression conditions used above (*33*, *84*). Although this method cannot differentiate the contributions of different proteases, it provides a live readout of net enzymatic activity through quantifiable fluorescence changes. Consistent with above results, $dlp^{A187/+}$ heterozygotes showed a significant ~35% reduction in proteolytic activity at the synapse compared to w^{1118} controls (Fig. 21A,B). Moreover, Dlp overexpression (*24B-Gal4>UAS-*dlp^{WT}) resulted in a significant ~50% increase in proteolytic activity at the synapse (Fig. 21A,C). We also tested whether the Dlp-mediated increase in proteolytic function required HS-GAG chains as above (*24B-Gal4>UAS-*dlp^{-HS}). These NMJs still displayed a significant ~60% increase in proteolytic activity compared to the matched driver control (*24B-Gal4/+*), with no detectable difference between Dlp^{WT} and Dlp^{-HS} overexpression conditions (Fig. 21A,C). Taken together, we conclude that Dlp abundance is a strong determinant of proteolytic gelatinase activity at the synapse, consistent with above measurements of Dlp-dependent synaptic Mmp1 abundance, with the enzymatic function reliant upon the Dlp core protein.

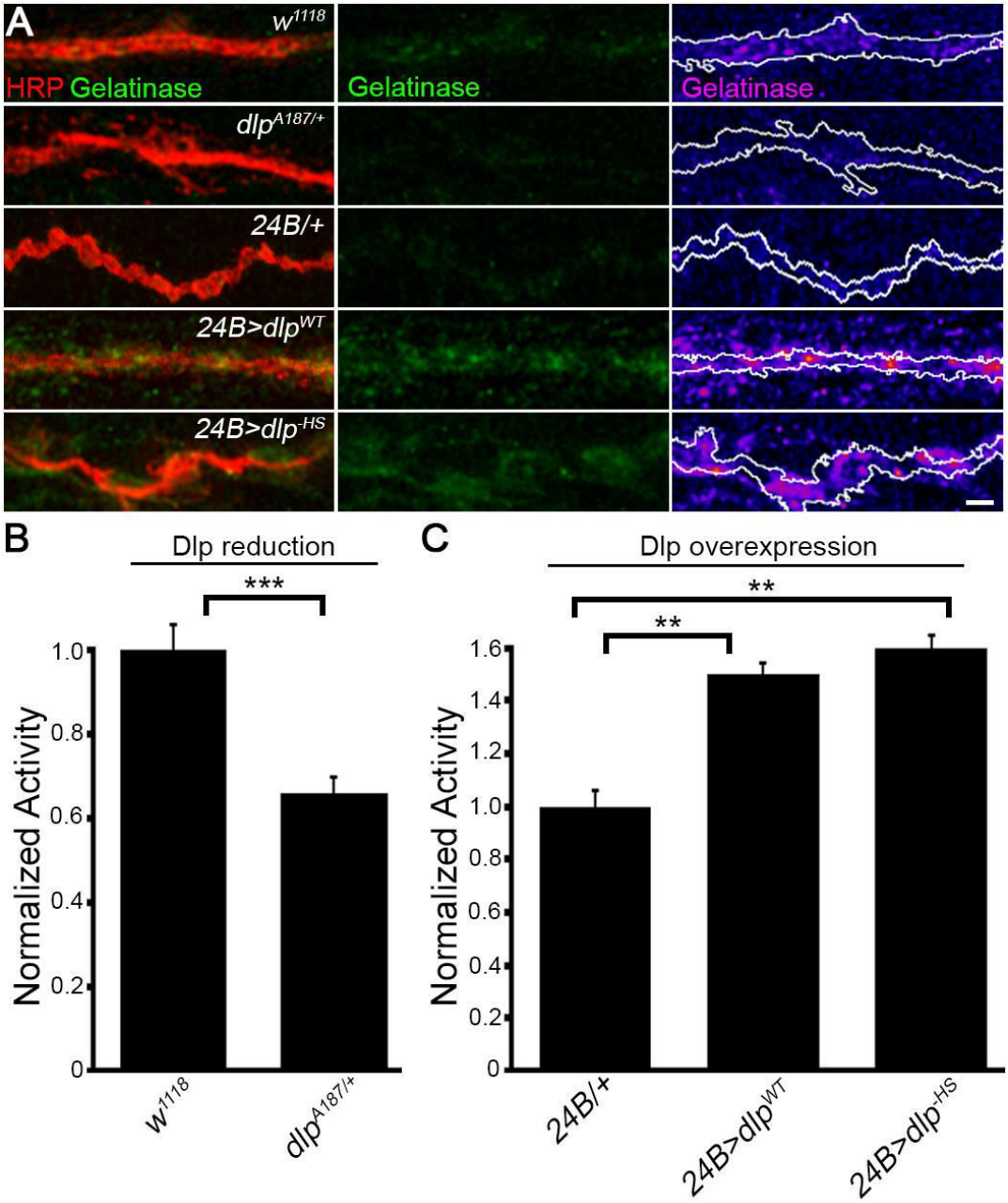

Figure 21

Figure 21: Dlp positively and bidirectionally regulates proteolytic activity at the synapse. (A) Images show NMJs from the indicated *dlp* reduction and overexpression co-labeled for HRP (red) and in situ zymography activity (green) compared to matched genetic controls. Gelatinase activity shown as a heat map with HRP synaptic outlines in white. Scale bar: 2 μm. **(B)** Quantified in situ zymography fluorescent intensity normalized to controls for *dlp* reduction: w^{1118} control (N=35, 1.0±0.06) and $dlp^{A187/+}$ heterozygote (N=33, 0.66±0.04). Significance determined by Unpaired t-test with Welch correction, indicated by ***p<0.0001. **(C)** Quantified in situ zymography fluorescent intensity normalized to controls for *dlp* overexpression conditions: *24B-Gal4/+* control (N=35, 1.0±0.05), *24B-Gal4>UAS-*dlp^{WT} (N=18, 1.5±0.09) and *24B-Gal4>UAS-*dlp^{-HS} (N=20, 1.6±0.18). Significance determined by nonparametric ANOVA (Kruskal-Wallis) and Dunn's multiple comparisons post-test, indicated by **p<0.01. Data show mean ± SEM from 3 independent replicates, with N representing NMJ number.

FMRP regulation of activity-dependent synaptic Mmp1 requires Dlp function

Dlp is upregulated in the *Drosophila* FXS disease model (*dfmr1* null mutant), Mmp1 and Dlp genetically interact with FMRP, and independently correcting either Dlp or Mmp1 in *dfmr1* mutants ameliorates FXS-associated synaptogenic defects (*13*, *28*, *33*). In conjunction with our above findings, this led us to hypothesize a coordinated FMRP-HSPG-Mmp axis converging in the synaptomatrix to enable activity-dependent synaptogenesis. To test this hypothesis, we first quantified synaptic Mmp1 in *dfmr1* null mutants (*74*). Mmp1 was significantly increased by >50% in *dfmr1* animals relative to controls (Fig. 22A,B). Consistently, we detected a parallel >40% increase in synaptic Dlp at *dfmr1* null synapses, a similar significant increase compared to controls (Fig. S18A,B). Our working model proposes Dlp positively regulates synaptic Mmp1, and we therefore hypothesized that increased Dlp is causative for the corresponding Mmp1 increase in the FXS model. To test this, we removed one copy of *dlp* in the *dfmr1* null background to reduce Dlp abundance, and then tested whether this restored normal synaptic Mmp1 intensity (Fig, 7A,B). As expected, Dlp expression was significantly reduced at $dlp^{A187/+}$, *dfmr1/dfmr1* synapses compared to the FXS model, with Dlp signal intensity comparable to wild-type controls (Fig. S18A,B). Moreover, the 50% Mmp1 increase observed in the FXS model was fully corrected in $dlp^{A187/+}$, *dfmr1/dfmr1* synapses, with Mmp1 signal intensity now indistinguishable from controls (Fig. 22A,B). Therefore, *dlp* co-removal in the FXS disease model is sufficient to restore normal synaptic Mmp1 abundance.

Finally, we asked whether FMRP is required for the activity-induced, Dlp-mediated synaptic Mmp1 enhancement. To test this hypothesis, we again stimulated synapses with high $[K^+]$ and quantified synaptic Mmp1 (Fig. 22C,D). Following stimulation, wild-type synapses displayed a significant >50% increase in Mmp1 compared to unstimulated controls (Fig. 22C,D). Conversely, there was no change in synaptic Mmp1 abundance following stimulation in *dfmr1* null mutants (Fig. 22C,D). Our model predicts that the FMRP requirement for activity-induced Mmp1 increase is mediated through Dlp. Therefore, we hypothesized that Dlp reduction in *dfmr1* null animals would restore activity-induced Mmp1 regulation. Consistently, removing a single copy of *dlp* in the FXS model was sufficient to fully restore the activity-induced Mmp1 increase following activity stimulation (Fig. 22C,D). Similar to the stimulated controls (w^{1118}), synaptic Mmp1 was significantly increased by >50% in the stimulated $dlp^{A187/+}$, *dfmr1/dfmr1* condition compared to unstimulated $dlp^{A187/+}$, *dfmr1/dfmr1* synapses (Fig. 22C,D). Accordingly, stimulated $dlp^{A187/+}$, *dfmr1/dfmr1* synapses now displayed a significant increase compared to stimulated *dfmr1* homozygous null mutants (Fig. 22D). Thus, *dlp* co-removal in the FXS disease model restores activity-induced Mmp1 regulation back towards the wild-type condition. Collectively, the findings provide the previously missing mechanistic link in the FMRP-Dlp-Mmp1 pathway,

leading us to propose Dlp misregulation mediates the disease-associated Mmp1 dysfunction casual for synaptogenic defects characterizing the FXS disease state

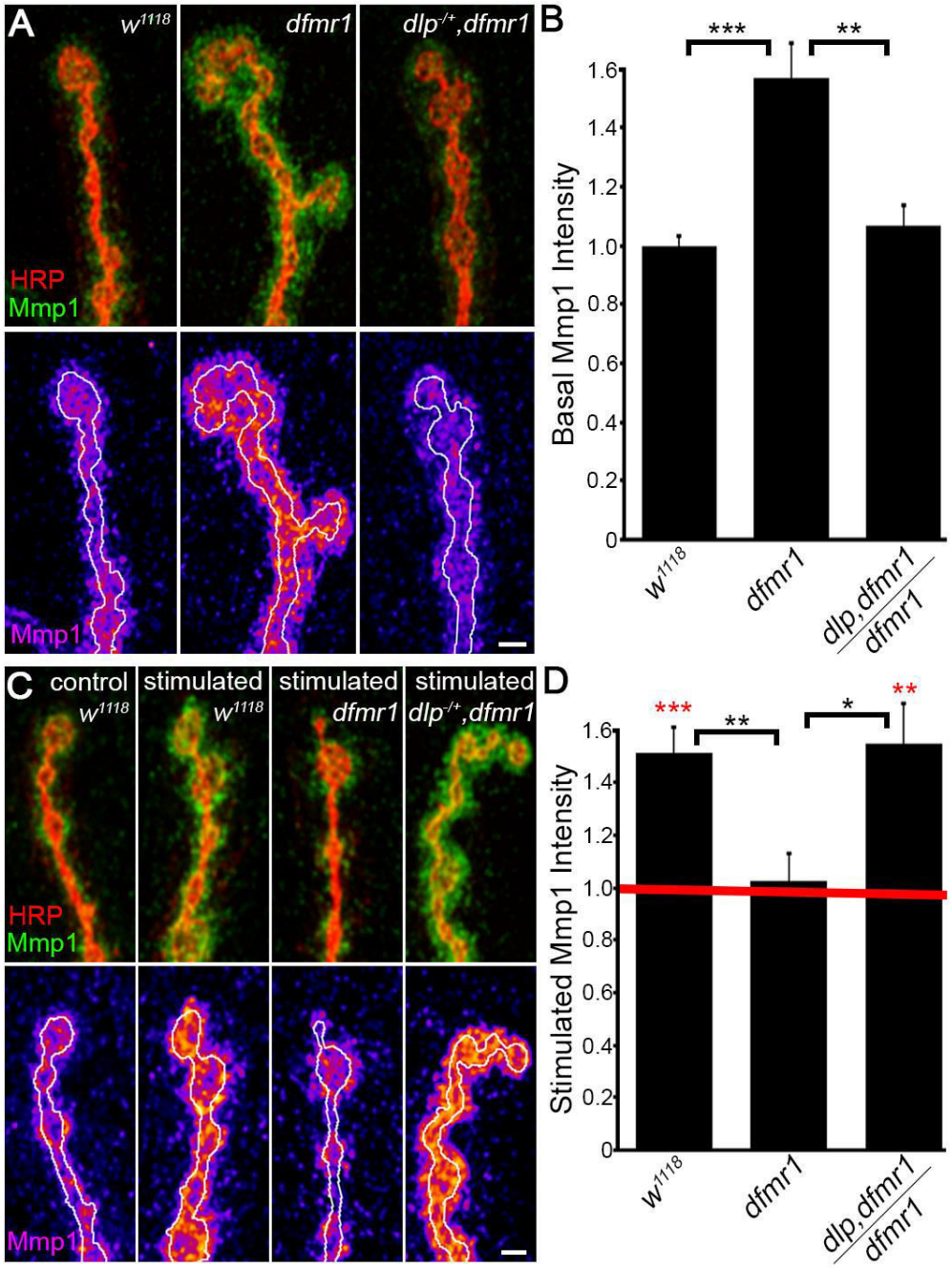

Figure 22

Figure 22: FMRP regulation of the activity-dependent Mmp1 enhancement requires Dlp. (A,C) Images show NMJs from the denoted genotypes co-labeled with HRP and Mmp1. Mmp1 intensity shown as a heat map with white HRP outlines. Scale bars: 2 μm. **(B)** Quantification of normalized Mmp1 fluorescence intensity: w^{1118} control (n=49, 1.0±0.03), $dfmr1^{50M/50M}$ (n=35, 1.57±0.12) and $dlp^{A187/+}$, $dfmr1^{50M/50M}$ (n=22, 1.07±0.07). **(C)** Images as in (A) treated with or without high [K^+]. **(D)** Mmp1 intensity in stimulated conditions (bar graphs) normalized to unstimulated controls (red line): w^{1118} control (unstimulated, n=13, 1.0±0.04) vs. w^{1118} stimulated (n=15, 1.51±0.1); $dfmr1^{50M/50M}$ control (unstimulated, n=15, 1.0±0.07) vs. $dfmr1^{50M/50M}$ stimulated (n=13, 1.02±0.11); and $dlp^{A187/+}$, $dfmr1^{50M/50M}$ control (unstimulated, n=14, 1.0±0.04) vs. $dlp^{A187/+}$, $dfmr1^{50M/50M}$ stimulated (n=17, 1.55±0.16). (D) Stimulated vs. unstimulated pair-wise comparisons, significance determined by Mann-Whitney U-Tests, indicated by **p<0.01 and ***p<0.001 (red). In (B) and across stimulated genotypes (D), significance determined by nonparametric ANOVA (Kruskal-Wallis) with Dunn's multiple comparisons post-test, indicated by *p<0.05, **p<0.01, and ***p<0.001 (black). Non-significant (p>0.05) comparisons for w^{1118} vs. $dlp^{A187/+}$, $dfmr1^{50M/50M}$ (B), stimulated vs. unstimulated $dfmr1^{50M/50M}$ (D) and stimulated w^{1118} vs. stimulated $dlp^{A187/+}$, $dfmr1^{50M/50M}$ (D) are not shown. Data show mean ± SEM from at least 3 independent replicates, with N representing separate NMJs.

Discussion

We report here that Mmp1, but not Mmp2, is required for rapid, activity-dependent synapse development (ghost bouton formation) (*47*, *75*). Although both *Drosophila* Mmps act to restrict NMJ growth over developmental time (*7*), there is a clear differential requirement in fast activity-dependent de novo synaptic bouton formation. Thus, distinct Mmp-dependent pathways control basal versus activity-induced synaptogenesis. Similarly separable roles have been shown for parallel molecular mechanisms. For example, the actin regulator Cortactin is required for fast activity-dependent ghost bouton formation, but has no detectable role in basal synaptic bouton maturation (*100*). Moreover, high $[K^+]$ depolarizing activity stimulation quickly restricts miRNA functions with exclusively activity-dependent roles (*101*, *102*). Our results suggest that Mmps (including proteolytic substrates or effectors) differentially control synaptic bouton formation in distinct time frames, revealing context-specific roles in long-term development versus acute, activity-dependent synaptogenesis. Consistent with the selective Mmp1 requirement, we also find that neuronal stimulation only elevated Mmp1, whereas Mmp2 is reciprocally suppressed by acutely increased activity. This bidirectional co-regulation by neuronal activity may reflect Mmp class interactions, since Mmp2 restricts synaptic Mmp1 abundance, spatial distribution and synaptogenesis requirements (*7*). This type of Mmp bidirectional co-regulation in response to activity likely represents an important extracellular regulatory mechanism at the synapse, controlling the function of Mmp-dependent synaptomatrix outputs.

Both thermogenic dTRPA1 stimulation and the much more acute high $[K^+]$ depolarization induce rapid synaptic Mmp1 elevation and Mmp1-dependent new bouton formation, suggesting activity-dependent Mmp1 function enables synaptogenesis. Given very rapid responses to high $[K^+]$ stimulation (10 minutes), the synaptic Mmp1 increase is most likely a post-transcriptional mechanism occurring directly at the synapse. Multiple molecular changes induced by acute high $[K^+]$ are cycloheximide-independent (*75*). We hypothesized the Mmp1 increase occurs through extracellular regulation, and identified a key interaction with the membrane-tethered HSPG Dlp. We show synaptic Dlp rapidly increases with acute stimulation, and tight spatial co-localization with Mmp1 in synaptic subdomains is heightened by increased activity. We demonstrate that Dlp is a strong, positive regulator of synaptic Mmp1, with Dlp bidirectionally determining Mmp1 abundance at the synapse. As a GPI-anchored glypican, Dlp can interact with many extracellular molecules to bring Mmp1 substrates within close proximity. In parallel, Mmp2 proteolytically cleaves Dlp to regulate Wg signaling in the *Drosophila* ovary (*68*), and a similar role likely occurs at the synapse, where Mmp2 spatially

confines Dlp in the synaptic domain (*7*). Thus, Mmp2-dependent Dlp processing may antagonize the Dlp-Mmp1 interaction, which would necessitate reciprocal co-regulation of Mmp1 and Mmp2.

We find that Dlp functions are context-dependent, with synaptic Dlp coordinating signaling mechanisms converging in the synaptomatrix. Consistently, synaptic defects observed in mutant conditions that also concurrently display misregulated Dlp are remediated by restoring Dlp back towards wild-type (*7*, *28*). HSPGs consist of a core protein linked to sulfated GAG chains, with both components contributing to ligand interactions (*38*, *46*, *96–99*, *71*). We find that an HS-GAG chain deficient Dlp is unable to efficiently retain Mmp1 at the synapse, or enhance activity-dependent control of Mmp1 abundance. We suggest this defect arises from loss of direct binding between Mmp1 and Dlp HS-GAG chains. Protease-HSPG interactions are bidirectional, with HS-GAG chains regulating protease localization, activity and inhibition, while proteases conversely mediate HSPG proteolytic processing and turnover through cleavage of core proteins (*34–39*, *103*). We suggest the Dlp-Mmp1 interaction is mediated through HS-GAG chains through a non-proteolytic mechanism (*7*). We further suggest that the synaptic co-localization of Dlp and Mmp1 is mediated through Dlp HS-GAG chains, with Dlp recruiting essential Mmp1 function driving activity-dependent bouton formation. With in situ zymography proteolytic function tests at the synapse (*33*, *84*), we consistently find reduced function with Dlp reduction and increased function with Dlp overexpression. However, enzymatic activity appears primarily dependent upon interaction with the Dlp core protein. Note that this assay reflects net proteolytic function, with likely context-dependent contributions by a variety of synaptic proteases.

In the *Drosophila* FXS disease model, we report that Mmp1 is constitutively increased and activity-dependent Mmp1 enhancement is lost, but that both defects are prevented when Dlp is suppressed. The mouse FXS model mirrors effects observed in *Drosophila*: mouse MMP-9 is similarly upregulated, and pharmacological and genetic inhibition of MMP-9 restores synaptic development (*13*, *104*, *105*). This suggests the HSPG-Mmp mechanism identified here is likely conserved in mammals as well. The FMRP mRNA-binding translational repressor is required for activity-dependent synaptogenesis and is itself directly upregulated by neuronal activity (*51–54*). Moreover, HSPGs are predicted FMRP targets (*32*), and synaptic HSPGs are increased in the *Drosophila* FXS model (*28*). Thus, FMRP might directly regulate *mmp1* and/or *dlp* translation in an activity-dependent mechanism. HSPG Dlp functions as a bifunctional Wg co-receptor during normal synaptogenesis, with impaired Wg *trans*-synaptic signaling causative in FXS disease state synaptogentic defects (*28*, *40*). Mmp1, Dlp and Wg are at least paritally inter-dependent, and all three are disrupted in the FXS disease state, which could therefore collectively impede the activity-induced Mmp1 enhancement

characterizing the FXS condition, dependent on the Dlp interaction. It will be of great interest in our future studies to dissect the differential activity requirements of this FMRP-Wg-Dlp-Mmp1 mechanism.

How do FMRP, Dlp and Mmp1 intersect in activity-dependent synaptogenesis? Dlp is a positive regulator of Mmp1, and absolutely required for any activity-dependent Mmp1 elevation. Why then is the activity-induced Mmp1 increase not present in the FXS disease model despite elevated synaptic Dlp? It seems counterintuitive that *dfmr1* mutants display increased Dlp, yet the activity-induced Mmp1 increase is completely abolished, and this defect can be corrected by reducing Dlp. One possibility is a ceiling effect in the FXS condition, in which maximal amounts of Dlp or Mmp1 no longer permit changes in response to activity. We feel this unlikely because Mmp1 and Dlp were both highly increased by Dlp overexpression, yet activity-induced Mmp1 elevation persists. Another possibility is the relative abundance of Dlp and Mmp1 control their interactions, with Dlp acting differently depending on relative abundance. Consistently, Dlp has biphasic functions as both a positive and a negative regulator of Wg *trans*-synaptic signaling, depending on relative abundance of Wg ligand, Frizzled-2 receptor and Dlp co-receptor (*40*, *46*). Is an unknown effector(s) regulated by FMRP modulating the Dlp-Mmp1 intersection? We feel this most likely, as numerous activity-dependent changes can increase Dlp in the synaptomatrix. As a core signaling platform, Dlp could interact with an unknown protein(s) in Mmp1 secretion or sequestration. In any case, it is apparent that FMRP loss impedes Dlp and Mmp1 interaction in response to neuronal activity, and that reducing Dlp in the FXS disease state restores this core activity-dependent intersection, allowing appropriate Mmp1 control at the synapse.

References

1. C. S. Barros, S. J. Franco, U. Müller, Extracellular Matrix: Functions in the Nervous System. *Cold Spring Harb. Perspect. Biol.* **3**, a005108 (2011).

2. N. Dani, K. Broadie, Glycosylated synaptomatrix regulation of trans-synaptic signaling. *Dev. Neurobiol.* **72**, 2–21 (2011).

3. D. L. Benson, G. W. Huntley, Building and remodeling synapses. *Hippocampus*. **22**, 954–968 (2012).

4. K. Conant, M. Allen, S. T. Lim, Activity dependent CAM cleavage and neurotransmission. *Front. Cell. Neurosci.* **9**, 305 (2015).

5. G. W. Huntley, Synaptic circuit remodelling by matrix metalloproteinases in health and disease. *Nat. Rev. Neurosci.* **13**, 743–57 (2012).

6. T. Shinoe, Y. Goda, Tuning synapses by proteolytic remodeling of the adhesive surface. *Curr. Opin. Neurobiol.* **December 2**, 148–155 (2015).

7. M. L. Dear, N. Dani, W. Parkinson, S. Zhou, K. Broadie, Two matrix metalloproteinase classes reciprocally regulate synaptogenesis. *Development*. **143**, 75–87 (2016).

8. I. M. Ethell, D. W. Ethell, Matrix metalloproteinases in brain development and remodeling: Synaptic functions and targets. *J. Neurosci. Res.* **85**, 2813–2823 (2007).

9. J. Wlodarczyk, I. Mukhina, L. Kaczmarek, A. Dityatev, Extracellular matrix molecules, their receptors, and secreted proteases in synaptic plasticity. *Dev. Neurobiol.* **71**, 1040–1053 (2011).

10. H. Nagase, R. Visse, G. Murphy, Structure and function of matrix metalloproteinases and TIMPs. *Cardiovasc. Res.* **69**, 562–573 (2006).

11. S. Nagappan-Chettiar, E. M. Johnson-Venkatesh, H. Umemori, Activity-dependent proteolytic cleavage of cell adhesion molecules regulates excitatory synaptic development and function. *Neurosci. Res.* **116**, 60–69 (2017).

12. S. M. Reinhard, K. Razak, I. M. Ethell, A delicate balance: role of MMP-9 in brain development and pathophysiology of neurodevelopmental disorders. *Front. Cell. Neurosci.* **9** (2015), doi:10.3389/fncel.2015.00280.

13. H. Sidhu, L. E. Dansie, P. W. Hickmott, D. W. Ethell, I. M. Ethell, Genetic removal of matrix metalloproteinase 9 rescues the symptoms of fragile X syndrome in a mouse model. *J. Neurosci.* **34**, 9867–9879 (2014).

14. E. Tsilibary, A. Tzinia, L. Radenovic, V. Stamenkovic, T. Lebitko, M. Mucha, R. Pawlak, R. Frischknecht, L. Kaczmarek, in *Progress in Brain Research*, A. Dityatev, B. Wehrle-Haller, A. Pitkanen, Eds. (Elsevier, Vol 214., 2014), pp. 135–157.

15. B. Vafadari, A. Salamian, L. Kaczmarek, MMP-9 in translation: from molecule to brain physiology, pathology, and therapy. *J. Neurochem.* **139**, 91–114 (2016).

16. K. Broadie, S. Baumgartner, A. Prokop, Extracellular matrix and its receptors in Drosophila neural development. *Dev. Neurobiol.* **71**, 1102–1130 (2011).

17. K. P. Harris, J. T. Littleton, Transmission, development, and plasticity of synapses. *Genetics*. **201**, 345–375 (2015).

18. K. Menon, R. Carrillo, K. Zinn, Development and Plasticity of the Drosophila Larval Neuromuscular Junction. *Wiley Interdiscip. Rev. Dev. Biol.* **2**, 647–670 (2013).

19. E. Llano, A. M. Pendas, P. Aza-Blanc, T. B. Kornberg, C. Lopez-Otin, Dm1-MMP, a matrix metalloproteinase from Drosophila with a potential role in extracellular matrix remodeling during neural development. *J. Biol. Chem.* **275**, 35978–35985 (2000).

20. E. Llano, G. Adam, A. M. Pendás, V. Quesada, L. M. Sánchez, I. Santamaría, S. Noselli, C. López-Otín, Structural and enzymatic characterization of Drosophila Dm2-MMP, a membrane-bound matrix metalloproteinase with tissue-specific expression. *J. Biol. Chem.* **277**, 23321–23329 (2002).

21. A. Page-McCaw, J. Serano, J. M. Sante, G. M. Rubin, Drosophila matrix metalloproteinases are required for tissue remodeling, but not embryonic development. *Dev. Cell*. **4**, 95–106 (2003).

22. K. LaFever, X. Wang, P. Page-McCaw, G. Bhave, A. Page-McCaw, Both Drosophila matrix metalloproteinases have released and membrane-tethered forms but have different substrates. *Sci. Rep.* **7** (2017), doi:10.1038/srep44560.

23. C. M. Miller, A. Page-McCaw, H. T. Broihier, Matrix metalloproteinases promote motor axon fasciculation in the Drosophila embryo. *Development*. **135**, 95–109 (2008).

24. C. M. Miller, N. Liu, A. Page-McCaw, H. T. Broihier, Drosophila Mmp2 Regulates the Matrix Molecule Faulty Attraction (Frac) to Promote Motor Axon Targeting in Drosophila. *J. Neurosci.* **31**, 5335–5347 (2011).

25. C. T. Kuo, L. Y. Jan, Y. N. Jan, Dendrite-specific remodeling of Drosophila sensory neurons requires matrix metalloproteases, ubiquitin-proteasome, and ecdysone signaling. *Proc. Natl. Acad. Sci. U. S. A.* **102**, 15230–15235 (2005).

26. K. I. Yasunaga, T. Kanamori, R. Morikawa, E. Suzuki, K. Emoto, Dendrite Reshaping of Adult Drosophila Sensory Neurons Requires Matrix Metalloproteinase-Mediated Modification of the Basement Membranes. *Dev. Cell*. **18**, 621–632 (2010).

27. A. Depetris-Chauvin, Á. Fernández-Gamba, E. A. Gorostiza, A. Herrero, E. M. Castaño, M. F. Ceriani, Mmp1 Processing of the PDF Neuropeptide Regulates Circadian Structural Plasticity of Pacemaker Neurons. *PLoS Genet.* **10**, e1004700 (2014).

28. S. H. Friedman, N. Dani, E. Rushton, K. Broadie, Fragile X mental retardation protein regulates trans-synaptic signaling in Drosophila. *Dis. Model. Mech.* **6**, 1400–1413 (2013).

29. G. J. Bassell, S. T. Warren, Fragile X Syndrome: Loss of Local mRNA Regulation Alters Synaptic Development and Function. *Neuron*. **60**, 201–214 (2008).

30. K. B. Garber, J. Visootsak, S. T. Warren, Fragile X syndrome. *Eur.J Hum.Genet.* **16**, 666–672 (2008).

31. A. J. Verkerk, M. Pieretti, J. S. Surtcliffe, Y.-H. Fu, D. P. Kuhl, A. Pizzuti, O. Reiner, S. Richards, M. F. Victoria, F. Zhang, B. E. Eussen, G.-J. B. van Ommen, L. A. Bionden, G. J. Riggins, J. L. Chastain, C. B. Kunst, H. Galjaard, C. T. Caskey, D. L. Nelson, *et al.*, Identification of a Gene (FMR-1) Containing a CGG Repeat Coincident with a Breakpoint Cluster Region Exhibiting Length Variation in Fragile X Syndrome. *Cell*. **65**, 905–914 (1991).

32. J. C. Darnell, S. J. Van Driesche, C. Zhang, K. Y. S. Hung, A. Mele, C. E. Fraser, E. F. Stone, C. Chen, J. J. Fak, S. W. Chi, D. D. Licatalosi, J. D. Richter, R. B. Darnell, FMRP stalls ribosomal translocation on mRNAs linked to synaptic function and autism. *Cell*. **146**, 247–261 (2011).

33. S. S. Siller, K. Broadie, Neural circuit architecture defects in a Drosophila model of Fragile X syndrome are alleviated by minocycline treatment and genetic removal of matrix metalloproteinase. *Dis. Model. Mech.* **4**, 673–685 (2011).

34. S. Georges, D. Heymann, M. Padrines, Modulatory effects of proteoglycans on proteinase activities. *Methods Mol Biol*, 307–322 (2012).

35. A. Tocchi, W. C. Parks, Functional interactions between matrix metalloproteinases and glycosaminoglycans. *FEBS J.* **280**, 2332–2341 (2013).

36. G. Murphy, H. Nagase, Localizing matrix metalloproteinase activities in the pericellular environment. *FEBS J.* **278**, 2–15 (2011).

37. V. C. Ramani, P. S. Pruett, C. A. Thompson, L. D. DeLucas, R. D. Sanderson, Heparan sulfate chains of syndecan-1 regulate ectodomain shedding. *J. Biol. Chem.* **287**, 9952–9961 (2012).

38. S. Sarrazin, W. C. Lamanna, J. D. Esko, Heparan sulfate proteoglycans. *Cold Spring Harb. Perspect. Biol.* **3**, a004952 (2011).

39. A. Theocharis, C. Gialeli, P. Bouris, E. Giannopoulou, S. Skandalis, A. Aletras, R. Iozzo, N. Karamanos, Cell-matrix interactions: focus on proteoglycan-proteinase interplays and pharmacological targeting in cancer. *FEBS J.* **281**, 5023–5042 (2014).

40. N. Dani, M. Nahm, S. Lee, K. Broadie, A Targeted Glycan-Related Gene Screen Reveals Heparan Sulfate Proteoglycan Sulfation Regulates WNT and BMP Trans-Synaptic Signaling. *PLoS Genet.* **8**, e1003031 (2012).

41. K. G. Johnson, A. P. Tenney, A. Ghose, A. M. Duckworth, M. E. Higashi, K. Parfitt, O. Marcu, T. R. Heslip, J. L. Marsh, T. L. Schwarz, J. G. Flanagan, D. Van Vactor, The HSPGs Syndecan and dallylike bind the receptor phosphatase LAR and exert distinct effects on synaptic development. *Neuron*. **49**, 517–531 (2006).

42. D. Minge, O. Senkov, R. Kaushik, M. K. Herde, O. Tikhobrazova, A. B. Wulff, A. Mironov, T. H. van Kuppevelt, A. Oosterhof, G. Kochlamazashvili, A. Dityatev, C. Henneberger, Heparan Sulfates Support Pyramidal Cell Excitability, Synaptic Plasticity, and Context Discrimination. *Cereb. Cortex*. **27**, 903–918 (2017).

43. Y. Yamaguchi, M. Inatani, Y. Matsumoto, J. Ogawa, F. Irie, *Roles of heparan sulfate in mammalian brain development Current views based on the findings from ext1 conditional knockout studies* (Elsevier Inc., 2010), vol. 93.

44. K. Kamimura, K. Ueno, J. Nakagawa, R. Hamada, M. Saitoe, N. Maeda, Perlecan regulates bidirectional Wnt signaling at the Drosophila neuromuscular junction. *J. Cell Biol.* **200**, 219–233 (2013).

45. Y. Wu, T. Y. Belenkaya, X. Lin, in *Methods in Enzymology*, M. Fukuda, Ed. (Elsevier Inc., 2010), vol. 480, pp. 33–50.

46. D. Yan, Y. Wu, Y. Feng, S.-C. Lin, X. Lin, The Core Protein of Glypican Daily-Like Determines Its Biphasic Activity in Wingless Morphogen Signaling. *Dev. Cell*. **17**, 470–481 (2009).

47. B. Ataman, J. Ashley, M. Gorczyca, P. Ramachandran, W. Fouquet, S. J. Sigrist, V. Budnik, Rapid activity-dependent modifications in synaptic structure and function require bidirectional Wnt signaling. *Neuron*. **57**, 705–718 (2008).

48. K. S. Kerr, Y. Fuentes-Medel, C. Brewer, R. Barria, J. Ashley, K. C. Abruzzi, A. Sheehan, O. E. Tasdemir-Yilmaz, M. R. Freeman, V. Budnik, Glial wingless/Wnt regulates glutamate receptor clustering and synaptic physiology at the Drosophila neuromuscular junction. *J. Neurosci.* **34**, 2910–2920 (2014).

49. C. Miech, H. U. Pauer, X. He, T. L. Schwarz, Presynaptic Local Signaling by a Canonical Wingless Pathway Regulates Development of the Drosophila Neuromuscular Junction. *J. Neurosci.* **28**, 10875–10884 (2008).

50. M. Packard, E. S. Koo, M. Gorczyca, J. Sharpe, S. Cumberledge, V. Budnik, The Drosophila Wnt, wingless, provides an essential signal for pre- and postsynaptic differentiation. *Cell*. **111**, 319–330 (2002).

51. L. N. Antar, R. Afroz, J. B. Dictenberg, R. C. Carroll, G. J. Bassell, Metabotropic Glutamate Receptor Activation Regulates Fragile X Mental Retardation Protein and FMR1 mRNA Localization Differentially in Dendrites and at Synapses. *J. Neurosci.* **24**, 2648–2655 (2004).

52. S. A. Irwin, R. Swain, C. A. Christmon, A. Chakravarti, I. J. Weiler, W. T. Greenough, Evidence for altered Fragile-X mental retardation protein expression in response to behavioral stimulation. *Neurobiol. Learn. Mem.* **73**, 87–93 (2000).

53. S. A. Irwin, C. A. Christmon, A. W. Grossman, R. Galvez, S. H. Kim, B. J. DeGrush, I. J. Weiler, W. T. Greenough, Fragile X mental retardation protein levels increase following complex environment exposure in rat brain regions undergoing active synaptogenesis. *Neurobiol. Learn. Mem.* **83**, 180–187 (2005).

54. I. J. Weiler, S. A. Irwin, A. Y. Klintsova, C. M. Spencer, A. D. Brazelton, K. Miyashiro, T. A. Comery, B. Patel, J. Eberwine, W. T. Greenough, Fragile X mental retardation protein is translated near synapses in response to neurotransmitter activation. *Proc. Natl. Acad. Sci. U. S. A.* **94**, 5395–5400 (1997).

55. C. A. Doll, K. Broadie, Neuron class-specific requirements for Fragile X Mental Retardation Protein in critical period development of calcium signaling in learning and memory circuitry. *Neurobiol. Dis.* **89**, 76–87 (2016).

56. C. A. Doll, K. Broadie, Impaired activity-dependent neural circuit assembly and refinement in autism spectrum disorder genetic models. *Front. Cell. Neurosci.* **8**, 30 (2014).

57. C. A. Doll, K. Broadie, Activity-dependent FMRP requirements in development of the neural circuitry of learning and memory. *Development*. **142**, 1346–1356 (2015).

58. C. L. Gatto, K. Broadie, Temporal requirements of the fragile X mental retardation protein in the regulation of synaptic structure. *Development*. **135**, 2637–2648 (2008).

59. C. R. Tessier, K. Broadie, Drosophila fragile X mental retardation protein developmentally regulates activity-dependent axon pruning. *Development*. **135**, 1547–1557 (2008).

60. S. Cavolo, D. Bulgari, D. Deitcher, E. Levitan, Activity Induces Fmr1-Sensitive Synaptic Capture of Anterograde Circulating Neuropeptide Vesicles. *J. Neurosci.* **36**, 11781–11787 (2016).

61. P. P. Jumbo-Lucioni, W. M. Parkinson, D. L. Kopke, K. S. Broadie, Coordinated movement, neuromuscular synaptogenesis and trans-synaptic signaling defects in Drosophila galactosemia models. *Hum. Mol. Genet.* **25**, 3699–3714 (2016).

62. X. Chen, R. Rahman, F. Guo, M. Rosbash, Genome-wide identification of neuronal activity-regulated genes in *Drosophila*. *Elife*. **5**, 1–21 (2016).

63. A. Fukui, M. Inaki, G. Tonoe, H. Hamatani, M. Homma, T. Morimoto, H. Aburatani, A. Nose, Lola regulates glutamate receptor expression at the Drosophila neuromuscular junction. *Biol. Open*. **1**, 362–75 (2012).

64. J. M. Gillespie, J. J. L. Hodge, CASK regulates CaMKII autophosphorylation in neuronal growth, calcium signaling, and learning. *Front. Mol. Neurosci.* **6** (2013), doi:10.3389/fnmol.2013.00027.

65. F. N. Hamada, M. Rosenzweig, K. Kang, S. R. Pulver, A. Ghezzi, T. J. Jegla, P. a Garrity, An internal thermal sensor controlling temperature preference in Drosophila. *Nature*. **454**, 217–220 (2008).

66. S. R. Pulver, S. L. Pashkovski, N. J. Hornstein, P. a Garrity, L. C. Griffith, Temporal dynamics of neuronal activation by Channelrhodopsin-2 and TRPA1 determine behavioral output in Drosophila larvae. *J. Neurophysiol.* **101**, 3075–88 (2009).

67. M. Uhlirova, D. Bohmann, JNK- and Fos-regulated Mmp1 expression cooperates with Ras to induce invasive tumors in Drosophila. *EMBO J.* **25**, 5294–5304 (2006).

68. X. Wang, A. Page-McCaw, A matrix metalloproteinase mediates long-distance attenuation of stem cell proliferation. *J. Cell Biol.* **206**, 923–936 (2014).

69. C. Han, T. Y. Belenkaya, B. Wang, X. Lin, Drosophila glypicans control the cell-to-cell movement of Hedgehog by a dynamin-independent process. *Development*. **131**, 601–11 (2004).

70. G. H. Baeg, X. Lin, N. Khare, S. Baumgartner, N. Perrimon, Heparan sulfate proteoglycans are critical for the organization of the extracellular distribution of Wingless. *Development*. **128**, 87–94 (2001).

71. D. Yan, Y. Wu, T. Y. Belenkaya, X. Tang, X. Lin, The cell-surface proteins Dally-like and Ihog differentially regulate Hedgehog signaling strength and range during development. *Development*. **137**, 2033–2044 (2010).

72. S. Nagarkar-Jaiswal, P. T. Lee, M. E. Campbell, K. Chen, S. Anguiano-Zarate, M. C. Gutierrez, T. Busby, W. W. Lin, Y. He, K. L. Schulze, B. W. Booth, M. Evans-Holm, K. J. T. Venken, R. W. Levis, A. C. Spradling, R. A. Hoskins, H. J. Bellen, A library of MiMICs allows tagging of genes and reversible, spatial and temporal knockdown of proteins in Drosophila. *Elife*. **2015**, 1–28 (2015).

73. K. J. T. Venken, K. L. Schulze, N. a Haelterman, H. Pan, Y. He, M. Evans-Holm, J. W. Carlson, R. W. Levis, A. C. Spradling, R. a Hoskins, H. J. Bellen, MiMIC: a highly versatile transposon insertion resource for engineering Drosophila melanogaster genes. *Nat. Methods*. **8**, 737–743 (2011).

74. Y. Q. Zhang, A. M. Bailey, H. J. G. Matthies, R. B. Renden, M. A. Smith, S. D. Speese, G. M. Rubin, K. Broadie, Drosophila fragile X-related gene regulates the MAP1B homolog Futsch to control synaptic structure and function. *Cell*. **107**, 591–603 (2001).

75. J. Lee, J. Geng, J. Lee, A. Wang, K. Chang, Activity-induced synaptic structural modifications by an activator of integrin signaling at the Drosophila neuromuscular junction. *J. Neurosci.* **37**, 3246–3263 (2017).

76. M. Baek, R. S. Mann, Lineage and birth date specify motor neuron targeting and dendritic architecture in adult Drosophila. *J. Neurosci.* **29**, 6904–6916 (2009).

77. A. Kolodziejczyk, X. Sun, I. A. Meinertzhagen, D. R. Nässel, Glutamate, GABA and acetylcholine signaling components in the lamina of the Drosophila visual system. *PLoS One*. **3** (2008), doi:10.1371/journal.pone.0002110.

78. A. Mahr, H. Aberle, The expression pattern of the Drosophila vesicular glutamate transporter: A marker protein for motoneurons and glutamatergic centers in the brain. *Gene Expr. Patterns*. **6**, 299–309 (2006).

79. H. H. Li, J. R. Kroll, S. M. Lennox, O. Ogundeyi, J. Jeter, G. Depasquale, J. W. Truman, A GAL4 driver resource for developmental and behavioral studies on the larval CNS of Drosophila. *Cell Rep.* **8**, 897–908 (2014).

80. B. D. Pfeiffer, A. Jenett, A. S. Hammonds, T.-T. B. Ngo, S. Misra, C. Murphy, A. Scully, J. W. Carlson, K. H. Wan, T. R. Laverty, C. Mungall, R. Svirskas, J. T. Kadonaga, C. Q. Doe, M. B. Eisen, S. E. Celniker, G. M. Rubin, Tools for neuroanatomy and neurogenetics in Drosophila. *Proc. Natl. Acad. Sci. U. S. A.* **105**, 9715–9720 (2008).

81. A. Jenett, G. M. Rubin, T. T. B. Ngo, D. Shepherd, C. Murphy, H. Dionne, B. D. Pfeiffer, A. Cavallaro, D. Hall, J. Jeter, N. Iyer, D. Fetter, J. H. Hausenfluck, H. Peng, E. T. Trautman, R. R. Svirskas, E. W. Myers, Z. R. Iwinski, Y. Aso, *et al.*, A GAL4-Driver Line Resource for Drosophila Neurobiology. *Cell Rep.* **2**, 991–1001 (2012).

82. J. Rohrbough, E. Rushton, E. Woodruff, T. Fergestad, K. Vigneswaran, K. Broadie, Presynaptic establishment of the synaptic cleft extracellular matrix is required for post-synaptic differentiation. *Genes Dev.* **21**, 2607–2628 (2007).

83. E. Rushton, J. Rohrbough, K. Broadie, Presynaptic secretion of mind-the-gap organizes the synaptic extracellular matrix-integrin interface and postsynaptic environments. *Dev. Dyn.* **238**, 554–571 (2009).

84. J. Shilts, K. Broadie, Secreted tissue inhibitor of matrix metalloproteinase restricts trans -synaptic signaling to coordinate synaptogenesis. *J. Cell Sci.* **130**, 2344–2358 (2017).

85. J. Schindelin, I. Arganda-Carreras, E. Frise, V. Kaynig, M. Longair, T. Pietzsch, S. Preibisch, C. Rueden, S. Saalfeld, B. Schmid, J.-Y. Tinevez, D. J. White, V. Hartenstein, K. Eliceiri, P. Tomancak, A. Cardona, Fiji: an open-source platform for biological-image analysis. *Nat. Methods*. **9**, 676–82 (2012).

86. E. M. M. Manders, F. J. Verbeek, J. A. Aten, Measurement of co-localization of objects in dual-colour confocal images. *J. Microsc.* **169**, 375–382 (1993).

87. C. A. Schneider, W. S. Rasband, K. W. Eliceiri, NIH Image to ImageJ: 25 years of image analysis. *Nat. Methods*. **9**, 671–675 (2012).

88. B. Ataman, J. Ashley, D. Gorczyca, M. Gorczyca, D. Mathew, C. Wichmann, S. J. Sigrist, V. Budnik, Nuclear trafficking of Drosophila Frizzled-2 during synapse development requires the PDZ protein dGRIP. *Proc. Natl. Acad. Sci. U. S. A.* **103**, 7841–7846 (2006).

89. Z. D. Piccioli, J. T. Littleton, Retrograde BMP signaling modulates rapid activity-dependent synaptic growth via presynaptic LIM kinase regulation of cofilin. *J. Neurosci.* **34**, 4371–81 (2014).

90. A. Vasin, L. Zueva, C. Torrez, D. Volfson, J. T. Littleton, M. Bykhovskaia, Synapsin regulates activity-dependent outgrowth of synaptic boutons at the Drosophila neuromuscular junction. *J. Neurosci.* **34**, 10554–63 (2014).

91. V. Dudu, T. Bittig, E. Entchev, A. Kicheva, F. Julicher, M. Gonzalez-Gaitan, Postsynaptic mad signaling at the Drosophila neuromuscular junction. *Curr. Biol.* **16**, 625–635 (2006).

92. E. S. Levitan, F. Lanni, D. Shakiryanova, In vivo imaging of vesicle motion and release at the Drosophila neuromuscular junction. *Nat. Protoc.* **2**, 1117–25 (2007).

93. B. M. Glasheen, A. T. Kabra, A. Page-McCaw, Distinct functions for the catalytic and hemopexin domains of a Drosophila matrix metalloproteinase. *Proc. Natl. Acad. Sci. U. S. A.* **106**, 2659–2664 (2009).

94. L. Lum, S. Yao, B. Mozer, A. Rovescalli, D. Von Kessler, M. Nirenberg, P. Beachy, Identification of Hedgehog Pathway Components by RNAi in Drosophila Cultured Cells. *Science (80-.).* **299**, 2039–2045 (2003).

95. K. W. Dunn, M. M. Kamocka, J. H. McDonald, A practical guide to evaluating colocalization in biological microscopy. *Am. J. Physiol. Cell Physiol.* **300**, C723–C742 (2011).

96. F. E. Poulain, H. J. Yost, Heparan sulfate proteoglycans: a sugar code for vertebrate development? *Development*. **142**, 3456–67 (2015).

97. P. D. Smith, V. J. Coulson-Thomas, S. Foscarin, J. C. F. Kwok, J. W. Fawcett, "GAG-ing with the neuron": The role of glycosaminoglycan patterning in the central nervous system. *Exp. Neurol.* **274**, 100–114 (2015).

98. M. Herndon, C. Stipps, A. Lander, Interactions of neural glycosaminoglycans and proteoglycans with protein ligands: assessment of selectivity, heterogeneity and the participation of core proteins in binding. *Glycobiology*. **9**, 143–55 (1999).

99. C. A. Kirkpatrick, S. M. Knox, W. D. Staatz, B. Fox, D. M. Lercher, S. B. Selleck, The function of a Drosophila glypican does not depend entirely on heparan sulfate modification. *Dev. Biol.* **300**, 570–582 (2006).

100. D. Alicea, M. Perez, C. Maldonado, C. Dominicci-Cotto, B. Marie, Cortactin is a regulator of activity-dependent synaptic plasticity controlled by Wingless. *J. Neurosci.* **37**, 2203–2215 (2017).

101. K. R. Nesler, R. I. Sand, B. A. Symmes, S. J. Pradhan, N. G. Boin, A. E. Laun, S. A. Barbee, The miRNA Pathway Controls Rapid Changes in Activity-Dependent Synaptic Structure at the Drosophila melanogaster Neuromuscular Junction. *PLoS One*. **8** (2013), doi:10.1371/journal.pone.0068385.

102. P. Jin, S. Warren, New insights into fragile X syndrome: from molecules to neurobehaviors. *Trends Biochem. Sci.* **28**, 152–158 (2003).

103. V. Kainulainen, H. M. Wang, C. Schick, M. Bernfield, Syndecans, heparan sulfate proteoglycans, maintain the proteolytic balance of acute wound fluids. *J. Biol. Chem.* **273**, 11563–11569 (1998).

104. T. V Bilousova, L. Dansie, M. Ngo, J. Aye, J. R. Charles, D. W. Ethell, I. M. Ethell, Minocycline promotes dendritic spine maturation and improves behavioural performance in the fragile X mouse model. *J. Med. Genet.* **46**, 94–102 (2009).

105. A. Janusz, J. Milek, M. Perycz, L. Pacini, C. Bagni, L. Kaczmarek, M. Dziembowska, The Fragile X mental retardation protein regulates matrix metalloproteinase 9 mRNA at synapses. *J. Neurosci.* **33**, 18234–41 (2013).

CHAPTER IV

CONCLUSIONS AND FUTURE DIRECTIONS

The MMP field has been ever changing since the identification of the first MMP in 1962 (*1*, *2*). Indeed, MMP research has exponentially evolved over the past decade with new approaches and findings challenging the canonical views of how, why and where MMPs function in the context of development and disease states (*3*–*5*). When I first started this project, most literature impressed the notion that MMPs were exclusive extracellular proteinases, collectively capable of acting on all components of the ECM, thus acting primarily on ECM (*6*–*8*). As such, primary MMP functions included matrix degradation and turnover with secondary roles in matrix-mediated signaling. Likewise, early studies of invertebrate Mmps reported matrix-mediated functions centered on tissue histolysis, remodeling and invasion events (*9*, *10*). Therefore, in conjunction with the belief that the ECM is an inhibitory environment, my original hypothesis was that the two *Drosophila* Mmps degrade the neural ECM to permit NMJ growth. However, our structural, functional and ultrastructural analyses largely argue against this hypothesis (Chapter II). Concurrent with my work, it become more widely appreciated that MMPs also act on non-ECM molecules and accumulating evidence from transgenic models and proteomic screens revealed an even wider array of substrates implicating primary MMP functions in active cell-signaling processes and within a broader proteolytic network (*11*–*14*). My data argue that co-regulated MMP proteolytic activities modulate *trans*-synaptic signaling pathways driving synaptogenesis and thereby support such a shift in the MMP functional paradigm. Now more than ever, MMPs are appreciated as tightly regulated, multifunctional proteins with catalytic, non-catalytic, intracellular and extracellular functions that display dynamic, interconnected and context-dependent activities. Accordingly, the idea that MMP activities are potent signaling regulators is no longer an exception to the rule but rather a common modality describing how MMPs influence cell behavior.

My thesis work sets a solid foundation for future studies interrogating proteolytic mechanisms driving synaptogenesis using the *Drosophila* NMJ genetic model. Before this work, very little was known about *Drosophila* Mmp functions in the nervous system and nothing was known about Mmp functions in synaptic mechanisms at the NMJ. Comparing to mammalian work is quite challenging as there are no single gene orthologues. Multiple mammalian MMPs are expressed in synapses, although most studies focus only on MMP-2 and -9 in one specific aspect of the nervous system, and early studies were performed *in vitro* or using neuronal cell culture (*5*). Moreover, functional redundancy and compensation are well documented in the

mammalian system, which might obscure essential MMP roles in the nervous system. My work aimed to disrupt all Mmps, alone and in combination, to genetically dissect Mmp mechanisms *in vivo*, to interrogate how Mmps are regulated in normal synaptic development and to place these questions in the context of the Fragile X syndrome (FXS) disease state. I developed new antibody tools to enable visualization of the entire *Drosophila* matrix metalloproteome at the synapse (Chapter II). I showed that synaptic Mmp1, Mmp2 and Timp are co-regulated, and that both Mmps normally put the brakes on structural and functional synaptic development. I found that synaptogenesis requires balanced Mmp activities in neuron, muscle and across the synaptic cleft (Chapter II). I found the two Mmps restrict Wnt Wg *trans*-synaptic signaling by differentially regulating HSPG Dlp to co-suppress each other's synaptogenic requirements. In turn, neural activity and Dlp HSPG reciprocally regulate Mmp1 and Mmp2 (Chapter III). I found neural activity and HSPGs are both upstream regulators and downstream effectors of Mmp functions. I discovered Mmp1 is required to promote activity-dependent bouton formation (Chapter III). Moreover, I found that HSPG Dlp and Mmp1 are both enhanced following neural stimulation in a Dlp-dependent mechanism that promotes Mmp1 synaptic localization via HS GAG chains. I showed that activity-stimulated Mmp1 upregulation requires the coordinated activities of both Dlp and FMRP (Chapter III). In the context of FXS, I find that aberrant Mmp1 enhancement following activity is restored by correcting synaptic Dlp. This work identifies convergence in the extracellular synaptomatrix contributing to synaptic defects underlying the FXS disease state. These findings suggest that synaptic Mmps do not play major roles in ECM degradation/turnover, but instead function as potent signaling regulators. Further, Mmp activities and Mmp regulation are dynamically coordinated through complex, bi-directional feedback loops intersecting with Dlp HSPG at the synapse. Overall, my work has significantly advanced our understanding of Mmp functions in normal and disease state synaptic development. However, much still remains to be investigated and there is undoubtedly an exciting future ahead exploring Mmp biology at the *Drosophila* NMJ.

Regulation of Synaptic Mmp and Timp Expression

At the NMJ, Mmp1 promotes Mmp2 and Mmp2 reciprocally restricts Mmp1 and Timp (Fig. 12). These interactions could reflect mechanisms of transcription, translation, secretion, internalization, localization, turnover or inhibition (*12*, *15*, *16*). Moreover, I find synaptic Mmps are derived from both neuron and muscle (Table S3 and Fig. 23), suggesting possibilities of intercellular interactions. Tissue-specific expression might dictate or compartmentalize Mmp function within the synaptomatrix. For Mmp1, there are ten alternatively

spliced isoforms originating from three alternative start sites, which are predicted to yield six unique polypeptides with variable C-terminal domains (*17*). The functional relevance for the various isoforms is unknown, but recent evidence suggests that catalytic inactivation of GPI-anchored Mmps can promote cell adhesion (*17*). The recently expanded definition of Mmp1 as both secreted and GPI-anchored protease (*17*) increases the possible modes of interaction in the extracellular synaptomatrix. For example, catalytically inactive, GPI-anchored Mmps induce cellular aggregation and *mmp1* mutant NMJs display aggregated boutons. Future studies could use available transgenic RNAi and overexpression lines in tissue-specific assays to test secreted versus GPI-anchored Mmp distributions and requirements for structural growth and plasticity exploring both *cis* (neuron:neuron or muscle:muscle) and *trans* (neuron:muscle) conditions at the NMJ. Mmp1 is a target gene of JNK-activated Fos and is commonly used as a read-out for JNK signal activation (*18*). The SWI/SNF (SWItch/ Sucrose Non-Fermentable) complex, which functions in chromatin remodeling and pre-mRNA processing, modulates the relative abundance of alternative Mmp1 isoforms (*19*, *20*). SWI/SNF orchestrates and spatio-temporally regulates various neurodevelopmental processes with defects linked to ASD, raising the possibility that differential cell-type and temporal expression of functionally diverse Mmp1 isoforms could be an important mediator of synaptogenesis (*20*). Studies should also test if Mmp1 isoforms are differentially expressed in FXS. ECM-mediated changes in gene expression are often transduced by SWI/SNF, suggesting HSPG or Mmp1-dependent matrix alterations might reciprocally influence gene expression (*20*, *21*).

For Mmp2, two of the three annotated transcripts are predicted to encode intracellular protein products with only one polypeptide being secreted (*17*). The Mmp2 antibody displays nuclear immunoreactivity that is reduced by peptide blocking and in *mmp2* LOF mutants, raising the possibility of intracellular Mmp2 functions (Fig. 24). However, antibodies produced in rabbit notoriously cross-react with an unidentified nuclear protein in *Drosophila* and warrant stringent follow-up studies. In the wing disc, both Mmp1 and Mmp2 appear to be regulated at the level of secretion/localization by cGMP production (*22*). At the NMJ, neural activity increases presynaptic cGMP synthesis which is coupled to synaptic vesicle exocytosis (*23*). The GMP signaling response (minutes) is dictated by the duration of neural stimulation (seconds) and could provide a biochemical signature instructing activity-dependent Mmp regulation (*23*). During *Drosophila* ovulation in mature follicles, steroid and octopaminergic signaling upregulate Mmp2 proteolytic activity, in the absence of detectable changes in Mmp2 expression (*24*–*26*). Therefore, like Mmp1, Mmp2 is likely spatially restricted and temporally regulated by many mechanisms.

Timp has just one annotated transcript encoding a single polypeptide (*27*). Similar to mammalian TIMP-2, *Drosophila* Timp has been identified as a direct transcriptional target of the co-activator Yorkie (*28*). Interestingly, Mmp1 and Mmp2 both display abnormal spatial distributions in *timp* LOF ovaries, suggesting Timp localizes Mmps (*29*). In my studies, Mmp2 spatially restricts the pericellular distribution of Timp at the NMJ (Fig. 12). Mmp2 similarly restricts the Dlp spatial domain at the NMJ (Fig. 14), raising the possibility that Timp localization could be regulated by HSPGs, as is the case for mammalian TIMP-3 (*30*). Secreted Mmps or Mmp-HSPG interactions might ferry Timp to the appropriate pericellular location. Conversely, Timp overexpression reduces Mmp1, and to a lesser extent Mmp2 (Fig. 12 and Table S3). However, Mmp1 appears "trapped" or enriched in axons or glia and Western blot analyses show an increase in total Mmp1 levels in the Timp overexpression condition (Figs. 12 and 25). I also analyzed Mmp1 using a monoclonal antibody raised against the hemopexin domain (Mmp1-hpx) (*17*, *31*), and similarly found synaptic Mmp1 severely reduced by Timp overexpression, but increased in axons (Fig. 25). Perhaps Mmp1 and Timp are co-secreted and overexpression somehow disrupts trafficking to NMJ terminals or turnover kinetics. Alternatively, Timp might promote Mmp1 internalization, compartmentalization or pericellular redistribution. Unfortunately, little is known regarding Mmp or Timp secretion and trafficking in *Drosophila*. Plasma membrane overgrowth causes ECM aggregation which triggers an immune response leading to Mmp upregulation (*32*). Our findings have yet to reveal any obvious differences in plasma membrane or ECM metabolism at the synapse, but we have not assayed more proximal axons or the nerve-glia interface.

Developing isoform specific tools and more sensitive live-imaging tools will greatly aid our understanding of specific Mmp functions and Mmp trafficking regulation in real-time. Employing *in situ* proximity ligation assays (PLA) would enable sensitive and specific visualization of protein-protein interactions occurring between Mmp1, Mmp2 and Timp (Fig. 26) (*33*). Utilizing antibody-based approaches that permit *in vivo* targeting and tracking of antigens (Mmps/Timp) with fluorescent nanobodies could shed light on Mmp/Timp dynamics at the synapse (*34*, *35*). A nanobody is derived from the smallest antigen-binding domain (V_HH) of single-domain antibodies produced by camelids (*34*). Nanobodies fused to a fluorescent protein function as biosensors which could be exogenously introduced or expressed as a transgene (*35*, *36*). Moreover, targeting nanobodies against specific Mmp or Timp domains could reveal functional domain requirements and offer a way to acutely inhibit proteolysis. Other mechanisms of extracellular Mmp regulation are discussed in the following sections.

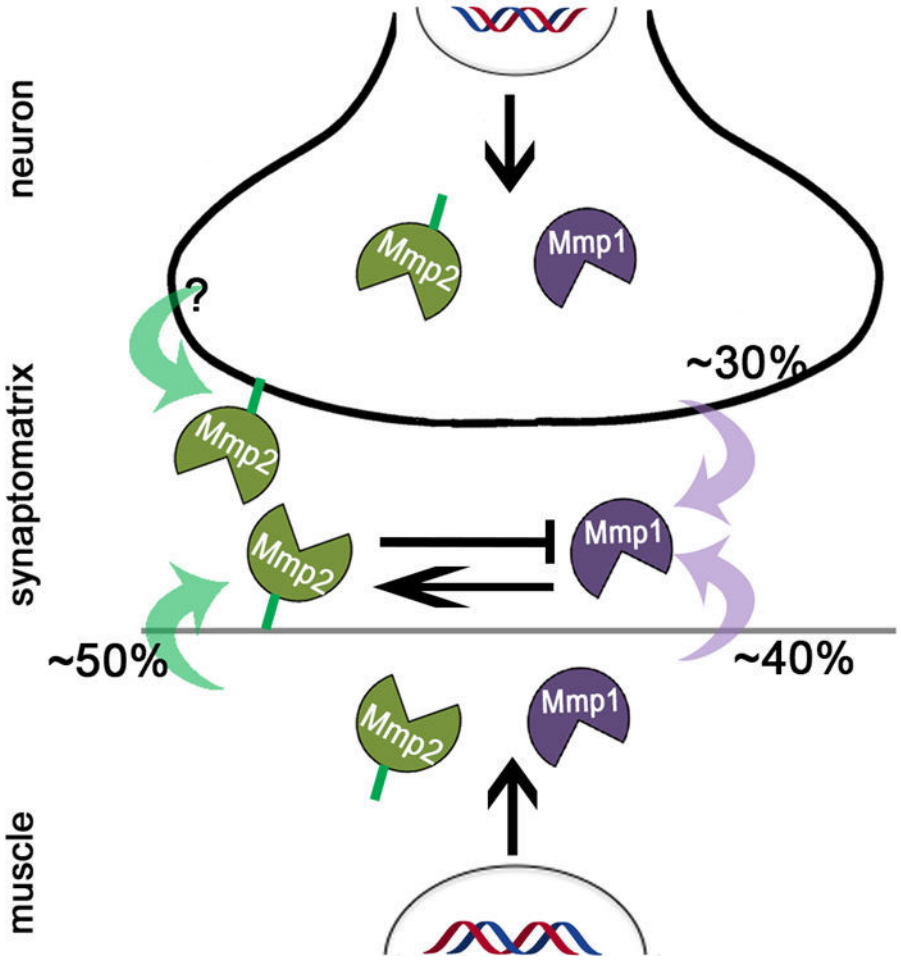

Figure 23

Figure 23: Synaptic Mmps are expressed by both neuron and muscle. Cell-type specific Mmp expression based on confocal imaging quantification of anti-Mmp fluorescence intensity following tissue-specific RNAi knockdown. Mmp1 is derived from both muscle and neuron. Mmp2 levels are reduced following postsynaptic *mmp2*^{RNAi} knockdown. However, presynaptic *mmp2*^{RNAi} knockdown has not yet been evaluated. Note also that glial-knockdown has not yet been performed for either Mmp. See Table S3 for raw values.

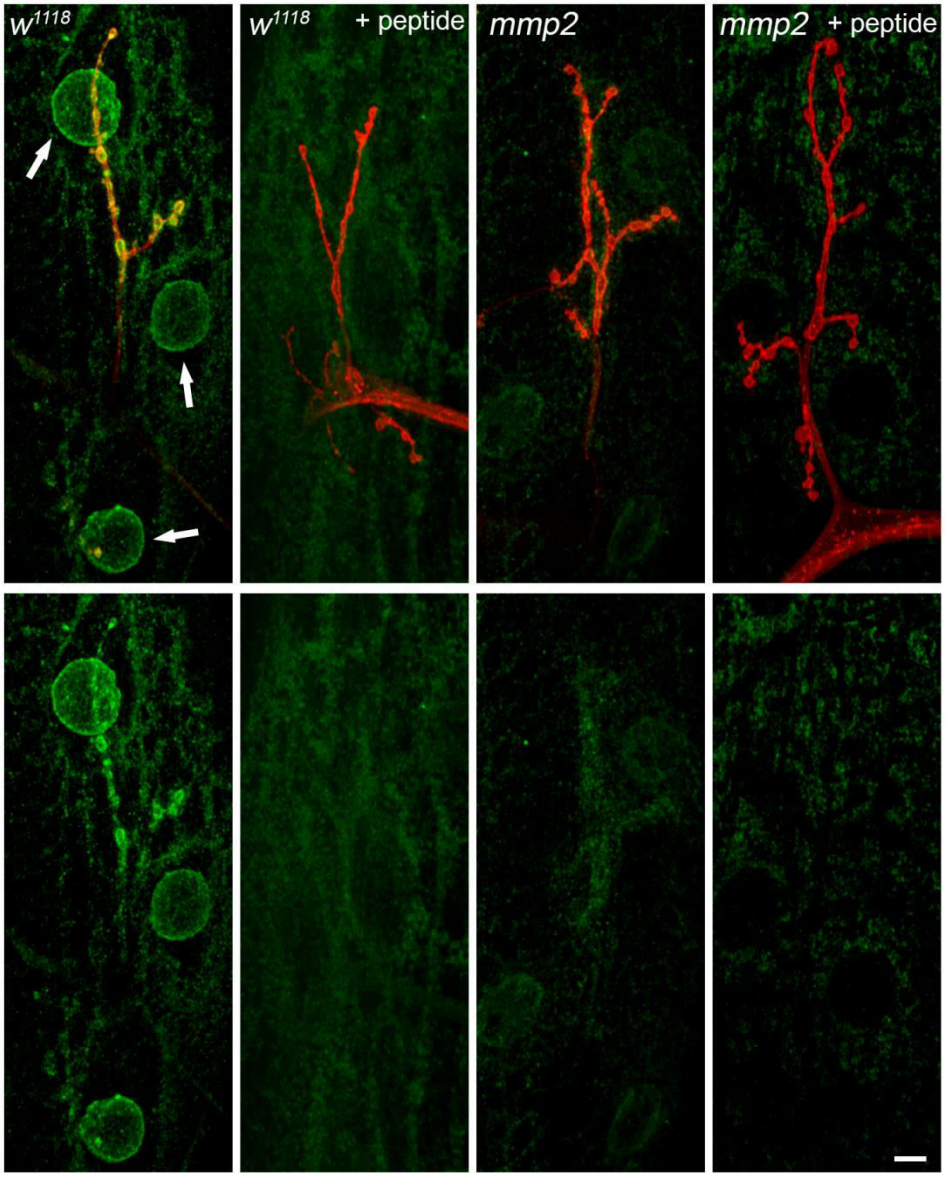

Figure 24

Figure 24: Mmp2 localizes to postsynaptic muscle nuclei. Images of NMJs (HRP, red) from the denoted genotypes labeled with non-affinity purified Mmp2 antibody (#446, green) that was pre-treated with or without Mmp2 peptide ("peptide blocking"). In w^{1118} control NMJs, Mmp2 is clearly visible at the NMJ as well as surrounding the muscle nuclei (white arrows). Synaptic and nuclear Mmp2 intensity is reduced by peptide blocking in controls (w^{1118}), in $mmp2^{W307*}$ mutants, and by peptide blocking in $mmp2^{W307*}$ mutant conditions. Scale bar is 10 μm. Similar results are obtained with $mmp2^{ss218/Df}$ (data not shown).

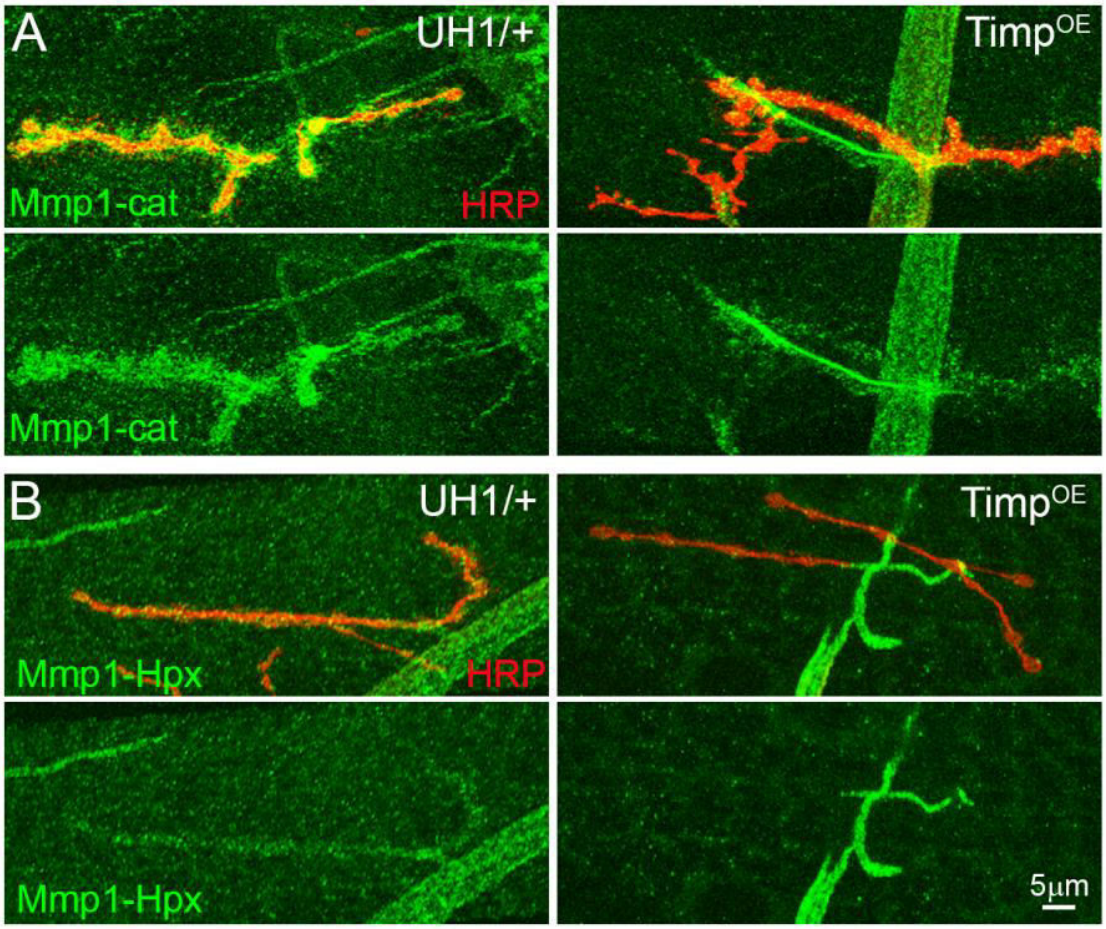

Figure 25

Figure 25: Mmp1 is abnormally sequestered at NMJs overexpressing Timp. (A) Representative NMJ images co-labeled with neuronal marker (HRP, red) and an anti-Mmp1 cocktail of antibodies targeting the catalytic domain (Mmp1-cat, green) in driver control (UH1-Gal4/+) compared to ubiquitous Timp overexpression (UH1-Gal4>UAS-Timp). (B) Representative NMJ images co-labeled with neuronal marker (HRP, red) and an anti-Mmp1 targeting the hemopexin domain (Mmp1-Hpx, green) in driver control (UH1-Gal4/+) compared to ubiquitous Timp overexpression (UH1-Gal4>UAS-Timp).

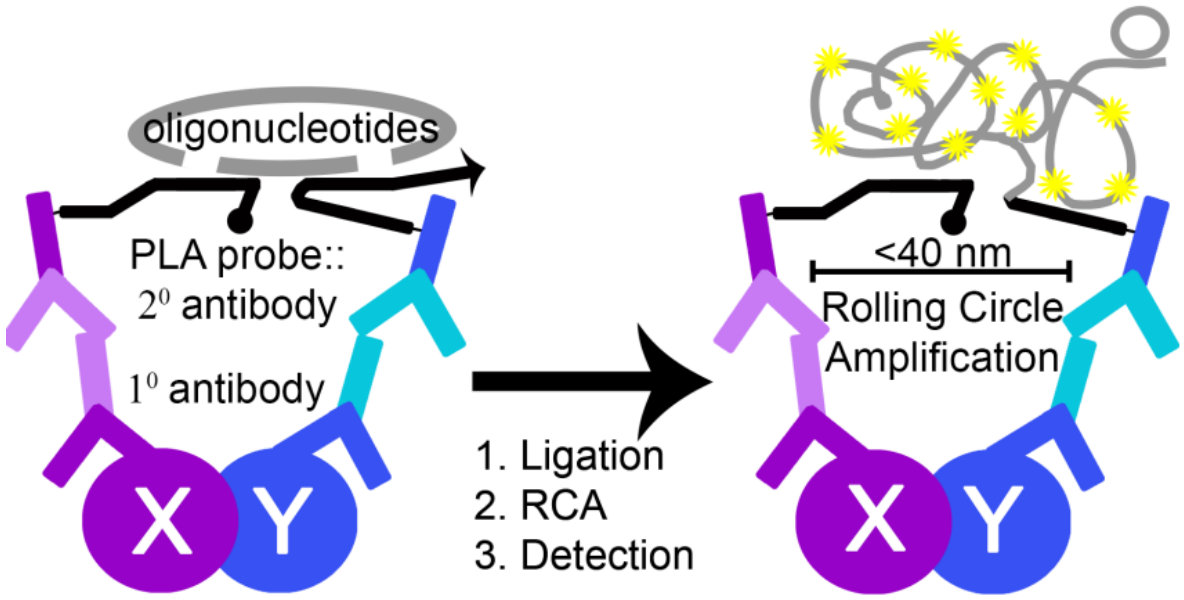

Figure 26

Figure 26: Proximity ligation assay (PLA) detects protein-protein interactions. Cartoon schematic illustrates the principle of proximity ligation assay (PLA) technology to detect protein-protein interactions. NMJ preparations are incubated with specific primary antibodies that bind protein X (purple) and protein Y (blue). Secondary antibodies conjugated to oligonucleotide proximity probes bind their respective primary antibody and are ligated to two additional DNA connector oligonucleotides forming a circular DNA strand if in close proximity (<40 nm). One of the proximity probes serves as a primer for the rolling circle amplification (RCA). The DNA circle is amplified by polymerase chain reaction with the amplification product remaining covalently bound to one of the proximity probes. The amplification product is detected with fluorescently labelled oligonucleotides and visualized using confocal microscopy.

Mmp Regulation of Presynaptic and Postsynaptic Molecular Machinery

My work shows a complex relationship between Mmp function and GluR regulation (Chapter II and Table S2). The *mmp1* mutants display significant increases in GluRIIA and GluRIIB. In contrast, *mmp2* mutants have reduced GluRIIA and extrasynaptic GluRIIB in muscles is observed far away from the synapse, suggesting Mmp2 might regulate B-type GluR mobility (Fig. 28). These interactions may be due to direct Mmp activities influencing GluR stability/mobility, or perhaps indirect differential modulation of diverse signaling pathways. What types of pathways could Mmp functions intersect with to regulate GluRs? Glia-derived Wg signaling regulates GluRIIA, and glial-knockdown of Mmp1 results in bouton overgrowth, raising the possibility that Mmp1 secreted from glia might control postsynaptic GluR levels through Wg signaling (Fig. 27) (*37*). Future studies should investigate how glial-Mmp activities play a role regulating synaptogenesis and modulating the *trans*-synaptic signaling pathways that drive this developmental process. Studies should include glia-specific RNAi and temporally-restricted UAS-mmp expression to overcome Mmp overexpression lethality concerns. GluRs are localized to the synapse through interactions with scaffolding proteins such as DLG and LGL (*38*, *39*). DLG loss increases GluR field sizes (*39*–*41*), and both *mmp* mutants display reduced DLG domains (Fig. 29). DLG and LGL scaffolds bind and recruit multiple interacting partners to the synapse, raising the possibility that scaffolds could be disrupted in *mmp* mutants (*38*). It has been proposed that FMRP may form a complex with DLG and LGL that specifically regulates B-type receptors and FMRP loss strongly impacts GluRIIA/B expression (*38*, *42*, *43*). Other signaling pathways that I did not investigate also contribute to GluR regulation at the NMJ. Loss of Dorsal/Cactus signaling is highly reminiscent of observed functional and GluRIIA synaptic phenotypes characterized by loss of Mmp2 (*44*, *45*). Dorsal domain-specific perturbations reveal bidirectional GluRIIA phenotypes: one domain promotes GluRIIA intensity whilst another domain restricts GluRIIA intensity (*45*). Perhaps extrasynaptic GluRIIB mislocalization is a secondary consequence. At the NMJ, GPI-anchored Mmp2 is well positioned to regulate TNF-α mediated signaling and/or Wnt inhibition and these neural mechanisms are likely similar to those observed in mammals (*45*). TNF-α – NFκB/Dorsal and IκB/Cactus and Pelle kinase mediate non-canonical Dorsal signaling in muscle helping to direct GluR density and mobility (*45*). WntD/8 functions as a secreted feedback inhibitor of Toll signaling, and Toll pathway components regulate NMJ structure and GluR delivery and density (*45*–*49*). It is tempting to speculate a role for WntD/8 as it is a known feedback inhibitor of Dorsal (*46*). However, WntD/8 functions at the NMJ remain to be shown, and this non-canonical signaling pathway may not intersect with WntD/8.

On the presynaptic side, loss of Mmp function results in reduced overall presynaptic active zone (AZ) abundance, as measured by anti-Brp labeling, but increased AZ density (*44*). These phenotypes are reminiscent of Wnt2 LOF defects at the *Drosophila* NMJ (*50*) as well as loss of Dlp (*51*), raising the possibility that Mmps, Wnt 2 and Dlp could intersect in presynaptic pathways. Defects in signaling cause changes in cytoskeletal elements that regulate synaptic machinery (*52*–*57*). These include the adapter protein Ankyrin, which is recruited to the NMJ via β-spectrin and instructs Wg signaling activity (*53*, *57*), as well as cell polarity scaffolds, such as DLG and LGL, and components that organize the spectrin network such as the Par complex (*38*, *39*, *58*–*60*). Disrupting polarity genes can result in JNK signaling activation and subsequent Mmp1 upregulation (*18*). Moreover, FMRP is a strong regulator of cytoskeletal machinery at the NMJ (*42*). Future studies should investigate any changes in the actin and microtubule cytoskeletal networks in *mmp* mutants to determine if such defects could influence synaptic machinery in the absence of Mmp function.

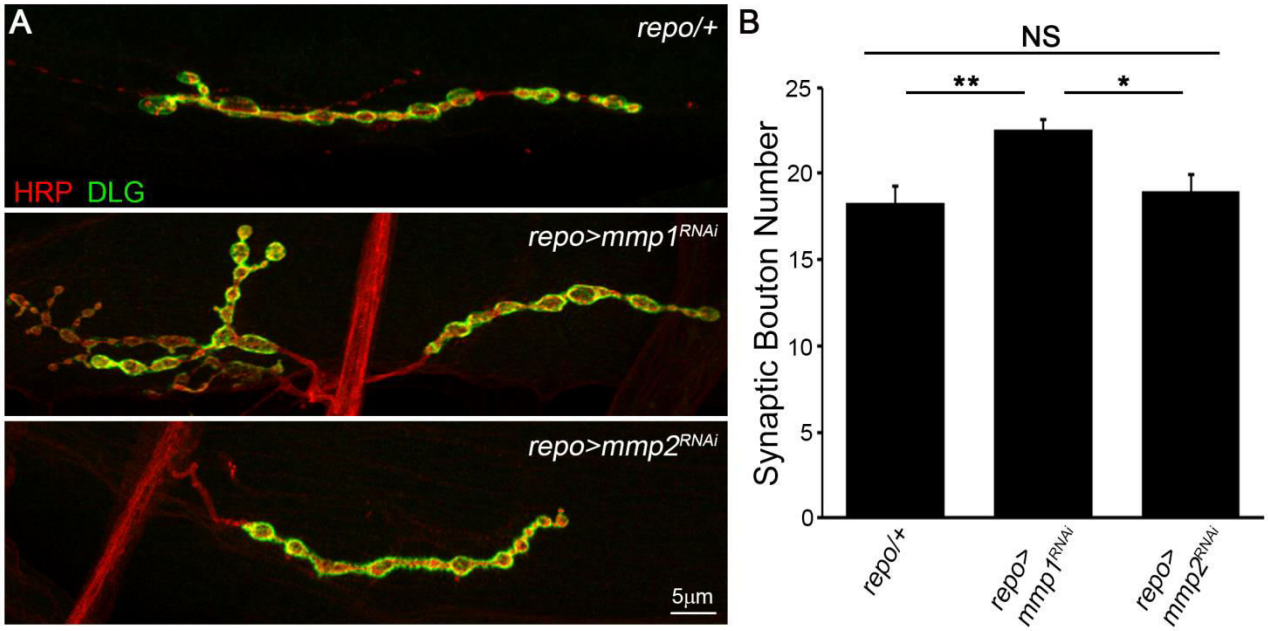

Figure 27

Figure 27: Glia-derived Mmp1 restricts NMJ growth. (A) Representative NMJ images co-labeled with presynaptic marker anti-HRP (red) and postsynaptic marker anti-Discs-large (DLG, green) in glia-driver control (*repo*-Gal4 crossed to w^{1118}) compared to Mmp knock-down in glia. Middle: *repo*-Gal4>UAS-$mmp1^{RNAi}$ and bottom: *repo*-Gal4>UAS-$mmp2^{RNAi}$. (B) Quantified bouton number from genotypes in (A) normalized to driver control. Sample size is ≥ 10 NMJs per genotype. Significance determined by one-way ANOVA indicated by *p<0.05, **p<0.01 and not significant (NS).

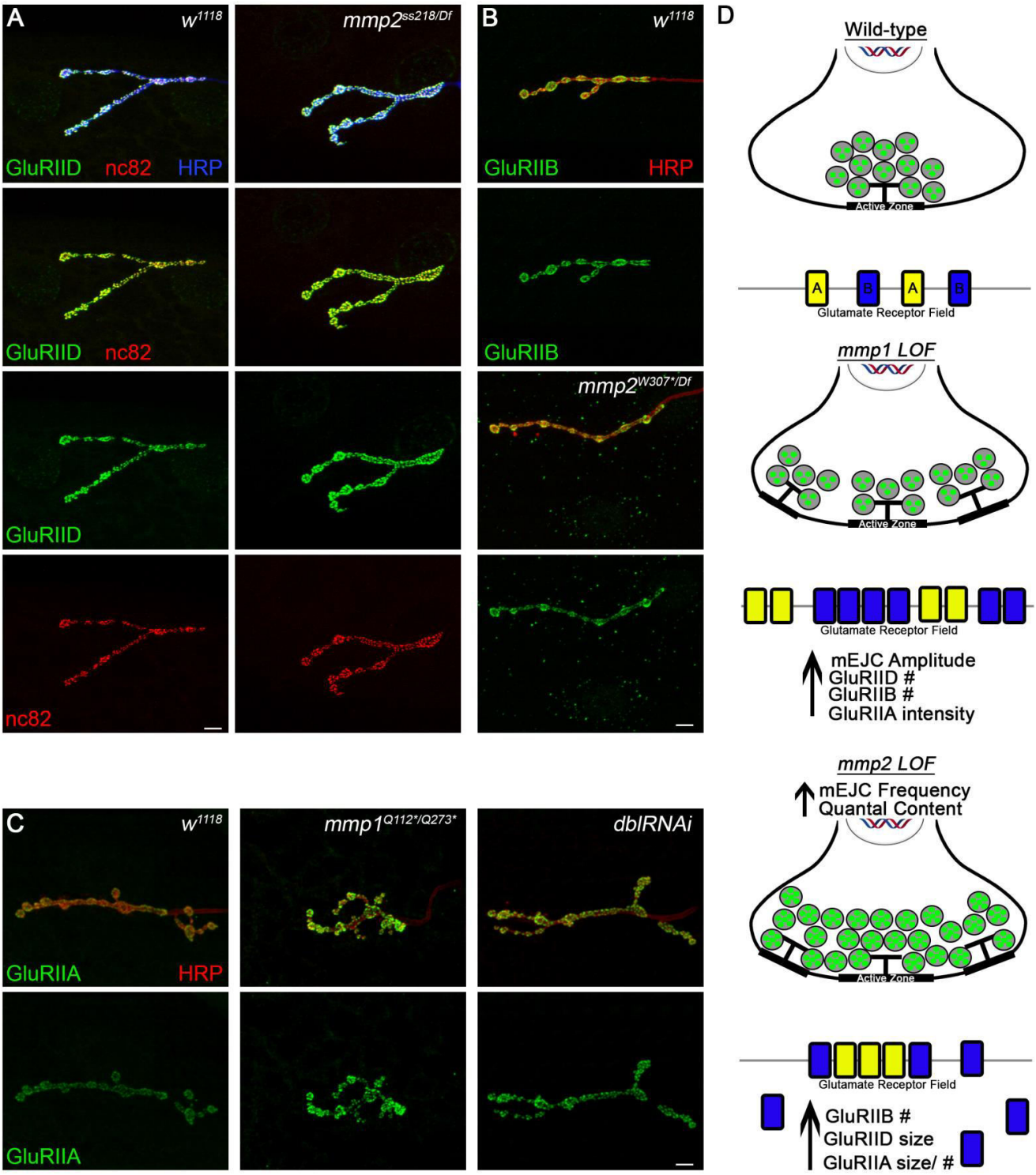

Figure 28

Figure 28: Mmps differentially regulate GluRs at the NMJ. (A) Representative NMJ images co-labeled with neuronal marker HRP (blue), presynaptic active zone marker anti-Bruchpilot (Brp, red) and postsynaptic, obligate glutamate receptor subunit anti-GluRIID (GluRIID, green) in control (w^{1118}) compared to $mmp2^{ss218/Df}$ genetic null. (B) Representative NMJ images co-labeled with neuronal marker HRP (red) and postsynaptic B-type glutamate receptor subunit anti-GluRIIB (GluRIIB, green) in control (w^{1118}) compared to $mmp2^{W307*/Df}$ genetic nulls. (C) Representative NMJ images co-labeled with neuronal marker HRP (red) and postsynaptic A-type glutamate receptor subunit anti-GluRIIA (GluRIIA, green) in control (w^{1118}) compared to $mmp1^{Q112*/Q273*}$ and ubiquitous double mmp1+2RNAi knock-down (dblRNAi). (D) Cartoon schematics illustrating synaptic machinery defects in *mmp* mutants (Chapter II). See table S2 for raw data values.

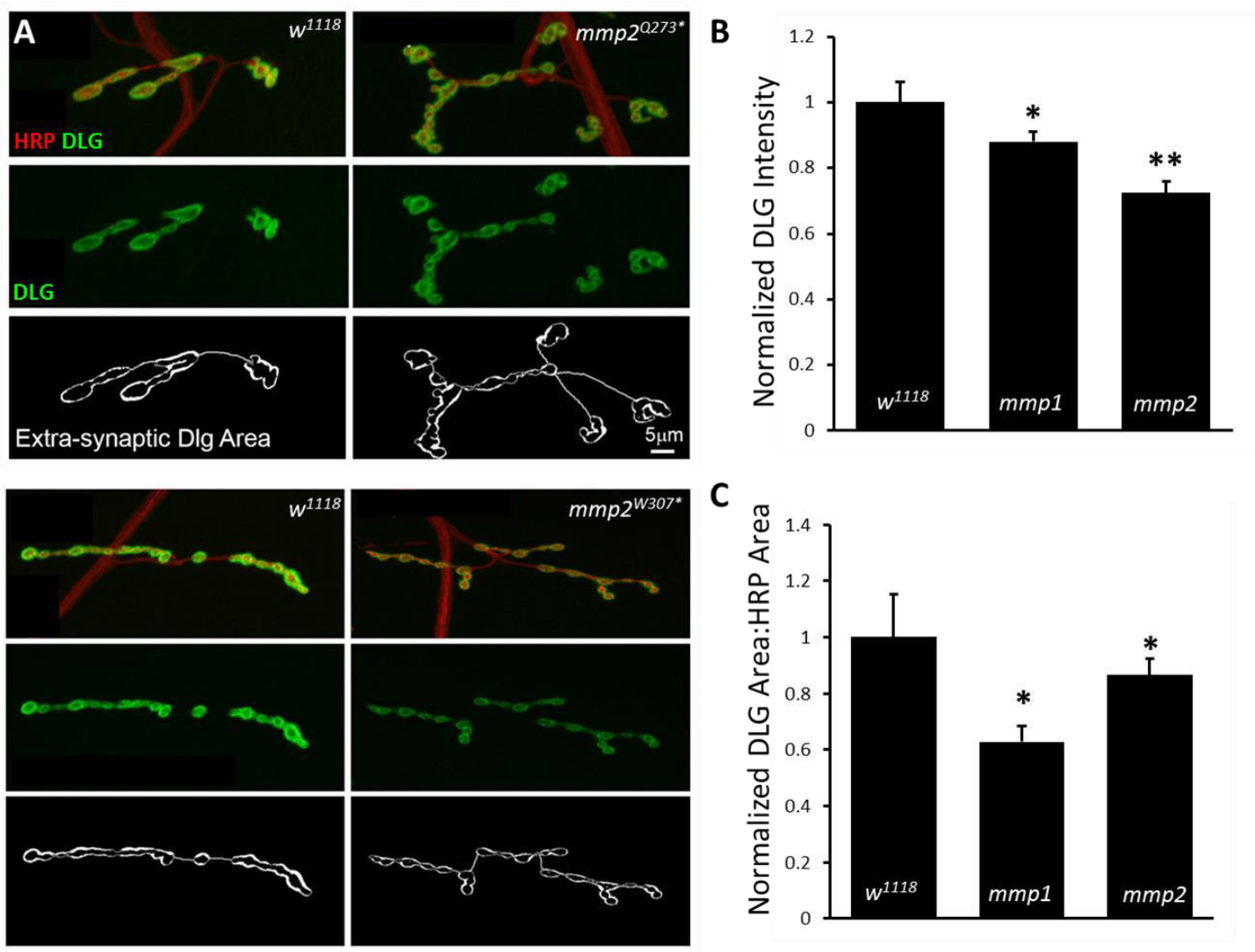

Figure 29

Figure 29: Mmp1 and Mmp2 promote DLG at the NMJ. (A) Representative NMJ images co-labeled with presynaptic marker anti-HRP (red) and postsynaptic marker anti-Discs-large (DLG, green) control (w^{1118}) compared to $mmp1^{Q273*}$ hypomorphs (top) and $mmp2^{W307*}$ genetic nulls (bottom). (B) Quantified DLG intensity from genotypes in (A) normalized to control. (C) Quantified DLG area: HRP area from genotypes in (A) normalized to control. Sample size is ≥ 10 NMJs per genotype. Significance determined by one-way ANOVA indicated by *p<0.05 and **p<0.01.

Heparan Sulfate and Wingless Regulation of Mmp1

My studies focused on extracellular mechanisms regulating Mmp1. I found HSPG Dlp is a potent, positive regulator of Mmp1 (Fig. 19). Dlp promotes extracellular Mmp1 localization at the NMJ, co-localizing with Mmp1 in a mechanism that requires HS GAG chains. This co-localization study was followed up with biochemical assays to test the predicted interaction. First, I treated NMJs with heparanase to enzymatically digest HS-GAG chains (*61*, *62*), and then visualized Mmp1 expression. Consistent with the prediction that Mmp1 would be reduced following heparanase treatment, extracellular Mmp1 signal intensity is significantly decreased compared to mock treated NMJ controls (Fig. 30). Using a similar paradigm, extracellular Wg abundance is reported to decrease following heparanase treatment while total Wg levels remain unchanged, suggesting HS-GAG chains restrict Wg internalization (*62*). In collaboration with Dr. Kay Grobe's laboratory (University of Munster, Germany, Institute for Physiological Chemistry & Pathobiochemistry), we next tested this interaction by employing an HS-Mmp1 binding assay (Figs. 31). HS was purified from *Drosophila* and coupled to an NHS-activated Sepharose column (*63*). Mmp proteins were obtained from the media of *Drosophila* S2 cells co-transfected with wild-type *UAS-Mmp* plasmids and *actin*-Gal4 (*actin*-Gal4>*UAS-Mmp1.F1* or *actin*-Gal4>*UAS-Mmp2*, kind gifts from Dr. Andrea Page-McCaw, Vanderbilt University, Cell and Developmental Biology). Mmp proteins were then applied to the column, washed and bound material was eluted with a linear NaCl gradient (0 to 1.5M in 0.1M sodium acetate buffer, pH 6.0) (*63*). Fractions were TCA-precipitated, resolved by SDS-PAGE, and immunoblotted with Mmp1-catalytic or Mmp2 antibodies (*17*, *44*). Mmp1 immunoreactivity is only detected in elution lanes, confirming a functional and direct Mmp1-HS interaction (Figs. 31). Conversely, Mmp2 does not appear to bind HS under these conditions (data not shown). Collectively, the co-localization assay (Chapter III), Mmp1 immunohistochemistry in the *dlp* genetic manipulations (Chapter III) and following heparanase treatment (Fig. 30), and the HS binding assay (Fig. 31) suggest that Mmp1 interacts with Dlp via HS GAG chains. In *mmp2* mutants, both Dlp and Mmp1 are upregulated at the NMJ and Dlp is a known Mmp2 substrate (Chapter II) (*64*). Reducing Dlp levels in the *mmp2* mutant background mostly suppressed NMJ overgrowth and neurotransmission phenotypes (Chapter II). I speculate that the Dlp increase is due to loss of proteolysis by Mmp2 and my model predicts this would cause the Mmp1 increase. Future studies should examine if Mmp1 levels are indeed lowered by restoring Dlp levels and if elevated Mmp1 abundance contributes to structural or functional synaptogenic defects observed in *mmp2* mutants. Interestingly, removing a single copy of *mmp1* in the *mmp2* homozygous mutant background does indeed suppress NMJ overgrowth (Chapter II). What is the functional relevance of the Mmp1-HSPG

interaction? More generally, HSPGs have known roles regulating protease expression, localization and function (*65–68*). As a GPI-anchored glypican, Dlp can interact with receptors, ligands, inhibitors, growth factors or cell adhesion molecules and may bring Mmp1 substrates in close proximity (Fig. 32). This interaction could be necessary to localize or stabilize Mmp1 activity, orient substrates for Mmp1-mediated proteolysis, or bridge some type of Mmp1-complex (Fig. 32). Mmp1 is secreted from both neuron and muscle; perhaps this interaction reflects a tissue-specific regulatory mechanism confining proteolysis to one side of the synapse. Co-localization analyses show that Dlp and Mmp1 appear to interact within a dynamic subset of boutons (Chapter III). What regulates this type of spatial specificity? Are Dlp and Mmp1 co-secreted or does this interaction occur independently in the synaptomatrix? Future approaches detailed in 'perspectives and future directions' could certainly be applied here to shed light on these questions. Does this interaction rely on GAG sulfation or some other particular GAG signature? This could be addressed by genetically manipulating enzymes in the HS-biosynthesis pathway with the caveat that all HSPGs would be modified (*69*). Alternatively, fractionated HS derived from *Drosophila*, synthetic oligosaccharides, and Mmp1 domain-bashing could be used to further interrogate Mmp1-HS binding requirements (*70*). Identifying and characterizing the specific molecular requirement is important to pursue GAG mimetics as a possible therapeutic strategy.

Dlp, Mmp1 and Wg are all interconnected with bidirectional regulation of Dlp and Mmp1 identified (*71*). I also find that Mmp1 promotes extracellular Wg ligand abundance but restricts Wg signal transduction (Chapter II) (*44*). Proposed transcriptional regulators of Mmp1 include C-terminal binding protein, Clock and Wg (*72–74*). This suggests that Wg might reciprocally regulate Mmp1 expression. Indeed, I find that Mmp1 is strongly upregulated at NMJs over-expressing Wg, suggesting that Wg activity promotes Mmp1 expression (Fig. 33). This raises the possibility that Mmp1 could be part of a Wg signaling feedback loop. In a negative feedback loop, Wg-induced Mmp1 upregulation might compete with Wg-receptor or co-receptor binding necessary for signal activation. Alternatively, Mmp1 induction might promote Wg signaling by activating factors that enhance signaling, dictate signaling directionality, or by inactivating Wg-inhibitors or other Wnt ligands. This also highlights that Mmp1, Dlp and Wg are interconnected through multiple nodes which contribute to FXS synaptogenic defects. Mmp2 similarly restricts Wg signal transduction and Mmp2 transcription is regulated by Eyeless, Dpp, Proneural, FGF signaling (possibly via dpERK), Cut, Sine oculis and Pumilio (*75–81*). Interestingly, the transcription factor Cut functions to restrict Mmp2 expression and Wg is a known regulator of Cut (*79*). Thus, increased Wg activity observed in either *mmp* single mutant condition could contribute to the identified co-regulated expression of Mmp1 and Mmp2. Future experiments should test if Mmp2 abundance is altered in Wg LOF or GOF studies and if reducing Wg in the *mmp2* mutant

background is sufficient to correct elevated Mmp1 levels. Moreover, both Wg and Dlp are sufficient to promote synaptic Mmp1 levels (Fig. 33 and Chapter III), raising the possibility that a Dlp-dependent Wg-Mmp1 interaction may instruct activity-dependent bouton formation. All of these molecular players are at least in part inter-dependent, and also each disrupted in the FXS disease state, which could therefore collectively impede the activity-induced Mmp1 enhancement that is lost in the FXS condition.

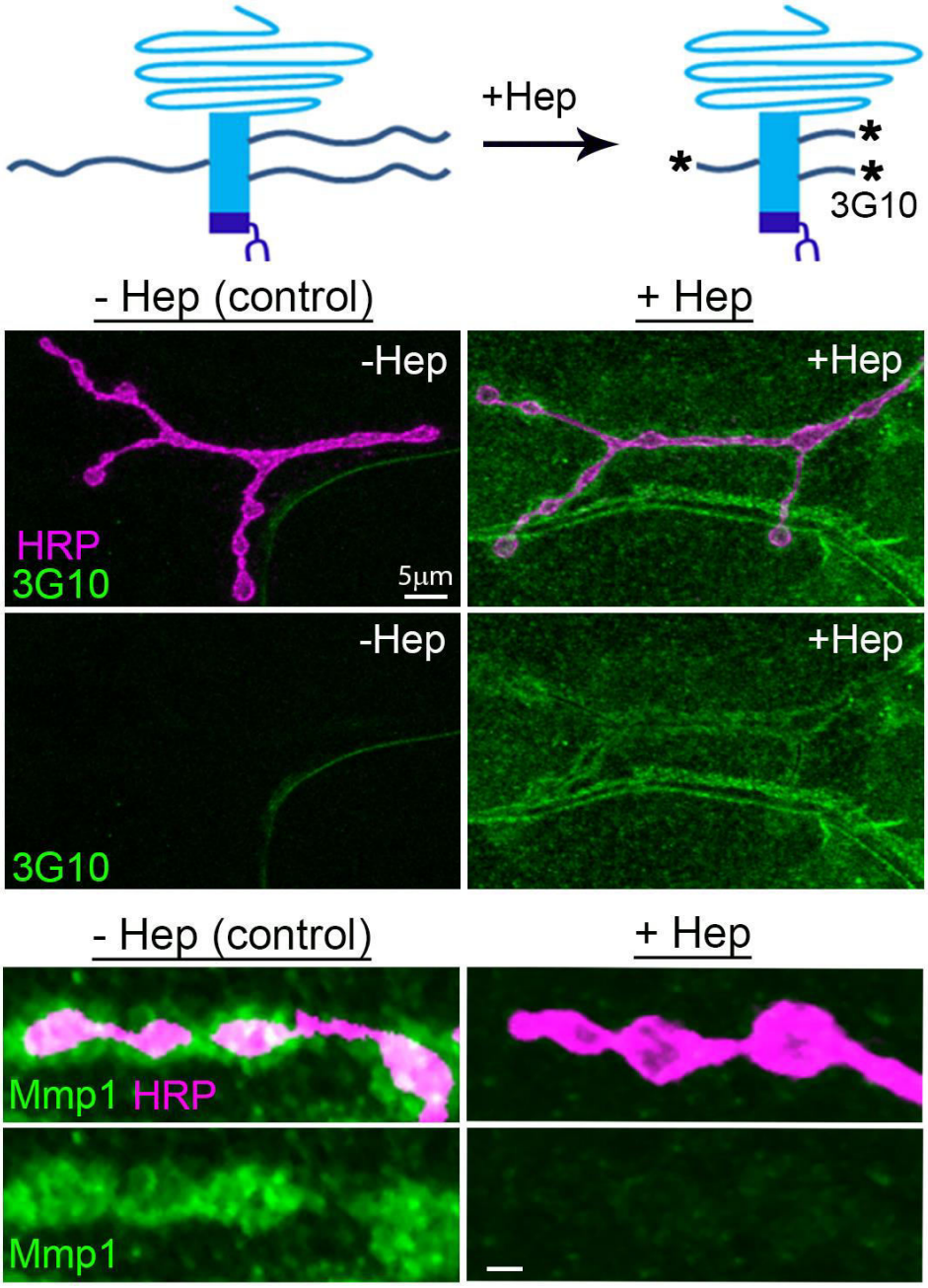

Figure 30

Figure 30: Reduced extracellular Mmp1 following Heparan Sulfate enzymatic digestion. Top: Cartoon schematic showing heparitinase (Hep) treatment enzymatically digests heparan sulfate (HS) of Dlp glypican (blue) and other HSPGs (not shown) exposing a new epitope (*) detected by 3G10 antibody. Middle: Positive control showing successful HS digestion which enables 3G10 antibody detection. NMJs were treated for 1 hour with (+ Hep) or without (- Hep) heparitinase in the presence of calcium according to manufacturer's instructions (Sigma) and fixed samples were co-labeled with synaptic marker (HRP, magenta) and anti-3G10 (green). Bottom: Representative images of NMJs processed as in (middle) and co-labeled with synaptic marker (HRP, magenta) and anti-Mmp1 targeting the catalytic domain (green). Images reflect representative results from two independent experiments.

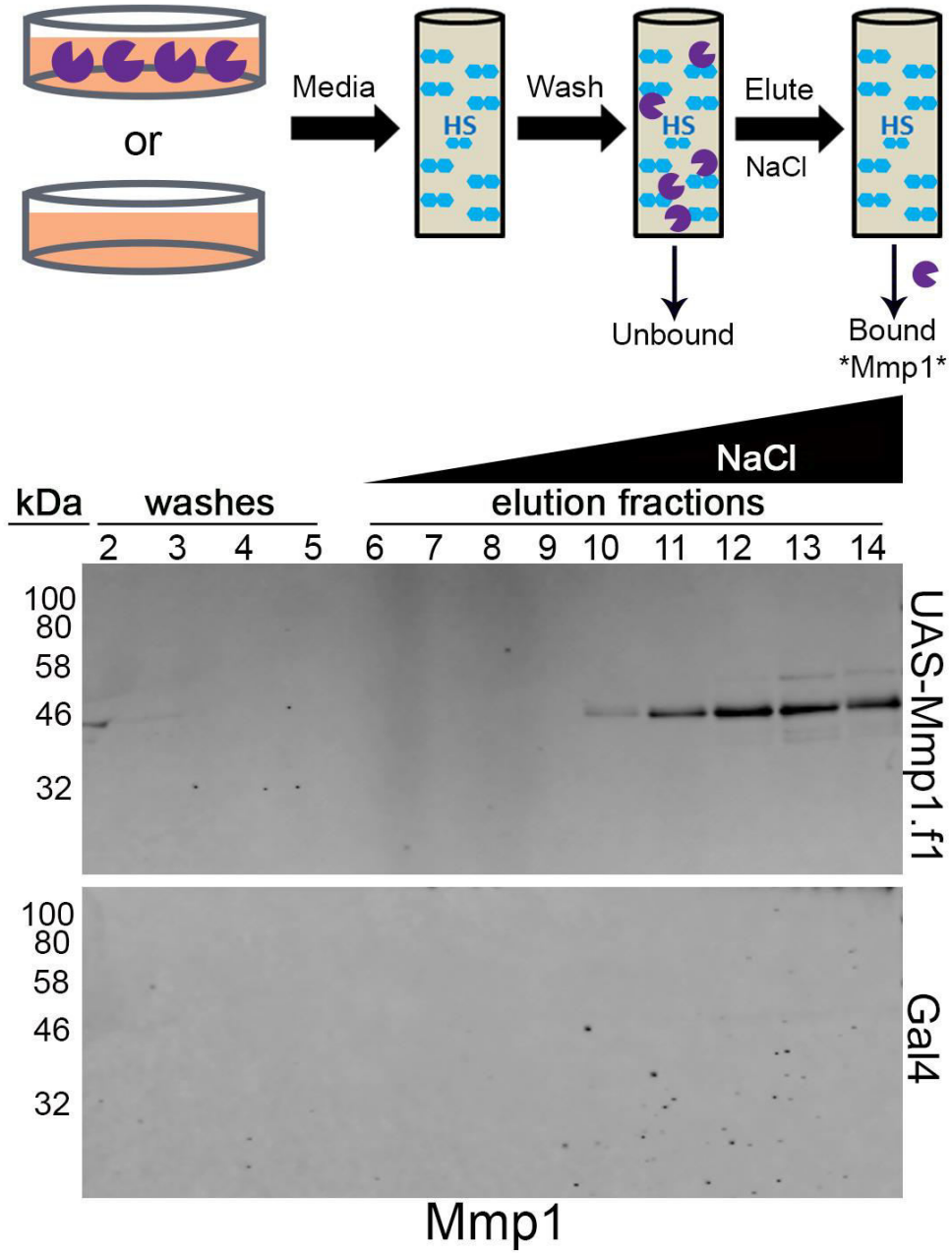

Figure 31

Figure 31: Mmp1 directly binds Heparan Sulfate. Top: Cartoon schematic illustrating the heparan sulfate (HS) binding assay. See text for complete description. In brief, Mmp1 (purple) was expressed in *Drosophila* S2 cells (peach petri dishes) and incubated with HS-conjugated (blue hexagons) to a Sepharose column. Unbound material was washed and bound material was eluted with NaCl. Bottom: Western blot analyses of fractions obtained from controls (actin-Gal4 alone) or actin-Gal4>UAS-Mmp1.f1 expressing cell culture media following HS-binding assay and immunoblotted for Mmp1 (anti-Mmp1 targeting the catalytic domain). Wash fractions (lanes 2-5) represent unbound material and elution fractions (lanes 6-14) represent bound material that was competed off the column by increasing NaCl gradient. Lanes 1 and 15 are molecular weight markers cropped out of the images.

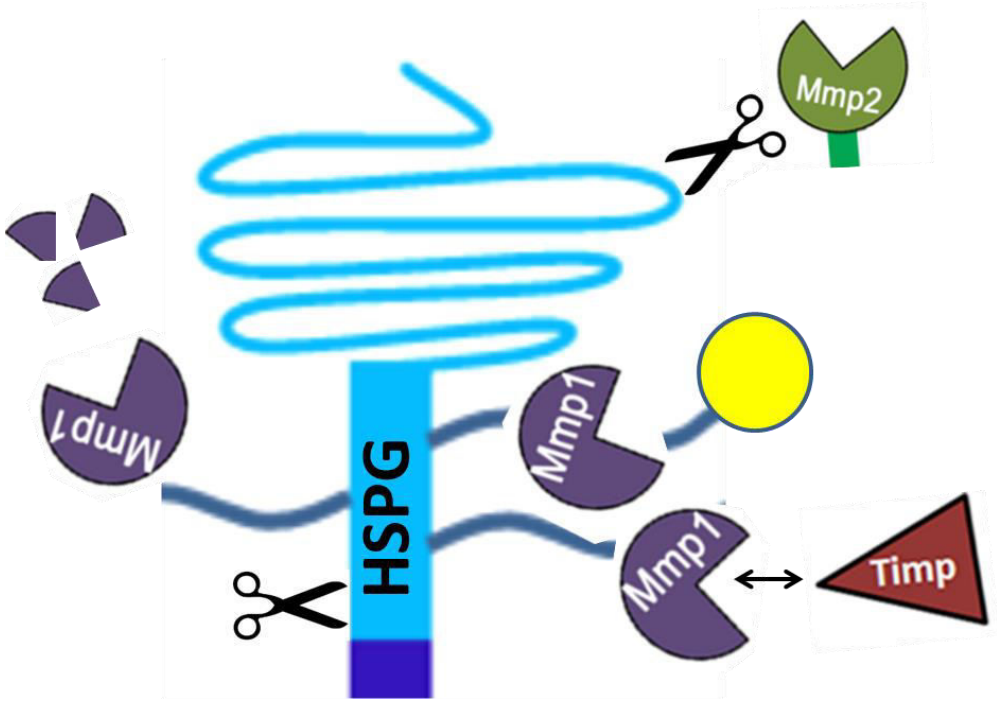

Figure 32

Figure 32: Possible functions of Mmp-HSPG interactions. Schematic illustrating possible functions of Mmp-HSPG interactions. Mmp2 (green) cleaves Dlp core protein to modulate Wnt/Wg signaling (*64*). HS GAG chains could alter Mmp-Timp inhibition (red), bring Mmp1 in close proximity to substrates (yellow), sequester Mmp1 (purple) or protect Mmp1 and/or other ligands (yellow) from degradation.

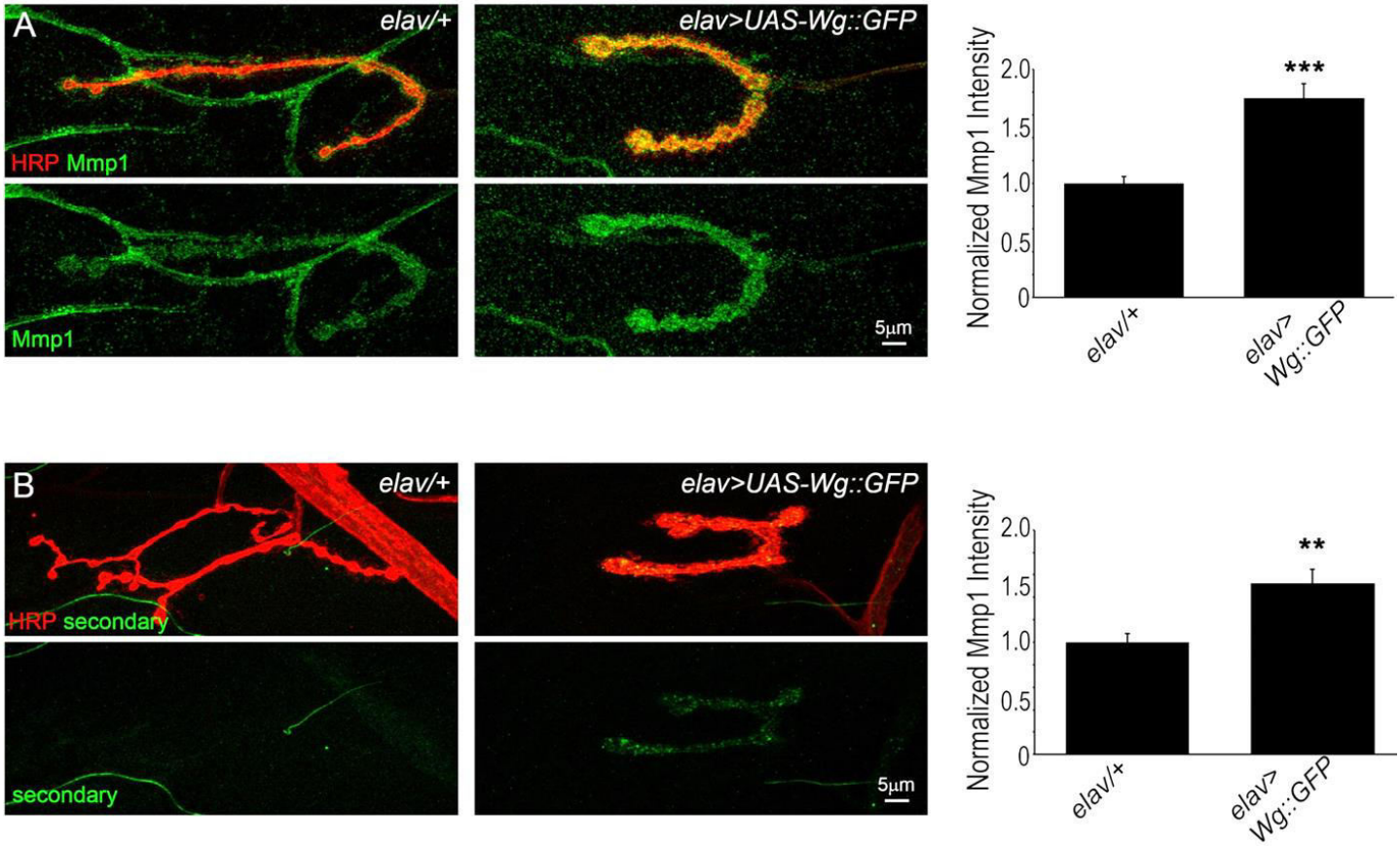

Figure 33

Figure 33: Wg promotes Mmp1 at the NMJ. (A) Confocal images of Mmp1 (green) at NMJs (red, HRP) in control (*elav*-GAL4/+) and presynaptic Wg overexpression conditions (*elav*-GAL4>UAS-*Wg::GFP*). Quantification of Mmp1 levels normalized to driver control. (B) Secondary-only labeling to control for Wg::GFP detection. The average signal intensity from (B) for controls (*elav*-GAL4/+) and presynaptic Wg overexpression (*elav*-GAL4>UAS-*Wg::GFP*) were subtracted from values obtained in (A) and normalized to the driver control condition. Significance was determined by nonparametric Mann-Whitney U-tests, and indicated by *p<0.05 and **p<0.01. Data show mean ± SEM from at least 2 independent replicates for each experiment, N>10, with N representing NMJ number.

Mmps and Activity-dependent Synaptogenesis

I found that Mmp1 is required for rapid synapse development in response to activity (*82*, *83*), with synaptic Mmp1 strongly upregulated by acute stimulation (Figs. 16 and 17). In mammals, low MMP levels are often upregulated in response to heightened activity (*84–88*), suggesting a conserved activity-dependent mechanism. Mammalian MMP levels can be upregulated by regular usage, such as Morris water maze training (*89*), with both temporal- and region-specific contributions to synaptogenesis (*90*, *91*). For example, mammalian MMP-9 is induced by glutamatergic signaling and seizure activity (*85*, *92*, *93*), with several studies showing MMP-9 is a critical regulator of activity-dependent synaptic remodeling (*84*, *94–97*). I found *Drosophila* Mmp1 restricts synaptic growth over developmental time, with *mmp1* null mutants making more, smaller boutons in expanded synaptic terminals (Fig. 9) (*44*). Mmp1 is also required to enable new bouton formation in response to acute activity (Fig. 16) (*71*). These distinct temporal requirements show different Mmp1-dependent pathways control developmental versus activity-dependent NMJ bouton formation.

Some studies induce ghost bouton formation using pulsed activity interspersed with rest intervals (*82*, *98*, *99*). This spaced paradigm is relatively mild compared to persistent stimulation. A recent study proposed that differences in synaptic usage activates distinct pathways with many synaptogenic mechanisms exclusively dependent on constant activity, but that both constant and spaced stimulation similarly drive ghost bouton formation (*83*). Consistently, acute high [K^+] depolarization (10 minutes) and prolonged thermogenic dTRPA1-stimulation (1 hour) both induce Mmp1- and activity-dependent molecular changes and ghost bouton formation (Fig. 17). These results suggest similar Mmp1 roles in both stimulation paradigms. I found Mmp1 upregulation following short-term intense and longer-term mild stimulation, suggesting Mmp1 is permissively increased by activity to enable new bouton formation. Moreover, Mmp1 is also increased following spaced activity and by long-term, increased chronic activity (Table S5).

A range of *trans*-synaptic signaling ligands play critical roles in activity-dependent synaptogenesis (*86*, *100–102*). For example, Wnt, BMP and integrin ligands are three classes that potently modulate both developmental and activity-dependent synaptogenic mechanisms (*82*, *83*, *103–105*). Milder spaced stimulation-induced bouton formation requires both pre- and postsynaptic Wg signaling (*82*, *106*), while stronger constant stimulation-induced bouton formation requires both pre- and postsynaptic integrin pathways (*83*). Both of these *trans*-synaptic signaling mechanisms are known to be strongly regulated by the extracellular synaptomatrix environment, making it intriguing to propose a likely Mmp1 involvement. Indeed, my work identified Mmp1 requirements for Wg *trans*-synaptic signaling (Fig. 13 and 16; Tables S3) (*44*). In

comparison, the activity-dependent Cortactin enhancement was recently shown to be Wg-dependent, although likewise required for rapid activity-dependent bouton formation (*106*). Mmps are glycosylated (*107*), and intimately inter-connected with integrins, integrin ligands and HSPGs which are all activity-regulated (*71*, *83*, *108*). Interestingly, reciprocal co-suppression was also identified in the glycan-related *pgant* mutants via misregulated integrin signaling presumably due to disrupted glycosylation states (*108*). More pertinently, in the extracellular synaptomatrix the Mmp target LanA is an integrin ligand critical for synapse formation and maintenance, and is also known to be regulated in both an activity- and Wg-dependent mechanism (*109–111*). Given that Mmp1 strongly controls Wg *trans*-synaptic signaling (*44*), and the number of secreted molecules, including Mmp1, that Wg is reported to modulate, I suggest that Wg is also a regulator of this mechanism. Future studies should investigate potential HSPG-Mmp-integrin intersections at the NMJ.

Future studies should add exogenous catalytically active or inactive recombinant Mmp1 to wild-type unstimulated NMJ preparations to address if Mmp1 is sufficient to induce plasticity and if this function requires proteolytic activity. We have shown that phosphomannomutase type 2-dependent Mmp N-glycosylation is likely necessary for Mmp-mediated synaptogenic functions driving proper neural development (*107*). Thus, recombinant Mmp production should utilize an expression system capable of synthesizing such PTMs such as the baculovirus-insect cell system (*17*, *112*). If exogenous Mmp1 alone is sufficient to induce ghost bouton formation then extending this experimental approach to *mmp1* LOF would help address if developmental defects in *mmp1* mutants restrict their ability to support activity-stimulated outgrowth. Moreover, spatio-temporal Mmp1 requirements could be addressed using an inducible binary expression system to turn on or off Mmp1 expression in neuron, muscle or glia at various time points. Unfortunately, transgenic UAS-Mmp1 expression is lethal in combination with ubiquitous-, neuronal-, glial- and muscle-specific Gal4 drivers. A recent initiative aiming to build a genome-wide GOF resource and circumvent exuberant UAS-Gal4 overexpression issues utilized catalytically-dead Cas9 as a transcriptional activator for target overexpression (*113*). With this method, transgenic flies ubiquitously expressing single guide RNA targeting upstream of the target (*mmp1*) transcriptional start site crossed to flies expressing the CRISPR activator (UAS) in a tissue specific (Gal4) and temporally restricted ($Gal80^{ts}$) manner would provide progeny with spatio-temporally controlled Mmp1 overexpression.

HSPGs and Activity-dependent Synaptogenesis

I find that Dlp mediates Mmp1-synaptic functions in both development and activity-dependent plasticity with Dlp likewise regulated by neural activity (Chapters II and III). Consistently, several studies show HSPGs are critical for synaptogenesis at the *Drosophila* NMJ (*51*, *61*, *62*, *69*), with similar activity-dependent roles for HSPGs in mammals (*114–121*). In mammals, enzymatic HS removal by acute heparitinase treatment affects synaptic scaling and attenuates activity-dependent modulation and synaptogenesis (*122–124*). More direct evidence for HSPG involvement in synaptic plasticity come from recent studies of a conditional, EXT1 knockout mouse model disrupting HS biosynthesis, which established a critical role for HSPGs in glutamatergic signaling (*121*, *125*, *126*). Future studies at the *Drosophila* NMJ should explore the possibility that other synaptic HSPGs (Perlecan, Cow and Syndecan) are activity-regulated.

Dlp and Mmp1 both show strong causative interactions with the Wg signaling pathway (*44*, *69*, *127*). However, whether correcting Dlp levels in the *mmp* mutants actually restores Wg signaling remains to be tested. *Trans*-synaptic Wg signaling could regulate activity-dependent Mmp1 translation and/or secretion at the synapse. Subsequently, extracellular localization via Dlp would then control synaptogenesis (*128*). This Wg-Dlp-Mmp1 interaction likely establishes a feedback loop bi-directionally modulating Mmp1 and Wg signaling, with Mmp1 negatively regulating Wg (*44*) and Wg promoting Mmp1 (*129–132*) (Fig. 13, 33 and Table S3). Alternatively, Dlp-dependent Wg-Mmp1 interactions could instruct activity-dependent changes, with Dlp as the central control node determining both Wg and Mmp1 levels, providing a synaptic binding scaffold for their activity-dependent interactions. Dlp has biphasic functions, serving as both a positive and negative regulator of Wg signal transduction depending on relative levels of Wg ligand, Frizzled-2 receptor and Dlp co-receptor (*69*, *133*). This interaction could determine co-localized Mmp1 abundance or activity at the synapse.

Secreted HSPG Perlecan also regulates bidirectional Wg signaling, with *trol* mutants exhibiting increased ghost bouton formation (*62*). Future studies should examine Mmp expression and localization in Perlecan LOF and GOF conditions, as well as test for Mmp-dependent processing of Perlecan. Perhaps Mmp1 cleaves Perlecan to regulate new bouton formation or instruct Wg signaling directionality. Dlp and Sdc both bind the receptor tyrosine phosphatase dLAR via HS-GAG chains (*51*), and disrupting HS-GAG chains results in severe synaptogenic defects at the *Drosophila* NMJ (*61*, *62*, *69*). In this coordinated mechanism, Dlp and Sdc bidirectionally antagonize functions with Dlp-dLAR instructing functional synaptogenesis and AZ morphogenesis, and Sdc-dLAR binding promoting structural growth (*51*, *134*). Perhaps Mmp activities regulate

such coordinated interactions during NMJ synaptogenesis. Future studies should test if reducing Sdc levels in either *mmp* mutant suppresses NMJ overgrowth and whether Mmp-dependent processing of Sdc occurs.

Disruption of two HS-GAG chain sulfation enzymes with opposing functions, *sulf1* and *hs6st*, restricts extracellular Wg ligand levels at the synapse with differential effects on Wg signal transduction (*69*). Moreover, heparin treatment reduces Wg levels, suggesting highly sulfated HS competes Wg away from the Dlp co-receptor (*62*, *69*). Interestingly, reducing postsynaptic HSPG sulfation by *sulfateless* knockdown augments ghost bouton formation in *trol* nulls, suggesting additional HSPG interactions (*62*). Sulfation state could be a key regulator of one or multiple convergent points in the FMRP-Dlp-Mmp axis, and reducing Dlp may restore the extracellular sulfation environment permitting activity-dependent Mmp1 enhancement. Biochemical approaches should be used to identify the HS landscape in FXS compared to controls. Protease-HSPG interactions are often bidirectional, with HS-GAG chains regulating protease localization, activity and inhibition, while proteases conversely mediate HSPG proteolytic processing and turnover through cleavage of the core protein (*65–68*, *135–137*). I propose that the Dlp-Mmp1 interaction is mediated through HS-GAG chains, suggesting a non-proteolytic mechanism. However, the functional consequence of this interaction on Mmp activity, stability, inhibition and/or substrate specificity have yet to be tested. Future studies should investigate the detailed consequences of HS-GAG chain interactions on the Dlp-Mmp1 mechanistic axis, in the context of FXS, and test the activity-regulation of this mechanism *in vivo* such as with PLA.

FMRP Regulation of Mmps and HSPGs

FMRP can directly and indirectly regulate MMP expression. In *Drosophila*, FMRP overexpression activates JNK signaling, which in turn increases Mmp1 expression (*138*, *139*). Mammalian MMPs are direct targets of FMRP translational regulation and loss of mammalian FMRP similarly increases MMP expression (*85*, *140–143*). Elevated Mmp1 levels in the absence of FMRP and loss of activity-dependent Mmp1 upregulation in FXS (Chapter III) along with the ability of FMRP to interact with *mmp* mRNA in other systems raise the possibility that part of this Mmp1 regulation is at the level of translational control (*71*, *144*). In collaboration with Dominic Vita (graduate student in the Broadie laboratory, Vanderbilt University, Department of Biological Sciences), we employed RNA immunoprecipitation (RIP) assays to test if the Mmp-FMRP intersection might be at the level of translation (Fig. 34). We find FMRP interacts with *mmp1* but not *mmp2* mRNA in *Drosophila* adult brain lysates, suggesting Mmp1 translation is regulated by FMRP (Fig. 34). In the mouse FXS model, MMP-9 is similarly upregulated, directly interacts with FMRP, and pharmacological and genetic inhibition of

MMP-9 restores normal synaptic development, again suggesting conserved functions (*142*, *145*, *146*). Future experiments could utilize several new or optimized strategies to investigate FMRP-*mmp* RNA interactions at the NMJ. In general, *mmp* mRNA localization could be spatially characterized by employing single molecule fluorescent *in situ* hybridization (FISH) on fixed NMJ preparations and visualized using confocal imaging approaches (*147*). Cell-specific RNA-tagging methods could be used to identify FMRP-RNA networks in either muscle or neuron (*148*, *149*). Specifically, a Gal4 driven UAS-FMRP product conjugated to poly(U) polymerase would covalently label FMRP-binding transcripts with 3' terminal uridines that can then be isolated and sequenced (*148*). A similar approach has been successful in *Drosophila* utilizing UAS-FMRP conjugated to the catalytic domain of ADAR to uncover targets of RNA-binding proteins identified by editing (TRIBE) in a tissue-specific manner (*149*). Cell-specific translational profiling techniques have been developed in *Drosophila* and could be used to identify actively translated mRNAs in the presence or absence of FMRP and/or activity stimulation (*150*, *151*). A combination of these approaches should shed light on FMRP-mediated control of Mmp1 at the NMJ and whether a single or multiple levels of translation-dependent and translation-independent mechanisms exist. It is possible that multiple spatially regulated and/or temporally restricted mechanisms contribute to the activity-induced Mmp1 upregulation. My work shows that Mmp1 and Mmp2 functions are coordinated at the synapse, with Mmp2 restricting Mmp1 expression, spatial distribution and synaptogenesis requirements (Fig. 9, 12 and Table S3) (*44*). Mmp2 is down-regulated following activity (Chapter III), possibly permitting the observed increase in Dlp and corresponding Mmp1 elevation (Fig. S12). Future studies should also investigate if activity-dependent Mmp2 reduction and activity-dependent Dlp enhancement still occur in the absence of FMRP. FMRP can also directly regulate HSPGs (*143*, *149*), and synaptic HSPGs are upregulated in the *Drosophila* FXS model (*127*). Thus, FMRP might directly regulate Dlp local translation at the synapse, in an activity-dependent mechanism. More indirectly, HS biosynthesis enzymes regulating the sulfation state of HS GAG chains could also be perturbed in FXS, which in turn would affect HSPG function (*125*, *152*).

I showed that loss of FMRP impedes the way in which Dlp and Mmp1 function in response to activity stimulation (context-dependent), and that reducing Dlp levels in the FXS disease state restores this core activity-dependent intersection, allowing for activity-stimulated Mmp1 enhancement (Chapter III). I propose that an unknown effector, regulated by FMRP and Dlp is causative for the defect in activity-dependent Mmp1 enhancement in FXS that is restored by Dlp reduction. As a core signaling platform, Dlp could interact with unknown proteins to modulate translation, secretion and/or sequestration of synaptic Mmp1. Screening for molecules that alter Mmp expression or co-localization with Dlp could identify such interacting molecules.

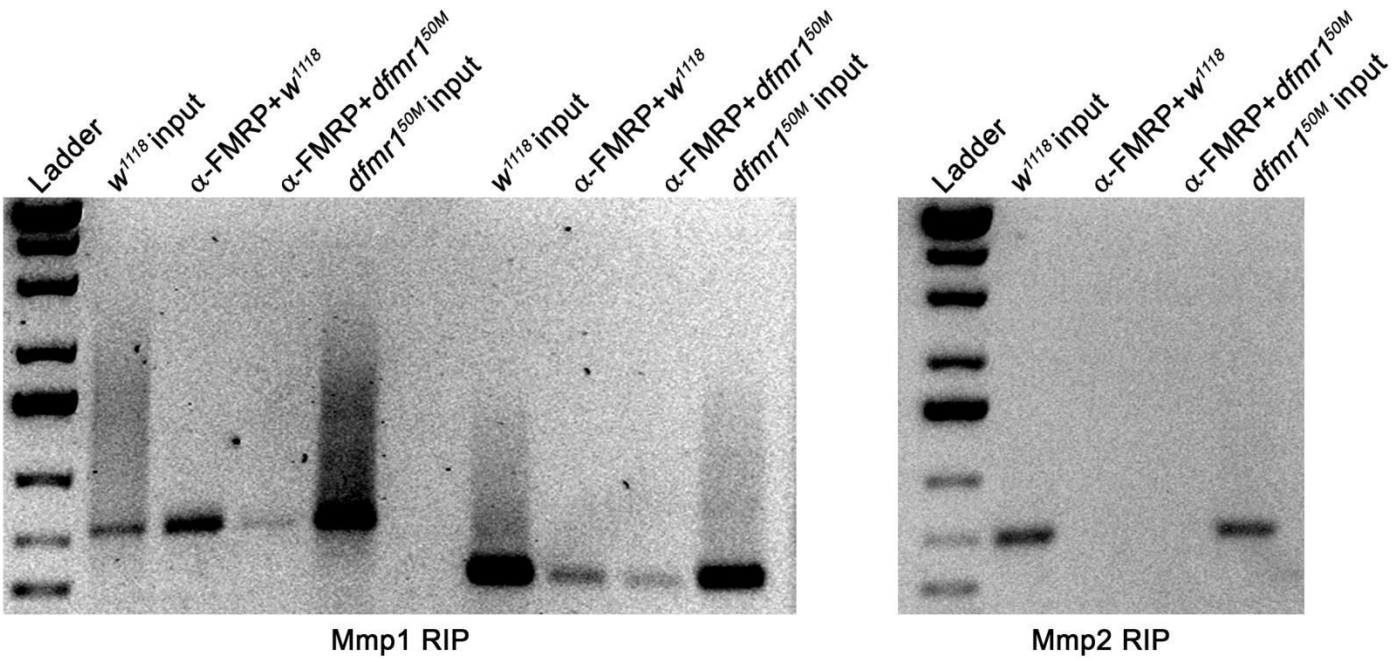

Figure 34 (RIP performed by Dominic Vita)

Figure 34: FMRP interacts with *mmp1* but not *mmp2* mRNA. RNA immunoprecipitation (RIP) using purified RNA extracted from adult heads, with or without anti-FMRP to pull-down RNA bound to FMRP. Standard techniques were used to reverse-transcribe RNA, with cDNA amplified using two different *mmp1* or *mmp2* primers. Input control lanes show that *mmp* mRNA is present in starting samples and that all primers detect *mmp* mRNA in total lysates. The second primer set for *mmp2* is not shown.

Mmp Regulation of Other *Trans*-synaptic Signaling Pathways

My work shows that Mmps have a core role as active signaling molecules instructing *trans*-synaptic signaling pathways (*44*). I assayed Mmp1 and Mmp2 requirements in two other *trans*-synaptic signaling pathways and found that *mmp* LOF mutants display differential defects in BMP signaling and Jeb-Alk (Jelly belly-Anaplastic lymphoma kinase) signaling at the NMJ (Fig. 35 and 36). While both Mmps restrict Wnt/Wg signaling (Fig. 13), Mmp1 also restricts BMP Glass Bottom Boat (Gbb) signaling and Mmp2 also regulates extracellular Jeb ligand levels (Figs. 35, 36 and Table S3). In conjunction with Dlp and Wg signaling, Mmps balance and coordinate other signaling activities important for synaptogenesis. Collectively, Mmps have intersecting and non-overlapping roles regulating *trans*-synaptic signaling pathways.

BMP *trans*-synaptic signaling

In testing the first pathway I find that Mmp1 limits BMP signal transduction (Fig. 35). TGF-β-BMP *trans*-synaptic Glass Bottom Boat (Gbb) signaling coordinates presynaptic and postsynaptic development by promoting structural growth, synapse stability, homeostasis and functional NMJ development (*153*–*156*). Gbb signaling is sensitive to synaptomatrix changes in Mmp activity, N-glycosylation and HSPG sulfation (*27*, *69*, *157*). The Gbb ligand is secreted by both neuron and muscle and both signals are transduced presynaptically through long-range and short-range signaling. In the long range, canonical BMP pathway, Gbb activates Wishful thinking (Wit, Type II BMPR), Saxophone (Sax, Type I BMPR) and/or Thickveins (Tkv, Type I BMPR) receptor complexes in MNs (*156*, *158*–*160*). Receptor activation results in phosphorylation of the transcription factor Mothers against decapentaplegic (pMad) and retrograde transport to the soma where pMad complexes with the co-Smad Medea (Med) to enter the nucleus and regulate the expression of BMP-responsive genes (*153*, *160*–*162*). BMP target genes include Trio, a guanine nucleotide exchange factor for the small GTPase Rac, Target of Wit (Twit) and a negative BMP regulator, Daughters against decapentaplegic (Dad) (*163*, *164*). Autocrine Gbb is packaged into dense-core vesicles (DCVs) by the BMP-binding protein Crimpy and both Gbb-containing DCVs and Crimpy-ectodomain release are observed following activity stimulation (*165*, *166*). Crimpy distinguishes the muscle-derived Gbb pool which promotes NMJ growth from the neural-derived, activity-induced Gbb signaling pool which promotes neurotransmission release (*166*). However, the functional relevance of Crimpy shedding is unknown and loss of Crimpy may shunt Gbb release from an activity-dependent pathway to constitutive secretion (*166*). Given that Mmp1 is regulated by activity (Chapter III), restricts NMJ development (Chapter II) and restricts pMad signaling (Fig. 35), Mmp1 might critically regulate

Gbb signaling by processing Crimpy. Crimpy may function as a Gbb co-receptor with ectodomain shedding terminating autocrine Gbb signaling or shed Crimpy may be necessary to compartmentalize or differentiate autocrine versus retrograde Gbb signaling in the synaptomatrix. In the first scenario, loss of Mmp1-dependent Crimpy processing could potentiate autocrine Gbb signal transduction contributing to the increased pMad and neurotransmission strength observed in *mmp1* mutants (Fig. 35). In the second scenario, mixed autocrine and retrograde Gbb signaling could enhance retrograde signaling, contributing to the increased synaptic pMad activity and NMJ overgrowth observed in *mmp1* mutants (Fig. 35). Finally, if Crimpy shedding is a prerequisite for neuronal Gbb release via the activity-dependent DCV pathway then loss of Mmp1 could trigger a switch in Gbb secretion toward constitutive release (*166*). This scenario would also cause aberrant presynaptic autocrine Gbb signaling by exacerbating retrograde pro-growth signaling which could contribute to the increased synaptic pMad activity and NMJ overgrowth observed in *mmp1* mutants (Fig. 35). Notably, *timp* LOF, integrin signaling defects, and Gbb overexpression all cause a wing blistering phenotype thought to be related to defects in Mmp-mediated adhesion and Crimpy overexpression is sufficient to suppress this phenotype in the Gbb overexpression condition (*27*, *167*, *168*). Retrograde BMP signaling is important for synaptic homeostasis and also activates a local (short-range), non-canonical Wit-LIMK pathway that promotes synapse stability limiting new synapse growth by restricting actin dynamics (*104*, *169*, *170*). Canonical Wit-signal transduction through pMad/Med potentiates activity-dependent ghost bouton formation while non-canonical Wit-LIMK signaling restricts actin turnover thereby inhibiting new bouton growth, highlighting opposing roles for Wit-signaling in structural plasticity (*104*). The BMP ligand Maverick (Mav) is secreted from glia signaling through activin-type receptor Punt on the muscle membrane resulting in intracellular activation of pMad and subsequent transcriptional regulation of Gbb and Dad in the muscle nuclei (*156*). Gbb is then secreted from the muscle and activates retrograde Gbb signaling through Wit in the presynaptic neuron (16). Therefore, glial cells regulate the magnitude of retrograde Gbb signaling. My data show that *mmp1* LOF mutants display a dramatic increase in postsynaptic pMad, suggesting Mmp1 limits Mav signaling from glia to muscle to restrict retrograde Gbb signaling in neurons (Fig. 35). This might be causative for the NMJ overelaboration observed following Mmp1 knock-down in glia (Fig. 27). Future studies should test if Mav is elevated in the glia-specific Mmp1 knock-down condition and if reducing Mav signaling is sufficient to suppress NMJ overgrowth. In neurons, excessive long-range, retrograde Gbb signaling downregulates FMRP abundance leading to increased Futsch/MAP1B translation and altered microtubule dynamics which permit synaptic overelaboration (*171*). Reducing long-range, retrograde Gbb signaling has the opposite effect (*171*). FMRP is a translational repressor of presynaptic Wit with FXS-associated neuroanatomical and locomotor defects enhanced by LIMK activation

and suppressed by either LIMK inhibition or reducing Wit receptor levels (*169*, *172*). Thus, presynaptic FMRP downregulation contributes to a feedforward loop as both an upstream and downstream effector of BMP-dependent signaling. Future studies should test if Mmp1-dependent Gbb signaling likewise regulates FMRP and interrogate potential Mmp requirements in this BMP feedforward loop. At the NMJ, *timp* LOF results in elevated Mmp activity, NMJ overgrowth, impaired motor function, defects in endocytosis and elevated *trans*-synaptic Gbb signaling (*27*). Tissue-specific *timp* knockdown and rescue studies suggest synaptogenic roles are mediated largely by muscle-derived Timp (*27*). Importantly, pharmacologic Mmp inhibition in the *timp* mutant background suppresses elevated proteolytic activity as well as Gbb signaling and largely mitigates structural and functional defects observed in the *timp* LOF condition (*27*). Likewise, genetically reducing BMP signaling in the *timp* null background via single copy *gbb* co-removal is sufficient to suppress structural and functional defects in *timp* mutants (*27*). These data suggest that Mmp proteolysis is balanced by Timp inhibition to limit BMP-mediated structural and functional synaptogenesis. To determine if one or both Mmps are causative for the *timp* LOF phenotypes described above, future studies could test single and double Mmp co-removal in the *timp* LOF background. I did not detect defects in Gbb or synaptic pMad abundance in *mmp2* mutants known to display elevated Mmp1 levels (Table S3 and Chapter II). Therefore, Mmp1 upregulation in the absence of Mmp2 is not sufficient to increase Gbb/pMad signaling, suggesting complete loss of Timp inhibition in combination with elevated Mmp activity might underlie this phenotype. Alternatively, Timp may have Mmp-independent requirements or Mmp2 gain of function might promote Gbb/pMad signaling. Notably, Mmp2 processing of the matrix molecule Frac enables LIMK signaling in embryonic MNs (*173*). I have not yet tested Mmp requirements for non-canonical Gbb signaling and Mmp2 could similarly regulate Wit-LIMK activation at the NMJ. Long-range retrograde pMad signaling to the MN nuclei also remains to be tested. Interestingly, *mir-124* mutant neurons have increased Mmp1 and BMP signaling components which also contain predicted mir-124 binding sites in their 3' UTRs, suggesting Mmp1 and BMP signaling might be co-regulated by the miRNA pathway (*174*). FMRP is documented to interact with the miRNA pathway and future studies should test if mir-124 mediated Mmp1-BMP signaling coordination is disrupted in the FXS condition (*174–177*).

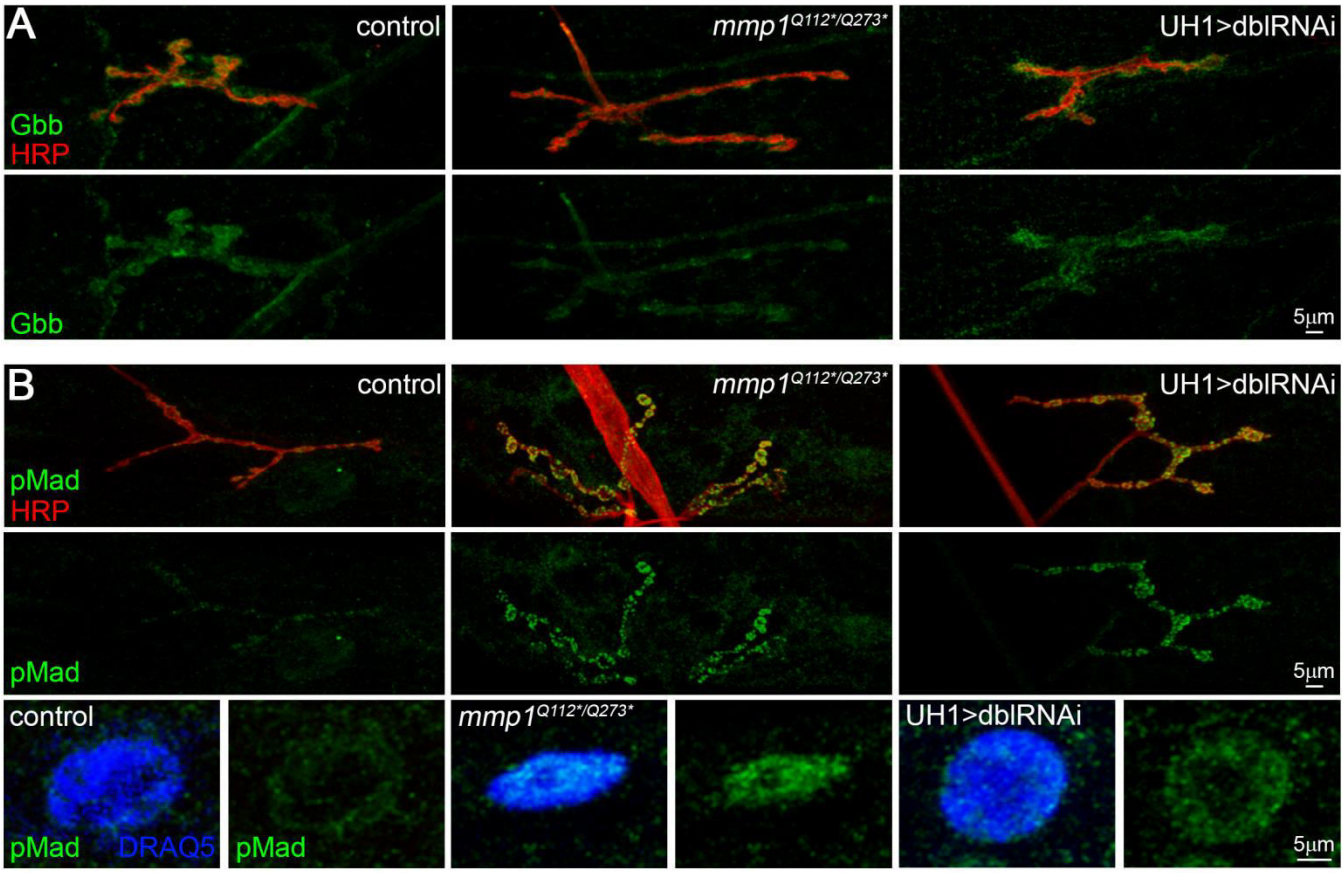

Figure 35

Figure 35. Mmp1 restricts BMP *trans*-synaptic signaling. (A) Representative NMJ images co-labeled with neuronal marker (HRP, red) and anti-Gbb (green) in genetic control (w^{1118}), *mmp1* mutant ($mmp1^{Q112/Q273}$) and ubiquitous double $mmp1{+}2^{RNAi}$ knock-down conditions (UH1>dblRNAi). (B) Representative images of individual muscle nuclei co-labeled with nuclear marker (DRAQ5, blue) and anti-phosphorylated mothers against decapentaplegic (pMad, green) in genetic control (w^{1118}), *mmp1* mutants ($mmp1^{Q112/Q273}$), *mmp2* genetic null ($mmp2^{ss218/Df}$) and ubiquitous double $mmp1{+}2^{RNAi}$ knock-down conditions (UH1>dblRNAi). See Table S3 for raw data values.

Jeb-Alk *trans*-synaptic signaling

In the second pathway, I find Mmp2 promotes extracellular Jeb ligand levels but restricts intracellular signal transduction (Fig. 36). Jeb ligand is secreted from the neuron to activate postsynaptic Alk receptors driving phosphorylation and nuclear import of extracellular signal-related kinase (dpERK) (*178*, *179*). Anterograde Jeb-Alk signaling restricts neurotransmission, limits synaptic expansion and localizes postsynaptic machinery including DLG and GluRs (*179*). Loss of *mmp2* leads to reduced extracellular Jeb ligand and increased dpERK signaling in the muscle nuclei (Fig. 36 and Table S3). Reduced ligand but increased signaling activation could be due to hyper-activated Alk receptors and increased ligand internalization. However, dpERK activation is predicted to reduce neurotransmission strength and lead to NMJ undergrowth, neither of which is a phenotype observed in *mmp2* mutants (Chapter II). Loss of *jeb* in presynaptic MNs leads to an increased number of undifferentiated boutons which lack postsynaptic scaffolds (*179*). It has been proposed that Jeb-Alk *trans*-synaptic signaling is coordinated by several negative regulators of ERK signaling which serve to balance development and activity-dependent structural and functional plasticity (*179*). Consistently, *mmp1* LOF leads to a striking increase in postsynaptic dpERK activity albeit in the absence of any observable changes in Jeb levels (Fig. 36 and Table S3). I reported elevated Wg signal transduction (FNI) for both *mmp* single mutants that was reciprocally co-suppressed by simultaneous knock-down of Mmp1+2 (Chapter II). Therefore I asked if a similar mechanism occurs in the Jeb-Alk pathway. Ubiquitous knock-down of both Mmps together resulted in extremely elevated dpERK activation; however, like *mmp2* single mutants, extracellular Jeb ligand was greatly diminished (Fig. 36 and Table S3). Jeb-Alk signaling is regulated by Mind-the-Gap (MTG), a critical regulator of the synaptomatrix that establishes the synaptic cleft signaling environment by recruiting and organizing integrins and various glycans (*180*–*182*). ERK is likewise a master integrator of signaling inputs and master regulator of transcriptional output. Currently, Jeb-Alk signaling is the only ERK-activating signal described for the postsynaptic muscle (*178*). In other cellular contexts, FGF and JNK signaling also feed into the dpERK pathway (*77*, *127*, *178*, *183*, *184*). Interestingly, Mmp2 is known to restrict FGF signaling in the *Drosophila* wing disc and could play a similar role at the NMJ (*77*, *78*). Future studies should test if Mmp2-dependent synaptogenic mechanisms involve FGF signaling by reducing FGF ligands or FGF receptors in the *mmp2* mutant background and testing for correction of structural, functional or signaling defects. JNK signaling activation and loss of *mmp2* both activate Mmp1 upregulation and feed into the dpERK pathway (*18*, *44*). Future studies should test if correcting Mmp1 abundance or modifying JNK signaling in the *mmp2* mutant background is sufficient to restore normal Jeb-Alk signaling. Likewise, studies should test if reducing JNK signaling in *mmp1* mutants is sufficient to correct elevated dpERK activation. Identifying target transcripts and

basal ERK signaling dynamics would aid in a better understanding of signal transduction at the NMJ. Signaling molecules, gene expression and cellular output are often discussed in terms of hierarchy or cause and effect; however, inputs and outputs are mutually interdependent. Perhaps loss of *mmp1 or mmp2* interfaces with MTG or MTG-targets and in doing so somehow alters signaling input, duration, specificity, stability, or output response. Mmp1 or Mmp2 may normally act as a molecular switch, somehow transcribing (input) or translating (output) ERK signaling to instruct the status of the NMJ. Other *trans*-synaptic signaling pathways, such as Wg or Gbb, likely intersect with ERK signaling and should be further investigated. The collective regulation of these pathways might contribute to the "co-suppressive" mechanism by which removal of both *mmps* offsets elevated structural and functional phenotypes observed by loss of either individual *mmp* alone (Chapter II). In this way, the strong dpERK activation in double-*mmp* knockdown studies is predicted to reduce structural and functional synaptogenesis and this might dampen the elevated FNI observed in single *mmp* mutants contributing to increased structural and functional development. Reduced Jeb and dpERK levels are observed in FXS but restored by decreasing HSPG abundance and accordingly neurotransmission strength is also corrected (*127*). This suggests that HSPGs may interact with Jeb-Alk signaling or Wg might influence ERK signaling. Finally, the magnitude of dpERK activation could be less important than when ERK is actually activated and perhaps for *mmp* mutants this is why elevated signaling occurs in the absence of predicted correlative phenotypes.

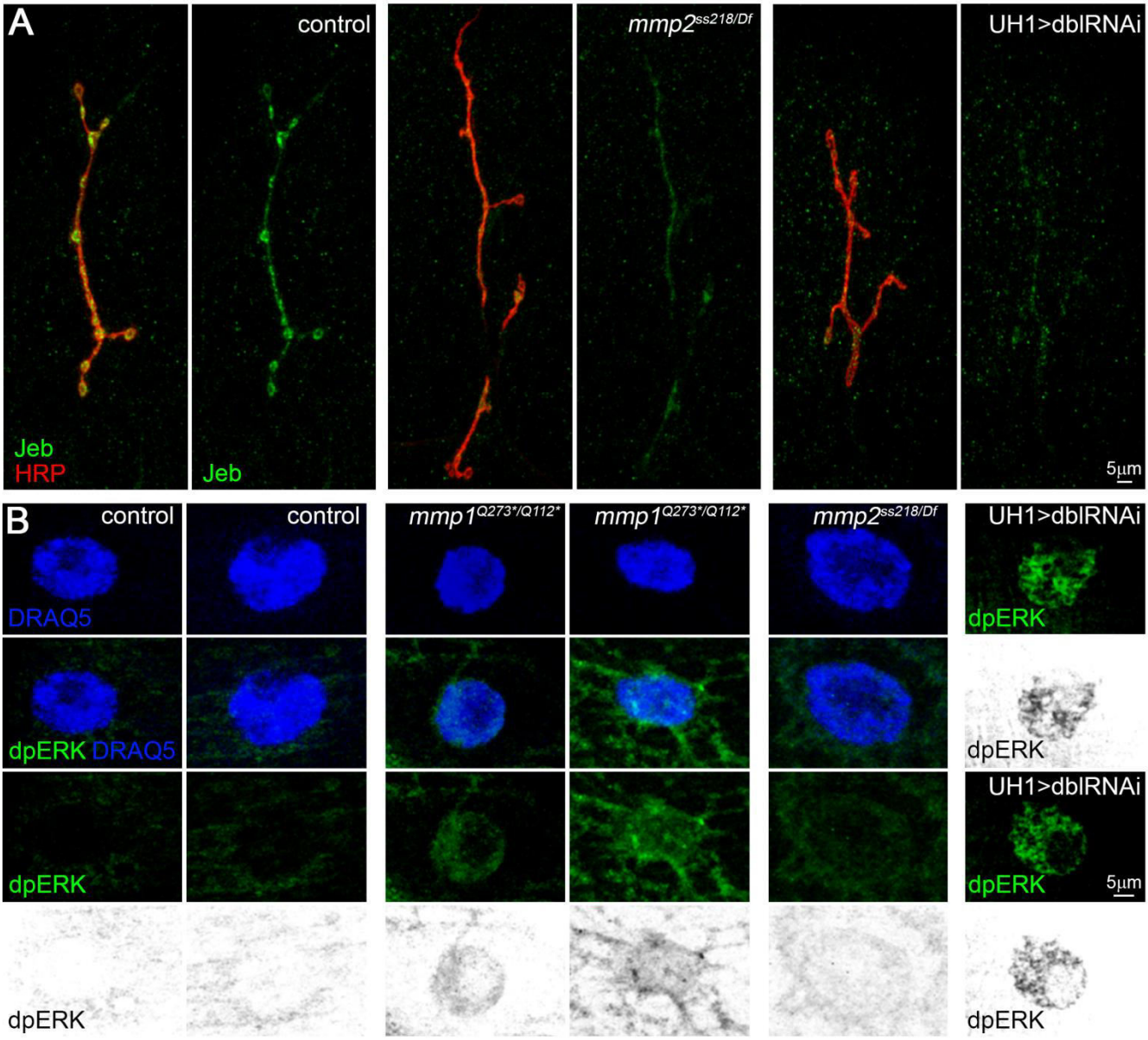

Figure 36

Figure 36: Mmp2 promotes extracellular Jeb ligand and both Mmps restrict dpERK signaling. (A) Representative NMJ images co-labeled with neuronal marker (HRP, red) and anti-Jeb (green) in genetic control (w^{1118}), *mmp2* genetic null ($mmp2^{ss218/Df}$) and ubiquitous double $mmp1{+}2^{RNAi}$ knock-down conditions (UH1>dblRNAi). (B) Representative images of individual muscle nuclei co-labeled with nuclear marker (DRAQ5, blue) and anti-diphosphorylated extracellular signal regulated kinase (dpERK, green) in genetic control (w^{1118}), *mmp1* mutants ($mmp1^{Q112/Q273}$), *mmp2* genetic null ($mmp2^{ss218/Df}$) and ubiquitous double $mmp1{+}2^{RNAi}$ knock-down conditions (UH1>dblRNAi). Black and white images show dpERK signal alone. See Table S3 for raw data values.

Perspectives and Extended Future Directions

The signaling functions of the synaptomatrix are mediated by dynamic protein-protein and protein-glycan interactions that are dependent on developmental and disease contexts. I identified a HS interaction that positions Mmp1 at the cell surface in a prime location to influence various signaling events. My findings suggest that the signaling input/output of the HS-interaction network and the signaling input/output of the Mmp-interaction network are mutually interconnected and collectively influence cellular behavior and intercellular signaling. Dlp::GFP binding proteins can be co-immunoprecipitated with a GFP-nanobody or streptavidin and identified by mass-spectrometry (*34*). At what level do the two Mmps regulate *trans*-synaptic signaling pathways and by extension structural and functional synaptogenesis? How direct or indirect is their involvement in these signaling events? Without identified proteolytic substrates the biologically relevant pathways can only be inferred. Degradomics encompasses genomic and proteomic approaches to identify protease-substrates, inhibitors and interactors related to protease function (*11*, *185*, *186*). A way forward is to pair my findings with degradomics to establish the Mmp substrate repertoire. Future proteomic analyses via mass-spectrometry could utilize the eight available iTRAQ (isobaric tags for relative and absolute quantitation) labels in conjunction with TAILS (terminal amine isotopic labeling of substrates) to compare substrate profiles following co-removal of Mmp1, Mmp2, and Timp in all possible pair-wise combinations (*12*, *185*–*187*). This provides a powerful approach for identifying substrates, cleavage-sites and cross-talk and can also be extended to assay temporal differences, such as during critical periods or to disease conditions like FXS. Highly conserved signaling processes, synaptogenic mechanisms, disease dysfunction, and *mmp* gene function all imply that *Drosophila* degradomics will be relevant and could critically accelerate our understanding of proteolytic processes in human development and disease. The question is how to match genetic LOF with the observed phenotypic consequences? One way forward is to exploit the power of *Drosophila* genetics and new CRISPR technology for domain bashing and to create live-imaging tools and Mmp/Timp sensors to interrogate temporal and cell-specific Mmp/Timp functions *in vivo*. A new generation of chemical tools permits cell-specific and temporal resolution of proteomes that can be defined, manipulated and quantified (*188*, *189*). These approaches are available for *Drosophila* and have been successfully employed at the NMJ (*188*). The methodology utilizes functionalized non-canonical amino acid tagging (NCAT) to label and identify synthesized proteins (*188*). Flies are fed a non-canonical amino acid which are incorporated in to nascent polypeptides in place of methionine using a UAS-Gal4 driven methionyl-tRNA synthetase (MetRS) mutant and utility is expanding as different variants are currently being optimized (*188*). The non-canonical amino acids contain a

reactive group that can be linked to various functional tags and this methodology compliments other labeling approaches such as fusion proteins, PLA, Stable Isotope Labeling with Amino acids in Cell culture (SILAC), iTRAQ and TAILS. BONCAT (bio-orthogonal non-canonical amino acid tagging) labels proteins with affinity tags, for example biotin, that can be quantified by blotting or purified and identified by mass spectrometry (*188*, *189*). Using presynaptic and postsynaptic MetRS expression in conjunction with BONCAT, iTRAQ, and TAILS labeling in controls versus FXS animals would reveal the cell-specific proteome and cleavage profiles which could be quantified and compared to identify changes relevant in the disease state. In this same way, future studies should profile the proteome and degradome of *mmp* LOF, GOF, and Dlp manipulations. FUNCAT (fluorescent non-canonical amino acid tagging) labels proteins with a fluorescent tag (*188*). Puromycylation (Puro) tagging permits the use of the tRNA analog, puromycin, to stop translation and release a truncated protein in order to identify the exact location of synthesis (*190*). To visualize a specific protein from the proteome, these approaches can be combined with PLA (*190*). PLA is amenable to multiplexing and could be used to monitor several synthesized proteins together. Overall, this could measure protein synthesis rates, the site of protein synthesis, chased to measure turnover, and whole proteome or single molecule analyses/dynamics during neural plasticity (*188*, *189*). This could be extended to measure Mmp parameters in Timp overexpression, Dlp manipulations, or the FXS condition. Cell-specific methionyl-tRNA synthetase (MetRS) mutant expression and NCAT-PLA can clarify what cell-type an extracellular protein originated from and track turnover. This might shed light on how Mmps, Dlp, or Timp are spatially and temporally regulated in the synaptomatrix and if tissue-specific differences influence these dynamics. In addition, a new modular expression system developed for *Drosophila* permits simultaneous targeting of different cell-types by using programmable transcription activator-like effector (TALE) proteins (*191*). In this way, parallel expression of multiple transgenes conjugated to a given variable activating sequence (VAS) can be activated in spatially distinct tissues (*191*). The VAS-TALE system can accommodate an unlimited number of combinations and is compatible with other binary expression systems (*191*). This provides a framework for investigating complex genetic manipulations *in vivo* that in conjunction with metabolic proteome labeling will address unsolved questions regarding Mmp interactions, dynamics and requirements during neural development and plasticity. In the same regard, studying *trans*-synaptic signaling has relied on indirect read-outs of signal activation and it remains challenging to parse out signaling directionality. Site-directed protein labeling and engineering by genetically encoding functionally targetable non-canonical amino acids into target proteins such as ligands, receptors, or Mmps could reveal a more detailed understanding of signaling dynamics (*192*). Ligand-directed, site-specific modifications of receptor proteins could be used as biosensors for monitoring *trans*-synaptic

signaling (*192*). Using this approach as a biosensor to detect Wg-Fz2 interactions could be paired with genetic manipulations of presynaptic or postsynaptic Dlp levels to directly test the consequence of HSPGs on *trans*-synaptic signaling. Future work at the NMJ should certainly include these approaches, live-imaging, activity and biosensors and proteomics for an integrated understanding of protease biology throughout synaptic development. Chemical biology paired with the power of *Drosophila* genetics will illuminate the previously elusive and complex biological functions of Mmps, HSPGs, and *trans*-synaptic signaling in normal physiology and in the context of the FXS disease state. Moreover, identifying Mmp interactors as well as potential novel substrates in disease conditions could instruct new therapeutic targets and approaches.

References

1. J. F. Woessner, Catabolism of collagen and non-collagen protein in the rat uterus during post-partum involution. *Biochem. J.* **83**, 304–14 (1962).
2. J. Gross, C. M. Lapiere, Collagenolytic Activity in Amphibian Tissues: a Tissue Culture Assay. *Proc. Natl. Acad. Sci.* **48**, 1014–1022 (1962).
3. B. Fingleton, Matrix metalloproteinases as regulators of inflammatory processes. *Biochim. Biophys. Acta - Mol. Cell Res.* **1864**, 2036–2042 (2017).
4. P. G. Jobin, G. S. Butler, C. M. Overall, New intracellular activities of matrix metalloproteinases shine in the moonlight. *Biochim. Biophys. Acta - Mol. Cell Res.* **1864**, 2043–2055 (2017).
5. M. E. De Stefano, M. T. Herrero, The multifaceted role of metalloproteinases in physiological and pathological conditions in embryonic and adult brains. *Prog. Neurobiol.* **155**, 36–56 (2017).
6. G. Murphy, H. Nagase, Progress in matrix metalloproteinase research. *Mol Asp. Med*. **29**, 290–308 (2008).
7. R. P. Iyer, N. L. Patterson, G. B. Fields, M. L. Lindsey, The history of matrix metalloproteinases: milestones, myths, and misperceptions. *AJP Hear. Circ. Physiol.* **303**, H919–H930 (2012).
8. H. Nagase, R. Visse, G. Murphy, Structure and function of matrix metalloproteinases and TIMPs. *Cardiovasc. Res.* **69**, 562–573 (2006).
9. A. Page-mccaw, Remodeling the Model Organism: Matrix Metalloproteinase Functions in Invertebrates. *Semin. Cell Dev. Biol.* **19**, 14–23 (2008).
10. A. Page-McCaw, J. Serano, J. M. Sante, G. M. Rubin, Drosophila matrix metalloproteinases are required for tissue remodeling, but not embryonic development. *Dev. Cell*. **4**, 95–106 (2003).
11. D. Rodríguez, C. J. Morrison, C. M. Overall, Matrix metalloproteinases: What do they not do? New substrates and biological roles identified by murine models and proteomics. *Biochim. Biophys. Acta - Mol. Cell Res.* **1803**, 39–54 (2010).
12. U. auf dem Keller, A. Prudova, U. Eckhard, B. Fingleton, C. Overall, Systems-level analysis of proteolytic events in increased vascular permeability and complement activation in skin inflammation. *Sci. Signal.* **6**, 2 (2013).
13. A. Page-McCaw, A. J. Ewald, Z. Werb, Matrix metalloproteinases and the regulation of tissue remodeling. *Nat Rev Mol Cell Biol.* **8**, 221–233 (2007).
14. A. Krüger, Functional genetic mouse models: Promising tools for investigation of the proteolytic

internet. *Biol. Chem.* **390**, 91–97 (2009).

15. J. Gaffney, I. Solomonov, E. Zehorai, I. Sagi, Multilevel regulation of matrix metalloproteinases in tissue homeostasis indicates their molecular specificity in vivo. *Matrix Biol.* **44–46**, 191–199 (2015).
16. K. Yamamoto, G. Murphy, L. Troeberg, Extracellular regulation of metalloproteinases. *Matrix Biol.* **44–46**, 255–263 (2015).
17. K. LaFever, X. Wang, P. Page-McCaw, G. Bhave, A. Page-McCaw, Both Drosophila matrix metalloproteinases have released and membrane-tethered forms but have different substrates. *Sci. Rep.* **7**, 44560 (2017).
18. M. Uhlirova, D. Bohmann, JNK- and Fos-regulated Mmp1 expression cooperates with Ras to induce invasive tumors in Drosophila. *EMBO J.* **25**, 5294–5304 (2006).
19. J. Waldholm, Z. Wang, D. Brodin, A. Tyagi, S. Yu, U. Theopold, A. Kristin, Ö. Farrants, N. Visa, SWI / SNF regulates the alternative processing of a specific subset of pre-mRNAs in Drosophila melanogaster. *BMC Mol. Biol.* **12**, 1471–2199 (2011).
20. G. Sokpor, Y. Xie, J. Rosenbusch, T. Tuoc, Chromatin Remodeling BAF (SWI/SNF) Complexes in Neural Development and Disorders. *Front. Mol. Neurosci.* **10**, 243 (2017).
21. R. Xu, V. A. Spencer, M. J. Bissell, Extracellular matrix-regulated gene expression requires cooperation of SWI/SNF and transcription factors. *J. Biol. Chem.* **282**, 14992–14999 (2007).
22. J. Schleede, S. S. Blair, The Gyc76C Receptor Guanylyl Cyclase and the Foraging cGMP-Dependent Kinase Regulate Extracellular Matrix Organization and BMP Signaling in the Developing Wing of Drosophila melanogaster. *PLoS Genet.* **11**, e1005576 (2015).
23. D. Shakiryanova, E. S. Levitan, Prolonged presynaptic posttetanic cyclic GMP signaling in Drosophila motoneurons. *Proc. Natl. Acad. Sci. U. S. A.* **105**, 13610–13613 (2008).
24. L. D. Deady, J. Sun, A Follicle Rupture Assay Reveals an Essential Role for Follicular Adrenergic Signaling in Drosophila Ovulation. *PLoS Genet.* **11**, e1005604 (2015).
25. E. Knapp, J. Sun, Steroid signaling in mature follicles is important for Drosophila ovulation. *Proc Natl Acad Sci USA*. **114**, 699–704 (2017).
26. L. D. Deady, W. Shen, S. A. Mosure, A. C. Spradling, J. Sun, Matrix Metalloproteinase 2 Is Required for Ovulation and Corpus Luteum Formation in Drosophila. *PLoS Genet.* **11**, e1004989 (2015).
27. J. Shilts, K. Broadie, Secreted tissue inhibitor of matrix metalloproteinase restricts trans -synaptic signaling to coordinate synaptogenesis. *J. Cell Sci.* **130**, 2344–2358 (2017).
28. A. Ikmi, B. Gaertner, C. Seidel, M. Srivastava, J. Zeitlinger, M. C. Gibson, Molecular Evolution of the Yap /

Yorkie Proto-Oncogene and Elucidation of Its Core Transcriptional Program. *Mol. Biol. Evol.* **31**, 1375–1390 (2014).

29. J. R. Pearson, F. Zurita, L. Tomás-Gallardo, A. Díaz-Torres, M. del C. Díaz de la Loza, K. Franze, M. D. Martín-Bermudo, A. González-Reyes, ECM-Regulator timp Is Required for Stem Cell Niche Organization and Cyst Production in the Drosophila Ovary. *PLoS Genet.* **12**, e1005763 (2016).
30. G. S. Butler, S. S. Apte, F. Willenbrock, G. Murphy, R. B. Y. Polyanions, G. S. Butler, S. S. Apte, F. Willenbrock, G. Murphy, Human Tissue Inhibitor of Metalloproteinases 3 Interacts with Both the N- and C-terminal Domains of Gelatinases A and B. *J Biol Chem*. **274**, 10846–10851 (1999).
31. B. M. Glasheen, A. T. Kabra, A. Page-McCaw, Distinct functions for the catalytic and hemopexin domains of a Drosophila matrix metalloproteinase. *Proc. Natl. Acad. Sci. U. S. A.* **106**, 2659–2664 (2009).
32. Y. Zang, M. Wan, M. Liu, H. Ke, S. Ma, L. Liu, J. C. Pastor-pareja, Plasma membrane overgrowth causes fibrotic collagen accumulation and immune activation in Drosophila adipocytes. *Elife*. **4**, e07187 (2015).
33. S. Wang, S. Yoo, H. Kim, M. Wang, C. Zheng, W. Parkhouse, C. Krieger, N. Harden, Detection of In Situ Protein-protein Complexes at the Drosophila Larval Neuromuscular Junction Using Proximity Ligation Assay. *JOVE*. **95**, e52139 (2015).
34. U. Rothbauer, K. Zolghadr, S. Tillib, D. Nowak, L. Schermelleh, A. Gahl, N. Backmann, K. Conrath, S. Muyldermans, M. C. Cardoso, H. Leonhardt, Targeting and tracing antigens in live cells with fluorescent nanobodies. *Nat. Methods*. **3**, 887–889 (2006).
35. A. Buchfellner, L. Yurlova, S. Nüske, A. M. Scholz, J. Bogner, B. Ruf, K. Zolghadr, S. E. Drexler, G. A. Drexler, S. Girst, C. Greubel, J. Reindl, C. Siebenwirth, T. Romer, A. A. Friedl, U. Rothbauer, A new nanobody-based biosensor to study endogenous PARP1 in vitro and in live human cells. *PLoS One*. **11**, e0151041 (2016).
36. S. Harmansa, thesis, Universität Basel (2016).
37. K. S. Kerr, Y. Fuentes-Medel, C. Brewer, R. Barria, J. Ashley, K. C. Abruzzi, A. Sheehan, O. E. Tasdemir-Yilmaz, M. R. Freeman, V. Budnik, Glial wingless/Wnt regulates glutamate receptor clustering and synaptic physiology at the Drosophila neuromuscular junction. *J. Neurosci.* **34**, 2910–2920 (2014).
38. J. Staples, K. Broadie, The cell polarity scaffold Lethal Giant Larvae regulates synapse morphology and function. *J. Cell Sci.* **126**, 1992–2003 (2013).
39. K. Chen, D. E. Featherstone, Discs-large (DLG) is clustered by presynaptic innervation and regulates postsynaptic glutamate receptor subunit composition in Drosophila. *BMC Biol.* **3**, 1 (2005).
40. S. M. Thomas, J. S. Brugge, Cellular functions regulated by Src family kinases. *Annu. Rev. Cell Dev. Biol.*

13, 513–609 (1997).

41. S. Karunanithi, L. Marin, K. Wong, H. L. Atwood, Quantal Size and Variation Determined by Vesicle Size in Normal and Mutant Drosophila Glutamatergic Synapses. *J. Neurosci.* **22**, 10267–10276 (2002).
42. Y. Q. Zhang, A. M. Bailey, H. J. G. Matthies, R. B. Renden, M. A. Smith, S. D. Speese, G. M. Rubin, K. Broadie, Drosophila fragile X-related gene regulates the MAP1B homolog Futsch to control synaptic structure and function. *Cell*. **107**, 591–603 (2001).
43. D. C. Zarnescu, P. Jin, J. Betschinger, M. Nakamoto, Y. Wang, T. C. Dockendorff, Y. Feng, T. A. Jongens, J. C. Sisson, J. A. Knoblich, S. T. Warren, K. Moses, Fragile X protein functions with Lgl and the PAR complex in flies and mice. *Dev. Cell*. **8**, 43–52 (2005).
44. M. L. Dear, N. Dani, W. Parkinson, S. Zhou, K. Broadie, Two matrix metalloproteinase classes reciprocally regulate synaptogenesis. *Development*. **143**, 75–87 (2016).
45. E. S. Heckscher, R. D. Fetter, K. W. Marek, S. D. Albin, W. Davis, NF-κB, I-κB and IRAK Control Glutamate Receptor Density at the Drosophila NMJ. *Neuron*. **55**, 859–873 (2007).
46. M. D. Gordon, M. S. Dionne, D. S. Schneider, R. Nusse, WntD is a feedback inhibitor of Dorsal/NF-kB in Drosophila development and immunity. *Nature*. **437**, 746–749 (2005).
47. J. B. Kearney, S. R. Wheeler, P. Estes, B. Parente, S. T. Crews, Gene expression profiling of the developing Drosophila CNS midline cells. *Dev Biol.* **275**, 473–492 (2004).
48. K. Janson, E. D. Cohen, E. L. Wilder, Expression of DWnt6, DWnt10, and DFz4 during Drosophila development. *Mech. Dev.* **103**, 117–120 (2001).
49. S. L. Ballard, D. L. Miller, B. Ganetzky, Retrograde neurotrophin signaling through tollo regulates synaptic growth in Drosophila. *J. Cell Biol.* **204**, 1157–1172 (2014).
50. F. L. W. Liebl, C. McKeown, Y. Yao, H. K. Hing, Mutations in Wnt2 Alter Presynaptic Motor Neuron Morphology and Presynaptic Protein Localization at the Drosophila Neuromuscular Junction. *PLoS One*. **5**, e12778 (2010).
51. K. G. Johnson, A. P. Tenney, A. Ghose, A. M. Duckworth, M. E. Higashi, K. Parfitt, O. Marcu, T. R. Heslip, J. L. Marsh, T. L. Schwarz, J. G. Flanagan, D. Van Vactor, The HSPGs Syndecan and dallylike bind the receptor phosphatase LAR and exert distinct effects on synaptic development. *Neuron*. **49**, 517–531 (2006).
52. C. Ruiz-Canada, V. Budnik, Introduction on the use of the Drosophila embryonic/larval neuromuscular junction as a model system to study synapse development and function, and a brief summary of pathfinding and target recognition. *Int. Rev. Neurobiol.* **75**, 1–31 (2006).

53. A. Luchtenborg, G. P. Solis, D. Egger-adam, A. Koval, C. Lin, M. G. Blanchard, S. Kellenberger, V. L. Katanaev, Heterotrimeric Go protein links Wnt-Frizzled signaling with ankyrins to regulate the neuronal microtubule cytoskeleton. *Development*. **141**, 3399–3409 (2014).

54. G. Ayalon, J. Q. Davis, P. B. Scotland, V. Bennett, An Ankyrin-Based Mechanism for Functional Organization of Dystrophin and Dystroglycan. *Cell*. **135**, 1189–1200 (2008).

55. A. Yao, S. Jin, X. Li, Z. Liu, X. Ma, J. Tang, Y. Q. Zhang, Drosophila FMRP regulates microtubule network formation and axonal transport of mitochondria. *Hum. Mol. Genet.* **20**, 51–63 (2011).

56. R. W. Ball, E. Peled, G. Guerrero, E. Y. Isacoff, BMP signaling and microtubule organization regulate synaptic strength. *Neuroscience*. **291**, 155–166 (2015).

57. J. Pielage, R. D. Fetter, G. W. Davis, A postsynaptic Spectrin scaffold defines active zone size, spacing, and efficacy at the Drosophila neuromuscular junction. *J. Cell Biol.* **175**, 491–503 (2006).

58. B. Ataman, V. Budnik, U. Thomas, Scaffolding Proteins at the Drosophila Neuromuscular Junction. *Int. Rev. Neurobiol.* **75**, 181–216 (2006).

59. C. Ruiz-Canada, J. Ashley, S. Moeckel-Cole, E. Drier, J. Yin, V. Budnik, New synaptic bouton formation is disrupted by misregulation of microtubule stability in aPKC mutants. *Neuron*. **42**, 567–580 (2004).

60. P. Ramachandran, R. Barria, J. Ashley, V. Budnik, A critical step for postsynaptic F-actin organization: Regulation of Baz/Par-3 localization by aPKC and PTEN. *Dev. Neurobiol.* **69**, 583–602 (2009).

61. Y. Ren, C. A. Kirkpatrick, J. M. Rawson, M. Sun, S. B. Selleck, Cell Type-Specific Requirements for Heparan Sulfate Biosynthesis at the Drosophila Neuromuscular Junction: Effects on Synapse Function, Membrane Trafficking, and Mitochondrial Localization. *J. Neurosci.* **29**, 8539–8550 (2009).

62. K. Kamimura, K. Ueno, J. Nakagawa, R. Hamada, M. Saitoe, N. Maeda, Perlecan regulates bidirectional Wnt signaling at the Drosophila neuromuscular junction. *J. Cell Biol.* **200**, 219–233 (2013).

63. S. Ohlig, U. Pickhinke, S. Sirko, S. Bandari, D. Hoffmann, R. Dreier, P. Farshi, M. Götz, K. Grobe, An emerging role of Sonic hedgehog shedding as a modulator of heparan sulfate interactions. *J. Biol. Chem.* **287**, 43708–43719 (2012).

64. X. Wang, A. Page-McCaw, A matrix metalloproteinase mediates long-distance attenuation of stem cell proliferation. *J. Cell Biol.* **206**, 923–936 (2014).

65. S. Georges, D. Heymann, M. Padrines, Modulatory Effects of Proteoglycans on Proteinase Activities. *Methods Mol. Biol.* **836**, 307–322 (2012).

66. G. Murphy, H. Nagase, Localizing matrix metalloproteinase activities in the pericellular environment. *FEBS J.* **278**, 2–15 (2011).

67. A. Theocharis, C. Gialeli, P. Bouris, E. Giannopoulou, S. Skandalis, A. Aletras, R. Iozzo, N. Karamanos, Cell-matrix interactions: focus on proteoglycan-proteinase interplays and pharmacological targeting in cancer. *FEBS J.* **281**, 5023–5042 (2014).

68. A. Tocchi, W. C. Parks, Functional interactions between matrix metalloproteinases and glycosaminoglycans. *FEBS J.* **280**, 2332–2341 (2013).

69. N. Dani, M. Nahm, S. Lee, K. Broadie, A Targeted Glycan-Related Gene Screen Reveals Heparan Sulfate Proteoglycan Sulfation Regulates WNT and BMP Trans-Synaptic Signaling. *PLoS Genet.* **8**, e1003031 (2012).

70. M. C. Z. Meneghetti, A. J. Hughes, T. R. Rudd, H. B. Nader, A. K. Powell, E. A. Yates, M. A. Lima, Heparan sulfate and heparin interactions with proteins. *J. R. Soc. Interface*. **12**, 20150589 (2015).

71. M. L. Dear, J. Shilts, K. Broadie, Neuronal activity drives FMRP- and HSPG-dependent matrix metalloproteinase function required for rapid synaptogenesis. *Sci. Signal.* **10**, 3181 (2017).

72. S. Kadener, D. Stoleru, M. Mcdonald, P. Nawathean, M. Rosbash, Clockwork Orange is a transcriptional repressor and a new Drosophila circadian pacemaker component. *Genes Dev.* **21**, 1675–1686 (2007).

73. A. Klebes, A. Sustar, K. Kechris, H. Li, G. Schubiger, T. B. Kornberg, Regulation of cellular plasticity in Drosophila imaginal disc cells by the Polycomb group, trithorax group and lama genes. *Development*. **132**, 3753–3765 (2005).

74. Y. W. Zhang, D. N. Arnosti, Conserved Catalytic and C-Terminal Regulatory Domains of the C-Terminal Binding Protein Corepressor Fine-Tune the Transcriptional Response in Development . *Mol. Cell. Biol.* **31**, 375–384 (2011).

75. E. J. Ostrin, Y. Li, K. Hoffman, J. Liu, K. Wang, L. Zhang, G. Mardon, R. Chen, Genome-wide identification of direct targets of the Drosophila retinal determination protein Eyeless. *Genome Res.* **16**, 466–476 (2006).

76. S. Aerts, X. Quan, A. Claeys, M. N. Sanchez, P. Tate, B. A. Hassan, Robust Target Gene Discovery through Transcriptome Perturbations and Genome-Wide Enhancer Predictions in Drosophila Uncovers a Regulatory Basis for Sensory Specification. *PLoS Biol.* **8**, e1000435 (2010).

77. Q. Wang, M. Uhlirova, D. Bohmann, Spatial Restriction of FGF Signaling by a Matrix Metalloprotease Controls Branching Morphogenesis. *Dev. Cell*. **18**, 157–164 (2010).

78. A. Guha, L. Lin, T. Kornberg, Regulation of Drosophila matrix metalloprotease Mmp2 is essential for wing imaginal disc:trachea association and air sac tubulogenesis. *Dev Biol.* **335**, 317–326 (2009).

79. C. Pitsouli, N. Perrimon, The Homeobox Transcription Factor Cut Coordinates Patterning and Growth

During Drosophila Airway Remodeling. *Sci. Signal.* **6**, 263 (2013).

80. M. Jin, S. Aibar, Z. Ge, R. Chen, S. Aerts, G. Mardon, Identification of Novel Direct Targets of Drosophila Sine Oculis by Integration of Genome-wide Data Sets. *Dev Biol.* **415**, 157–167 (2016).
81. W.-H. Lin, C. Giachello, R. Baines, Seizure control through genetic and pharmacological manipulation of Pumilio in Drosophila: a key component of neuronal homeostasis. *Dis. Model. Mech.* **10**, 141–150 (2017).
82. B. Ataman, J. Ashley, M. Gorczyca, P. Ramachandran, W. Fouquet, S. J. Sigrist, V. Budnik, Rapid activity-dependent modifications in synaptic structure and function require bidirectional Wnt signaling. *Neuron*. **57**, 705–718 (2008).
83. J. Lee, J. Geng, J. Lee, A. Wang, K. Chang, Activity-induced synaptic structural modifications by an activator of integrin signaling at the Drosophila neuromuscular junction. *J. Neurosci.* **37**, 3246–3263 (2017).
84. K. Conant, M. Allen, S. T. Lim, Activity dependent CAM cleavage and neurotransmission. *Front. Cell. Neurosci.* **9**, 305 (2015).
85. M. Dziembowska, J. Milek, a. Janusz, E. Rejmak, E. Romanowska, T. Gorkiewicz, a. Tiron, C. R. Bramham, L. Kaczmarek, Activity-Dependent Local Translation of Matrix Metalloproteinase-9. *J. Neurosci.* **32**, 14538–14547 (2012).
86. E. Tsilibary, A. Tzinia, L. Radenovic, V. Stamenkovic, T. Lebitko, M. Mucha, R. Pawlak, R. Frischknecht, L. Kaczmarek, Neural ECM proteases in learning and synaptic plasticity. *Prog. Brain Res.* **214**, 135–157 (2014).
87. B. Vafadari, A. Salamian, L. Kaczmarek, MMP-9 in translation: from molecule to brain physiology, pathology, and therapy. *J. Neurochem.* **139**, 91–114 (2016).
88. C. Vaillant, M. Didier-baze, M. Belin, N. Thomasset, Spatiotemporal Expression Patterns of Metalloproteinases and Their Inhibitors in the Postnatal Developing Rat Cerebellum. *J. Neurosci.* **19**, 4994–5004 (1999).
89. S. E. Meighan, P. C. Meighan, P. Choudhury, C. J. Davis, M. L. Olson, P. A. Zornes, J. W. Wright, J. W. Harding, Effects of extracellular matrix-degrading proteases matrix metalloproteinases 3 and 9 on spatial learning and synaptic plasticity. *J. Neurochem.* **96**, 1227–1241 (2006).
90. L. L. Phillips, J. L. Chan, A. E. Doperalski, T. M. Reeves, Time dependent integration of matrix metalloproteinases and their targeted substrates directs axonal sprouting and synaptogenesis following central nervous system injury. *Neural Regen. Res.* **9**, 362–376 (2014).

91. S. M. Reinhard, K. Razak, I. M. Ethell, A delicate balance: role of MMP-9 in brain development and pathophysiology of neurodevelopmental disorders. *Front. Cell. Neurosci.* **9**, 280 (2015).

92. P. Michaluk, L. Kolodziej, B. Mioduszewska, G. M. Wilczynski, J. Dzwonek, J. Jaworski, D. C. Gorecki, O. P. Ottersen, L. Kaczmarek, B-Dystroglycan as a target for MMP-9, in response to enhanced neuronal activity. *J. Biol. Chem.* **282**, 16036–16041 (2007).

93. A. Szklarczyk, J. Lapinska, M. Rylski, R. D. G. McKay, L. Kaczmarek, Matrix metalloproteinase-9 undergoes expression and activation during dendritic remodeling in adult hippocampus. *J. Neurosci.* **22**, 920–930 (2002).

94. S. Murase, C. L. Lantz, E. Kim, N. Gupta, R. Higgins, M. Stopfer, D. A. Hoffman, E. M. Quinlan, Matrix Metalloproteinase-9 Regulates Neuronal Circuit Development and Excitability. *Mol. Neurobiol.* **53**, 3477–3493 (2016).

95. S. Nagappan-Chettiar, E. M. Johnson-Venkatesh, H. Umemori, Activity-dependent proteolytic cleavage of cell adhesion molecules regulates excitatory synaptic development and function. *Neurosci. Res.* **116**, 60–69 (2017).

96. M. Stawarski, M. Stefaniuk, J. Wlodarczyk, Matrix metalloproteinase-9 involvement in the structural plasticity of dendritic spines. *Front. Neuroanat.* **8**, 68 (2014).

97. X. Wang, O. Bozdagi, J. S. Nikitczuk, Z. W. Zhai, Q. Zhou, G. W. Huntley, Extracellular proteolysis by matrix metalloproteinase-9 drives dendritic spine enlargement and long-term potentiation coordinately. *Proc. Natl. Acad. Sci. U. S. A.* **105**, 19520–19525 (2008).

98. A. Vasin, L. Zueva, C. Torrez, D. Volfson, J. T. Littleton, M. Bykhovskaia, Synapsin regulates activity-dependent outgrowth of synaptic boutons at the Drosophila neuromuscular junction. *J. Neurosci.* **34**, 10554–10563 (2014).

99. K. R. Nesler, R. I. Sand, B. A. Symmes, S. J. Pradhan, N. G. Boin, A. E. Laun, S. A. Barbee, The miRNA Pathway Controls Rapid Changes in Activity-Dependent Synaptic Structure at the Drosophila melanogaster Neuromuscular Junction. *PLoS One*. **8**, e68385 (2013).

100. V. Y. Poon, S. Choi, M. Park, Growth factors in synaptic function. *Front. Synaptic Neurosci.* **5**, 6 (2013).

101. K. Shen, C. W. Cowan, Guidance Molecules in Synapse Formation and Plasticity. *Cold Spring Harb. Perspect. Biol.* **2**, a001842 (2010).

102. T. Wang, A. Hauswirth, A. Tong, D. Dickman, G. Davis, Endostatin is a Trans-Synaptic Signal for Homeostatic Synaptic Plasticity. *Neuron*. **83**, 616–629 (2014).

103. M. Packard, E. S. Koo, M. Gorczyca, J. Sharpe, S. Cumberledge, V. Budnik, The Drosophila Wnt, wingless,

provides an essential signal for pre- and postsynaptic differentiation. *Cell*. **111**, 319–330 (2002).

104. Z. D. Piccioli, J. T. Littleton, Retrograde BMP signaling modulates rapid activity-dependent synaptic growth via presynaptic LIM kinase regulation of cofilin. *J. Neurosci.* **34**, 4371–4381 (2014).
105. J. Rohrbough, M. S. Grotewiel, R. L. Davis, K. Broadie, Integrin-mediated regulation of synaptic morphology, transmission, and plasticity. *J. Neurosci.* **20**, 6868–6878 (2000).
106. D. Alicea, M. Perez, C. Maldonado, C. Dominicci-Cotto, B. Marie, Cortactin is a regulator of activity-dependent synaptic plasticity controlled by Wingless. *J. Neurosci.* **37**, 2203–2215 (2017).
107. W. M. Parkinson, M. Dookwah, M. L. Dear, C. L. Gatto, K. Aoki, M. Tiemeyer, K. Broadie, Synaptic roles for phosphomannomutase type 2 in a new Drosophila congenital disorder of glycosylation disease model. *Dis. Model. Mech.* **9**, 513–527 (2016).
108. N. Dani, H. Zhu, K. Broadie, Two Protein N-Acetylgalactosaminyl Transferases Regulate Synaptic Plasticity by Activity-Dependent Regulation of Integrin Signaling. *J. Neurosci.* **34**, 13047–13065 (2014).
109. I. M. Ethell, D. W. Ethell, Matrix metalloproteinases in brain development and remodeling: Synaptic functions and targets. *J. Neurosci. Res.* **85**, 2813–2823 (2007).
110. B. L. Patton, Laminins of the neuromuscular system. *Microsc. Res. Tech.* **51**, 247–261 (2000).
111. P.-I. Tsai, M. Wang, H.-H. Kao, Y.-J. Cheng, Y.-J. Lin, R.-H. Chen, C.-T. Chien, Activity-dependent retrograde laminin A signaling regulates synapse growth at Drosophila neuromuscular junctions. *Proc. Natl. Acad. Sci. U. S. A.* **109**, 17699–17704 (2012).
112. X. Shi, D. L. Jarvis, Protein N-glycosylation in the baculovirus-insect cell system. *Curr. Drug Targets*. **8**, 1116–11125 (2007).
113. B. Ewen-Campen, D. Yang-Zhou, V. R. Fernandes, D. P. González, L.-P. Liu, R. Tao, X. Ren, J. Sun, Y. Hu, J. Zirin, S. E. Mohr, J.-Q. Ni, N. Perrimon, Optimized strategy for in vivo Cas9-activation in Drosophila. *Proc. Natl. Acad. Sci.* **114**, 9409–9414 (2017).
114. A. Barik, B. Zhang, G. S. Sohal, W. C. Xiong, L. Mei, Crosstalk between Agrin and Wnt signaling pathways in development of vertebrate neuromuscular junction. *Dev. Neurobiol.* **74**, 828–838 (2014).
115. J. DeWit, M. L. O'Sullivan, J. N. Savas, G. Condomitti, M. C. Caccese, K. M. Vennekens, J. R. Yates, A. Ghosh, Unbiased discovery of Glypican as a receptor for LRRTM4 in regulating excitatory synapse development. *Neuron*. **79**, 696–711 (2013).
116. T. J. Edwards, M. Hammarlund, Syndecan promotes axon regeneration by stabilizing growth cone migration. *Cell Rep.* **8**, 272–283 (2014).
117. M. Gautam, P. G. Noakes, L. Moscoso, F. Rupp, R. H. Scheller, J. P. Merlie, J. R. Sanes, Defective

neuromuscular synaptogenesis in agrin-deficient mutant mice. *Cell*. **85**, 525–535 (1996).

118. M. Kaksonen, I. Pavlov, V. Voikar, S. E. Lauri, A. Hienola, R. Riekki, M. Lakso, T. Taira, H. Rauvala, Syndecan-3-deficient mice exhibit enhanced LTP and impaired hippocampus-dependent memory. *Mol. Cell. Neurosci.* **21**, 158–172 (2002).
119. T. J. Siddiqui, P. Tari, S. A. Connor, P. Zhang, F. A. Dobie, K. She, H. Kawabe, Y. Wang, N. Brose, A. Craig, An LRRTM4-HSPG complex mediates excitatory synapse development on dentate gyrus granule cells. *Neuron*. **79**, 680–695 (2013).
120. Y. Yamaguchi, Heparan sulfate proteoglycans in the nervous system: their diverse roles in neurogenesis, axon guidance, and synaptogenesis. *Semin. Cell Dev. Biol.* **12**, 99–106 (2001).
121. Y. Yamaguchi, M. Inatani, Y. Matsumoto, J. Ogawa, F. Irie, Roles of heparan sulfate in mammalian brain development Current views based on the findings from ext1 conditional knockout studies. *Prog. Mol. Biol. Transl. Sci.* **93**, 133–152 (2010).
122. A. Dityatev, G. Dityateva, V. Sytnyk, M. Delling, N. Toni, I. Nikonenko, D. Muller, M. Schachner, Polysialylated Neural Cell Adhesion Molecule Promotes Remodeling and Formation of Hippocampal Synapses. *J. Neurosci.* **24**, 9372–9382 (2004).
123. S. Korotchenko, L. a Cingolani, T. Kuznetsova, L. L. Bologna, M. Chiappalone, A. Dityatev, Modulation of network activity and induction of homeostatic synaptic plasticity by enzymatic removal of heparan sulfates. *Philos. Trans. R. Soc. Lond. B. Biol. Sci.* **369**, 20140134 (2014).
124. D. Minge, O. Senkov, R. Kaushik, M. K. Herde, O. Tikhobrazova, A. B. Wulff, A. Mironov, T. H. van Kuppevelt, A. Oosterhof, G. Kochlamazashvili, A. Dityatev, C. Henneberger, Heparan Sulfates Support Pyramidal Cell Excitability, Synaptic Plasticity, and Context Discrimination. *Cereb. Cortex*. **27**, 903–918 (2017).
125. F. Irie, H. Badie-Mahdavi, Y. Yamaguchi, Autism-like socio-communicative deficits and stereotypies in mice lacking heparan sulfate. *Proc. Natl. Acad. Sci. U. S. A.* **109**, 5052–5056 (2012).
126. F. E. Poulain, H. J. Yost, Heparan sulfate proteoglycans: a sugar code for vertebrate development? *Development*. **142**, 3456–3467 (2015).
127. S. H. Friedman, N. Dani, E. Rushton, K. Broadie, Fragile X mental retardation protein regulates trans-synaptic signaling in Drosophila. *Dis. Model. Mech.* **6**, 1400–1413 (2013).
128. S. D. Speese, J. Ashley, V. Jokhi, J. Nunnari, R. Barria, Y. Li, B. Ataman, A. Koon, Y.-T. Chang, Q. Li, M. J. Moore, V. Budnik, Nuclear envelope budding enables large ribonucleoprotein particle export during synaptic Wnt signaling. *Cell*. **149**, 832–846 (2012).

129. L. Blavier, A. Lazaryev, X. H. Shi, F. J. Dorey, G. M. Shackleford, Y. A. DeClerck, Stromelysin-1 (MMP-3) is a target and a regulator of Wnt1-induced epithelial-mesenchymal transition (EMT). *Cancer Biol. Ther.* **10**, 198–208 (2010).

130. I. Kondratiuk, S. Łęski, M. Urbańska, P. Biecek, H. Devijver, B. Lechat, F. van Leuven, L. Kaczmarek, T. Jaworski, GSK-3β and MMP-9 Cooperate in the Control of Dendritic Spine Morphology. *Mol. Neurobiol.* **54**, 200–211 (2017).

131. E. B. M. Landman, P. C. Periyasamy, C. A. van Blitterswijk, J. N. Post, M. Karperien, Distinct Effect of TCF4 on the NFκB Pathway in Human Primary Chondrocytes and the C20/A4 Chondrocyte Cell Line. *Cartilage*. **5**, 181–189 (2014).

132. B. Ma, C. van Blitterswijk, M. Karperien, Wnt/β-catenin negative feedback loop inhibits interleukin-1–induced matrix metalloproteinase expression in human articular chondrocytes. *Arthritis Rheumatol.* **64**, 2589–2600 (2012).

133. D. Yan, Y. Wu, Y. Feng, S.-C. Lin, X. Lin, The Core Protein of Glypican Daily-Like Determines Its Biphasic Activity in Wingless Morphogen Signaling. *Dev. Cell*. **17**, 470–481 (2009).

134. A. N. Fox, K. Zinn, The heparan sulfate proteoglycan syndecan is an in vivo ligand for the Drosophila LAR receptor tyrosine phosphatase. *Curr. Biol.* **15**, 1701–1711 (2005).

135. V. Kainulainen, H. M. Wang, C. Schick, M. Bernfield, Syndecans, heparan sulfate proteoglycans, maintain the proteolytic balance of acute wound fluids. *J. Biol. Chem.* **273**, 11563–11569 (1998).

136. V. C. Ramani, P. S. Pruett, C. A. Thompson, L. D. DeLucas, R. D. Sanderson, Heparan sulfate chains of syndecan-1 regulate ectodomain shedding. *J. Biol. Chem.* **287**, 9952–9961 (2012).

137. S. Sarrazin, W. C. Lamanna, J. D. Esko, Heparan sulfate proteoglycans. *Cold Spring Harb. Perspect. Biol.* **3**, a004952 (2011).

138. A. Srivastava, A novel link between FMR gene and the JNK pathway provides clues to possible role in malignant pleural mesothelioma. *FEBS Open Bio*. **5**, 705–711 (2015).

139. S. Schultz-Pedersen, H. Hasle, J. H. Olsen, U. Friedrich, Evidence of decreased risk of cancer in individuals with fragile X. *Am. J. Med. Genet.* **103**, 226–230 (2001).

140. C. G. Gkogkas, A. Khoutorsky, R. Cao, S. M. Jafarnejad, M. Prager-Khoutorsky, N. Giannakas, A. Kaminari, A. Fragkouli, K. Nader, T. J. Price, B. W. Konicek, J. R. Graff, A. K. Tzinia, J. C. Lacaille, N. Sonenberg, Pharmacogenetic Inhibition of eIF4E-Dependent Mmp9 mRNA Translation Reverses Fragile X Syndrome-like Phenotypes. *Cell Rep.* **9**, 1742–1756 (2014).

141. K. Lepeta, K. J. Purzycka, K. Pachulska-Wieczorek, M. Mitjans, M. Begemann, B. Vafadari, K. Bijata, R. W.

Adamiak, H. Ehrenreich, M. Dziembowska, L. Kaczmarek, A normal genetic variation modulates synaptic MMP-9 protein levels and the severity of schizophrenia symptoms. *EMBO*. **9**, 1100–1116 (2017).

142. A. Janusz, J. Milek, M. Perycz, L. Pacini, C. Bagni, L. Kaczmarek, M. Dziembowska, The Fragile X mental retardation protein regulates matrix metalloproteinase 9 mRNA at synapses. *J. Neurosci.* **33**, 18234–18241 (2013).
143. J. C. Darnell, S. J. Van Driesche, C. Zhang, K. Y. S. Hung, A. Mele, C. E. Fraser, E. F. Stone, C. Chen, J. J. Fak, S. W. Chi, D. D. Licatalosi, J. D. Richter, R. B. Darnell, FMRP stalls ribosomal translocation on mRNAs linked to synaptic function and autism. *Cell*. **146**, 247–261 (2011).
144. S. S. Siller, K. Broadie, Neural circuit architecture defects in a Drosophila model of Fragile X syndrome are alleviated by minocycline treatment and genetic removal of matrix metalloproteinase. *Dis. Model. Mech.* **4**, 673–685 (2011).
145. T. V Bilousova, L. Dansie, M. Ngo, J. Aye, J. R. Charles, D. W. Ethell, I. M. Ethell, Minocycline promotes dendritic spine maturation and improves behavioural performance in the fragile X mouse model. *J. Med. Genet.* **46**, 94–102 (2009).
146. H. Sidhu, L. E. Dansie, P. W. Hickmott, D. W. Ethell, I. M. Ethell, Genetic removal of matrix metalloproteinase 9 rescues the symptoms of fragile X syndrome in a mouse model. *J. Neurosci.* **34**, 9867–9879 (2014).
147. J. Titlow, L. Yang, R. Parton, A. Palanca, I. Davis, Super-Resolution Single Molecule FISH at the Drosophila Neuromuscular Junction. *Methods Mol. Biol.* **1649**, 163–175 (2018).
148. C. Lapointe, M. Wickens, RNA Tagging: Preparation of High-Throughput Sequencing Libraries. *Methods Mol. Biol.* **1649**, 455–471 (2018).
149. A. C. McMahon, R. Rahman, H. Jin, J. L. Shen, A. Fieldsend, W. Luo, M. Rosbash, Hijacking an RNA-editing enzyme to identify cell-specific targets of RNA-binding proteins. *Cell*. **165**, 742–753 (2016).
150. S. Nagarajan, S. S. Grewal, An investigation of nutrient-dependent mRNA translation in Drosophila larvae. *Biol. Open*. **3**, 1020–1031 (2014).
151. A. Thomas, P. J. Lee, J. E. Dalton, K. J. Nomie, L. Stoica, M. Costa-Mattioli, P. Chang, S. Nuzhdin, M. N. Arbeitman, H. A. Dierick, A Versatile Method for Cell-Specific Profiling of Translated mRNAs in Drosophila. *PLoS One*. **7**, e40276 (2012).
152. H. Pantazopoulos, S. Berretta, In sickness and in health: Perineuronal nets and synaptic plasticity in psychiatric disorders. *Neural Plast.* **2016**, 9847696 (2016).
153. B. D. McCabe, G. Marques, A. P. Haghighi, R. D. Fetter, M. L. Crotty, T. E. Haerry, C. S. Goodman, M. B.

O'Connor, The BMP homolog Gbb provides a retrograde signal that regulates synaptic growth at the Drosophila neuromuscular junction. *Neuron*. **39**, 241–254 (2003).

154. R. A. Baines, Synaptic strengthening mediated by bone morphogenetic protein-dependent retrograde signaling in the Drosophila CNS. *J. Neurosci.* **24**, 6904–6911 (2004).
155. V. Dudu, T. Bittig, E. Entchev, A. Kicheva, F. Julicher, M. Gonzalez-Gaitan, Postsynaptic mad signaling at the Drosophila neuromuscular junction. *Curr. Biol.* **16**, 625–635 (2006).
156. Y. Fuentes-Medel, J. Ashley, R. Barria, R. Maloney, M. Freeman, V. Budnik, Integration of a retrograde signal during synapse formation by glia-secreted TGF-β ligand. *Curr. Biol.* **22**, 1831–1838 (2012).
157. W. Parkinson, M. L. Dear, E. Rushton, K. Broadie, N-glycosylation requirements in neuromuscular synaptogenesis. *Development*. **140**, 4970–4981 (2013).
158. H. Aberle, A. P. Haghighi, R. D. Fetter, B. D. McCabe, T. R. Magalhaes, C. S. Goodman, wishful thinking encodes a BMP type II receptor that regulates synaptic growth in Drosophila. *Neuron*. **33**, 545–558 (2002).
159. G. Marques, H. Bao, T. E. Haerry, M. J. Shimell, P. Duchek, B. Zhang, M. B. O'Connor, The Drosophila BMP type II receptor wishful thinking regulates neuromuscular synapse morphology and function. *Neuron*. **33**, 529–543 (2002).
160. J. M. Rawson, M. Lee, E. L. Kennedy, S. B. Selleck, Drosophila neuromuscular synapse assembly and function require the TGF-beta type I receptor saxophone and the transcription factor mad. *J. Neurobiol.* **55**, 134–150 (2003).
161. B. D. McCabe, S. Hom, H. Aberle, R. D. Fetter, G. Marques, T. E. Haerry, H. Wan, M. B. O'Connor, C. S. Goodman, A. P. Haghighi, Highwire regulates presynaptic BMP signaling essential for synaptic growth. *Neuron*. **41**, 891–905 (2004).
162. B. A. Eaton, R. D. Fetter, G. W. Davis, Dynactin is necessary for synapse stabilization. *Neuron*. **34**, 729–741 (2002).
163. R. W. Ball, M. Warren-Paquin, K. Tsurudome, E. H. Liao, F. Elazzouzi, C. Cavanagh, B.-S. An, T.-T. Wang, J. H. White, A. P. Haghighi, Retrograde BMP signaling controls synaptic growth at the NMJ by regulating trio expression in motor neurons. *Neuron*. **66**, 536–549 (2010).
164. N. . M. Kim G., Identification of downstream targets of the Bone Morphogenetic Protein pathway in the Drosophila nervous system. *Dev. Dyn.* **239**, 2413–2425 (2010).
165. R. E. James, H. T. Broihier, Crimpy inhibits the BMP homolog Gbb in motoneurons to enable proper growth control at the Drosophila neuromuscular junction. *Development*. **138**, 3273–3286 (2011).

166. R. E. James, K. M. Hoover, D. Bulgari, C. N. McLaughlin, C. G. Wilson, K. A. Wharton, E. S. Levitan, H. T. Broihier, Crimpy Enables Discrimination of Presynaptic and Postsynaptic Pools of a BMP at the Drosophila Neuromuscular Junction. *Dev. Cell*. **31**, 586–598 (2014).

167. D. Martin, S. Zusman, X. Li, E. L. Williams, N. Khare, S. DaRocha, R. Chiquet-Ehrismann, S. Baumgartner, wing blister, a new Drosophila laminin alpha chain required for cell adhesion and migration during embryonic and imaginal development. *J. Cell Biol.* **145**, 191–201 (1999).

168. T. A. Godenschwege, N. Pohar, S. Buchner, E. Buchner, Inflated wings, tissue autolysis and early death in tissue inhibitor of metalloproteinases mutants of Drosophila. *Eur. J. Cell Biol.* **79**, 495–501 (2000).

169. R. Kashima, S. Roy, M. Ascano, V. Martinez-Cerdeno, J. Ariza-Torres, S. Kim, J. Louie, Y. Lu, P. Leyton, K. D. Bloch, T. B. Kornberg, P. J. Hagerman, R. Hagerman, G. Lagna, A. Hata, Augmented noncanonical BMP type II receptor signaling mediates the synaptic abnormality of fragile X syndrome. *Sci. Signal.* **9**, 58 (2016).

170. C. P. Goold, G. W. Davis, The BMP ligand Gbb gates the expression of synaptic horneostasis independent of synaptic growth control. *Neuron*. **56**, 109–123 (2007).

171. M. Nahm, M. Lee, W. Parkinson, M. Lee, H. Kim, Y.-J. Kim, S. Kim, Y. S. Cho, B. Min, Y. C. Bae, K. Broadie, S. Lee, Spartin Regulates Synaptic Growth and Neuronal Survival by Inhibiting BMP-Mediated Microtubule Stabilization. *Neuron*. **77**, 680–695 (2013).

172. R. Kashima, P. L. Redmond, P. Ghatpande, S. Roy, T. B. Kornberg, T. Hanke, S. Knapp, G. Lagna, A. Hata, Hyperactive locomotion in a Drosophila model is a functional readout for the synaptic abnormalities underlying fragile X syndrome. *Sci. Signal.* **10**, 8133 (2017).

173. C. M. Miller, N. Liu, A. Page-McCaw, H. T. Broihier, Drosophila Mmp2 Regulates the Matrix Molecule Faulty Attraction (Frac) to Promote Motor Axon Targeting in Drosophila. *J. Neurosci.* **31**, 5335–5347 (2011).

174. K. Sun, J. O. Westholm, K. Tsurudome, J. W. Hagen, Y. Lu, M. Kohwi, D. Betel, F. Gao, A. P. Haghighi, C. Q. Doe, E. C. Lai, Neurophysiological Defects and Neuronal Gene Deregulation in Drosophila mir-124 Mutants. *PLoS Genet.* **8**, e1002515 (2012).

175. X.-L. Xu, Y. Li, F. Wang, F.-B. Gao, The steady-state level of the nervous-system-specific microRNA-124a is regulated by dFMR1 in Drosophila. *J. Neurosci.* **28**, 11883–11889 (2008).

176. I. P. Sudhakaran, J. Hillebrand, A. Dervan, S. Das, E. E. Holohan, J. Hulsmeier, M. Sarov, R. Parker, K. VijayRaghavan, M. Ramaswami, FMRP and Ataxin-2 function together in long-term olfactory habituation and neuronal translational control. *Proc. Natl. Acad. Sci.* **111**, 99–108 (2014).

177. F. V Bolduc, K. Bell, H. Cox, K. Broadie, T. Tully, Excess protein synthesis in Drosophila Fragile X mutants impairs long-term memory. *Nat. Neurosci.* **11**, 1143–1145 (2008).

178. J. Rohrbough, K. Broadie, Anterograde jelly belly ligand to Alk receptor signaling at developing synapses is regulated by mind the gap. *Development*. **137**, 3523–3533 (2010).

179. J. Rohrbough, K. S. Kent, K. Broadie, J. B. Weiss, Jelly Belly Trans-Synaptic Signaling to Anaplastic Lymphoma Kinase Regulates Neurotransmission Strength and Synapse Architecture. *Dev. Neurobiol.* **73**, 189–208 (2013).

180. J. Rohrbough, E. Rushton, E. Woodruff, T. Fergestad, K. Vigneswaran, K. Broadie, Presynaptic establishment of the synaptic cleft extracellular matrix is required for post-synaptic differentiation. *Genes Dev.* **21**, 2607–2628 (2007).

181. E. Rushton, J. Rohrbough, K. Broadie, Presynaptic secretion of mind-the-gap organizes the synaptic extracellular matrix-integrin interface and postsynaptic environments. *Dev. Dyn.* **238**, 554–571 (2009).

182. E. Rushton, J. Rohrbough, K. Deutsch, K. Broadie, Structure-function analysis of endogenous lectin mind-the-gap in synaptogenesis. *Dev. Neurobiol.* **72**, 1161–1179 (2012).

183. H. H. Lee, A. Norris, J. B. Weiss, M. Frasch, Jelly belly protein activates the receptor tyrosine kinase Alk to specify visceral muscle pioneers. *Nature*. **425**, 507–512 (2003).

184. J. Singh, S. A. Aaronson, M. Mlodzik, Drosophila Abelson kinase mediates cell invasion and proliferation via two distinct MAPK pathways. *Oncogene*. **29**, 4033–4045 (2010).

185. P. Schlage, U. auf dem Keller, Proteomic approaches to uncover MMP function. *Matrix Biol.* **44–46**, 232–238 (2015).

186. U. Eckhard, G. Marino, G. S. Butler, C. M. Overall, Positional proteomics in the era of the human proteome project on the doorstep of precision medicine. *Biochimie*. **122**, 110–118 (2016).

187. P. F. Lange, C. M. Overall, Protein TAILS: When termini tell tales of proteolysis and function. *Curr. Opin. Chem. Biol.* **17**, 73–82 (2013).

188. I. Erdmann, K. Marter, O. Kobler, S. Niehues, J. Abele, A. Müller, J. Bussmann, E. Storkebaum, T. Ziv, U. Thomas, D. C. Dieterich, Cell-selective labelling of proteomes in Drosophila melanogaster. *Nat. Commun.* **6**, 7521 (2015).

189. F. I. Hinz, D. C. Dieterich, E. M. Schuman, Teaching old NCATs new tricks: Using non-canonical amino acid tagging to study neuronal plasticity. *Curr. Opin. Chem. Biol.* **17**, 738–746 (2013).

190. S. Tom Dieck, L. Kochen, C. Hanus, M. Heumller, I. Bartnik, B. Nassim-Assir, K. Merk, T. Mosler, S. Garg, S. Bunse, D. A. Tirrell, E. M. Schuman, Direct visualization of newly synthesized target proteins in situ.

Nat. Methods. **12**, 411–414 (2015).

191. M. Toegel, G. Azzam, E. Y. Lee, D. J. H. F. Knapp, Y. Tan, M. Fa, T. A. Fulga, A multiplexable TALE-based binary expression system for in vivo cellular interaction studies. *Nat. Commun.* **8**, 1663 (2017).

192. Y. Gong, L. Pan, Recent advances in bioorthogonal reactions for site-specific protein labeling and engineering. *Tetrahedron Lett.* **56**, 2123–2132 (2015).

APPENDIX

Supplementary Figures

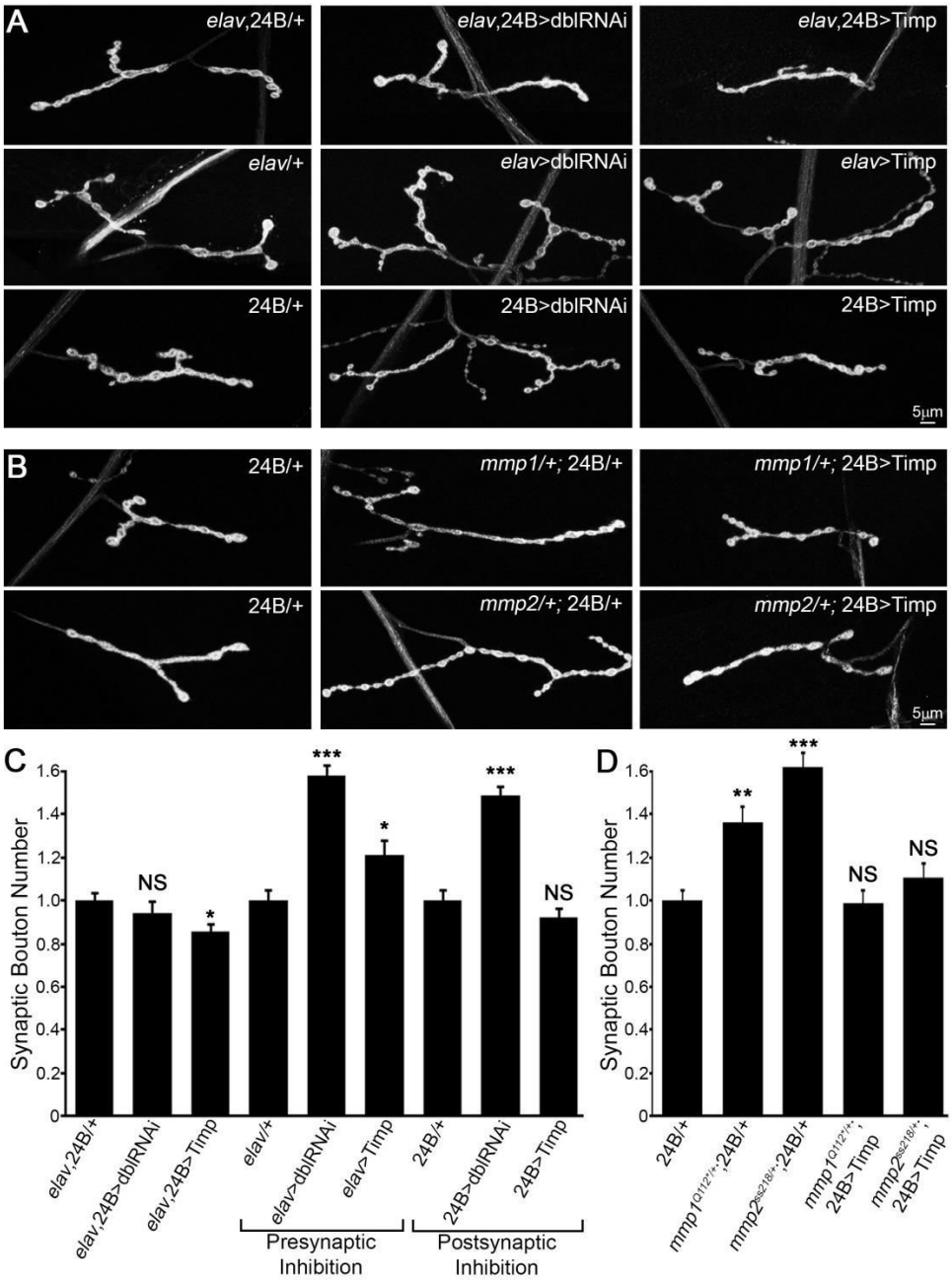

Figure S1

Figure S1: Postsynaptic Timp expression suppresses NMJ morphology defects.
(A) Representative wandering 3rd instar NMJs labeled for synaptic markers α-HRP and α-Dlg. Top row: Recombined dual pre- and postsynaptic *elav, 24B*/+ transgenic control (left), *elav, 24B*>*mmp1+2*^{RNAi} knockdown (dblRNAi; center) and *elav, 24B*>UAS-Timp (Timp; right). Middle row: *elav*/+ transgenic control (left), *elav*>dblRNAi (center), and *elav*>Timp (right). Bottom row: *24B*/+ transgenic control (left), *24B*>dblRNAi (center), and *24B*>Timp. **(B)** NMJs labeled for synaptic markers α-HRP and α-Dlg in specified genotypes. Top row: *24B*/+ transgenic control (left), *mmp1*^{Q112*}/+; *24B*/+ (center) and *mmp1*^{Q112*}/+; *24B*>Timp (right). Bottom row: *24B*/+ transgenic control (left), *mmp2*^{ss218}/+; *24B*/+ (center) and *mmp2*^{ss218}/+; *24B*>Timp (right). **(C)** Quantification of synaptic bouton number normalized to controls from genotypes shown in above (A). **(D)** Quantification of synaptic bouton number normalized to controls from genotypes shown in above (B). Significance: *p<0.05, **p<0.01, ***p<0.001 and not significant (NS). See Table S1A for raw data values and sample sizes.

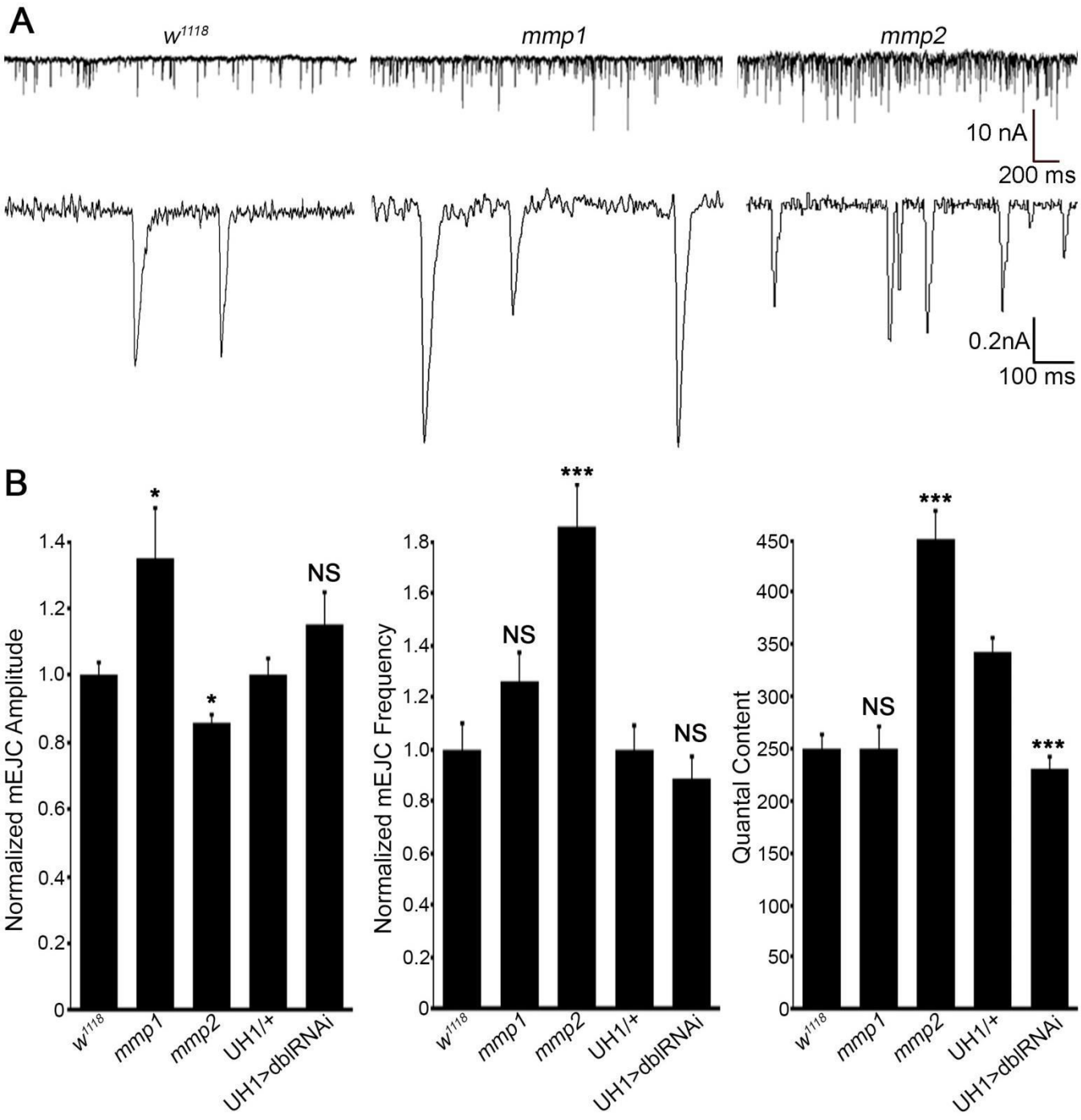

Figure S2

Figure S2: Mmp1 and Mmp2 regulate spontaneous SV fusion rate and response amplitude. (A) Representative spontaneous miniature EJC (mEJC) two-electrode voltage-clamp (TEVC) recording traces in genetic control (w^{1118}), *mmp1* ($mmp1^{Q273*}$) and *mmp2* ($mmp2^{W307*/Df}$) mutants. Top: Sample long time scale recordings of mEJC events for all 3 genotypes. Bottom: Magnified mEJC event traces for all 3 genotypes. **(B)** Quantification of mEJC amplitude (left), mEJC frequency (middle) and quantal content (right) normalized to respective control conditions. Significance indicated as **P*<0.05, ****P*<0.001 and not significant (NS). See Table S2B for raw data values and sample sizes.

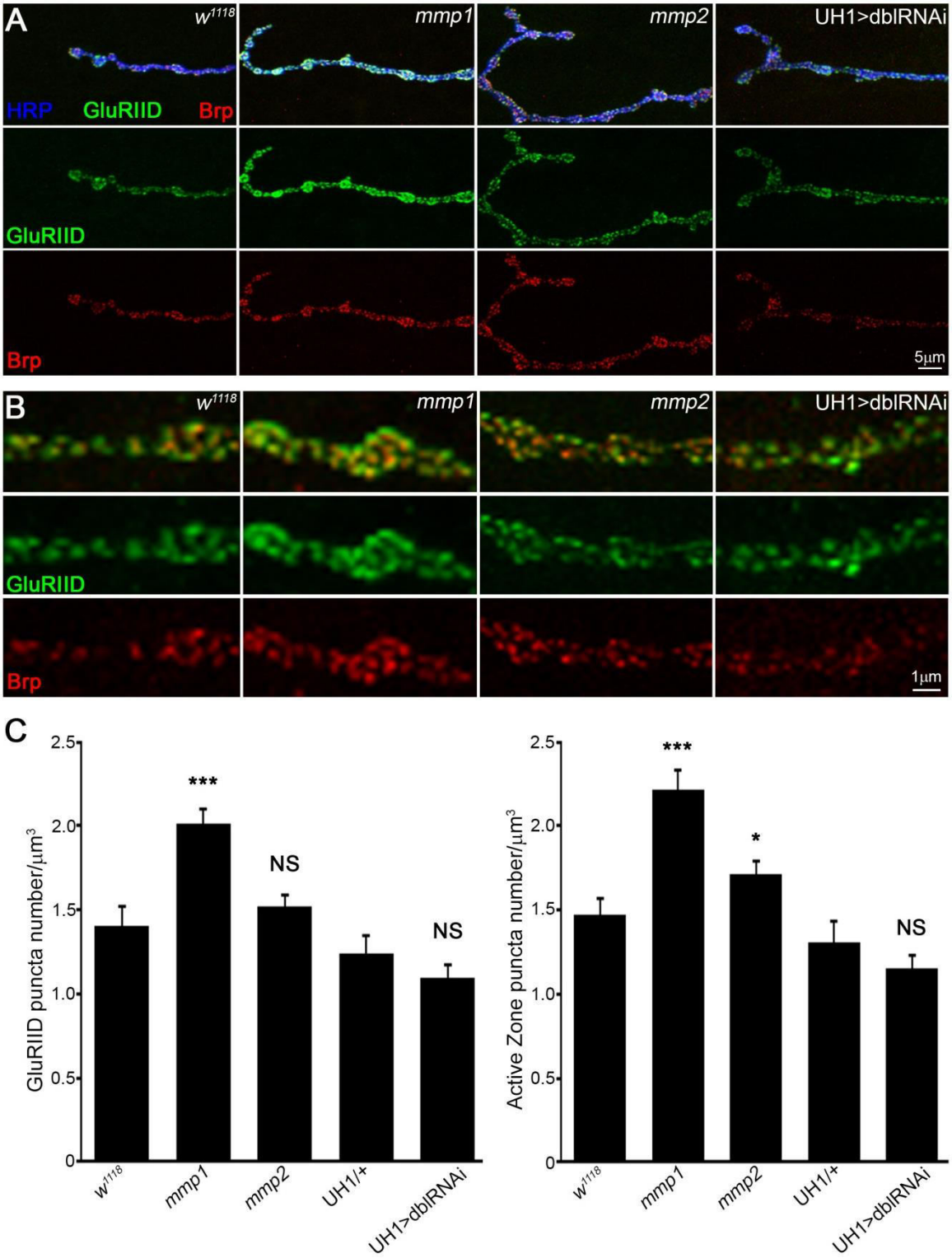

Figure S3

Figure S3: Loss of Mmp1 and Mmp2 differentially regulate NMJ molecular assembly. (A) Representative low magnification images wandering 3rd instar NMJs triple-labeled for synaptic membrane marker α-HRP (blue), core glutamate receptor subunit (GluRIID, green) and presynaptic active zone marker Bruchpilot (Brp, red) in genetic background control (w^{1118}), *mmp* mutants ($mmp1^{Q112*/Q273*}$ and $mmp2^{ss218/Df}$) and the double *mmp* RNAi condition (UH1>$mmp1+2^{RNAi}$ (dblRNAi)). (B) Higher magnification images of synaptic boutons from the same genotypes. (C) Quantification of GluRIID puncta number (left) and Brp puncta number (right) normalized to bouton volume. Significance indicated as *p<0.05, **p<0.01, ***p<0.001 and not significant (NS) based on Mann-Whitney tests. See Tables S1B and S2C for raw data values and sample sizes.

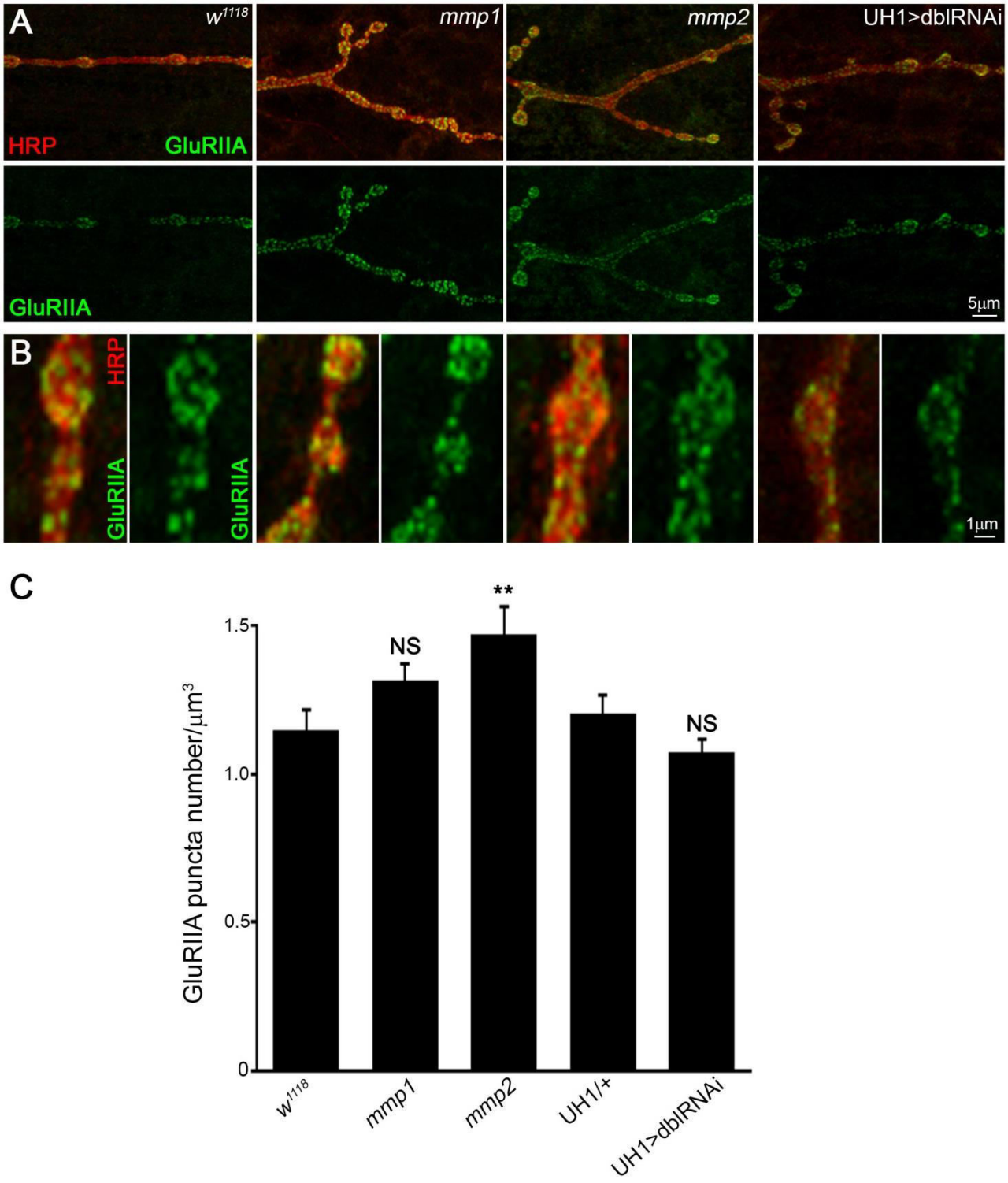

Figure S4

Figure S4: Mmp2 negatively regulates GluRIIA-containing receptors. (A) Representative low magnification images of wandering 3rd instar NMJs co-labeled for the GluRIIA subunit (green) and the synaptic membrane marker α-HRP (red) in genetic background control (w^{1118}), *mmp* mutants ($mmp1^{Q112*/Q273*}$ and $mmp2^{ss218/Df}$) and UH1>$mmp1+2^{RNAi}$ condition (dblRNAi). Bottom row shows GluRIIA subunit (green) labeling alone. (B) Higher magnification images of synaptic boutons from the same genotypes. Right panels show GluRIIA subunit (green) labeling alone. (C) Quantification of GluRIIA puncta number normalized to bouton volume. Significance indicated as **p<0.01 and not significant (NS). See Tables S1B and S2C for raw data values and sample sizes.

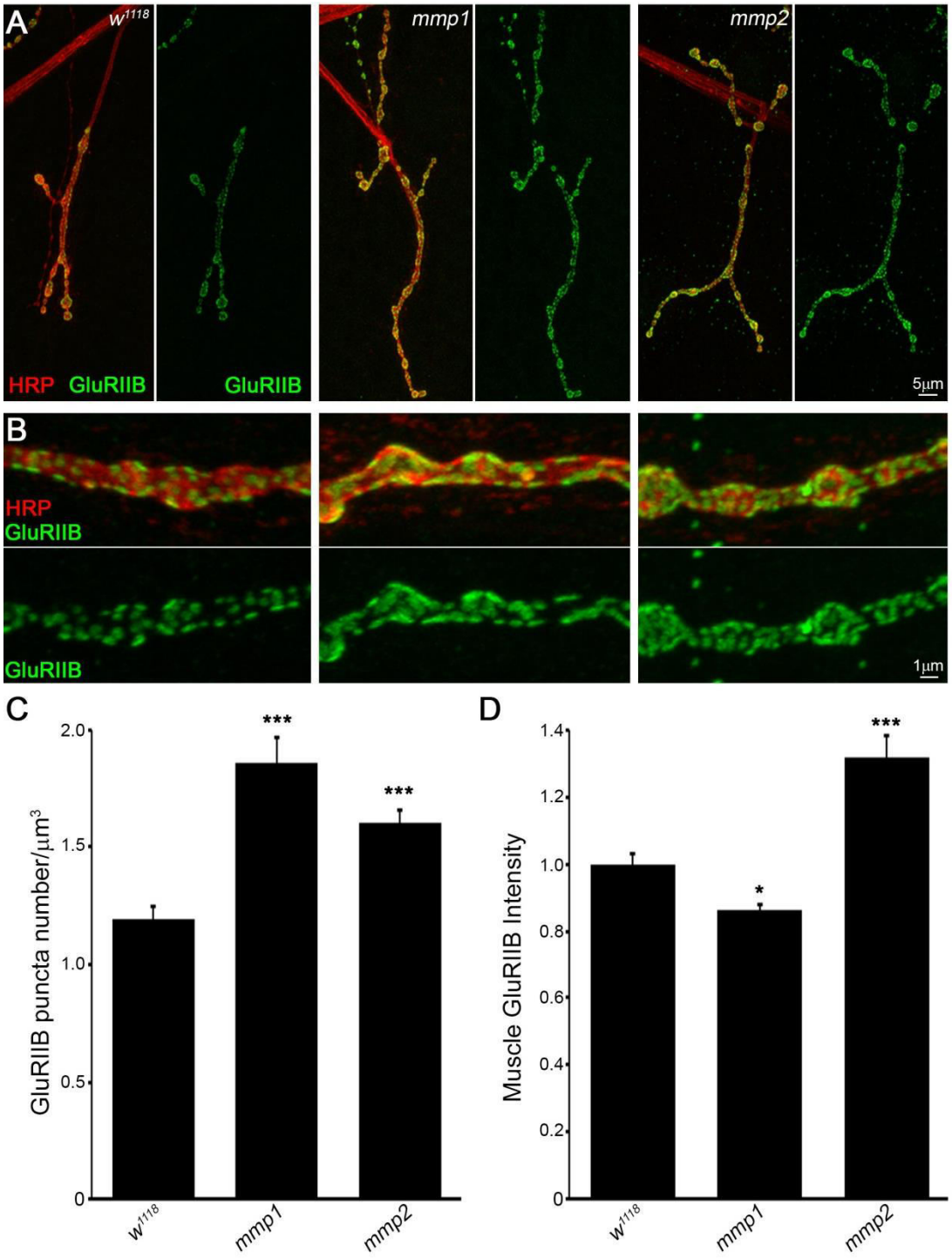

Figure S5

Figure S5: Mmp1 and Mmp2 negatively regulate GluRIIB-containing receptors. (A) Representative low magnification images of wandering 3rd instar NMJs co-labeled for the GluRIIB subunit (green) and synaptic membrane marker α-HRP (red) in genetic background control (*w* ^{1118}, left), *mmp1* (*mmp1*$^{Q112*/Q273*}$, middle) and *mmp2* (*mmp2*$^{ss218/Df}$, right). (B) Higher magnification images of synaptic boutons from the same genotypes. (C) Quantification of GluRIIB puncta number normalized to bouton volume. (D) Quantification of GluRIIB intensity in the muscle of each genotype normalized to genetic control. Significance indicated as *p<0.05, ***p<0.001 and not significant (NS). See Tables S1B and S2C for raw values and sample sizes.

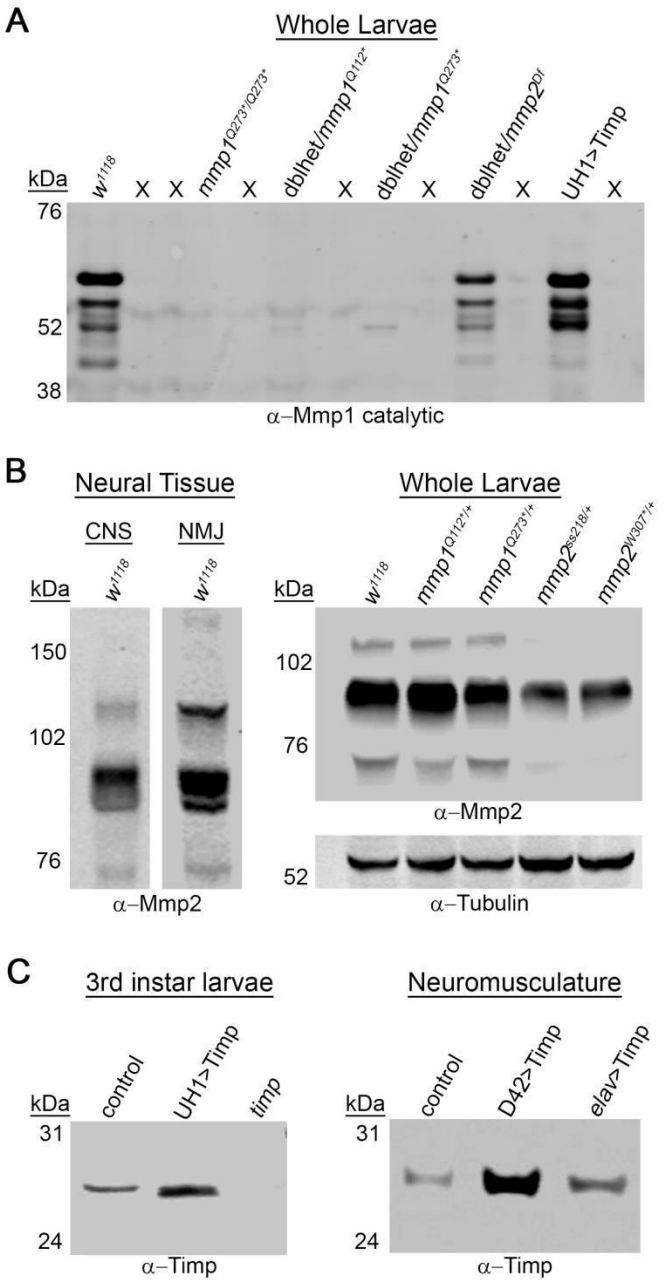

Figure S6

Figure S6: Western blot characterization and specificity of Mmp2 and Timp antibodies. (A) Western blot shows Mmp1 immunoreactivity in wandering 3rd instar whole larval tissue from genetic background control (w^{1118}), strong Mmp1 hypomorph ($mmp1^{Q273*}$), three different $mmp1^{Q112*/+}$,$mmp2^{W307*/+}$ double, heterozygous (dblhet) dosage combinations (dblhet/$mmp1^{Q112*}$; dblhet/$mmp1^{Q273*}$; dblhet/$mmp2^{Df}$) and the ubiquitous double inhibition condition (UH1>Timp). The 74kDa band corresponds to a predicted GPI-anchored Mmp1 isoform while the 64, 52 and 46 kDa bands correspond to secreted and activated Mmp1 isoforms. (B) Left: α-Mmp2 Western blots from 3rd instar central nervous system (CNS, left) and neuromusculature (NMJ, right) lysates from control (w^{1118}). Right: Whole larvae α-Mmp2 Western blots from w^{1118}, two *mmp1* heterozygotes ($mmp1^{Q112*/+}$, $mmp2^{Q273*/+}$) and two *mmp2* heterozygotes ($mmp2^{ss218/+}$, $mmp2^{W307*/+}$). Predominant ~90kDa band corresponds to predicted Mmp2 activated/processed form, and fainter ~120kDa band corresponds to predicted full-length/pre-processed Mmp2 form. Source of the ~76 kDa Mmp2 immunoreactive band is unknown. (C) Left: α-Timp Western blot of wandering 3rd instar larvae shows a single ~28kDa band at the predicted Timp molecular weight in transgenic control animals (UH1/+), which is elevated by transgenic Timp overexpression (UH1>Timp) and absent in *timp* null mutants. Right: α-Timp Western blot of isolated neuromusculature from transgenic control (D42/+), motor neuron D42>Timp and panneuronal *elav*>Timp shows endogenous and overexpressed Timp.

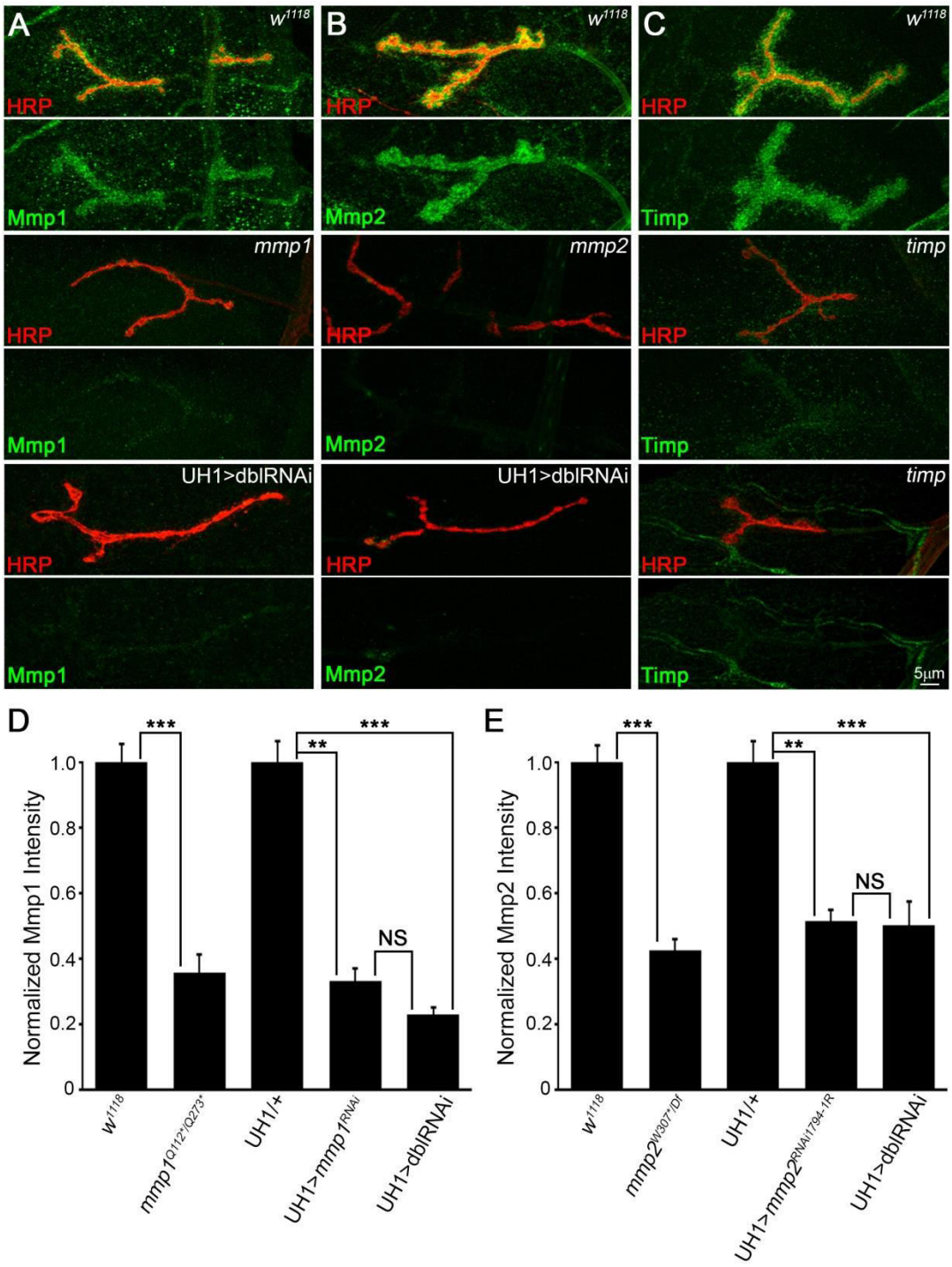

Figure S7

Figure S7: Imaging characterization and specificity of Mmp2 and Timp antibodies. (A) Representative images of α-Mmp1 (green) co-labeled with the NMJ marker α- HRP (red) in w^{1118} genetic control (top), $mmp1^{Q112*/Q273*}$ mutant (middle) and with UH1>$mmp1{+}2^{RNAi}$ (dblRNAi, bottom panel). (B) α-Mmp2 (green) co-labeled with α-HRP (red) in w^{1118} (top), $mmp2^{W307*/Df}$ mutant (middle) and UH1>dblRNAi, (bottom). (C) α-Timp (green) co-labeled with α-HRP (red) in w^{1118} (top) and *timp* mutants (middle and bottom panels). (D) Quantification of Mmp1 fluorescent intensity normalized to genetic controls (w^{1118}, UH1) for $mmp1^{Q112*/Q273*}$, UH1>$mmp1^{RNAi}$ and UH1>dblRNAi. (E) Quantification of Mmp2 fluorescent intensity normalized to genetic controls (w^{1118}, UH1) for $mmp2^{W307*/Df}$, UH1>$mmp2^{RNAi1794\text{-}1R}$ and UH1>dblRNAi. Significance indicated as **p<0.01, ***p<0.001 and not significant (NS). See Table S4A for raw data values and sample sizes.

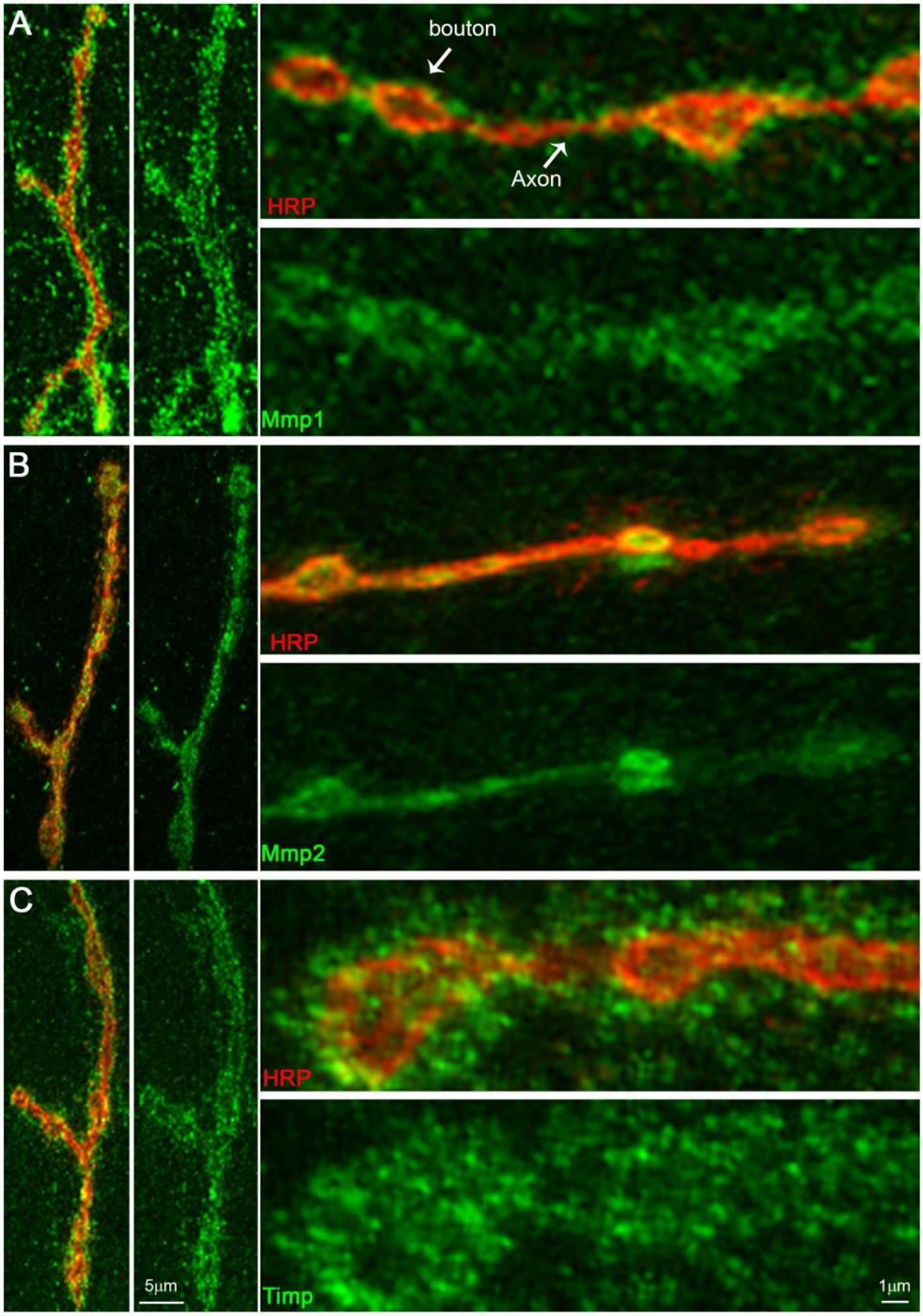

Figure S8

Figure S8: Characterization of Mmp1, Mmp2 and Timp localization at the NMJ. Representative wandering 3rd instar NMJ images from w^{1118} control animals showing (A) α- Mmp1 (green), (B) α-Mmp2 (green) and (C) α-Timp (green) relative to α-HRP presynaptic membrane marker (red) at low (left) and high (right) magnifications. Arrows label a representative bouton and axon/inter-bouton space.

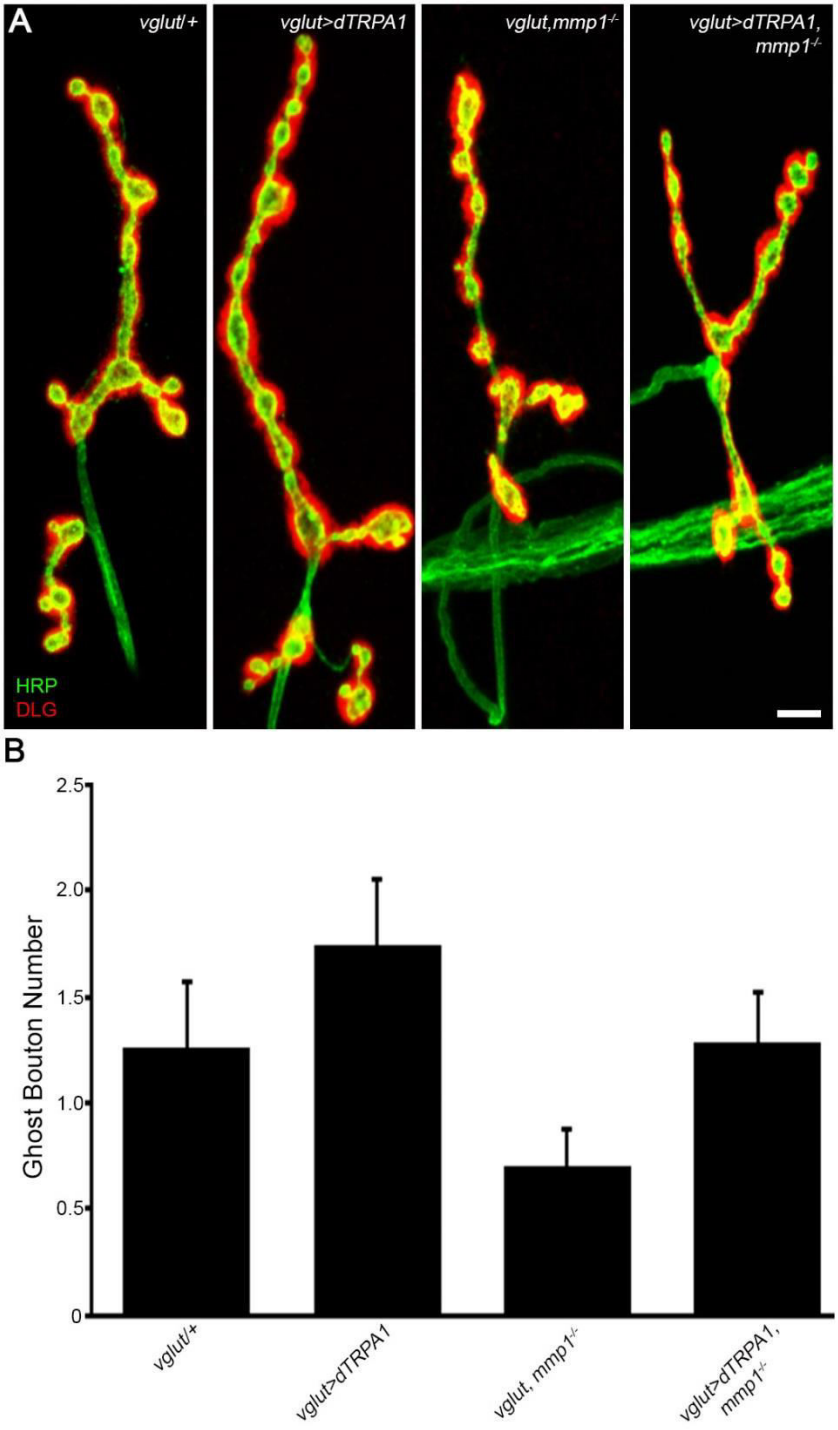

Figure S9

Figure S9. Temperature controls for dTRPA1 activity-induced synaptic bouton formation. (A) Animals from the 4 genotypes shown were raised at 18°C to the wandering third instar stage, and then the NMJs were co-labeled for presynaptic HRP and postsynaptic DLG. Scale bar: 5 μm. (B) Quantification of ghost bouton number: *vglut-Gal4*/+ (N=23, 1.26±0.31), *vglut-Gal4>UAS-dTRPA1* (N=35, 1.74±0.31), *vglut-Gal4,mmp1*^{Q112*}/*mmp1*^{Q112*} (N=34, 0.71±0.17) and *vglut-Gal4>UAS-dTRPA1,mmp1*^{Q112*}/*mmp1*^{Q112*} (N=42, 1.29±0.24). The significance was determined by nonparametric ANOVA (Kruskal-Wallis) and Dunn's multiple comparisons post-test. All comparisons were non-significant (p>0.05). Data show mean ± SEM from at least 3 independent replicates, with N representing the NMJ number.

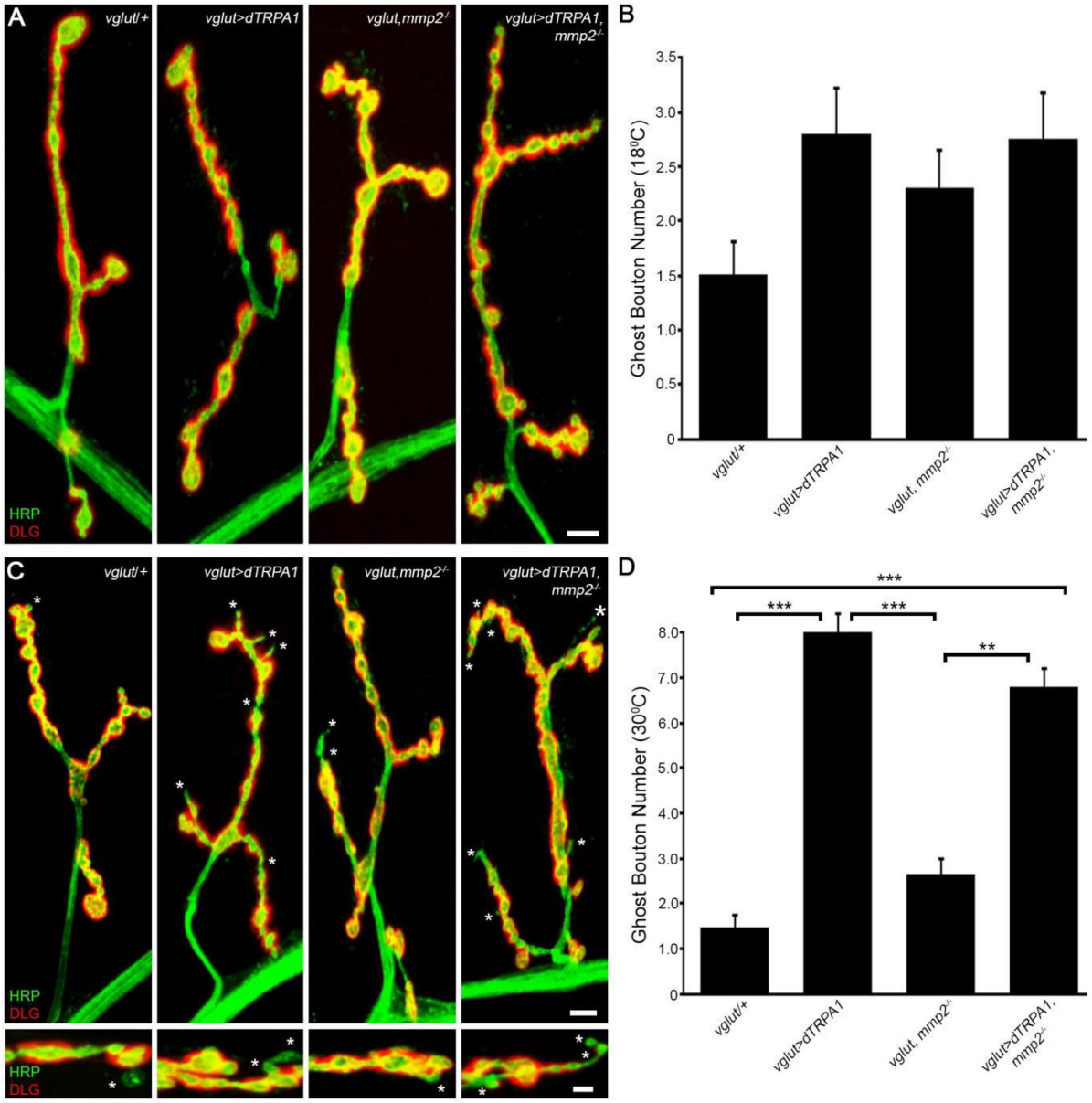

Figure S10

Figure S10. Mmp2 is not required for activity-dependent synaptic bouton formation. (A,C) NMJs co-labeled for HRP and DLG at 18°C (A) or after dTRPA1 activity stimulation (C) in the 4 genotypes shown. Scale bars: 5 μm. Higher magnification images of synaptic boutons are shown in (C). Scale bar: 2 μm. White asterisks mark ghost boutons. (B) Quantification of the ghost bouton number at constant 18°C: *vglut-Gal4/+* (N=29, 1.52±0.3), *vglut-Gal4>UAS-dTRPA1* (N=25, 2.8±0.42), *vglut-Gal4, mmp2^{W307*}/Df(2R)BSC132* (N=23, 2.3±0.34) and *vglut-Gal4>UAS-dTRPA1,mmp2^{W307*}/Df(2R)BSC132* (N=20, 2.75±0.42). Significance was determined by nonparametric ANOVA (Kruskal-Wallis) and Dunn's multiple comparisons post-test. All comparisons were non-significant (p>0.05). (D) Quantified ghost bouton number following dTRPA1 activation (1-hour at 30°C): *vglut-Gal4/+* (N=26, 1.46±0.31), *vglut-Gal4>UAS-dTRPA1* (N=28, 8.0±0.83), *vglut-Gal4, mmp2^{W307*}/ Df(2R)BSC132* (N=26, 2.65±0.36) and *vglut-Gal4>UAS-dTRPA1,mmp2^{W307*}/Df(2R)BSC132* (N=24, 6.79±0.79). Significance was determined by nonparametric ANOVA (Kruskal-Wallis) and Dunn's multiple comparisons post-test, and indicated as ***p<0.001 and **p<0.01. Non-significant (p>0.05) comparisons 1) *vglut-Gal4/+* vs. *vglut-Gal4, mmp2^{W307*}/Df(2R)BSC132* and 2) *vglut-Gal4>UAS-dTRPA1* vs. *vglut-Gal4> UAS-dTRPA1,mmp2^{W307*}/Df(2R)BSC132* are not shown. Data show mean ± SEM from at least 3 independent replicates, with N = NMJ number.

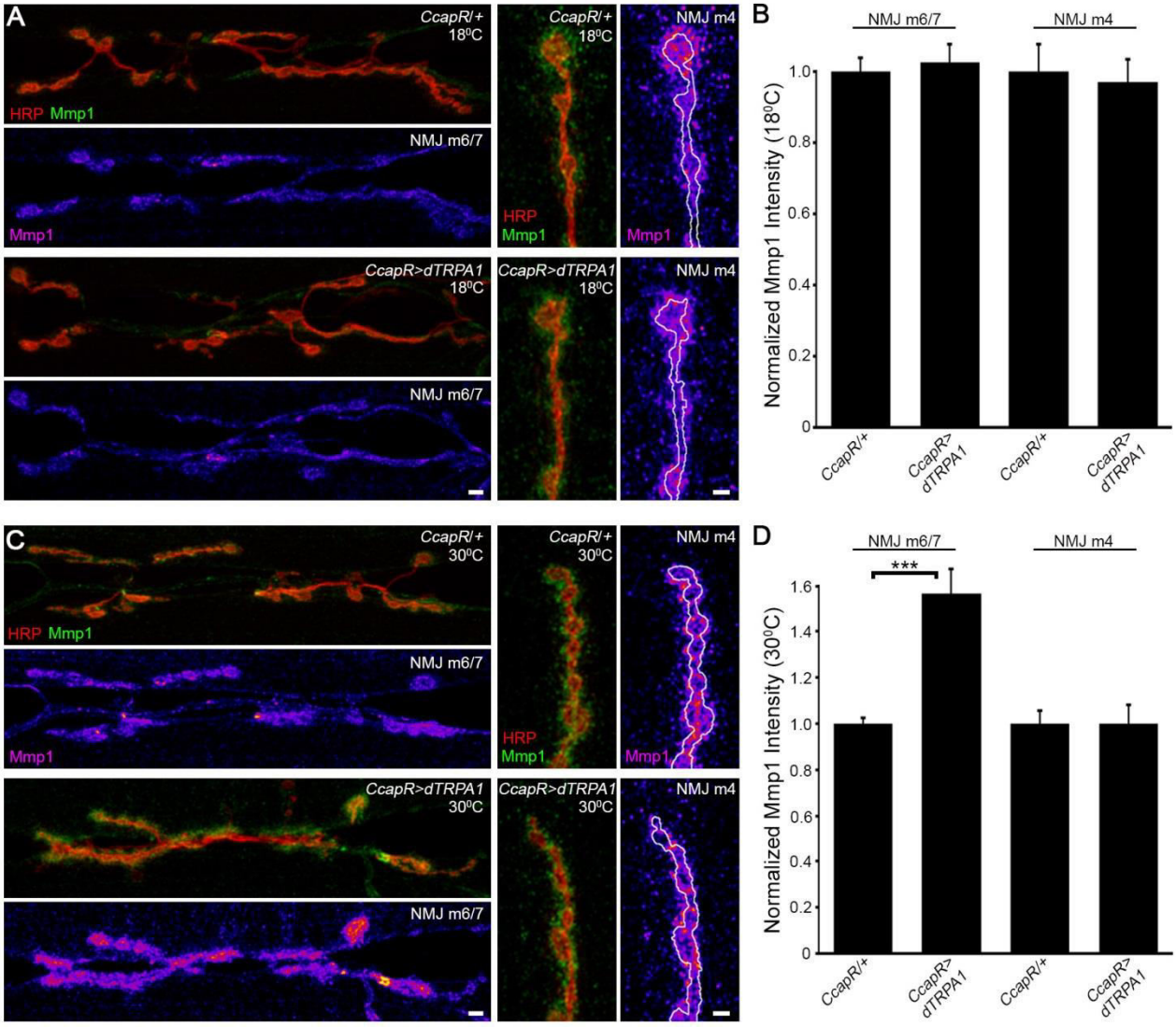

Figure S11

Figure S11. Mmp1 is rapidly and specifically increased following dTRPA1 neuronal stimulation. (A,C) Images show NMJs co-labeled with HRP and Mmp1 at m6/7 NMJ (scale bar: 5 μm) and m4 NMJ (scale bar: 2 μm) in animals reared at dTRPA1-restrictive 18°C (A) or following dTRPA1 stimulation at 30°C for 1 hour (C) in the genotypes indicated. Mmp1 intensity is shown as a heat map. (B) Quantification of normalized Mmp1 intensity in the dTRPA1-restrictive condition at m6/7 and m4 NMJs: *CcapR-Gal4/+* m6/7 NMJ (N=12, 1.0±0.04) vs. *CcapR-Gal4>UAS-dTRPA1* m6/7 NMJ (N=12, 1.03±0.05) and *CcapR-Gal4/+* m4 NMJ (N=16, 1.0±0.08) vs. *CcapR-Gal4>UAS-dTRPA1* m4 NMJ (N=14, 0.97±0.07). Significance determined by Unpaired t-test with Welch correction was non-significant for both ($p>0.05$) and is not shown. (D) Quantification of normalized Mmp1 intensity in the dTRPA1-permissive condition at m6/7 and m4 NMJs: *CcapR-Gal4/+* m6/7 NMJ (N=16, 1.0±0.03) vs. *CcapR-Gal4>UAS-dTRPA1* m6/7 NMJ (N=13, 1.57±0.1) and *CcapR-Gal4/+* m4 NMJ (N=21, 1.0±0.05) vs. *CcapR-Gal4>UAS-dTRPA1* m4 NMJ (N=24, 0.99±0.08). Significance determined by Unpaired t-test with Welch correction (NMJ m6/7), indicated by ***$p<0.001$. Data show mean ± SEM from at least 3 independent replicates, with N = NMJ number.

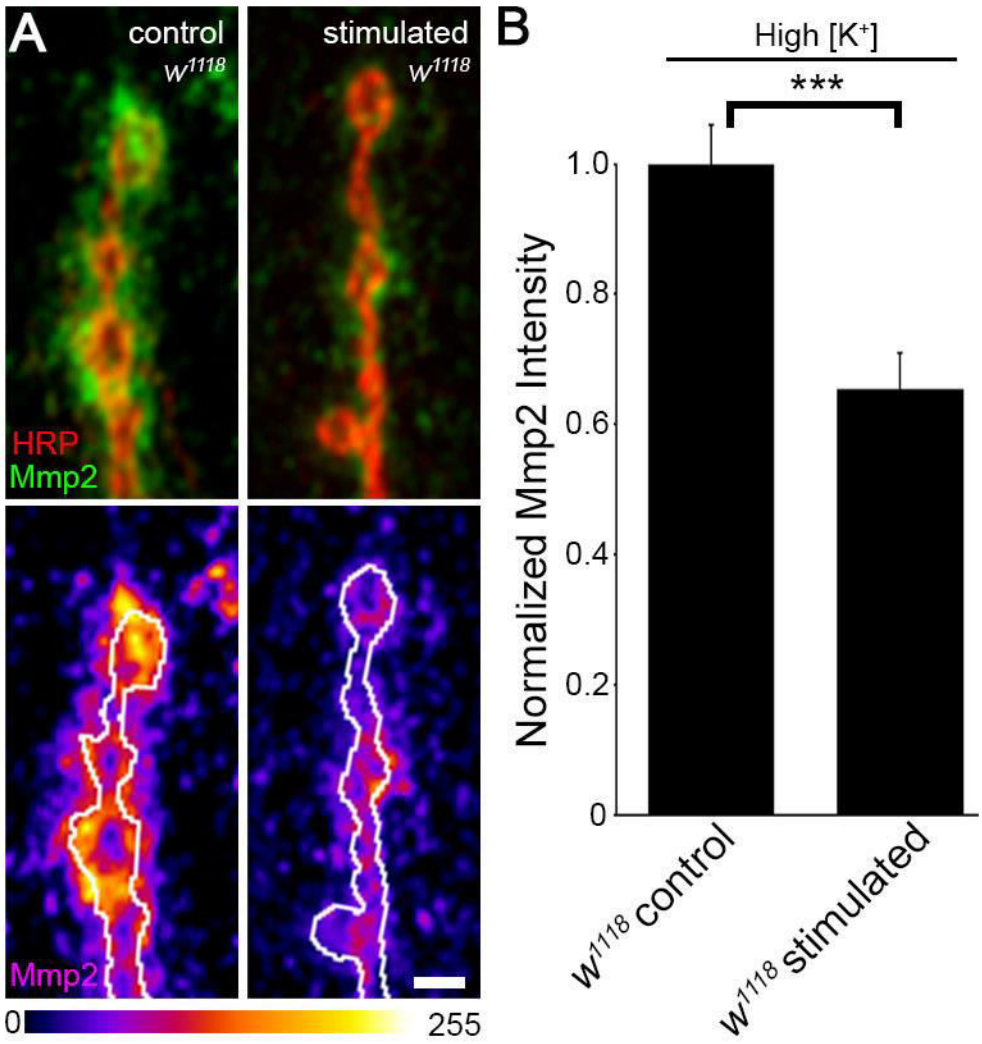

Figure S12

Figure S12. Synaptic Mmp2 is rapidly reduced following acute neuronal stimulation. (A) Images show NMJs co-labeled for HRP and Mmp2 in either the w^{1118} mock-treated (control) or following 10 minute high [K^+] stimulation. Heat map shows Mmp2 alone (with intensity scale below) and HRP synaptic outlines in white. Scale bar: 2 μm. (B) Quantification of Mmp2 fluorescent intensity normalized to the unstimulated controls: w^{1118} control (unstimulated, N=25, 1.0±0.06) vs. w^{1118} stimulated (high [K^+], N=28, 0.66±0.06). Significance was determined by Unpaired t-test, indicated as ***p<0.001. Data show mean ± SEM from at least 3 independent experimental replicates, with N = NMJ number.

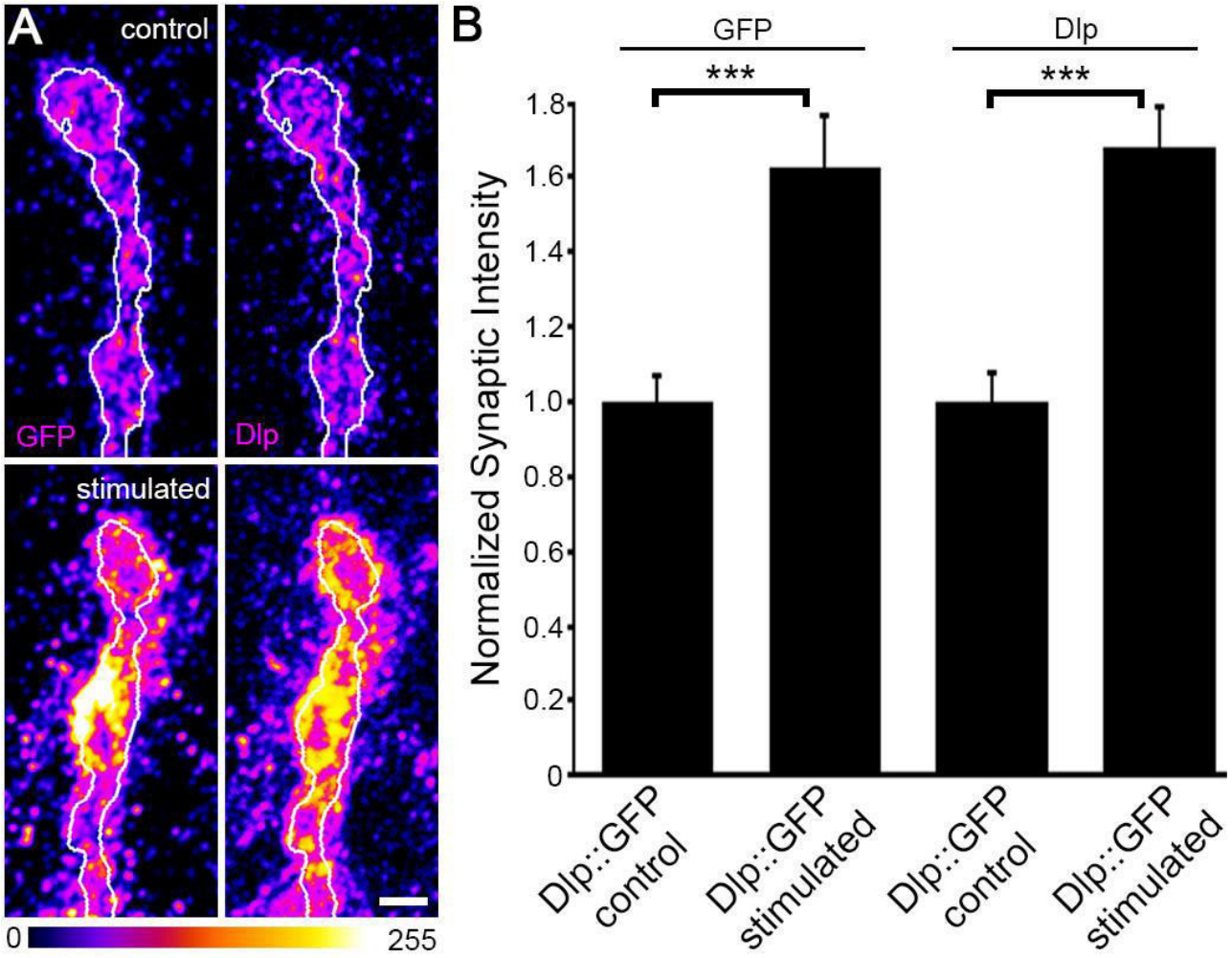

Figure S13

Figure S13 Synaptic Dlp is rapidly increased following acute neuronal stimulation. (A) Images show NMJs from Dlp::GFP animals co-labeled for GFP and Dlp under standard conditions (control) or following 10 minutes high [K^+] stimulation. Dlp::GFP and Dlp are shown as a heat map (with intensity scale below) and HRP synaptic outlines in white. Scale bar: 2 μm. (B) Quantification of GFP and Dlp fluorescence intensities normalized to unstimulated controls. GFP: control (N=24, 1.0±0.07) vs. stimulated (N=23, 1.62±0.14) and Dlp: control (N=14, 1.0±0.07) vs. stimulated (N=15, 1.68±0.11). Significance was determined by Unpaired t-test with Welch correction, indicated as ***p<0.001. Data show mean ± SEM from at least 3 independent replicates, with N = NMJ number.

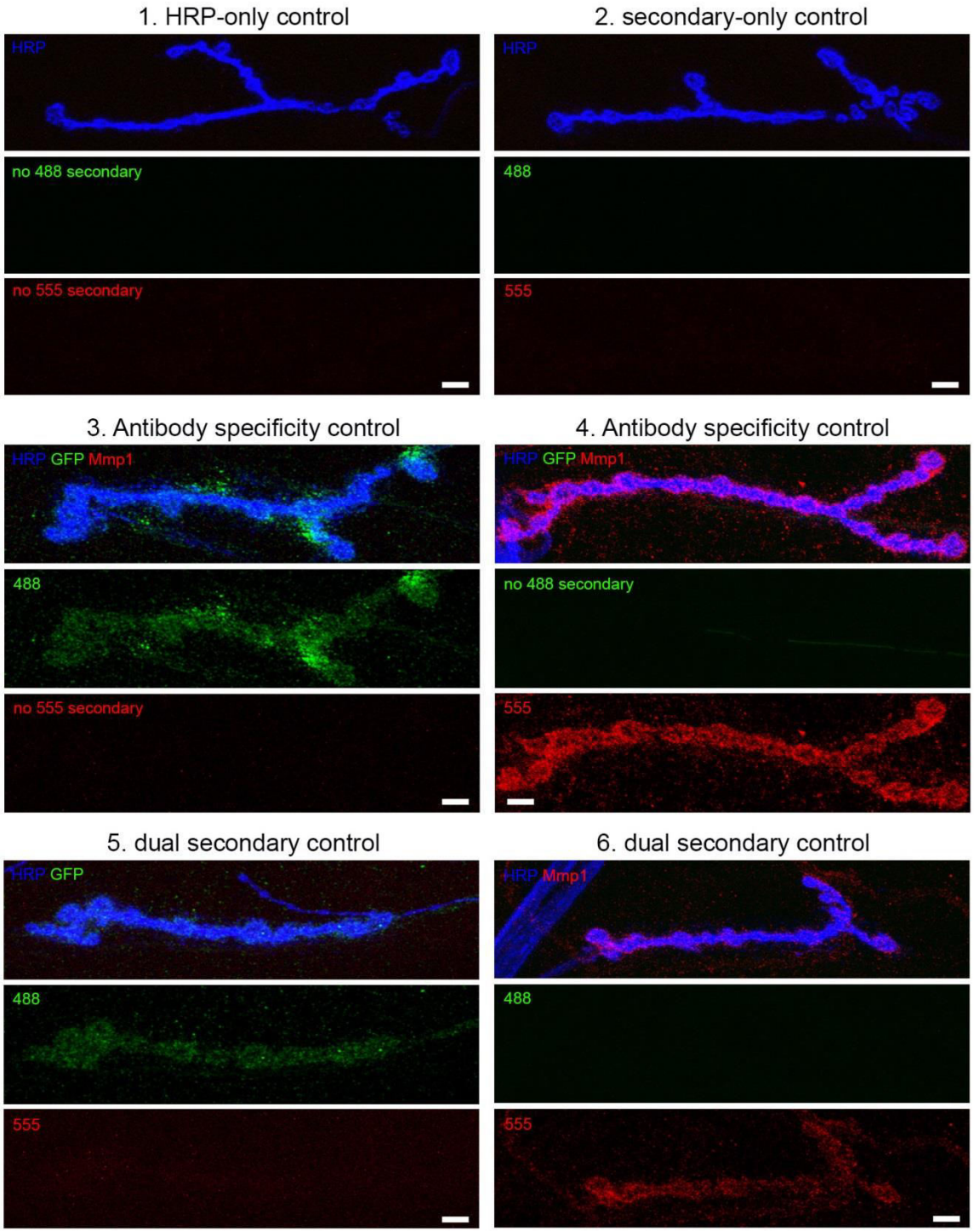

Figure S14

Figure S14. Synaptic Mmp1 and Dlp imaging controls at the NMJ terminal. Confocal images of Dlp::GFP NMJs labeled with denoted primary (specified in top panels) and secondary antibodies (specified in the middle and bottom panels), processed side-by-side with studies shown in Figure 3. Scale bars: 2 μm. All conditions included HRP::Cy5 to mark NMJs. Controls included: control 1 terminals labeled with HRP alone; control 2 terminals labeled with HRP and secondary antibodies only (rabbit::488 and mouse::555); control 3 terminals labeled with three primary antibodies (HRP, GFP and Mmp1) but incubated with rabbit::488 secondary only; control 4 terminals labeled with three primary antibodies (HRP, GFP, and Mmp1) and then incubated with mouse::555 secondary only; control 5 terminals labeled with the two primary antibodies (HRP and GFP) and then incubated with the two secondary antibodies (rabbit::488 and mouse::555); and control 6 terminals labeled with two primary antibodies (HRP and Mmp1) and then incubated with the two secondary antibodies (rabbit::488 and mouse::555).

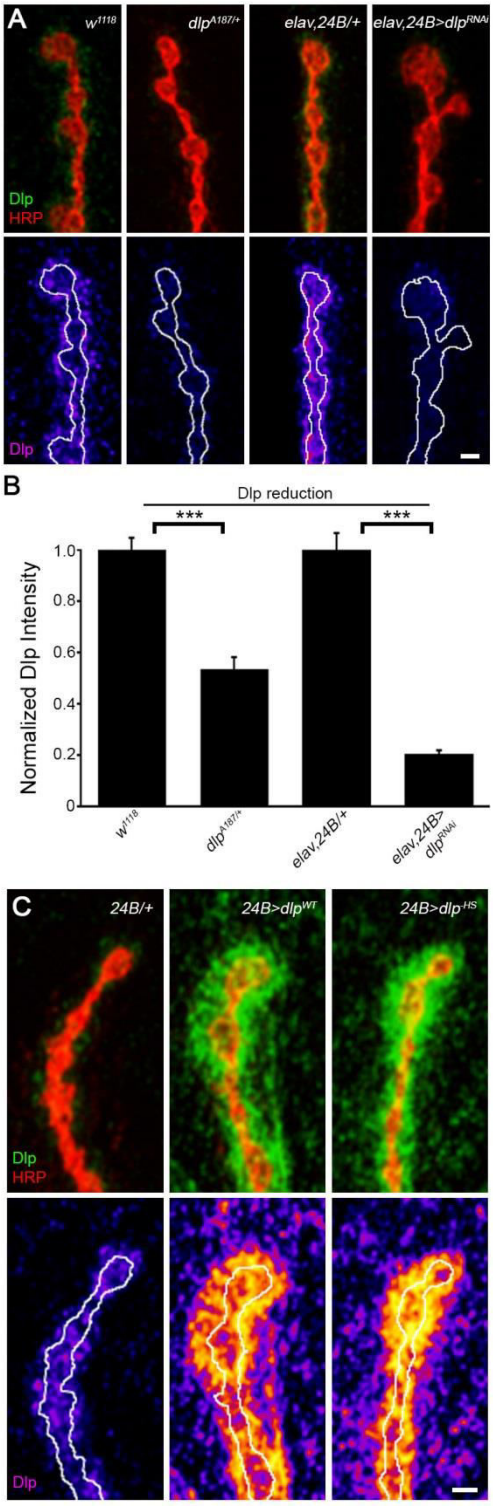

Figure S15

Figure S15. Synaptic Dlp changes with bidirectional *dlp* genetic manipulations. (A) Images show NMJs co-labeled for HRP and Dlp in the 2 indicated *dlp* reduction conditions compared to matched genetic controls. Dlp is shown in a heat map and HRP synaptic outlines in white. Scale bar: 2 μm. (B) Quantified Dlp fluorescence intensity normalized to controls: w^{1118} (N=21, 1.0±0.04), $dlp^{A187/+}$ (N=23, 0.54±0.04), *elav-Gal4, 24B-Gal4/+* (N=9, 1.0±0.06) and *elav-Gal4, 24B-Gal4>UAS-*dlp^{RNAi} (N=11, 0.21±0.01). Significance was determined by Unpaired t-test (w^{1118} vs. $dlp^{A187/+}$) or Unpaired t-test with Welch correction, indicated as ***p<0.001. Data show mean ± SEM from at least 3 independent replicates, with N representing NMJ number. (C) NMJ images co-labeled as in (A) for the 2 indicated *dlp* overexpression conditions compared to transgenic control. Scale bar: 2 μm. N=5 NMJs.

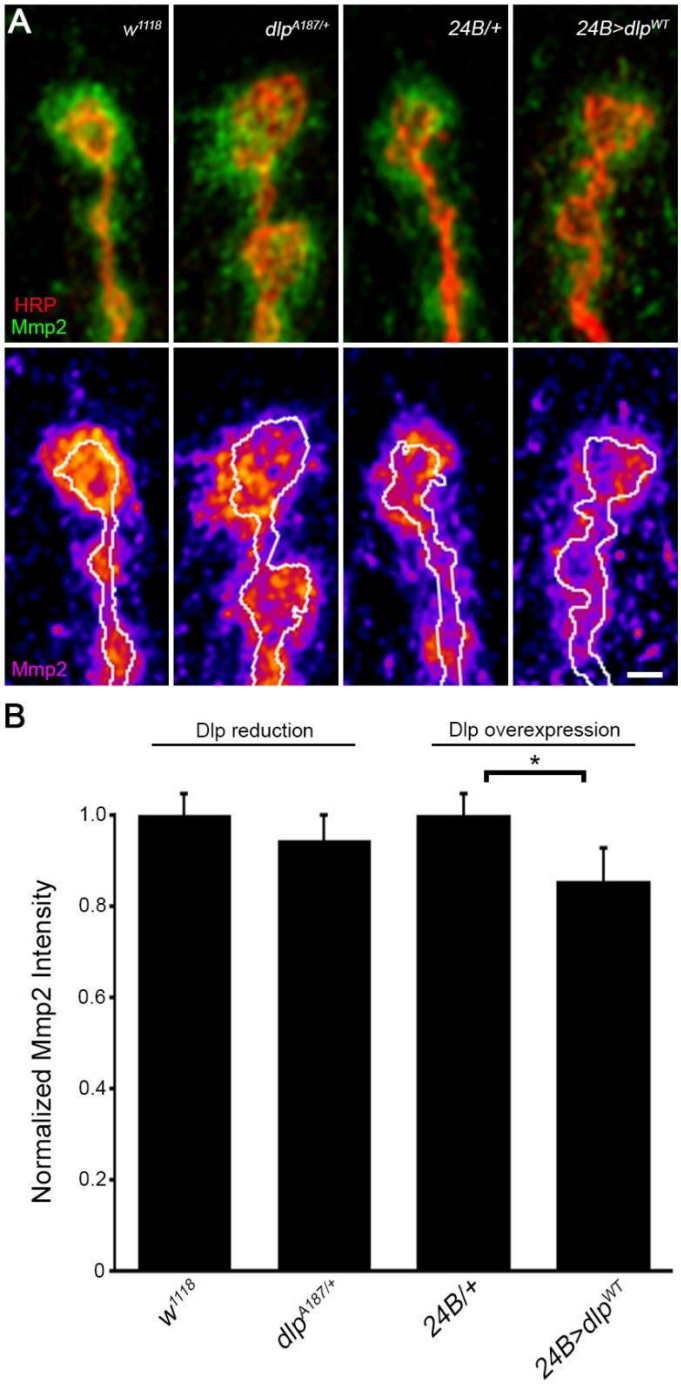

Figure S16

Figure S16. Synaptic Mmp2 changes with bidirectional *dlp* genetic manipulations. (A) Images show NMJs co-labeled for HRP and Mmp2 in the indicated *dlp* genotypes compared to matched controls. Mmp2 is shown in a heat map and HRP synaptic outlines in white. Scale bar: 2 μm. (B) Quantification of Mmp2 fluorescence intensity normalized to matched genetic controls: w^{1118} (N=39, 1.0±0.05) vs. $dlp^{A187/+}$ (N=44, 0.94±0.06), and *24B-Gal4/+* driver control (N=29, 1.0±0.05) vs. *24B-Gal4>UAS-*dlp^{WT} (N=31, 0.86±0.07). Significance determined by Unpaired t-test (w^{1118} vs. $dlp^{A187/+}$) was non-significant (p>0.05; not shown). Significance determined by the Mann-Whitney U-Test (*24B-Gal4/+* vs. *24B-Gal4>UAS-*dlp^{WT}) indicated as *p<0.05. Data show mean ± SEM from at least 3 independent replicates, with N = NMJ number. See Figure S7 for Dlp abundance in the genetic manipulations reported here.

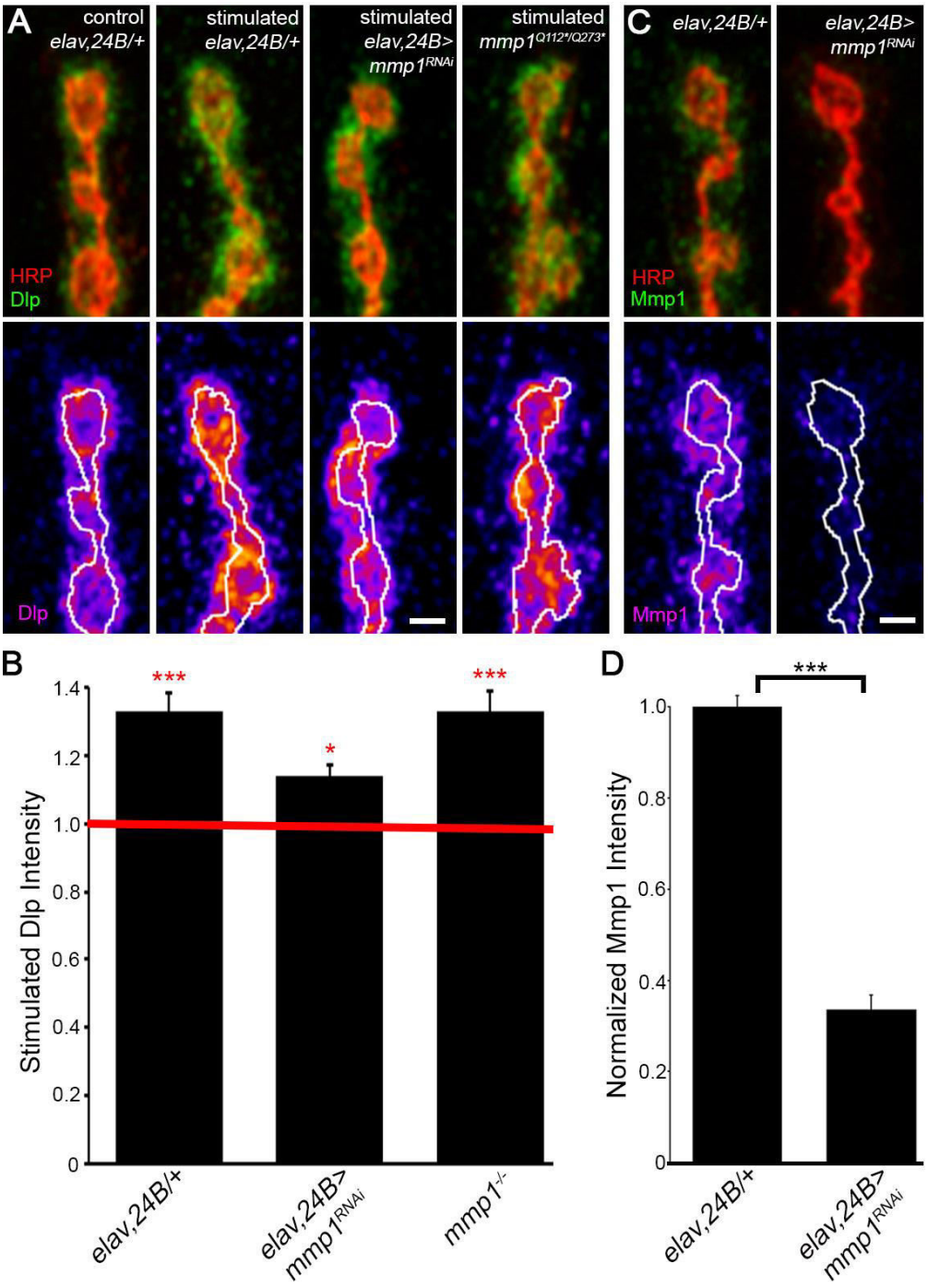

Figure S17

Figure S17. Activity-dependent synaptic Dlp increase occurs in the absence of Mmp1. (A) Images show NMJs co-labeled for HRP and Dlp in the indicated genotypes, mock treated (unstimulated) or stimulated with high [K^+]. Dlp is shown in a heat map and HRP synaptic outlines in white. Scale bar: 2 μm. (B) Quantification of stimulated Dlp intensity (bar graphs) normalized to unstimulated controls (red line): *elav-Gal4, 24B-Gal4/+* control (unstimulated, N=14, 1.0±0.05) vs. stimulated *elav-Gal4, 24B-Gal4/+* (N=14, 1.33±0.05), and *elav-Gal4, 24B-Gal4>UAS-mmp1^{RNAi}* (unstimulated, N=21, 1.0±0.04) vs. stimulated *elav-Gal4, 24B-Gal4>UAS-mmp1^{RNAi}* (N=20, 1.14±0.04) and unstimulated *mmp1^{Q112*}/mmp1^{Q273*}* (N=22, 1.0±0.04) vs. stimulated *mmp1^{Q112*}/mmp1^{Q273*}* (N=25, 1.33±0.06). (C) Images show NMJs co-labeled for HRP and Mmp1 in the indicated genotypes. Heat map shows Mmp1 alone and HRP synaptic outlines in white. Scale bar: 2 μm. (D) Quantification of Mmp1 intensity: *elav-Gal4, 24B-Gal4/+* control (N=18, 1.0±0.02) and *elav-Gal4, 24B-Gal4>UAS-mmp1^{RNAi}* (N=21, 0.34±0.03). (B,D) Significance determined by Unpaired t-test, indicated as *p<0.05 and ***p<0.001. Data show mean ± SEM from at least 3 independent replicates, with N = NMJ number.

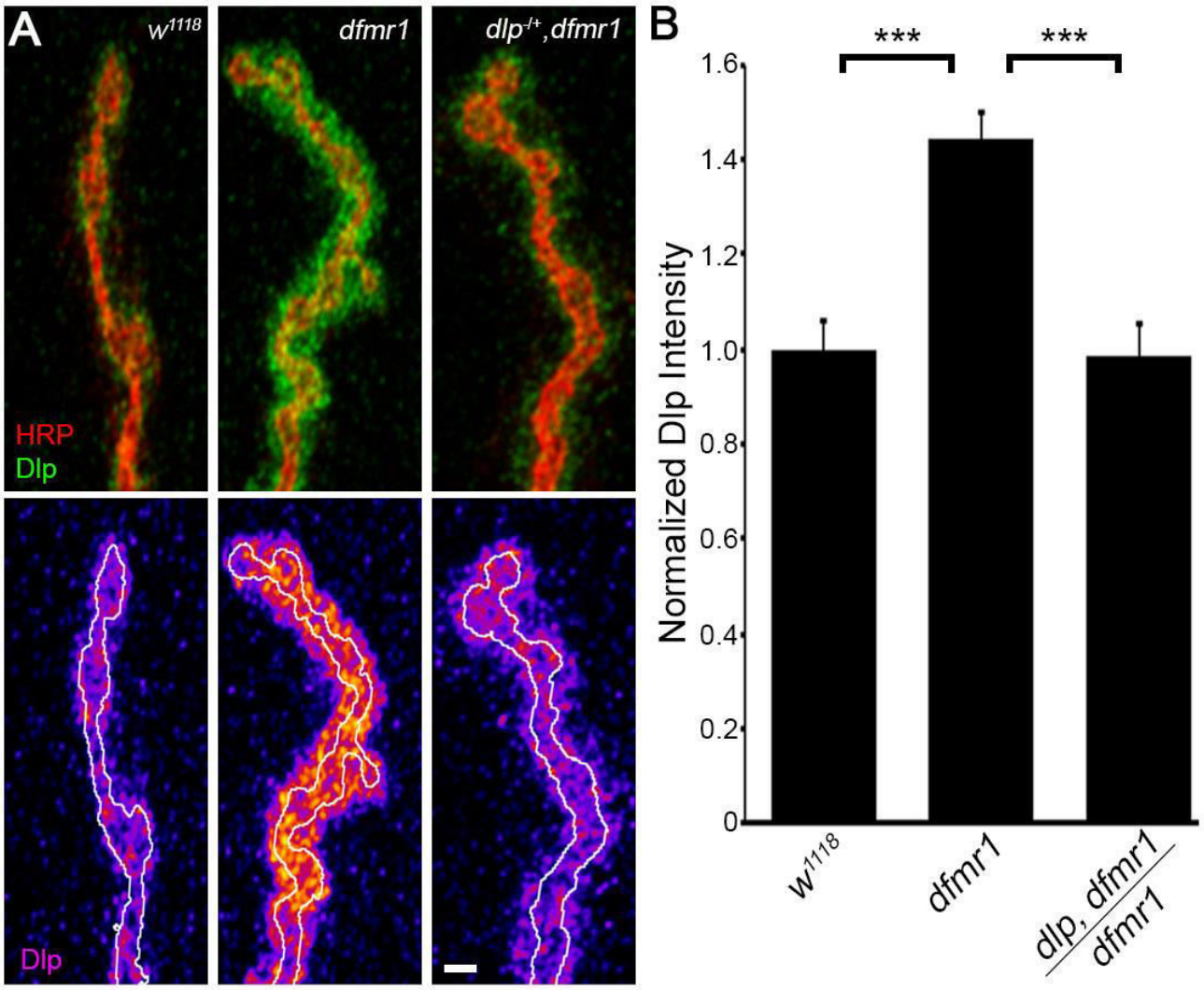

Figure S18

Figure S18. Synaptic Dlp in FXS disease model is restored by single copy *dlp* co-removal. (A) Images show NMJs co-labeled for HRP and Dlp in the 3 indicated genotypes. Dlp is shown in a heat map and HRP synaptic outlines in white. Scale bar: 2 μm. (B) Quantification of normalized Mmp1 fluorescence intensity: w^{1118} control (N=13, 1.0±0.06), $dfmr1^{50M/50M}$ (N=16, 1.44±0.06) and $dlp^{A187/+}$, $dfmr1^{50M/50M}$ (N=20, 0.98±0.07). Significance was determined by nonparametric ANOVA (Kruskal-Wallis) and Dunn's multiple comparisons post-test, indicated as ***p<0.001. The non-significant (p>0.05) comparison for w^{1118} vs. $dlp^{A187/+}$, $dfmr1^{50M/50M}$ is not shown. Data show mean ± SEM from at least 3 independent replicates, with N = NMJ number.

Supplementary Tables

Table S1: Raw data values for synaptic bouton number and ultrastructure

A. Synaptic Bouton Number			
	Genotype	***n***	***mean ± sem***
Genetic LOF	w^{1118} †	31	18.2 ± 0.99
	w^{1118}	23	21.5 ± 0.87
	$mmp1^{Q112*/Q112*}$ †	13	23.4 ± 1.3
	$mmp1^{Q273*/Q273*}$	21	28 ± 1.1
	$mmp2^{W307*/Df}$	19	29.7 ± 1.3
	$mmp2^{ss218/Df}$	21	29.1 ± 1.3
Heterozygotes	w^{1118}	12	21.9 ± 1.2
	$mmp1^{Q112*/+}$	15	31.4 ± 1.6
	$mmp1^{Q273*/+}$	22	32.5 ± 1.6
	$mmp2^{W307*/+}$	20	34.1 ± 1.5
	$mmp2^{ss218/+}$	22	37.6 ± 1.2
	$mmp2^{W307*/+}$, $mmp1^{Q112*/+}$ (dhet)	22	21.7 ± 1.1
	$mmp2^{W307*/+}$, $mmp1^{Q112*/Q112*}$ †	12	25.0 ± 1.7
	$mmp2^{W307*/+}$, $mmp1^{Q112*/Q273*}$	20	31.2 ± 1.2
	$mmp2^{W307*/Df}$, $mmp1^{Q112*/+}$	22	17.8 ± 0.90
Ubiquitous Inhibition	UH1/+ †	21	18.9 ± 0.50
	UH1>dblRNAi	23	19.8 ± 1.5
	UH1>Timp †	18	16.8 ± 0.63
	UH1/+	23	21.4 ± 0.74
	UH1>$mmp1^{RNAi}$	22	25.3 ± 1.1
	UH1>$mmp2^{RNAi}$	35	28.3 ± 0.74
	UH1>$mmp2^{RNAi1794-1R}$	20	35.6 ± 1.3
Pre & Post Inhibition	*elav*,24B/+	24	25.1 ± 0.78
	elav,24B>$mmp1^{RNAi}$	20	35.8 ± 0.99
	elav,24B>$mmp2^{RNAi}$	21	31.3 ± 0.85
	elav,24B>$mmp2^{RNAi1794-1R}$	21	35 ± 1.0
	elav,24B>dRNAi	23	23.7 ± 1.3
	elav,24B>$Timp^{OE}$	22	21.5 ± 0.92
Presynaptic Inhibition	*elav*/+	24	21.3 ± 0.94
	elav>$mmp1^{RNAi}$	27	28.6 ± 0.96
	elav>$mmp2^{RNAi}$	26	25.5 ± 1.38
	elav>$mmp2^{RNAi1794-1R}$	14	36.9 ± 0.91
	elav>dRNAi	26	33.7 ± 0.99
	elav>$Timp^{OE}$	18	25.8 ± 1.5
Postsynaptic Inhibition	24B/+	29	21.1 ± 1.1
	24B>$mmp1^{RNAi}$	23	26 ± 1.1
	24B>$mmp2^{RNAi}$	21	25.4 ± 1.4
	24B>$mmp2^{RNAi1794-1R}$	17	30.8 ± 0.88
	24B/+	27	23.1 ± 1.06
	24B>dblRNAi	23	34.3 ± 0.91
	24B>Timp	23	21.3 ± 0.84
	24B/+	29	20.4 ± 0.97
	$mmp1^{Q112*/+}$; 24B/+	19	27.8 ± 1.52
	$mmp2^{ss218/+}$; 24B/+	18	33.1 ± 1.34

	mmp1$^{Q112*/+}$; 24B>Timp	21	20.1 ± 1.28
	mmp2$^{ss218/+}$; 24B>Timp	19	22.6 ± 1.33

	Genotype	***n***	***mean ± sem***
Dlp Modulation	24B/+ †	20	19.4 ± 1.1
	mmp1$^{Q112*/Q273*}$ †	20	25.4 ± 1.4
	mmp1$^{Q112*/Q273*}$; 24B>dlp †	18	17.8 ± 0.83
	w^{1118}	33	22.7 ± 0.67
	mmp2$^{W307*/Df}$; *dlp*$^{A187/+}$	19	21.8 ± 0.2
Glial Inhibition	*Repo*/+	19	18.3 ± 1.0
	Repo>mmp1^{RNAi}	17	22.5 ± 0.6
	Repo>mmp2^{RNAi}	19	18.9 ± 1.0

B. Synaptic Ultrastructure

		Bouton Area (μm^2)		**Bouton Volume (μm^3)**		**Muscle Surface Area ($\mu m^2 x 10^4$)**		**Avg. # Boutons/Section**	
Morphology	**Genotype**	***n***	***mean ± sem***	***n***	***mean ± sem***	***n***	***mean ± sem***	***n***	***mean ± sem***
	w^{1118}	31	8.9 ± 1.3	61	8.4 ± 0.6	35	4.8 ± 0.10	30	1.1 ± 0.05
	mmp1$^{Q112*/Q273*}$	47	3.7 ± 0.4	62	4.9 ± 0.3	31	3.0 ± 0.11	36	1.6 ± 0.14
	mmp2$^{ss218/Df}$	36	5.8 ± 0.5	70	7.5 ± 0.4	37	5.1 ± 0.12	31	1.3 ± 0.11
	UH1/+	-	-	78	8.3 ± 0.5	41	4.6 ± 0.12	-	-
	UH1>dblRNAi	44	8.0 ± 0.7	83	8.8 ± 0.5	41	4.5 ± 0.12	42	1.2 ± 0.06

		SV Density		**SV's 0-250 nm**	**SV's 250-500 nm**	**SV's > 75 nm**	**SV's > 75 / Bouton Area**
Synaptic Vesicles	**Genotype**	***n***	***mean ± sem***	***mean ± sem***	***mean ± sem***	***mean ± sem***	***mean ± sem***
	w^{1118}	31	34.5 ±3.1	14.7 ± 0.5	18.6 ± 0.79	4.45 ± 0.52	0.67 ± 0.08
	mmp1$^{Q112*/Q273*}$	47	42.2 ± 3.2	15.7 ± 0.2	23.8 ± 1.4	3.85 ± 0.42	1.37 ± 0.22
	mmp2$^{ss218/Df}$	36	48 ± 3.1	18.5 ± 0.5	29.0 ± 1.3	4.47 ± 0.46	0.77 ± 0.07
	UH1>dblRNAi	44	33.4 ± 2.4	15.6 ± 0.4	19.6 ± 1.2	11.4 ± 1.38	1.55 ± 0.16

		MVB Density		**Mitochondria Density**	**SSR:Bouton Area**
Misc. Structures	**Genotype**	***n***	***mean ± sem***	***mean ± sem***	***mean ± sem***
	w^{1118}	31	0.06 ± 0.02	0.23 ± 0.04	1.84 ± 0.28
	mmp1$^{Q112*/Q273*}$	47	0.07 ± 0.03	0.16 ± 0.04	2.61 ± 0.27
	mmp2$^{ss218/Df}$	36	0.05 ± 0.02	0.17 ± 0.03	1.43 ± 0.13
	UH1>dblRNAi	43	0.02 ± 0.01	0.12 ± 0.02	1.37 ± 0.16

† Denotes size matched comparisons.

Table S2: Raw data values for functional neurotransmission and molecular assembly

A. Evoked Neurotransmission (TEVC)			
	Genotype	***n***	***Amplitude (nA)***
Genetic LOF	w^{1118}	10	191 ± 10
	$mmp1^{2/Q273*}$	10	244 ± 10
	$mmp1^{Q273*/Q273*}$	11	251 ± 21
	$mmp2^{W307*/Df}$	11	296 ± 18
	$mmp2^{ss218/Df}$	12	319 ± 13
Ubiquitous Inhibition	UH1/+	18	263 ± 9
	UH1>dblRNAi	11	202 ± 10
	UH1>Timp	10	192 ± 9
	UH1>$mmp1^{RNAi}$	16	292 ± 10
	UH1>$mmp2^{RNAi}$	12	310 ± 14
Cell-Targeted Inhibition	*elav*/+	10	264 ± 16
	elav>$mmp1^{RNAi}$	10	257 ± 14
	elav>$mmp2^{RNAi}$	11	281 ± 15
	24B/+	11	267 ± 8
	24B>$mmp1^{RNAi}$	12	301 ± 13
	24B>$mmp2^{RNAi}$	11	326 ± 21
	24B>dblRNAi	13	213 ± 17
	24B>Timp	11	210 ± 14
	24B/+	11	224 ± 13
	$mmp1^{Q112*/+}$; 24B/+	12	184 ± 13
	$mmp2^{ss218/+}$; 24B/+	11	224 ± 14
	$mmp1^{Q112*/+}$; 24B>Timp	13	199 ± 16
	$mmp2^{ss218/+}$; 24B>Timp	11	246 ± 15
	elav,24B/+	10	216 ± 14
	elav,24B> $mmp1^{RNAi}$	10	195 ± 12
	elav,24B> $mmp2^{RNAi}$	10	195 ± 12
	elav,24B>dblRNAi	10	230 ± 7
	elav,24B>Timp	10	200 ± 15
Dlp Modulation	24B/+	11	224 ± 13
	$mmp1^{Q112*/Q273*}$; 24B>*dlp*	10	139 ± 17
	w^{1118}	11	194 ± 14
	$mmp2^{W307*/Df}$	10	313 ± 13
	$mmp2^{W307*/Df}$; $dlp^{A187/+}$	10	234 ± 12

B. Spontaneous mEJC Analysis					
	Genotype	***n***	***Amplitude (nA)***	***Frequency (Hz)***	***Quantal Content***
LOF	w^{1118}	15	0.77 ± 0.1	2.07 ± 1.1	250 ± 13
	$mmp1^{Q273*/Q273*}$	19	1.0 ± 0.6	2.4 ± 1.2	251 ± 21
	$mmp2^{W307*/Df}$	15	0.66 ± 0.1	3.9 ± 1.5	451 ± 27
Ubiquitous Inhibition	UH1/+	15	0.67 ± 0.02	1.3 ± 0.1	393 ± 14
	UH1>$mmp1^{RNAi}$	8	0.4 ± 0.02	0.7 ± 0.1	729 ± 24
	UH1>$mmp2^{RNAi}$	11	1.5 ± 0.4	2.2 ± 0.4	207 ± 9.4
	UH1>dblRNAi	10	0.71 ± 0.03	3.9 ± 0.6	285 ± 14
	UH1/+	15	0.77 ± 0.05	9.3 ± 0.9	344 ± 12

	UH1>dblRNAi	14	0.88 ± 0.08	8.5 ± 0.8	230 ± 12

C. Glutamate Receptors							
Essential GluR Subunit	***Genotype***	***n***	***Total AZ #***	***AZ Density***	***Total GluRIID #***	***GluRIID Density***	***Apposition (GluRIID:nc82)***
	w^{1118}	13	216 ± 14	1.47 ± 0.10	203 ± 14	1.4 ± 0.12	0.94 ± 0.03
	$mmp1^{Q112*/Q273*}$	13	216 ± 11	2.22 ± 0.11	201 ± 11	2.0 ± 0.09	0.90 ± 0.02
	$mmp2^{ss218/Df}$	13	295 ± 10	1.74 ± 0.08	263 ± 8	1.52 ± 0.07	0.90 ± 0.03
	UH1/+	16	173 ± 11	1.31 ± 0.12	178 ± 11	1.24 ± 0.11	0.95 ± 0.02
	UH1>dblRNAi	17	184 ± 7	1.15 ± 0.08	200 ± 11	1.12 ± 0.07	0.98 ± 0.02
Alternative GluR Subunits	***Genotype***	***n***	***GluRIIA Density***	***GluRIIA Muscle Intensity (A.U.)***	***n***	***GluRIIB Density***	***GluRIIB Muscle Intensity (A.U.)***
	w^{1118}	13	1.15 ± 0.07	1.0 ± 0.09	27	1.18 ± 0.05	1.0 ± 0.03
	$mmp1^{Q112*/Q273*}$	14	1.32 ± 0.05	0.90 ± 0.12	13	1.86 ± 0.11	0.86 ± 0.02
	$mmp2^{ss218/Df}$	14	1.47 ± 0.09	0.98 ± 0.11	24	1.60 ± 0.06	1.32 ± 0.06
	UH1/+	16	1.20 ± 0.06	1.0 ± 0.1	-	-	-
	UH1>dblRNAi	16	1.07 ± 0.05	0.59 ± 0.09	-	-	-

Table S3: Raw data values for selected IHC experiments.

A. IHC: NMJ Mmp Levels					
	Genotype	**Mmp1 Levels (A.U.)**		**Mmp2 Levels (A.U.)**	
		n	***mean ± sem***	***n***	***mean ± sem***
Genetic LOF	w^{1118}	19	1.0 ± 0.06	15	1.0 ± 0.05
	$mmp1^{Q112*/Q273*}$	12	0.36 ± 0.06	10	0.45 ± 0.06
	$mmp2^{W307*}$	-	-	15	0.43 ± 0.03
	$mmp2^{ss218/Df}$	24	1.64 ± 0.09	11	0.4 ± 0.07
Ubiquitous Knockdown	UH1/+	13	1.0 ± 0.06	25	1.0 ± 0.04
	UH1>$mmp1^{RNAi}$	9	0.33 ± 0.04	-	-
	UH1>$mmp2^{RNAi}$	-	-	15	0.56 ± 0.07
	UH1>$mmp2^{RNAi1794\text{-}1R}$	-	-	11	0.51 ± 0.04
	UH1/+	23	1.0 ± 0.07	22	1.0 ± 0.06
	UH1>dblRNAi	24	0.23 ± 0.02	15	0.50 ± 0.07
	UH1/+	8	1.0 ± 0.06	10	1.0 ± 0.12
	UH1>Timp	7	0.50 ± 0.04	14	0.70 ± 0.04
Neuronal KD	*elav*/+	16	1.0 ± 0.08	-	-
	elav>$mmp1^{RNAi}$	19	0.67 ± 0.05	-	-
	elav>$mmp2^{RNAi}$	-	-	-	-
	elav>$mmp2^{RNAi1794\text{-}1R}$	-	-	-	-
Muscle KD	24B/+	15	1.0 ± 0.07	11	1.0 ± 0.09
	24B>$mmp1^{RNAi}$	17	0.54 ± 0.06	11	0.44 ± 0.10
	24B>$mmp2^{RNAi}$	11	1.4 ± 0.12	9	0.57 ± 0.07
	24B>$mmp2^{RNAi1794\text{-}1R}$	12	1.5 ± 0.20	13	0.48 ± 0.06

B. IHC: NMJ Timp Levels and Area					
	Genotype	**Timp Levels (A.U.)**		**Perisynaptic Timp Domain (μm^2)**	
		n	***mean ± sem***	***n***	***mean ± sem***
Genetic LOF	w^{1118}	15	1.0 ± 0.09	15	0.65 ± 0.07
	$mmp1^{Q112*/Q273*}$	21	1.1 ± 0.10	21	0.69 ± 0.06
	$mmp2^{ss218/Df}$	15	0.84 ± 0.06	15	1.4 ± 0.09
	timp	6	0.43 ± 0.02	-	-

C. IHC: NMJ Wg Signaling Pathway					
	Genotype	**Intensity (A.U.)**		**% Wg-Expressing Boutons**	
		n	***mean ± sem***	***n***	***mean ± sem (%)***
Extracellular Wg Ligand	w^{1118}	31	1.0 ± 0.03	31	68 ± 5
	$mmp1^{Q112*/Q273*}$	17	0.63 ± 0.05	20	31 ± 5
	$mmp2^{W307*/Df}$	35	0.92 ± 0.02	36	75 ± 3
	$mmp2^{ss218/Df}$	29	0.93 ± 0.02	27	77 ± 3
	UH1/+	22	1.0 ± 0.08	24	72 ± 6
	UH1>$mmp1^{RNAi}$	20	0.88 ± 0.06	10	39 ± 5
	UH1>dblRNAi	22	0.97 ± 0.08	23	74 ± 8

	Genotype	NMJ Intensity (A.U.)		Nuclear Intensity (A.U.)	
		n	*mean ± sem*	*n*	*mean ± sem*
FrzC2 Receptor	w^{1118}	20	1.0 ± 0.06	20	1.0 ± 0.05
	$mmp1^{Q112*/Q273*}$	19	1.16 ± 0.07	19	1.25 ± 0.08
	$mmp2^{ss218/Df}$	22	1.21 ± 0.07	22	1.35 ± 0.07
	UH1/+	26	1.0 ± 0.03	26	1.0 ± 0.03
	UH1>dblRNAi	22	0.88 ± 0.04	22	1.08 ± 0.08
	Genotype	**Intensity (A.U.)**		**Perisynaptic Dlp Area:HRP Area**	
		n	*mean ± sem*	*n*	*mean ± sem*
Dlp Co-receptor	w^{1118}	22	1.0 ± 0.06	23	0.60 ± 0.04
	$mmp1^{Q112*/Q273*}$	12	0.73 ± 0.06	13	0.38 ± 0.03
	$mmp2^{ss218/Df}$	22	0.93 ± 0.05	24	1.11 ± 0.06
	UH1/+	26	1.0 ± 0.02	35	0.58 ± 0.04
	UH1>dblRNAi	26	0.93 ± 0.07	35	0.59 ± 0.02

D. IHC: NMJ BMP Signaling Pathway			
	Genotype	Intensity (A.U.)	
		n	*mean ± sem*
Extracellular Gbb Ligand	w^{1118}	22	1.0 ± 0.05
	$mmp1^{Q112*/Q273*}$	25	0.73 ± 0.06
	$mmp2^{W307*/Df}$	30	0.93 ± 0.05
	UH1/+	23	1.0 ± 0.07
	UH1>dblRNAi	17	1.01 ± 0.08
Intracellular pMAD (NMJ)	w^{1118}	21	1.0 ± 0.18
	$mmp1^{Q112*/Q273*}$	20	2.2 ± 0.21
	$mmp2^{ss218/Df}$	17	0.9 ± 0.06
	UH1/+	17	1.0 ± 0.09
	UH1>dblRNAi	17	2.0 ± 0.21

E. IHC: NMJ Jeb Signaling Pathway					
	Genotype	Intensity (A.U.)		% Jeb-Expressing Boutons	
		n	*mean ± sem*	*n*	*mean ± sem (%)*
Extracellular Jeb Ligand	w^{1118}	25	1.0 ± 0.06	25	100 ± 6
	$mmp2^{W307*/Df}$	38	0.76 ± 0.04	-	-
	$mmp2^{ss218/Df}$	22	0.58 ± 0.03	22	59 ± 8
	UH1/+	23	1.0 ± 0.05	23	100 ± 6
	UH1>$mmp1^{RNAi}$	14	0.88 ± 0.06	13	64 ± 10
	UH1>dblRNAi	21	0.5 ± 0.05	21	48 ± 10
	Genotype	**NMJ Intensity (A.U.)**		**Nuclear Intensity (Muscle)**	
		n	*mean ± sem*	*n*	*mean ± sem*
Intracellular dpERK Signaling	w^{1118}	8	1.0 ± 0.04	17	1.0 ± 0.1
	$mmp1^{Q112*/Q273*}$	7	1.1 ± 0.1	14	2.4 ± 0.26
	$mmp2^{ss218/Df}$	6	0.79 ± 0.07	9	1.4 ± 0.17
	UH1/+	8	1.0 ± 0.3	6	1.0 ± 0.42
	UH1>dblRNAi	9	8.1 ± 2.1	23	20.4 ± 2.6

Table S4: Raw data values for *in situ* zymography assays.

***in situ* Zymography Proteolytic Activity Assays**							
		Gelatinase Activity (A.U.)			**Collagenase Activity Intensity (A.U.)**		
	genotype	*n*	*mean*	*sem*	*n*	*mean*	*S.D.*
Genetic Manipulations	w^{1118}	35	1	0.06			
	$dlp^{A187/+}$	33	0.66	0.04			
	elav,24B/+	7	1	0.5			
	elav,24B>dlp^{RNAi}	7	0.58	0.3			
	24B/+	35	1	0.07			
	24B>dlp^{WT}	18	1.5	0.09			
	24B>dlp^{-HS}	20	1.6	0.18			
	w^{1118}	31	1	0.05	8	1	0.29
	$dfmr1^{\Delta 50M}$	36	1.25	0.06	7	1.47	0.46
dTrpA1 Activity Assays (1hr 30C)	vglut/+	8	1	0.23	8	1	0.35
	vglut>dTrpA1	9	0.69	0.17	7	1.4	0.59
	vglut/+*	14	1	0.08			
	vglut>dTrpA1*	13	1.04	0.12			

Table S5: Raw data values for activity assays.

A. Chronic Activity Manipulations (NMJ IHC)

		Mmp1 Intensity (A.U.)			Mmp2 Intensity (A.U.)			Sdc Intensity (A.U.)		
	genotype	*n*	*mean*	*sem*	*n*	*mean*	*sem*	*n*	*mean*	*S.D.*
Chronic Increased Activity	elav,24B/+	12	1	0.064081	11	1	0.111113			
	elav,24B>shaw^{DN}	12	1.74	0.128275	10	1.4020634	0.116577			
	elav/+	23	1	0.044	5	1	0.09			
	elav>shaw^{DN}	25	1.78	0.076	6	1.49	0.322			
	vglut/+	16	1	0.031	17	1	0.056	4	1	0.152707
	vglut>shaw^{DN}	16	1.3	0.052	17	1.28	0.067	5	1.053383	0.25152
Chronic Inhibition	vglut/+	18	1	0.03673	19	1	0.054			
	vglut>shaw^{55719}	14	0.784	0.06786	17	0.69	0.049	4	1.25094	0.3619
	vglut>shaw^{55710}				10	0.72	0.075			
	vglut/+				13	1	0.07577			
	vglut>ork$^{\Delta NC1}$				11	0.604	0.07926			

B. Acute dTrpA1 Activity Manipulations (NMJ IHC)

		Mmp1 Intensity (A.U.)			Dlp Intensity (A.U.)		
	genotype	*n*	*mean*	*sem*	*n*	*mean*	*sem*
Acute dTrpA1 Activity Stimulation	vglut/+ 18C				10	1	0.07
	vglut>dTrpA1 18C				7	0.79	0.06
	vglut/+ 1hr 30C	10	1.00	0.06658	17	1	0.04
	vglut>dTrpA1 1hr 30C	13	1.42	0.09817	16	0.77	0.02
	ccapr/+ 18C	16	1.00	0.077324			
	ccapr>dTrpA1 18C	14	0.97	0.065302			
	ccapr/+ 1hr 30C	21	1.00	0.054872			
	ccapr>dTrpA1 1hr 30C	24	1.00	0.080717			
	*ccapr/+ 18C	12	1.00	0.040916			
	*ccapr>dTrpA1 18C	12	1.03	0.052798			
	*ccapr/+ 1hr 30C	16	1.00	0.026777			
	*ccapr>dTrpA1 1hr 30C	13	1.57	0.103862			
	vglut/+ 10' 30C						
	vglut>dTrpA1 10' 30C						

C. Acute Activity Stimulation High [K^+] (NMJ IHC)

			Mmp1			Mmp2			Timp			Dlp		
	genotype	*paradigm*	*n*	*mean*	*sem*	*n*	*mean*	*sem*	*n*	*mean*	*sem*	*n*	*mean*	*sem*
Wild-type Stimulation	w^{1118} unstimulated	2'	16	1	0.054377									
	w^{1118} stimulated	2'	14	1.37412	0.155506									
	w^{1118} unstimulated	10'	56	1	0.03077	25	0.999993	0.059885	17	1	0.051532			
	w^{1118} stimulated	10'	57	1.537821	0.07275	28	0.654831	0.055001	12	0.844929	0.041385			
	w^{1118} unstimulated	30'	11	1	0.090184									
	w^{1118} stimulated	30'	10	0.83522	0.061688									
	w^{1118} unstimulated	60'	17	1.000018	0.051078									
	w^{1118} stimulated	60'	16	1.444849	0.090526									
	w^{1118} unstimulated	spaced	25	1	0.051	4	1	0.281294				21	1	0.037772
	w^{1118} stimulated	spaced	27	1.48	0.0749	5	0.748762	0.200908				23	1.325707	0.057211
	w^{1118} unstimulated*	spaced*	19	1	0.1									
	w^{1118} stimulated*	spaced*	19	0.99	0.08									
	dlp::GFP unstimulated	10'	20	1	0.05							14	1.000086	0.073672
	dlp::GFP stimulated	10'	19	1.56	0.14							15	1.683304	0.106671
Stimulated Mmp Manipulations	$mmp2^{W307*}$ unstimulated	spaced	8	1	0.2									
	$mmp2^{W307*}$ stimulated	spaced	4	0.62234	0.18									
	$mmp1^{Q273*}$ unstimulated	spaced				4	1.000006	0.125516						
	$mmp1^{Q273*}$ stimulated	spaced				6	0.623	0.031442						
	elav,24B/+ unstimulated	10'										14	1.00	0.05
	elav,24B/+ stimulated	10'										14	1.33	0.05
	elav,24B>$mmp1^{RNAi}$ unstimulated	10'										21	1.00	0.04
	elav,24B>$mmp1^{RNAi}$ stimulated	10'										20	1.14	0.04
	$mmp1^{Q112*/Q273*}$ unstimulated	10'										22	1.00	0.04
	$mmp1^{Q112*/Q273*}$ stimulated	10'										25	1.33	0.06
Stimulated FXS Manipulations	*50M* unstimulated	spaced	17	1	0.15	8	0.999991	0.083291						
	50M stimulated	spaced	14	0.8	0.08	7	0.90669	0.134733						
	w^{1118} unstimulated	10'	13	1.00	0.04									
	w^{1118} stimulated	10'	15	1.51	0.10									
	50M unstimulated	10'	15	1.00	0.07									
	50M stimulated	10'	13	1.02	0.11									
	$dlp^{A187/+}$ unstimulated	10'	14	1.000004	0.044857									
	$dlp^{A187/+}$ stimulated	10'	15	0.912679	0.059003									
	dlp^{A187},*50M* unstimulated	10'	14	1.00	0.04									
	dlp^{A187},*50M* stimulated	10'	17	1.55	0.16									
Stimulated Wg Manipulations	elav/+ unstimulated	10'	4	1	0.22									
	elav/+ stimulated	10'	5	1.51	0.43									
	elav>Wg::GFP unstimulated	10'	5	1	0.09									
	elav>Wg::GFP stimulated	10'	5	0.85	0.09									
Stimulated Dlp Manipulations	w^{1118} unstimulated	10'	17	0.99988	0.08									
	w^{1118} stimulated	10'	19	1.338305	0.06									
	$dlp^{A187/+}$ unstimulated	10'	19	1	0.03									
	$dlp^{A187/+}$ stimulated	10'	21	0.853783	0.06									
	elav,24B/+ unstimulated	10'	26	1.00	0.04									
	elav, 24B/+ stimulated	10'	24	1.34	0.06									
	elav, 24B>dlp^{RNAi} unstimulated	10'	25	1.00	0.06									
	elav, 24B>dlp^{RNAi} stimulated	10'	18	0.88	0.06									
	elav, 24B>dlp^{WT} unstimulated	10'	16	1	0.06197									
	elav, 24B>dlp^{WT} stimulated	10'	14	1.504664	0.087135									
	24B/+ unstimulated	10'	21	1.00	0.06									
	24B/+ stimulated	10'	18	1.39	0.07									
	24B>dlp^{WT} unstimulated	10'	21	1.00	0.03									
	24B>dlp^{WT} stimulated	10'	16	1.64	0.16									
	24B>dlp^{-HS} unstimulated	10'	23	1.00	0.05									
	24B>dlp^{-HS} stimulated	10'	13	1.19	0.08									